

The *Arabidopsis* RNA Polymerase II Transcript Elongation
Complex and the role of post-translational modifications on
the histone chaperone FACT



DISSERTATION ZUR ERLANGUNG DES
DOKTORGRADES DER NATURWISSENSCHAFTEN (DR. RER. NAT.)
DER FAKULTÄT BIOLOGIE UND VORKLINISCHE MEDIZIN
DER UNIVERSITÄT REGENSBURG

vorgelegt von
Philipp, Michl-Holzinger, geb. Holzinger
aus Passau

im Jahr 2021

Das Promotionsgesuch wurde eingereicht am:

07.05.2021

Die Arbeit wurde angeleitet von:

PROF. DR. KLAUS D. GRASSER

Unterschrift:

PHILIPP MICHL-HOLZINGER

Für Josephine und Theodor

Acknowledgment

I would like to thank all people that have supported me or contributed to my work during my PhD.

I am entirely grateful to my PhD supervisor Prof. Dr. Klaus Grasser, who has guided and supported my entire academic career ever since my bachelor's thesis, enabled the research visit at the University of Southern Denmark which laid the groundwork for this PhD thesis and always showed patience when starting a family took its toll.

I would like to thank Prof. Dr. Thomas Dresselhaus, for creating a friendly, respectful, and stimulating environment over all those years and for leading my examination committee as a chairperson.

I thank my mentoring team Prof. Dr. Gernot Längst and Prof. Dr. Isabel Bäurle for their time, encouragement, and insight. Besides my advisors, I would like to thank Prof. Dr. Dina Grohmann for assessing this thesis and Dr. Jan Medenbach for the evaluation of my work as a 3rd examiner.

Additional thanks go to Dr. Astrid Bruckmann, Dr. Thomas Stempf, Dr. Uwe Schwartz, Elisabeth Silberhorn and Klaus-Jürgen Tiefenbach for their help with different experiments. Warm thanks go to Kinga Ay for her ever friendly and supportive work for the Graduate Research Academies.

A ton of thanks goes to my fellow labmates: Wojciech, Hans, Silvia, Alex, Brian, Simon, Amelie, Valentin, Henna, Hanna, Marion, Ina, Antje and Michael and all students that I joyfully encountered. Especially I would like to thank Simon for his patient bioinformatic support, Silvia for co-suffering through blotchy western blots, Hans for putting things into perspective, Hanna for sticking around and Wojciech for his sharp and helpful views.

My final thanks go to my wife, for providing space, making plenty of sacrifices and providing lovingly for our family.

Abbreviations

-/-	Homozygous mutant	Me1/2/3	Mono/Di/Tri-methylation
+/-	Heterozygous mutant	MS/MS	Tandem mass spectrometry
<i>A. thaliana</i>	<i>Arabidopsis thaliana</i>	<i>N. benthamiana</i>	<i>Nicotiana Benthamiana</i>
<i>A. tumefaciens</i>	<i>Agrobacterium tumefaciens</i>	NDR	Nucleosome depleted region
aa	Amino acids	Ni-NTA	Nickel nitriloacetic acid
Ac	Lysine Acetylation	PAM	protospacer adjacent motif
Acetyl+	Acetylation-mimetic	Phos	Phosphorylation
Acetyl0	Acetylation-insensitive	Phos+	Phosphorylation-mimetic
AID	Acidic intrinsic disordered	Phos0	Phosphorylation-insensitive
AU	Acid Urea	Pol II	RNA polymerase II
BID	Basic intrinsic disordered	PTM	Post translational modification
bp	Base pairs	SDU	University of Southern Denmark
CBB	Coomassie Brilliant Blue	sgRNA	single guide RNA
CD	Circular dichroism	SHL	Superhelix location
CDS	Coding sequence	SPT	Suppressor of Ty
CK2	Casein Kinase 2 complex	SSRP1	Structure specific recognition protein 1
CLSM	Confocal laser scanning microscopy	TCE	2,2,2-Trichloroethanol
Col-0	Columbia Ecotype	TES	Transcription end site
DAF	Days after flowering	TSS	Transcription start site
DAS	Days after stratification	UR	University of Regensburg
<i>E. coli</i>	<i>Escherichia coli</i>	WT	Wildtype
eGFP	Enhanced green fluorescence protein	Y2H	Yeast-2-Hybrid
ELF1	Elongation factor 1		
EMSA	Electrophoretic mobility shift assay	TSS	Transcription start site
FRAP	Fluorescence recovery after photobleaching	WT	Wildtype
FRET	Förster resonance electron transfer	UR	University of Regensburg
GS-tag	Protein G and streptavidin-binding peptide- tag	Y2H	Yeast-2-Hybrid
GST-tag	Glutathione S-transferase -tag		
His-tag	6 x Polyhistidine tag		
HMG	High mobility group		
IDR	Intrinsic disordered region		
LC	Liquid chromatography		

References of Manuscripts

This thesis is composed of/contains Data or Figures of the following manuscripts

Michl-Holzinger, P., Mortensen, S.A., and Grasser, K.D. (2019). The SSRP1 subunit of the histone chaperone FACT is required for seed dormancy in *Arabidopsis*. *J. Plant Physiol.* 236, 105–108.

Disclaimer: Most experimental work was performed by Philipp Michl-Holzinger, except: Initial observations were made by Simon Arnold Mortensen (Mortensen, 2012); T0 seeds of of *ssrp1-2* mutants with an additional copy of DOG1 were obtained from Marcel Kaljanac (Kaljanac, 2014). Text and Figures section **2.7**. Text section **3.5.1**, **6.1.9** and **6.2.4.4**

Pfab, A., Grønlund, J.T., **Holzinger, P.**, Längst, G., and Grasser, K.D. (2018). The *Arabidopsis* Histone Chaperone FACT: Role of the HMG-Box Domain of SSRP1. *J. Mol. Biol.* 430, 2747–2759.

Disclaimer: Philipp Michl-Holzinger (former Holzinger) contributed by performing major revisions. These revisions included a more detailed look on the phenotypic aspects leaf and flower morphology and a validation of SSRP1 and SSRP1 Δ HMG protein levels in the *ssrp1-1* background under control of the native or the 35s promoter via western blot and subsequent signal quantification. Figures section **2.6**

Antosz, W., Pfab, A., Ehrnsberger, H.F., **Holzinger, P.**, Köllen, K., Mortensen, S.A., Bruckmann, A., Schubert, T., Längst, G., Griesenbeck, J., et al. (2017). The Composition of the *Arabidopsis* RNA Polymerase II Transcript Elongation Complex Reveals the Interplay between Elongation and mRNA Processing Factors. *Plant Cell* 29, 854–870.

Disclaimer: Philipp Michl-Holzinger (former Philipp Holzinger) contributed to this work by affinity purification coupled to mass spectrometry (AP-MS) analysis of the GS-tagged FACT subunits (SPT16-GS and SSRP1-GS). This included the affinity purification, western blotting the sample preparation for LC-MS/MS and the bioinformatic analysis of the MS data. The mentioned experiments were performed in this PhD thesis, except α -SPT16 and α -SSRP1 immunostainings in my master's thesis (Holzinger, 2015). Datasets SPT16 and SSRP1, Section **2.1**

Contents

1	Introduction	1
1.1	Chromatin Organisation	1
1.2	Transcription by RNA Polymerase II.....	2
1.3	Histone Chaperones.....	3
1.4	ELF1	4
1.5	SPT6.....	5
1.6	The FACT complex.....	7
1.6.1	FACT – Architecture.....	8
1.6.2	FACT – Mode of Action	9
1.6.3	FACT in <i>Arabidopsis thaliana</i>	10
1.7	Aims of the thesis	11
1.7.1	Determination of the Transcript Elongation Histone Chaperone Complex	11
1.7.2	Generation of Mutant lines.....	11
1.7.3	ELF1 as a histone chaperone.....	12
1.7.4	Impact of PTMs on the FACT complex.....	12
1.7.5	The HMGbox of SSRP1.....	13
1.7.6	An effect of SSRP1 on seed dormancy	13
2	Results	14
2.1	The Transcript Elongation Histone Chaperone Complex	14
2.1.1	Experimental Setup and Affinity Purification.....	14
2.1.2	Data analysis – Generals and Considerations	16
2.1.3	Association with the Transcript Elongation Complex	18
2.1.3.1	FACT.....	18
2.1.3.2	SPT6l.....	19
2.1.3.3	ELF1	20
2.1.3.4	Orientation of histone Chaperones on Pol II.....	20
2.1.3.5	Histones.....	21

2.1.3.5 Association with CK2	22
2.1.4 Summary	22
2.2 Mutant lines for ELF1 and SPT6l	23
2.3 ELF1 has histone chaperone like qualities	26
2.3.1 ELF1-BID binds DNA	27
2.3.2 Association of ELF1 with CK2 is independent of phosphorylation	28
2.3.3 ELF1 binds to H2A-H2B; synergistic phenotypes with histone chaperones	29
2.4 Acetylation and Phosphorylation modulate the binding properties of the <i>Arabidopsis</i> Histone Chaperone FACT	31
2.4.1 SPT16 AID is phosphorylated by CK2	32
2.4.2 Direct interaction studies between CK2 and FACT by Y2H	34
2.4.3 Increase of H2A-H2B binding by phospho-mimetic SPT16_AID	36
2.4.4 Influence of Charge Alterations on Histone Immunoprecipitation	39
2.4.5 Altering the charge pattern of SPT16 displays effects on plant development	40
2.4.5.1 Line creation and validation	41
2.4.5.2 Phenotypic analysis of SPT16 phospho-variants	43
2.4.6 Phosphorylation of SPT16 plays a role in clearing nucleosome depleted regions..	47
2.5 Acetylation of SSRP1 BID and HMGbox.....	55
2.5.1 Putative KDACs	55
2.5.2 Putative KATs	58
2.5.3 Acetylation mimicking amino acid substitutions affect the binding of linear DNA	58
2.5.4 Influences on Histone immunoprecipitation by SSRP1 acetylation variants.....	62
2.5.5 No obvious defect on subcellular localisation.....	63
2.5.6 Acetylation-mimicking in SSRP1 leads to no severe defects on plant development	64
2.5.6.1 Line creation and validation	65
2.5.6.2 Phenotypic analysis of SSRP1 acetyl-variants.....	66

2.6	The <i>Arabidopsis</i> Histone Chaperone FACT: Role of the HMG-Box Domain of SSRP1	70
2.7	The SSRP1 subunit of the histone chaperone FACT is required for seed dormancy in <i>Arabidopsis</i>	71
3	Discussion	76
3.1	The Transcript Elongation Histone Chaperone Complex	76
3.2	The histone chaperone ELF1.....	80
3.3	Phosphorylation of SPT16 AID	82
3.4	Acetylation of SSRP1 BID and HMGbox.....	88
3.5	A role for SSRP1 in seed dormancy.....	90
3.5.1	The SSRP1 subunit of the histone chaperone FACT is required for seed dormancy in <i>Arabidopsis</i>	90
3.5.2	General Discussion.....	91
4	Summary	92
5	Materials.....	93
5.1	Instruments	93
5.2	Chemicals and Enzymes.....	93
5.2	Oligonucleotides.....	93
5.4	Plasmids	96
5.5	T-DNA insertion lines	98
5.6	Bacteria and yeast strains	98
5.7	Databases, Online Tools and Software	99
6	Methods.....	99
6.1	Plant based Methods.....	99
6.1.1	Cultivation of <i>A. thaliana</i> on soil.....	99
6.1.2	Surface sterilisation of seeds and cultivation of <i>A. thaliana</i> on MS-media	100
6.1.3	Crossing of <i>A. thaliana</i>	100
6.1.4	Stable transformation of <i>A. thaliana</i>	100

6.1.5 Selection of transgenic lines.....	101
6.1.6 Soil based phenotypic analysis.....	101
6.1.7 Abiotic stress treatment.....	101
6.1.8 Photometric determination of anthocyanins.....	102
6.1.9 Germination assays	102
6.1.10 Transient transformation of <i>N. benthamiana</i>	102
6.1.11 Cultivation of <i>Arabidopsis</i> PSB-D cells.....	103
6.1.12 Transformation of <i>Arabidopsis</i> PSB-D cells.....	103
6.1.13 Upscaling of <i>Arabidopsis</i> PSB-D cells	103
6.2 Nucleic Acid based methods	104
6.2.1 Isolation of genomic DNA from <i>Arabidopsis</i> leaves	104
6.2.2 Isolation of RNA from <i>Arabidopsis</i> seeds	104
6.2.3 cDNA Synthesis	104
6.2.4 Polymerase Chain Reaction (PCR)	105
6.2.5 Agarose Gel Electrophoresis	106
6.2.6 Annealing of Oligonucleotides.....	107
6.2.7 Restriction-ligation cloning.....	107
6.2.8 Gateway cloning.....	107
6.2.9 Sequencing	107
6.3 Cell based methods.....	107
6.3.1 Preparation of chemically competent yeast cells	107
6.3.2 Co-transformation of yeast cells by heat shock	108
6.3.3 Yeast-2-Hybrid (Y2H) Assay.....	108
6.3.4 Preparation of Rubidium Chloride competent cells	108
6.3.5 Transformation of <i>E. coli</i> and <i>A. tumefaciens</i> by heat shock.....	109
6.3.6 Plasmid Miniprep	109
6.3.7 Plasmid Midiprep	109
6.3.8 Protein expression in <i>E. coli</i>	110

6.4 Protein based methods.....	110
6.4.1 SDS-PAGE.....	110
6.4.2 Native PAGE.....	111
6.4.3 Acid Urea (AU) PAGE	111
6.4.4 Coomassie Brilliant Blue staining (CBB).....	111
6.4.5 Protein Quantification	111
6.4.5 Protein/Affinity Purification	112
6.4.6 Desalting and Protein Concentration.....	114
6.4.7 Electrophoretic mobility shift assay (EMSA)	114
6.4.8 Circular dichroism (CD).....	114
6.4.9 GST-pulldowns	114
6.4.10 “hot” CK2 <i>in vitro</i> phosphorylation assay	115
6.4.11 “cold” CK2 <i>in vitro</i> phosphorylation assay.....	115
6.4.12 ChIP-Seq	115
6.4.13 Western Blotting	118
6.4.14 Mass-Spectrometry.....	119
6.4.14.1 MALDI-TOF.....	119
6.4.14.2 In-gel digestion of proteins	119
6.5.14.3 LC-MS/MS.....	119
6.5 Confocal laser scanning microscope (CLSM)	120
6.5.1 Fluorescence recovery after photobleaching (FRAP)	120
6.5.2 Förster resonance energy transfer (FRET)	120
7 Supplementary.....	121
References	135

1 Introduction

The fundamental dogma of molecular biology states, that DNA is transcribed into RNA and that RNA is translated into proteins (Crick, 1970). This holds true for transcription of mRNA by RNA Polymerase II (Pol II), which will be in the focus of this thesis. Transcription overall is the most magnificent process, as it allows to determine from one set of DNA a multitude of cell types by generating and maintaining distinct gene expression patterns during development (Chen and Dent, 2014). Unsurprisingly, many aspects of transcription must be heavily regulated to accomplish this.

1.1 Chromatin Organisation

The first obstacle in the way of the transcription machinery is the organization of the genome into chromatin (Shandilya and Roberts, 2012). The core particle of chromatin, the nucleosome, consists of two copies of each histone protein, H2A, H2B, H3 and H4, which are assembled into an octamer with 145-147 base pairs (bp) of DNA wrapped around it (Luger et al., 1997). The major grooves of DNA face the octamer in distinct, so called superhelix locations (SHL). The nucleosome dyad is located in the middle of the symmetry (SHL 0) and extends to each side up to the DNA bound at the borders (SHL +7 to -7) (Luger et al., 1997; Zhou et al., 2019). This module is arranged into beads on a string, compacting the genome five- to tenfold. Additionally, chromatin contains a linker histone, H1, which binds between nucleosomes. Thereby the core histones get linked to form a condensed fibre, compacting the DNA higher (Bell et al., 2011). The view on the organization of these higher-order structures has undergone a change: From a regular 30 nm fibre, which can be visualised via Cryo-EM *in vitro* (Song et al., 2014), towards an irregular folded nucleosome fibre *in vivo* (Nishino et al., 2012; Ricci et al., 2015). There, nucleosomes arrange into discrete groups of various sizes and densities. Dense patches associate with linker histone H1. Individual groups can be interspaced by nucleosome-depleted regions (Ricci et al., 2015). Chromatin does not only pack the genome into the nucleus, but it also acts as repressive barrier (Petesch and Lis, 2012). Hence, it has regulatory implications on all DNA-depending processes including transcription, replication and repair (Luger et al., 2012). An important role in distinguishing open, euchromatin and closed heterochromatin play post-translational modifications (PTMs) of histones. In *Arabidopsis* heterochromatin states are associated with H3K9me2 and H3K27me1 (Roudier et al., 2011; Sequeira-Mendes et al., 2014) while open chromatin states are associated with histone acetylation and further mono- di- and tri-methylation marks (Leng et al., 2020; Sequeira-

Mendes et al., 2014). Generally, the acetylation of histone tails reduces the affinity to DNA in nucleosomes (Brower-Toland et al., 2005). Further, histone turnover becomes important to regain access to repressed regions. Here, the rigid nucleosomes are partly, or completely exchanged. Increasing the histone exchange can increase the accessibility of a certain genomic region, e.g. proximal promoters which are targeted by transcription factors and start the transcription cascade. Exchanging histones for certain histone variants can block further rounds of exchange and will limit DNA accessibility and hence transcription. While increasing nucleosome density (heterochromatin) correlates with H2A.W levels in *Arabidopsis*, H2A.Z is present in the 5' end of the gene bodies (Yelagandula et al., 2014). Several factors regulate histone exchange during transcription, including writers and erasers of histone post-translational modifications, energy dependent chromatin remodellers and histone chaperones (Venkatesh and Workman, 2015).

1.2 Transcription by RNA Polymerase II

The transcription cycle begins with initiation. The preinitiation complex assembles on promoters, containing Pol II and general transcription factors. This complex unwinds promoter-DNA and synthesizes the first 8-9 bp of RNA, forming the so-called transcription bubble. Pol II escapes the promoter and extends the pre-messenger RNA, thereby entering the elongation phase. Here, co-transcriptional processes like RNA 5'-end capping, promoter-proximal pausing, the subsequent release of pausing, splicing and backtracking take place. At all times obstacles like the nucleosome must be removed. In the end pre-mRNA is cleaved, polyadenylated and Pol II terminates the cycle (Osman and Cramer, 2020).

Many additional layers can be added to this rather simplified version of the transcription cycle, e.g., the phosphorylation status of the Pol II C-terminal heptad repeat domain. In yeast the phosphorylation patterns change during the course of transcription: S7P spikes at promoters, S5P during early elongation and S2P later in the gene body (Vinayachandran et al., 2018). A similar pattern can be observed in *Arabidopsis* (Antosz et al., 2020). During the onset of transcript elongation, initiation factors are exchanged for transcript elongation factors (TEFs) by reusing the respective interaction interfaces (Schier and Taatjes, 2020). TEFs associated with Pol II are for example SPT6 and IWS1 (SPN1 in yeast), the DSIF-complex (SPT4 and SPT5), the PAF-complex and ELF1. Elongation factors are absent at the promoter and sharply increase downstream of the transcription start site (TSS) within a narrow window of ~50 nucleotides (nt), indicating a coordinated transcript elongation complex (TEC) formation (Mayer et al., 2010), thereby enabling the onset of efficient transcription.

However, the obstacle of the nucleosome remains. *In vitro* Pol II can unwrap the nucleosome without any additional factors until SHL-1, still binding the complete octamer partly (Kujirai et al., 2018). After passage of the dyad no obvious stalling of Pol II can be detected (Weber et al., 2014) as histones might be removed from the Pol II nucleosome complex (Kujirai et al., 2018). Next to the stimulation of elongation activity (Vos et al., 2020) some TEFs are needed to circumvent the complete disassembly of the nucleosome and hence the loss of spatially stored information. Recent cryogenic electron microscopy (cryo-EM) structures of Pol II (Bernecky et al., 2016) could accommodate the PAF-complex, SPT6, ELF1 and DSIF-complex (Ehara et al., 2017; Vos et al., 2018, 2020) embedding huge portions of Pol II. The FACT complex (SPT16 and SSRP1) could be crystalized encasing the nucleosome making contacts with all histones (Liu et al., 2020). Many of these factors contain acidic intrinsic disordered regions (AID) which could cover and hold exposed histone DNA binding surfaces in the wake of transcription (Ehara et al., 2019). TEFs which assist the disassembly of nucleosomes in an ATP independent way can be grouped in the class of histone chaperones (Van Lijsebettens and Grasser, 2014).

1.3 Histone Chaperones

The basic principle of histone chaperones is to interact with histones to shield the strong interactions with DNA. Classically, a negative charged chaperone binds to positive charged histones to free negative charged DNA. Thereby, an ordered assembly and disassembly of nucleosomes under physiological conditions is mediated (Philpott et al., 2000). Due to their very basic nature and their high content of hydrophobic amino acids, histones are prone to interact unspecific with many other macromolecules. Hence, there is a need to tether unwinding nucleosomes and similarly to store free pools of histones. Histone chaperones are defined as a group of ATP independent proteins that bind to histones but also stimulate their transfer onto DNA or to other proteins (Warren and Shechter, 2017).

During, e.g. transcription, the nucleosome must be removed ahead of the polymerase, however the octasome is stably bound to the DNA due to its many DNA-Histone contacts (see SHLs). To make removal more efficient, histones and DNA are bound in a coordinated manner by chaperones (Formosa, 2012). In the progression of Pol II the nucleosome is unwrapped, exposing a histone octamer where DNA is gradually removed. The octamer alone is very unstable at physiological conditions and the unwrapping of the nucleosome causes a serious risk for its integrity. Uncoordinated exposure of histones to DNA would cause histones to bind rapidly and thereby forming unwanted aggregates (Gurova et al., 2018). Indeed, anchor away

assays in yeast removing the TEC-associated histone chaperones SPT6 and SPT16 show an increase in scrambling of histone modifications, indicating a loss of histones during transcription (Jeronimo et al., 2019).

There is not a single feature which defines a histone chaperone. Both, structural folds and intrinsically disordered regions (IDR) are used to bind histones and shield functional interfaces (Hammond et al., 2017). A nice example for the use of structural folds would be the histone chaperone NAP1, which manages to mimic the structure and electrostatics of nucleosomal DNA and thereby provides an acidic binding surface for H2A–H2B (Aguilar-Gurrieri et al., 2016). Other chaperones, like e.g. SPT16 are dependent on its IDR, as the initial step of invading the nucleosome cannot be accomplished without it (Tsunaka et al., 2016). Generally, IDRs are extremely flexible and dynamic regions of proteins, resulting from a lack of stable secondary structure. This confers many advantages compared to structured domains in protein-protein interactions. IDRs can extend far from the protein core enabling them capture binding partners further away. When bound, IDRs can make many transient contacts with potential ligands with fast on and off rates and eventually fold upon proper binding. Within the context of histone chaperones, they are mostly very negatively charged (acidic intrinsic disordered =AID) to complement the very basic nature of histones (Warren and Shechter, 2017). Many interaction partners of the core TEC (ELF1, SPT5, SPT6, CTR9, SPT16 and POB3 (SSRP1 in higher eukaryotes) contain at least one AID and each of them might bind basic regions of the nucleosome exposed during transcription (Ehara et al., 2019; Kujirai and Kurumizaka, 2020). In the focus of this thesis are four histone chaperones associated with Pol II: ELF1, SPT6 and SPT16 together with its complex partner SSRP1.

1.4 ELF1

ELF1 (*elongation factor 1*) was first described in yeast as a factor causing synthetic lethality with other known transcript elongation factor mutants (SPT6, SPT4, SPT5, TFIIS and members of the PAF-complex). For the ELF1 and SPT16 combination, a synthetic Spt- phenotype was observed (Prather et al., 2005), which indicates defects in chromatin and transcription (Tomson and Arndt, 2013). ELF1 is a small protein of ~80-150 amino-acids (aa), containing a basic N-terminus, a defined Zn-Ribbon in the middle and an acidic C-terminus, which is present in yeast and *Arabidopsis*, however absent from *Drosophila melanogaster* to human (Prather et al., 2005). Both N- and C-terminus are intrinsically disordered (Ehara et al., 2017, 2019). Yeast ELF1 is phosphorylated by CK2 in its C-terminus *in vitro* (Kubinski et al., 2006) and associates early during transcript elongation with Pol II (Joo et al., 2019; Mayer et al., 2010). This

association stays put even after the polyadenylation site (Mayer et al., 2010). In a recent Cryo-EM structure ELF1 filled the gap between core and clamp module, thereby completing the DNA entry tunnel by direct interaction with RPB1, RPB2 (**Figure 1a**). Further direct interaction was observed with the outer shell of TEC factors by directly binding to SPT5 (Ehara et al., 2017). Adding the unwinding nucleosome in this scenario, places ELF1 directly on the surface of the incoming nucleosome (**Figure 1b**). It was proposed that the basic N-terminus (unresolved) competes for DNA and the C-terminus (not present in the crystal) extends towards H2A-H2B, with H2B showing the nearest exposed surface (Ehara et al., 2019). Hence, ELF1 would qualify as a histone chaperone by binding and eventually releasing histones during transcript elongation. In line, *in vitro* transcription runoff essays show that ELF1 alone minimally enhances the progression through the nucleosome, in combination with DSIF it leads to a synergistic effect to overcome the nucleosomal barrier (Ehara et al., 2019). In plants ELF1 has not been studied so far. The unique situation that the acidic C-terminus is present in higher eukaryotes (Prather et al., 2005) make it a desirable candidate to study.

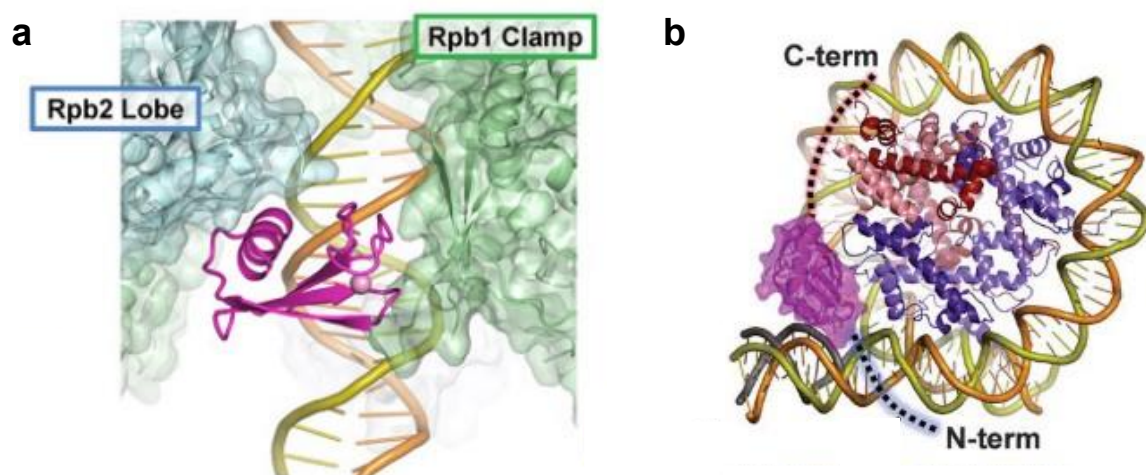


Figure 1 ELF1 bridges the DNA entry tunnel and faces the unwrapping nucleosome during transcript elongation

(a) ELF1 (magenta) binds directly to Rpb1 (green) and Rpb2 (cyan) completing the DNA entry tunnel (b) ELF1 faces the unwrapping nucleosome at SHL-1 (approximately half the DNA peeled of). The acidic C-terminus is suggested to extend towards the exposed histones and the basic N-terminus competes for DNA. H2A dark red, H2B light red, H3 light blue, H4 dark blue. Figure (a) is taken from Ehara et al., 2017); Figure (b) from Ehara et al., 2019)

1.5 SPT6

SPT6 has been first identified in the screen for suppressing the Ty phenotype (*Suppressor of Ty* 6) (Winston et al., 1984). SPT6 is a conserved histone chaperone critical in managing chromatin

during transcription (Duina, 2011). Traditionally considered as a H3-H4 chaperone, recent publications suggest similar binding affinity to H2A-H2B (McCullough et al., 2015). SPT6 consists of three functionally distinct regions: N-terminus, core, and C-terminus. The acidic intrinsically disordered N-terminal region is essential for the histone chaperone activity of SPT6. Binding of SPN1 (IWS1 in *Arabidopsis*) to the N-terminus blocks nucleosome interaction (Kato et al., 2013; McDonald et al., 2010). The C-terminal domain reads phosphorylation patterns of the C-terminal domain of RPB1 (Brázda et al., 2020). In yeast SPT6 is recruited to transcribed regions as a component of the general RNAPII transcription complex, like other factors of the core TEC, this happens rapidly (Joo et al., 2019) within a narrow frame of 50 bp after transcript initiation which is independent of the binding of the C-terminus of SPT6 to RPB1-CTD (Mayer et al., 2010). Recent Cryo-EM (Vos et al., 2018, 2020) structures place SPT6 on transcribing Pol II and indeed the tight binding of the SPT6 C-terminus to the CTD of RPB1 was mapped as well as interaction of the SPT6 core with the stalk (RPB4-7) and SPT5 (Figure 2).

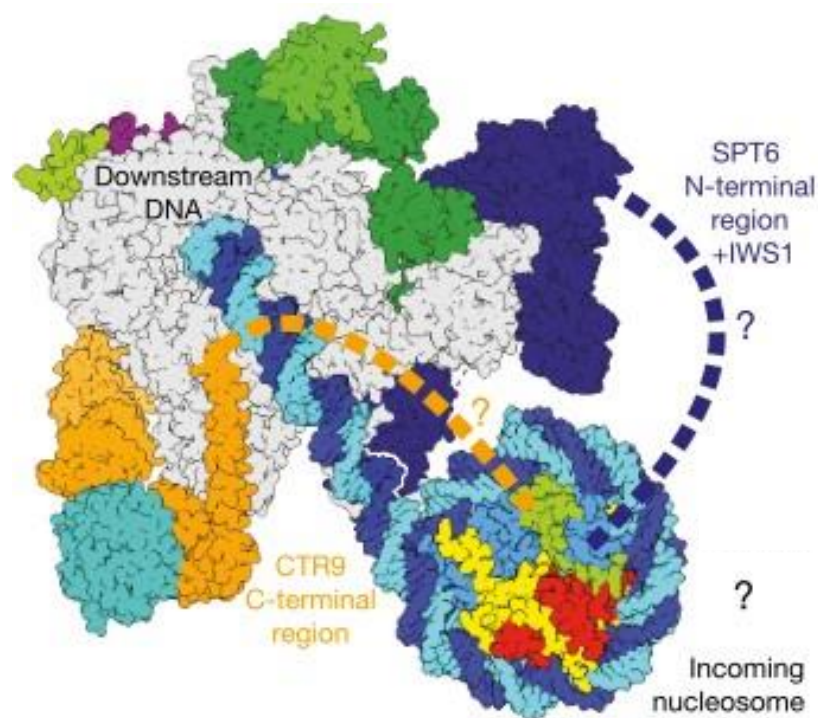


Figure 2 SPT6 is in direct contact with Pol II and SPT5. The SPT6 core (dark blue, upper part) binds to the stalk (RPB4-7, grey) and SPT5 (dark green). SPT6 C-terminus (dark blue, lower part) binds to RPB1 CTD (grey) where the linker emerges from Pol II body. The N-terminus possibly extends to the incoming nucleosome. Figure is taken from Vos et al., 2018

The constrained location between upstream and downstream DNA is consistent with the idea that SPT6 tethers histones while Pol II transcribes through a nucleosome (Vos et al., 2018). In

yeast, SPT6 depleted cells showed biggest defects on transcription in highest transcribed genes (Pathak et al., 2018). In *Arabidopsis* there are two version of SPT6. SPT6 and SPT6like (SPT6l). *SPT6* is barely detectable in contrast to *SPT6l* which is ubiquitously expressed. A T-DNA insertion knockout line for *spt6l* displays undeveloped roots, deformed cotyledons and is unable to develop true leaves. In good agreement with data obtained from other organisms, SPT6l associates with Pol II transcribed genes. Additionally, Pol II occupancy along transcribed genes is reduced in *spt6l*, indicating a similar role in transcription in *Arabidopsis* (Chen et al., 2019a; Gu et al., 2012).

1.6 The FACT complex

FACT (*facilitates chromatin transcription*) was identified as a complex to release Pol II from initiation by bypassing the nucleosome to start productive transcription (Orphanides et al., 1998). FACT is a heterodimer, consisting of two subunits termed SPT16 (*suppressor of Ty 16*) and SSRP1 (*structure-specific recognition protein 1*) (Orphanides et al., 1999). The FACT complex is highly conserved among eukaryotes, but yeast FACT includes POB3 instead of SSRP1 - showing significant sequence similarity but lacking the HMG-box domain. The DNA binding function of the HMG-box domain of SSRP1 (Stros et al., 2007) is mediated by NHP6, a small HMG B-type protein (Brewster et al., 2001). FACT has been implicated in all aspects of chromatin transactions, e.g. replication and repair, preserving histone modifications and in establishing centromeres, however it is best studied for its role in transcription (Formosa, 2012; Formosa and Winston, 2020). While the role in transcript elongation has given FACT its name (Orphanides et al., 1998) and genome-wide enrichment at coding regions of transcribed genes are observed in a temporal distinct manner linked to Pol II (Mayer et al., 2010; Mylonas and Tessarz, 2019; Vinayachandran et al., 2018), there seems to be an additional role for FACT during initiation. Histone occupancy measured by ChIP-Seq in the yeast strain *spt16-197* showed an increase of nucleosome density just upstream of TSS and a depletion of nucleosomes over the gene body (Jeronimo et al., 2019; True et al., 2016). In line, SPT16 occupancy determined by ChIP is found across transcribed genes but also in the TATA box (Pathak et al., 2018). Intriguingly, FACT recruitment to G1 cyclin promoters preceded nucleosome eviction and gene expression (Takahata et al., 2009), indicating an additional role in keeping the TSS nucleosome free (Gurova et al., 2018).

1.6.1 FACT – Architecture

All eukaryotic forms of the SPT16 protein contain three distinct structurally defined domains - N-terminal domain (NTD), dimerization domain (DD) and middle domain (MD) – and a disordered, highly acidic C-terminal domain (CTD, an AID) (**Figure 3a**). SSRP1 is composed of three defined domains termed N-terminal dimerization domain (NTD/DD), MD and HMG-box domain, which is surrounded by charged intrinsically disordered regions (IDD and CTD) (Formosa, 2012; Winkler and Luger, 2011).

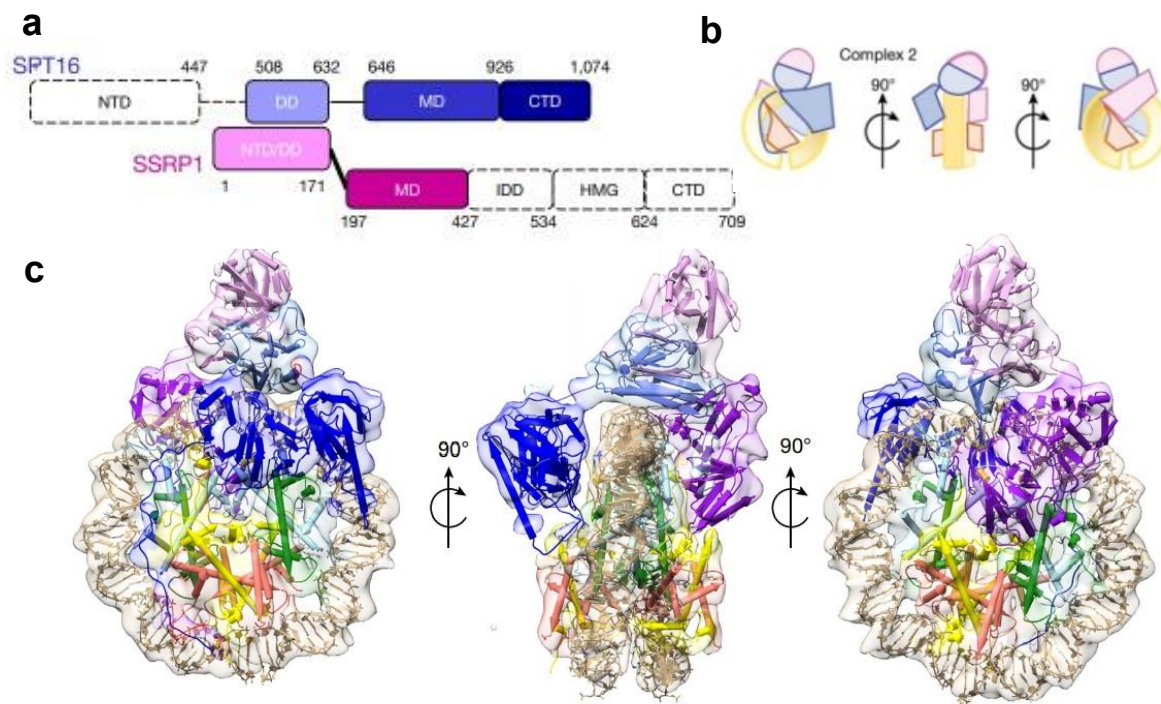


Figure 3 The FACT-complex forms contacts with all histones and the nucleosome dyad (a) SPT16 (blue) is organized in a structured N-terminal domain (NTD), a dimerization domain (DD), middle domain and a disordered highly acidic C-terminal domain (CTD). SSRP1 (magenta) is organized in a structured DD, MD and a HMGbox domain (HMG), surrounded by intrinsically disordered domains (IDD and CTD) **(b)** schematic representation of **(c)** Cryo-EM structure of the FACT complex with H2A-H2B subjected to 79 bp of the 601 sequence and the tetrasome core (H3-H4)₂: SPT16-DD interacts with the dyad, SSRP1-DD stacks on top; MD of SSRP1 and SPT16 make contact with DNA and H3-H4, SPT16-CTD binds to the exposed DNA binding surface of H2A-H2B. SPT16-NTD, SSRP1-IDD/HMG/CTD were not resolved. Figures are taken from Liu et al., 2020

It has been shown that the N-terminal domain (NTD) of SPT16 provides distinct binding pockets for the N-termini of H3 and H4 but not for H2A and H2B (Stuwe et al., 2008). Recent Cryo-EM structures have shed light on how most of the FACT complex assembles on the nucleosome (**Figure 3b, c**) (Liu et al., 2020). As human FACT binds only to nucleosomes with a destabilized H2A–H2B dimer (Tsunaka et al., 2016) a special set-up was used: First the

FACT complex was incubated with H2A-H2B, forming a complex. This complex was mixed with the tetrasomal core (H3-H4)₂, which was wrapped with 79 bp of the 601 sequence, lacking on both sides the DNA bound to by the respective H2A-H2B interface. In this setup (**Figure 3c**) the SPT16 dimerization domain (DD) was sitting on nucleosome dyad (SHL 0) and the SSRP1 dimerization domain stacks on top of the SPT16 dimerization domain. To each side the middle domain (MD) of SPT16 or SSRP1 expands, both binding additional DNA and H3-H4 thereby encasing the tetrasomal core (Liu et al., 2020). The SPT16 CTD, which has been shown to be disordered (Miyagi et al., 2008), binds the exposed, positively charged H2A-H2B DNA-binding surface and this H2A-H2B dimer is docked onto the tetrasome. SSRP1 is not resolved further, however a second H2A-H2B can be accommodated (Liu et al., 2020). The unresolved missing parts of SSRP1 contain an intrinsically disordered region (Miyagi et al., 2008), split first in an acidic part (AID) and then a basic intrinsic disordered part (BID) (Tsunaka et al., 2009). The acidic part extends from the MD, potentially facing the remaining H2A-H2B dimer (Mayanagi et al., 2019), while the basic part is followed by the DNA binding HMG-box motif. The HMGbox motif preferentially binds to bent and cruciform DNA (Gurova et al., 2018). *In vitro* studies have narrowed this DNA interaction and shown the HMGbox preferentially binds best when linker DNA is present (Winkler et al., 2011). The NTD of SSRP1 (absent in plants) has been shown to bind alternative DNA structures as well, however here the preference lies on Z-DNA (Safina et al., 2017).

In Summary, the FACT complex covers the entire nucleosome (Zhou et al., 2020). From the H2A-H2B DNA binding sites on one side bound by the acidic C-terminal domain of SPT16 (Liu et al., 2020; Mayanagi et al., 2019), to the most distal linker DNA bound by the HMGbox of SSRP1 (Winkler et al., 2011).

1.6.2 FACT – Mode of Action

FACT binds to the intact nucleosome with DNA wrapped around poorly. Hence, some removal of DNA is required for FACT to enter (Tsunaka et al., 2016). During processive transcription the progression of Pol II has been shown to be sufficient to peel of the DNA from a nucleosome (Farnung et al., 2018; Kujirai et al., 2018) and even more efficient in the presence of TEFs (Ehara et al., 2019). The exposed H2A-H2B DNA surface is used by SPT16 AID to invade and tether H2A-H2B. Further binding of SPT16 MD leads to steric clashes and removal of the H2A-H2B dimer and hexasome formation (Liu et al., 2020; Mayanagi et al., 2019). In line with a peeling of model during transcription and subsequent invasion by SPT16 AID, it has been shown in yeast that FACT is recruited to chromatin *in vivo* as a consequence of transcription

by RNA Polymerase I-III (Martin et al., 2018). Interestingly, SPT16 has been shown to invade and remove the more proximal H2A-H2B dimer and SSRP1 the more distal H2A-H2B dimer (Ramachandran et al., 2017). This puts an orientation on the FACT-complex with SPT16 sitting on the nucleosome dyad facing the DNA entry tunnel of Pol II, invading the nucleosome upon DNA-peeling (Farnung et al., 2021; Liu et al., 2020). An important role for SPT16-AID binding seems to lie in its phosphorylation level. It was shown that a phosphorylated truncated form of SPT16 containing only MD-AID binds to a nucleosome with only 112bp of DNA wrapped around (leaving the DNA binding interface of one H2A-H2B free). However, the unphosphorylated form did not (Mayanagi et al., 2019). Additional NMR studies have shown that the H3 N-termini gain more flexibility upon invasion by the phosphorylated SPT16 AID (Tsunaka et al., 2020). The SSRP1 HMGbox has also been shown to be important in tethering the nucleosome to DNA: By the use of single molecule magnetic tweezers it was determined that the SSRP1 HMGbox is responsible for keeping the nucleosome integrity even when the DNA wraps are removed of the nucleosome. In consequence, removal of the HMGbox led to a loss of the FACT- bound nucleosome from the DNA (Chen et al., 2018).

In summary: The domains of FACT invade and destabilize the nucleosome and tether the components (Wang et al., 2018) while at the same time enhancing the accessibility for DNA (Formosa and Winston, 2020) and H3- N-termini (Tsunaka et al., 2020).

1.6.3 FACT in *Arabidopsis thaliana*

In *Arabidopsis thaliana* the FACT complex was first described in 2004 (Duroux et al., 2004) and since then a number of useful T-DNA insertion lines have been identified. The complete loss of either SSRP1 (*ssrp1-1*) or SPT16 (*spt16-3*) is critical for plant viability (Frost et al., 2018; Lolas et al., 2010). T-DNA insertion lines which show reduced levels of *SSRP1* (*ssrp1-2*) or *SPT16* (*spt16-1* and *spt16-2*) display early flowering, severe defects in flower- and leaf-architecture, an impaired seed production and an increased number of leaves and inflorescences, thereby appearing more bushy (Lolas et al., 2010). FACT is rather conserved, with *Arabidopsis* SPT16 and SSRP1 being 120.6 and 71.6 kDa big, compared to human FACT with 119.9, 81.1 kDa, sharing 34.7% and 35.8% amino acid identity (Duroux et al., 2004). The overall architecture is very similar, however SSRP1 is lacking the CTD (compare **Figure 3a**). Transcript profiling of *Arabidopsis ssrp1-2* and *spt16-1* seedlings showed that only a small subset of genes is differentially expressed (Pfab et al., 2018a), in line with studies in yeast (Pathak et al., 2018). Genes linked to phenotypes which need temporal and spatial distinct expression seem to be more deregulated in the knockdown mutants, e.g. early bolting in

consequence to downregulation of the floral repressor *FLC* (Lolas et al., 2010) or reduced anthocyanin production linked to reduced expression of anthocyanin biosynthesis genes during stress response (Pfab et al., 2018a). A prior PhD thesis has shown that the knockdown mutants *spt16-1* and *ssrp1-2* show reduced seed dormancy, in line with reduced *Delay of Germination 1 (DOG1)* expression (Mortensen, 2012). This indicates that also the second major transition in a plant life could be particularly affected by FACT: The transition from seed dormancy to germination.

1.7 Aims of the thesis

1.7.1 Determination of the Transcript Elongation Histone Chaperone Complex

A diverse group of transcript elongation factors is required for efficient mRNA synthesis. The family of histone chaperones is particularly important in removing, stabilising, and repositioning of the incoming nucleosome along elongating Pol II. Here, affinity purification coupled to mass spectrometry (AP-MS) in the *Arabidopsis* cell culture system transformed with GS-tagged proteins (Van Leene et al., 2008) will be used. This *in vivo* system has the potential to validate and extend studies from other organisms and highlight their relevance in the plant kingdom in the model organism *Arabidopsis thaliana*. Especially the side-by-side comparison will reveal similarities and differences in the targeted histone chaperones SSRP1, SPT16, SPT6l and ELF1.

1.7.2 Generation of Mutant lines

For the rather well studied FACT complex set of T-DNA insertion lines exist (Section 1.6.3). ELF1 has not been studied in plants and consequently no T-DNA insertion lines have been established in *Arabidopsis*. Here, a knockout mutant will be created with the means of the CRISPR/Cas9-system, (Wang et al., 2015; Xing et al., 2014) which can be used further to test for synergistic effects in other TEF depletion mutants.

Likewise, a set of mutant lines will be created for SPT6l to bypass the originally described embryo lethality of the *spt6l-1/2/3* T-DNA knockout lines (Chen et al., 2019a; Gu et al., 2012), employing a β -estradiol inducible RNAi system (Brand et al., 2006; Dürr, 2013). In these T-DNA insertion lines the respective inserts are located approximately in the middle leaving a substantial part of the gene intact, including the nuclear localisation sequence (NLS). The respective transcripts have been characterized with *in situ* hybridization in the 3' part of the

gene (Gu et al., 2012). As the inserts of T-DNA insertion lines contain e.g. resistance markers including regulatory elements (Ülker et al., 2008) this does not exclude the formation of aberrant or truncated *SPT6l* transcripts. Hence, a CRISPR mediated knockout approach will be designed to obtain a clean *spt6l* knockout line in the very first exons of the coding sequence.

1.7.3 ELF1 as a histone chaperone

The obtained Mass-spec dataset together with the *Arabidopsis* knockout mutant will give a starting point to evaluate and place ELF1 into context in *Arabidopsis thaliana*. Biochemic interaction studies of the basic N-terminal part and DNA and the C-terminal part and histones will complement *in vivo* studies to evaluate the role of ELF1 as a putative histone chaperone, like proposed before (Ehara et al., 2019).

1.7.4 Impact of PTMs on the FACT complex

A research visit to the Proteomics Department at the University of Southern Denmark in my master's thesis (Holzinger, 2015) led to the creation of a dataset, where transgenic *Arabidopsis* cell suspension culture (GS-tagged SSRP1, SPT16 or empty GS) was affinity purified and subsequently analysed via LC-MS/MS in a label free quantitative way. Next to the interactome, PTMs like acetylation and phosphorylation were included in the analysis. Indeed, in SPT16 phosphorylations were detected in the histone binding acidic region. In SSRP1, acetylations were found in the basic disordered region next to the HMGbox and in the HMGbox itself. In respect to charge this seemed intriguing. For SPT16, the already negatively charge H2A-H2B histone binding patch becomes even more negative. For SSRP1, positive charges in the DNA binding elements of SSRP1 get neutralized. Both, phosphorylations and acetylations are reversible and are therefore suitable to transiently modulate binding affinity. With the complex array of binding events upon nucleosome unwrapping and the subsequent release after Pol II progression a way to modulate histone and DNA binding contacts could be required for FACT.

This led to the formulation of two hypotheses which will be analysed further in this PhD thesis: On the one hand, phosphorylation might have an impact in regulating SPT16; Making the AID more negative could lead to an increase in histone binding affinity. On the other hand, acetylation of the SSRP1 HMGbox might alter DNA binding affinity. Taking away positive charge could lead to a decrease in DNA binding affinity.

Additionally, the respective-writers and -erasers are of the modifications are of interest. A starting point will be the obtained interactome from the LC-MS/MS analysis, which will be evaluated by the means of FRET and Y2H. Further, the interaction of the truncated domains

with DNA or histones will be studied *in vitro* via biochemical assays like EMSAs or GST-pulldown experiments. To obtain a more complete picture *in vivo*, immunoprecipitation of modified FACT versions could tell differences in the efficiency of nucleosome binding. This will be studied with the *Arabidopsis* cell culture system together with subsequent analysis of the immuno-precipitates by western blot.

Finally, phenotypic analysis of the FACT knockdown/knockout mutants *spt16-1/ssrp1-1* will help to elucidate the effect of the respective modification. Hereby, the mutants will be rescued with different transgenes, mimicking the presence of the PTM, the absence or the wildtype (WT) state. Interesting candidates will be analysed by H3 ChIP-seq to understand the molecular consequences genome wide.

1.7.5 The HMGbox of SSRP1

FACT is best studied in yeast, however there is one major difference. Yeast FACT outsources the DNA binding of its HMGbox to a third protein, NHP6. However, SPT16, POB3 and NHP6 do not form a stable complex (Formosa et al., 2001). Yeast lacking NHP6 are severely affected, however still viable (Stillman, 2010). Here, the role of the HMGbox in *Arabidopsis thaliana* was studied by a former colleague Alexander Pfab. Among other essays, he successfully rescued the *ssrp1-1* knockout line with full or truncated *SSRP1* versions lacking the *HMGbox*. Here, final evaluation of the respective lines considering phenotypic details and the *SSRP1* protein level were performed.

1.7.6 An effect of SSRP1 on seed dormancy

To confirm the initial observation of reduced seed dormancy in FACT mutants (Mortensen, 2012), germination rates of the FACT-knockdown mutant *ssrp1-2* next to controls will be measured. *ssrp1-2* lines will be transformed with an additional copy of *DOG1*, to restore wildtype *DOG1* levels. Measured germination rates will be cross correlated with *DOG1* levels via quantitative reverse transcribed PCR (qRT-PCR).

2 Results

2.1 The Transcript Elongation Histone Chaperone Complex

To identify proteins that co-purify with transcription associated histone chaperones, bait proteins fused to a GS tag (2 protein G domains and a streptavidin binding peptide, **Figure 5a**, Van Leene et al., 2008) were expressed in *Arabidopsis* PSB-D suspension culture cells, upscaled and harvested (**Figure 4a**). One step Protein G affinity purification was conducted with 15 g of cell culture using magnetic beads coupled to IgG (**Figure 4b**). This included a benzonase endonuclease digest to reduce purely RNA- or DNA-mediated interactions. Subsequently, proteins were separated and fractionated via SDS-page, digested with trypsin, and analysed via shotgun proteomics (Zhang et al., 2013) (**Figure 4c**).

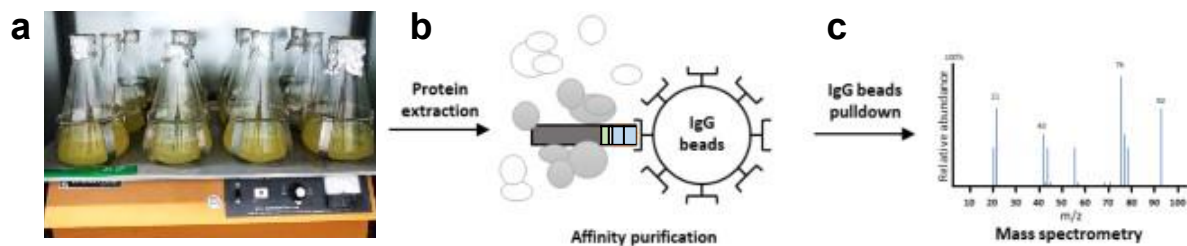


Figure 4 From upscaled transgenic cell culture to data acquisition. (a) Transgenic PSB-D cells are upscaled to yield sufficient amount of starting material (b) Bait proteins are purified together with their putative interactors from the whole protein extract using IgG coupled magnetic beads (c) Co-purified proteins are further processed and eventually identified by mass spectrometry. PSB-D: *Arabidopsis Landsberg erecta* cell culture; IgG: Immunoglobulin G. Panels (b) and (c) are modified from (Antosz, 2019)

2.1.1 Experimental Setup and Affinity Purification

Due to their prior association with the TEC in yeast (Krogan et al., 2002), and their similar structural properties - all containing AIDs (Ehara et al., 2019) - a set of SPT16, SSRP1, ELF1 and SPT61 was selected (**Figure 5a**). Additionally, to extract a list of unspecific interactors an empty GS-tag was treated accordingly. For SPT16-GS and SSRP1-GS, frozen cell culture material was available provided by Alexander Pfab. The missing ELF1-GS and SPT61-GS were expressed in PSB-D suspension cultured cells and upscaled to ~10 L. All constructs were under control of the 35s promoter and terminator (**Figure 5a**) and the respective AID was next to the GS-tag.

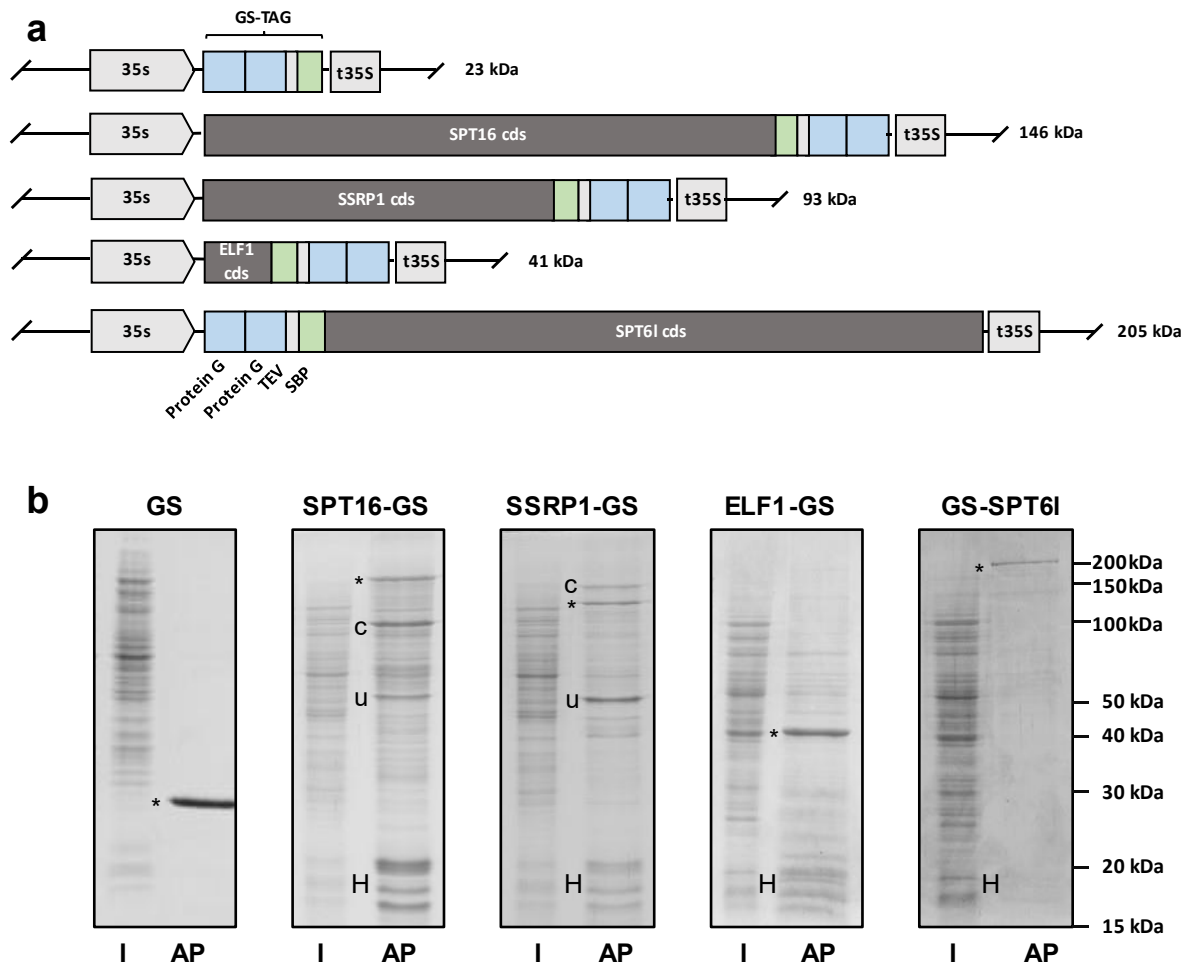


Figure 5 Affinity purification of transcription associated histone chaperones (a) Schematic illustration of different bait proteins fused to a GS tag under control of the 35s promoter and terminator (bait in dark grey, streptavidin-binding protein in green; TEV cleavage site in light grey; Protein G domains in light blue) (b) Total protein extracts (Input, 0.01 % of total) of transgenic cells expressing the bait proteins next to the eluates (1/3 of total) of the one-step affinity purifications (AP) using IgG coupled magnetic beads. The proteins were separated by 18 % SDS-PAGE and the gels were stained with Coomassie Blue. Asterisks indicate the bands corresponding to the bait proteins fused to the GS-tag. In case of the FACT subunits c indicates the other complex partner of the heterodimer (Holzinger 2015). Bands marked with H putatively correspond to histones, u was analysed further by LC-MS/MS analysis.

After one step affinity purification (AP) and subsequent analysis by SDS-PAGE electrophoreses and coomassie brilliant blue (CBB) staining the expected migration positions of all baits can be assigned to a prominent band (**Figure 5b**; asterisks, AP lane). Although an overexpression system was used, no prominent band in the expected migration position can be determined in the input lanes (**Figure 5b**; I). This indicates no massive overexpression of the bait and hence a good likelihood for native complex formation. In the empty GS-control AP (**Figure 5b**, first panel) no other (prominent) bands appear. In the SPT16-GS and SSRP1-GS

AP (**Figure 5b**, panel 2 and 3) several prominent bands can be distinguished. The upper two bands mark the FACT complex. The identity of the respective FACT complex partner has been confirmed by western blot analysis before (Holzinger, 2015) and is not shown here. The height of these bands varies from the SPT16-GS to the SSRP1-GS lane (**Figure 5b**, panel 2 and 3, * and c). This can be explained by reciprocal tagging of the subunits. The GS-tag with its size of 23 kDa widens the gap in the migration patterns when SPT16 is tagged and narrows it when SSRP1 is tagged. From top to bottom a third prominent band can be found in the FACT APs (**Figure 5b**, panel 2 and 3, u). The single band was cut out from the gel (SPT16-GS), trypsin digested and analysed by LC-MS/MS (Supplementary Data Table 1). This screen identified RecA, a chloroplastic protein, containing large patches of charged amino acids. Hence, it was considered an unspecific interaction which probably arises when cellular compartments get lysed during purification.

A cluster of proteins can be seen in the range from 15-20 kDa, which could be different histone variants, in line with FACTs role as a histone chaperone (**Figure 5b**, panel 2 and 3, h). Interestingly the same patterning can be observed in the ELF1-GS AP (**Figure 5b**, panel 4, h), making up for most of the prominent bands next to the bait. In GS-SPT6l the overall signal intensity was weaker (**Figure 5b**, panel 5). However also here, quite faintly, at least two bands can be detected in the range from 15-20 kDa. Next, a more detailed look at the underlying interactome will follow by comparing the lists of the complex partners derived by shotgun proteomic analysis.

2.1.2 Data analysis – Generals and Considerations

The here collected datasets of SSRP1-GS and SPT16-GS were published in (Antosz et al., 2017). Minor differences in the obtained lists for SSRP1 and SPT16 are due to different filtering (**Figure 6**): A newer, more extensive empty GS-List was created (Supplementary Data Table 2), the list of common copurifying proteins presented in (Van Leene et al., 2015) has been used less stringently to retain some of the histones on the list (>9 groups, Supplementary Data Table 3). Additionally, a further filtering step has been implemented, keeping nuclear and subcellular unassigned proteins only (based on TAIR10, Supplementary Data Table 4). After all filtering steps (**Figure 6**) a final number of 99 proteins remain for SPT16-, 53 in SSRP1-, 317 in ELF1- and 263 in SPT6l-datasets in 2 out of 3 replicates (Supplementary Data Table 6-9.) The different number in acquired hits can be explained by cutting the gel into more pieces for ELF1, SPT6l and empty GS, which leads to more analysis time in the mass spectrometer and more

hits accordingly. However, sample input and the respective sample complexity were comparable (**Figure 5b**).

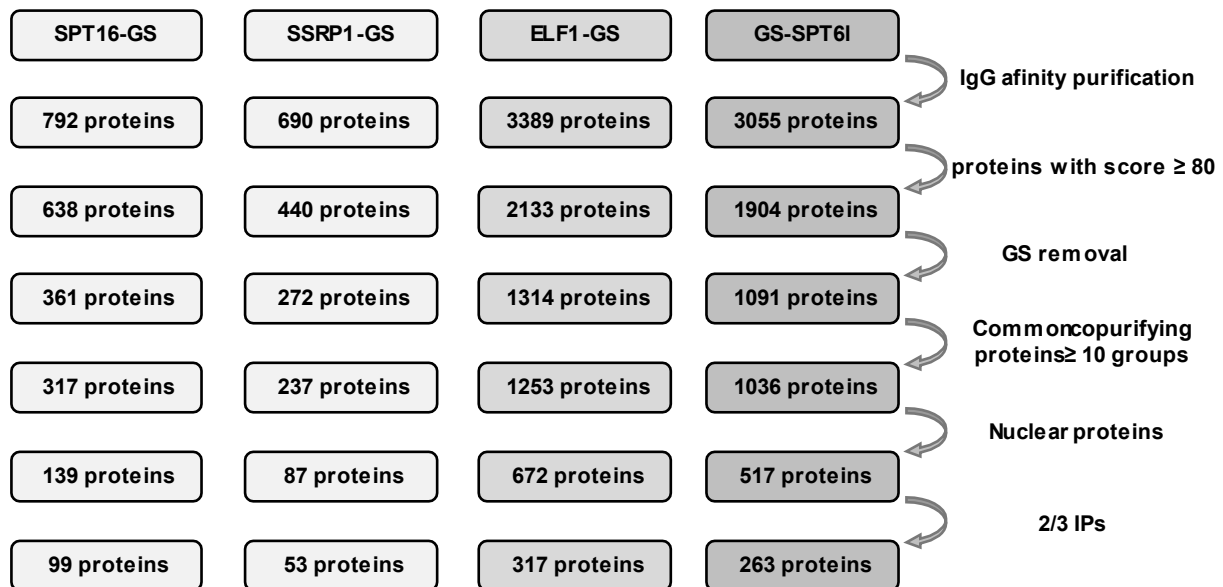


Figure 6 Schematic illustration of the Data analysis workflow following mass spectrometry. The list of common copurifying proteins is taken from (Van Leene et al., 2015). Please Note: The datasets for SPT16 and SSRP1 were raised at a different timepoint as ELF1, SPT6l and the empty GS negative control. Sample input were comparable, however the preparation differed in the number of gel pieces cut out from the gel, leading to less analysis time in the mass spectrometer and subsequent lower number of detected hits for SPT16 and SSRP1

Two final considerations before comparing the datasets: The principal behind the Mascot score is, to sum the score for the individual peptides and thereby create an overall score for the protein (Koenig et al., 2008). This can introduce biases. Bigger proteins will usually be digested into more, suitable peptides (~ 7- 30 aa), leading to an overall higher mascot score. Smaller proteins will lead to very little suitable peptides, in the worst case there is not a single peptide which can be ionized during electro spray ionization and thereby assigned to a protein (although present in huge amounts). Additionally, there are further criteria like charge or a certain amino acid composition which are prone to be reactive during sample preparation, like e.g. aspartic acid (Koenig et al., 2008). While a high score does not happen accidentally, a lower score must not translate into lower abundance in e.g. a small protein. Two examples: ELF1 (13.9 kDa) displays a prominent band in the CBB stain (**Figure 5b**), can be theoretically digested in 2-3 good peptides (determined with the online tool PeptideCutter (EXPASY); Wilkins et al., 1999). In line an average of only 8 different peptides were found (this includes varieties of the same peptide due to missed trypsin cutting sites and amino acid oxidations), which translates into an average mascot score of 791 (Supplementary Data Table 8). With SPT6l (184,9 kDa) as bait, an average

of 136 peptides were found, leading to a score of 12026 (Supplementary Data Table 9). Similarly, H2B (AT5G22880) produces more suitable peptides than H2A (AT3G20670), which is reflected in the number of peptides identified (an average of 5 vs. an average of 16, Supplementary Data Table 8). Nonetheless, assuming similar complexity of the sample, similar abundance should lead to a similar score concerning the same protein. Each round the most intense peptide ions are picked in MS1 (data dependent acquisition). Hence, additional analysis time is hereby more crucial for detecting additional low abundant interactors. A big challenge in proteomics is to properly assign peptides to proteins (Zhang et al., 2013). Ideally, one finds unique peptides to assign to proteins. However, in plants there are many copies of histones, e.g. there are 13 genes coding for H2A variants with a great deal of sequence identity (Lei and Berger, 2020). Due to a huge sequence overlap, most of the peptides detected can be assigned to more than one histone variant. To avoid unnecessary assumptions, these so-called razor peptides are assigned to a prior found unique peptide. One example, in case of the ELF1-GS AP (Supplementary Data Table 8): In each of the three replicates, a H2B variant has the 3rd highest mascot score (H2B.10, -4 and -8). This is a notable hit, for such a small protein (138-145 aa; 15.1 – 15.7 kDa). It is unlikely, that each immuno-precipitate contains only the one selected variant but a mixture of variants which are then assigned to one variant (due to one unique peptide). Because unnecessary assumptions are avoided in MASCOT, filtering hits into being present in 2 out of 3 APs here would deplete the list of high interacting histones. Hence, the comparisons shown in the following chapter (**Table 1-4**) include hits when present in only one AP (**Figure 6**, second to last row).

2.1.3 Association with the Transcript Elongation Complex

Overall, the AP-MS datasets of SPT16, SSRP1, ELF1 and SPT6l reflect the ascribed architecture determined in other studies by cryogenic electron microscopy (cryo-EM; Ehara et al., 2019; Vos et al., 2020). In the following, notable hits for each factor will be highlighted and put into perspective in the published landscape (Section 2.1.3.1 – 2.1.3.3) with a focus on their associations with Pol II (Section 2.1.3.4), histones (2.1.3.5) and their common interactor CK2 (2.1.3.6).

2.1.3.1 FACT

For the FACT complex subunits SSRP1 and SPT16 the respective bait protein had the highest score. The respective other subunit ranks second (**Table 1**). This is in agreement with prominent bands in the CBB stain (**Figure 5b**; *, c). Similar to reciprocal AP-MS assays in yeast (Bedard et al., 2016; Krogan et al., 2002) all 6 subunits of the PAF-Complex can be found in SPT16

(**Table 1**). RTF1 (VIP5 in *Arabidopsis*), which shows labile association with the PAF-complex in organisms other than *S. cerevisiae* and has been shown to sit at the DNA exit tunnel (Vos et al., 2020), is present with high score in both FACT AP-MS datasets, ranking 5th in SSRP1 and 12th in SPT16. It has been proposed before that the “Histone Chaperones Spt6 and FACT Collaborate to Assemble, Inspect, and Maintain Chromatin Structure” (McCullough et al., 2015). In the SPT16-GS dataset SPT6l ranks 17 with a score of 823; and 26 in the SSRP1-GS dataset with a score of 321. Vice versa in the GS-SPT6l dataset SPT16 and SSRP1 rank 3 and 7 (**Table 1**).

2.1.3.2 SPT6l

Similar to FACT, the SPT6l bait had the highest score (**Table 1**). In the cryo-EM structure, SPT6 displayed a direct interaction interface with SPT5 (Vos et al., 2020), reflected here in rank 5 (**Table 1**). In contrast to FACT, RTF1/VIP5 is present in only 1 out of 3 APs with a low score (**Table 1**) In human, RNA extension assays have shown, that stimulation of Pol II by RTF1 is independent from SPT6 (Vos et al., 2020). This potentially indicates that labile association of RTF1 might also occur in *Arabidopsis*. Further IWS1 (interacts with SPT6) was also found with a score ~ 3x as high as in the empty GS-list (141, Supplementary Data Table 2).

Table 1 TEFs co-purifying with transcription associated histone chaperones. \emptyset = no rank assigned; factor is present in the empty GS-list

SPT16		SSRP1		ELF1		SPT6l		Interactor	AGI	Complex
Rank	Score/#IPs	Rank	Score/#IPs	Rank	Score/#IPs	Rank	Score/#IPs			
1	4205/3	2	2885/3	6	1356/3	3	2390/3	SPT16	AT4G10710	FACT
2	2657/3	1	3152/3	17	816/3	7	1376/3	SSRP1	AT3G28730	FACT
				20	791/3			ELF1	AT5G46030	ELF1
17	823/3	26	321/3	10	1040/2	1	12026/3	SPT6l	AT1G65440	SPT6
19	758/3	43	180/3	8	1133/3	5	1578/3	SPT5-2	AT4G08350	DSIF
				468	117/1	58	325/2	SPT4-2	AT5G63670	DSIF
38	389/2	33	232/2	185	231/3	103	239/2	PAF1, ELF7	AT1G79730	PAF-C
70	203/2			92	333/3	39	382/3	CDC73	AT3G22590	PAF-C
29	464/3	34	222/3					CTR9, ELF8	AT2G06210	PAF-C
15	859/3	20	422/3	86	344/3	107	236/3	LEO1, VIP4	AT5G61150	PAF-C
12	968/3	5	1068/2	130	277/3	360	110/1	RTF1, VIP5	AT1G61040	PAF-C
\emptyset	1274/3	\emptyset	542/3	\emptyset	317/3	\emptyset	311/3	WDR61, VIP3	AT4G29830	PAF-C
				594	95/1	482	88/1	TFIIS	AT2G38560	TFIIS
\emptyset	130/2	\emptyset	82/1	\emptyset	360/3	\emptyset	537/3	IWS1	AT1G32130	IWS1

2.1.3.3 ELF1

ELF1 as bait ranked in 20th place (**Table 1**) and is therefore probably underrepresented due to its small size and high portion of charged aa and the resulting low number of peptides suitable for electro spray ionisation (Section 2.1.2). This contrasts the CBB stain where ELF1 can be seen as the most prominent band (**Figure 5b**). In the Cryo-EM structure ELF1 directly interacts with SPT5 (Ehara et al., 2017), which is displayed in rank 8 (**Table 1**). Surprisingly, SPT16 has an even higher score than the direct interactor SPT5, potentially indicating potential interplay of transcription associated histone chaperones. In line with this SPT6l ranked 10 and SSRP1 ranked 17. The PAF-complex, another component of the core transcript elongation complex is present albeit with lower scores, compared to the datasets of the FACT subunits (**Table 1**). In reciprocal assays, ELF1 was not detected. Overall untagged ELF1 could not be found in any other AP-MS shown in this thesis and in the other TEF datasets from our group (Antosz et al., 2017).

2.1.3.4 Orientation of histone Chaperones on Pol II

ELF1 has been shown to close the DNA entry tunnel formed by RPB1 and RPB2 (Ehara et al., 2017). This is displayed in the respective dataset with the ranks 1 and 2 (**Table 2**). SPT6 bound directly to the CTD of RBP1 with its C-terminus (Vos et al., 2018), which is reflected in the highest rank after the bait for NRPB1. Direct interactions determined by Cryo-EM are further reflected by the interaction of SPT6 with the Pol II stalk (NRPB7, rank 48).

Table 2 Subunits of Pol II co-purifying with transcription associated histone chaperones. \emptyset = no rank assigned; factor is present in the empty GS-list

SPT16		SSRP1		ELF1		SPT6l		Interactor	AGI	Complex
Rank	Score/#IPs	Rank	Score/#IPs	Rank	Score/#IPs	Rank	Score/#IPs			
11	986/3	6	1040/2	2	2598/3	2	2581/3	NRPB1	AT4G35800	Pol II
21	705/3	8	809/3	1	2617/3	4	2079/3	NRPB2	AT4G21710	Pol II
\emptyset	518/2	\emptyset	507/3	\emptyset	1296/3	\emptyset	1053/3	NRPB3	AT2G15430	Pol II, IV, V
						406	101/1	NRPB4	AT5G09920	Pol II
				469	117/1	390	104/1	NRPB6	AT5G51940	Pol II, III, IV, V
137	85/1			89	340/2	48	351/3	NRPB7	AT5G59180	Pol II
				259	181/2	101	240/2	NRPB8	AT3G59600	Pol II
				637	88/1	267	138/2	NRPB9	AT4G16265	Pol II, IV, V
103	128/2	51	157/1	408	133/2	160	188/3	NRPB11	AT3G52090	Pol II, IV, V

Recent cryo-EM structures have shown that SPT16 sits at the nucleosome dyad with SSRP1 on top (Liu et al., 2020). SPT16 has been shown to affect the proximal H2A-H2B (in respect to Pol II) and SSRP1 the distal H2A-H2B (Ramachandran et al., 2017) This orientation has been

confirmed by a recent cryo-EM structure containing nucleosome bound FACT and Pol II (Farnung et al., 2021). The nucleosome dyad enters the TEC facing the RPB1 clamp head and the RPB2 lobe (Farnung et al., 2018). In line NRPB1 and NRPB2 can be found with similar high scores in both SSRP1 and SPT16 AP-MS datasets (**Table 2**), while other subunits of Pol II are barely detected. This can also explain the high score obtained for SPT16 in the ELF1 dataset (**Table 1**), as ELF1 is sitting on the DNA entry tunnel facing the incoming nucleosome (Ehara et al., 2019) and hence SPT16.

2.1.3.5 Histones

In agreement with FACT's and SPT6's role as a histone chaperone, numerous, high ranking interactions with histones are detected (**Table 3**). For ELF1 it was proposed that the acidic region of ELF1 could bind to histones (Ehara et al., 2019) and indeed very high scores were obtained for H2Bs (**Table 3**, rank 3-5) together with hits for members of H2A, H3, H4. This supports the hypothesis that the incoming nucleosome could be bound by the C-terminal AID of ELF1 (Ehara et al., 2019).

Table 3 Histones co-purifying with transcription associated histone chaperones. \emptyset = no rank assigned; factor is present in the empty GS-list

SPT16		SSRP1		ELF1		SPT6I		Interactor	AGI	Family
Rank	Score/#IPs	Rank	Score/#IPs	Rank	Score/#IPs	Rank	Score/#IPs			
5	1423/1							H2B.11	AT5G59910	H2B
6	1344/2	3	1180/2					H2B.7	AT3G46030	H2B
4	1433/2	4	1159/1	3	1599/1	6	1512/1	H2B.10	AT5G22880	H2B
						9	1087/1	H2B.9	AT5G02570	H2B
				4	1592/1	10	957/1	H2B.4	AT2G37470	H2B
8	1188/2	11	675/1	5	1485/1	8	1253/2	H2B.8	AT3G53650	H2B
32	442/3	42	185/3	61	395/2	115	222/2	H2A.2	AT3G20670	H2A
72	193/3	49	162/2	53	425/2	138	198/3	H2A.7	AT5G59870	H2A.W
88	154/3	62	135/3	103	323/2	206	157/3	H2A.5	AT5G27670	H2A.W
51	304/1	23	376/1					H2A5	AT1G08880	H2A.X
68	207/3	56	152/3	269	177/2	158	188/3	H2A.9	AT1G52740	H2A.Z
80	168/1	66	126/2					H3	AT1G09200	H3
\emptyset	666/3	\emptyset	307/3	\emptyset	486/2	\emptyset	479/3	H4	AT1G07660	H4
28	488/3							H1.2	AT2G30620	H1
39	388/2							H1.1	AT1G06760	H1

While all factors show strong association with histones, the FACT complex displays a greater variety of detected variants. Although analysis time was decreased compared to ELF1-GS and GS-SPT6I (Section 2.1.2), both SPT16-GS and SSRP1-GS showed H2A.X (**Table 3**), a marker for DNA damage (Lei and Berger, 2020). This is in line with FACT's association with not only

transcription but also DNA-damage repair (Formosa, 2012) and the exchange of H2A.X by FACT in human cell culture (Heo et al., 2008). Another distinct feature of the FACT complex is the presence of linker histone H1 (**Table 3**), in contrast to ELF1 and SPT6l. Indeed, it has been found that FACT interacts with H1 and SSRP1 potentially evicts H1 in *X. laevis* and human (Falbo et al., 2020; Kalashnikova et al., 2013).

2.1.3.5 Association with CK2

Another shared feature of the histone chaperones SPT6, SSRP1, SPT16 and ELF1 is its association with the Casein Kinase 2 complex (CK2) in literature (Bedard et al., 2016; Gouot et al., 2018; Keller and Lu, 2002; Krohn et al., 2003; Mayanagi et al., 2019; Tsunaka et al., 2009). CK2 is a heterodimeric complex, consisting of CKA and CKB, with CKA being the catalytically active subunit. The CK2 consensus sequence is S/T-x(-x)-E/D/pS (Meggio and Pinna, 2003). In *Arabidopsis* ELF1, SPT6l, SPT16 and SSRP1 all show an AID rich in E, D and S. In *Arabidopsis* each CK2 subunit has 4 different variants (CKA1-4, CKB1-4). In agreement with data from other organisms, the CK2 complex was present in each dataset (**Table 4**). The role of CK2 for FACT was further shown in a second independent dataset (**Supplementary Table 1**, (Holzinger, 2015)). Strikingly, although direct interaction of FACT with CK2 was shown in human (Keller and Lu, 2002), here ELF1-GS shows strongest association with CK2 complex, with CKA-variants ranking three times in the top 20 (of 627 proteins). This is in line with prior direct interaction in GST-pulldown assays in yeast with both CK α and CK β (Kubinski et al., 2006).

Table 4 Subunits of CK2 co-purifying with transcription associated histone chaperones

SPT16		SSRP1		ELF1		SPT6l		Interactor	AGI	Complex
Rank	Score/#IPs	Rank	Score/#IPs	Rank	Score/#IPs	Rank	Score/#IPs			
		86	82/1	15	892/3	41	381/2	CKA1	AT5G67380	CK2
41	368/2			11	1009/3	28	486/3	CKA2	AT3G50000	CK2
				41	483/3	80	271/3	CKA3	AT2G23080	CK2
96	145/2			9	1065/3	20	586/3	CKA4	AT2G23070	CK2
81	168/1	47	163/2	90	336/3			CKB1	AT5G47080	CK2
				371	142/2			CKB2	AT4G17640	CK2
111	110/2	76	109/1	176	236/3	213	152/1	CKB3	AT3G60250	CK2
						322	121/1	CKB4	AT2G44680	CK2

2.1.4 Summary

The transcription associated histone chaperones in *Arabidopsis*, integrate nicely into the framework obtained from other organisms. Differences in rank and score might reflect different

interaction interfaces with core transcript elongation factors (**Table 1**) and Pol II (**Table 2**), e.g. RTF1/VIP5 and FACT. All of them interacted with histones (**Table 3**): The established histone chaperones FACT and SPT6L, as well as the putative histone chaperone ELF1. The here tagged variants associated with each other (**Table 1**): As all of them locate at the DNA entry site, or show flexible domains potentially protruding to the DNA entry site (Ehara et al., 2019; Liu et al., 2020; Vos et al., 2018) they could collaborate to tether and hand over the unwrapping nucleosome during transcription. Additionally, all showed association with CK2, strongest in ELF1, indicating a general role for CK2 in transcription in *Arabidopsis thaliana*.

2.2 Mutant lines for ELF1 and SPT6L

There is a good set of T-DNA insertion mutants available for FACT, including knockdowns and knockouts for both SSRP1 and SPT16. However, no T-DNA insertion lines have been established for ELF1. To study the effects of ELF1 knockout, a plasmid was created employing the CRISPR-Cas9 endonuclease system under the control of the egg cell-specific (EC1) promoter (Wang et al., 2015), to make use of the error prone double strand break (DSB) repair mechanism (**Figure 7a**). A single guide in the beginning of the CDS (**Figure 7b**) was selected with the help of the tool CRISPR-P 2.0 (Liu et al., 2017) and inserted via annealed oligo cloning in the pHEE401 vector system (Wang et al., 2015; Xing et al., 2014).

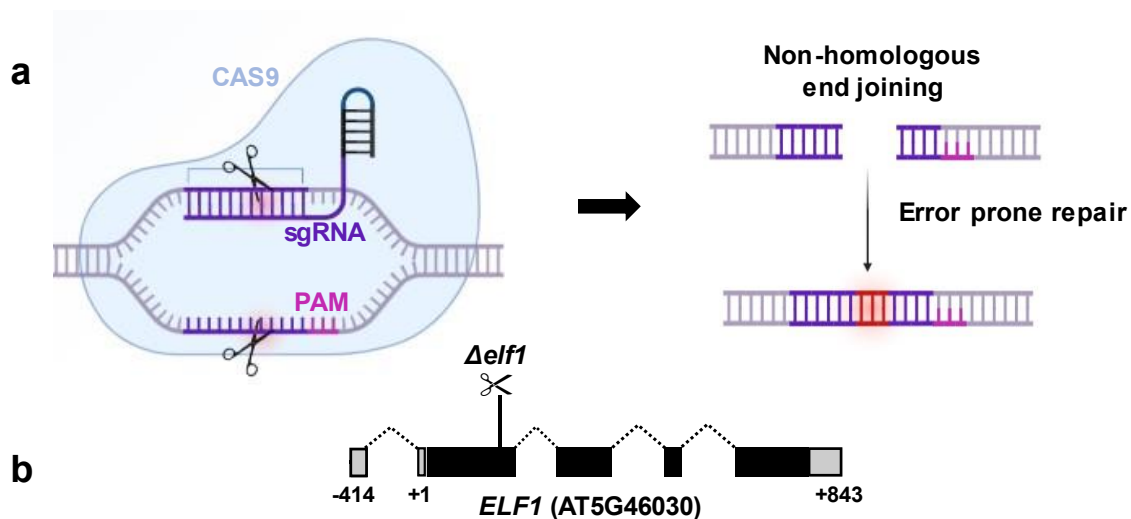


Figure 7 CRISPR-CAS9 mediated gene disruption by insertions or small deletions at the example of *ELF1* (a) Schematic illustration of CAS9 endonuclease cutting at PAM (protospacer adjacent motif) directed by sgRNA (single guide RNA). Purple: Regions corresponding to guide RNA sequence; magenta PAM site; red: Error prone ds break repair (b) Gene model for *ELF1*. Grey bars UTRs; black bars: exons; dashed lines: introns; scissors: complementary regions for sgRNA guides. Panel (a) was created with biorender.com

The T-DNA insertion lines for *SPT6l* (*spt6l-1/2/3*, **Figure 8b**) show a severe phenotype and do not form a viable seedling (Chen et al., 2019a; Gu et al., 2012). To bypass this, an inducible two component β -estradiol inducible system was used to mediate dsRNAi (**Figure 8a**, Brand et al., 2006). A suitable 500 bp region (bp 464-946 of the cDNA, exons 4-7, **Figure 8b**) was predicted with the help of the tool dsCheck (Naito et al., 2005). The plasmid was created by amplification of the predicted sequence from cDNA in sense and antisense and inserted via restriction-ligation cloning to obtain the double stranded hairpin scaffold, which was transferred to the destination vector containing the β -estradiol inducible cassette to obtain the final plasmid (**Figure 8a**).

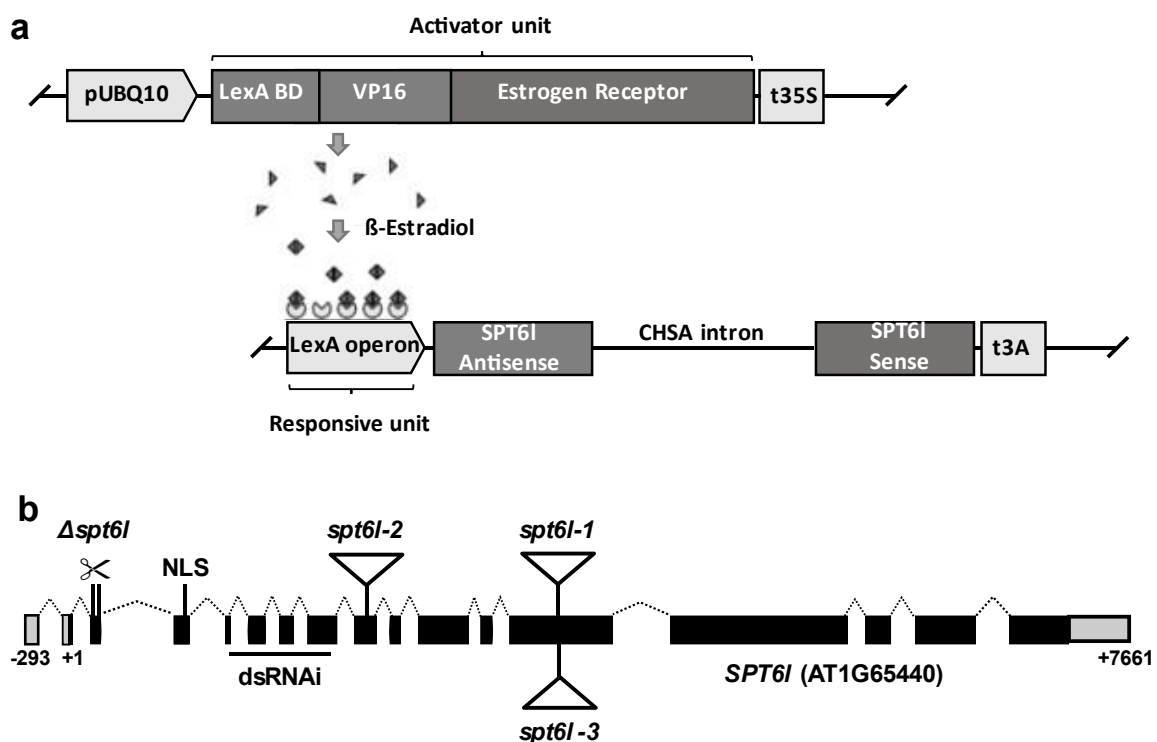


Figure 8 Gene Induction by the β -estradiol system at the example of SPT6l dsRNAi (a) Schematic illustration of β -estradiol system created for inducible expression of double stranded RNAi. The activator unit (grey triangles) is constitutively expressed and binds to the responsive unit in the presence of β -estradiol, activating dsRNAi expression. pUBQ10: native promoter of *Arabidopsis* Ubiquitin 10; LexA BD: binding domain of LexA operon; VP16: acidic transactivation (b) Gene model for SPT6l: Grey bars UTRs; black bars: exons; dashed lines: introns; big empty triangles: T-DNA insertions; scissors: complementary regions for sgRNA guides. Panel (a) is modified from (Antosz, 2019)

The described lines for *SPT6l* (*spt6l-1/2/3*) have been characterised by *in situ* hybridisation in the 3' region of the transcript (Begum et al., 2012). However, huge portions including the NLS stay intact (**Figure 8b**). This leaves the question unanswered whether an aberrant or truncated *SPT6l* transcript is produced. To address this, another plasmid was planned *in silico* to employ

the CRISPR-Cas9 system, containing two guides. With the assumption, that a *SPT6l* knockout would still be lethal, two sgRNA guides in close proximity (~50 bp) within the 2nd exon of the gene were selected (**Figure 8b**). In case of the CRISPR event at both sites, 50 bp of the genomic DNA would be deleted. This would lead to stop codons in two frames early in the CDS, which would allow visualization of heterozygous plants via PCR and subsequent agarose gel electrophoresis, avoiding money and labour-intensive work. The plasmid was planned with the tools described above. While the *SPT6l* project was handed over to PhD Student Henna Kapoor at this point, the *ELF1* knockout lines ($\Delta elf1$) was realized in the *Col-0* genomic background by *Agrobacterium*-mediated transformation. In total 19 lines were selected in T1 via hygromycin based selection. A PCR reaction spanning the genomic locus (450 bp) was sent to sequencing and a total 8 of the 19 plants showed alterations in T1 in the genomic sequence (Data not shown). Two independent T1 lines were picked (line 8 and 15, $\Delta elf1$ +/- *pHEE401* guide_ *ELF1* +/-), each containing a 1 bp insertion, leading to a frameshift and a premature stop codon within the first exon (**Figure 9a**, red box).



Figure 9 *ELF1* gene disruption with CRISPR-Cas9 system (a) *ELF1* disruption by one sgRNA. Two independent lines with the same 1bp insertion (Red highlight, Line 8 and 15), leading to a premature stop codon within Exon1 (red square). After segregation, lines were picked which are homozygous for $\Delta elf1$ (-/-) and Cas9-free. (b) First phenotypic evaluation of two independent $\Delta elf1$ lines show a comparable phenotype to wildtype (Col-0), here 28 days after stratification (DAS). Purple: Guide RNA sequence. Magenta: PAM site. The guide was predicted with the tool CRISPR-P 2.0 (Liu et al., 2017). Pictures in b were shot by Hanna Markusch in her Bachelor's thesis (Markusch 2018)

With the help of Hanna Markusch in her bachelor's thesis (Markusch, 2018), Line 8 and 15 were made homozygous for the CRISPR event in T2 (*Elf1* ^{-/-}), while the vector driving the construct was segregated out to reduce the time for potential off-target effects to one generation of active egg cell-specific promoter. Initial phenotyping of line 8 and 15 (data not shown, Markusch 2018) showed no obvious alterations compared to the wildtype *Col-0* (**Figure 9b**).

2.3 ELF1 has histone chaperone like qualities

A basic principle of histone chaperones is to form electrostatic reactions with histones, to shield the strong interactions with DNA (Philpott et al., 2000). ELF1, containing both basic or acidic regions at the N- or C-termini could hereby shield both: The basic N-terminus binding to negatively charged DNA, potentially guiding DNA into the DNA entry tunnel and the acidic C-terminus binding to the otherwise DNA bound nucleosome during the DNA unwrapping mediated by transcription of Pol II.

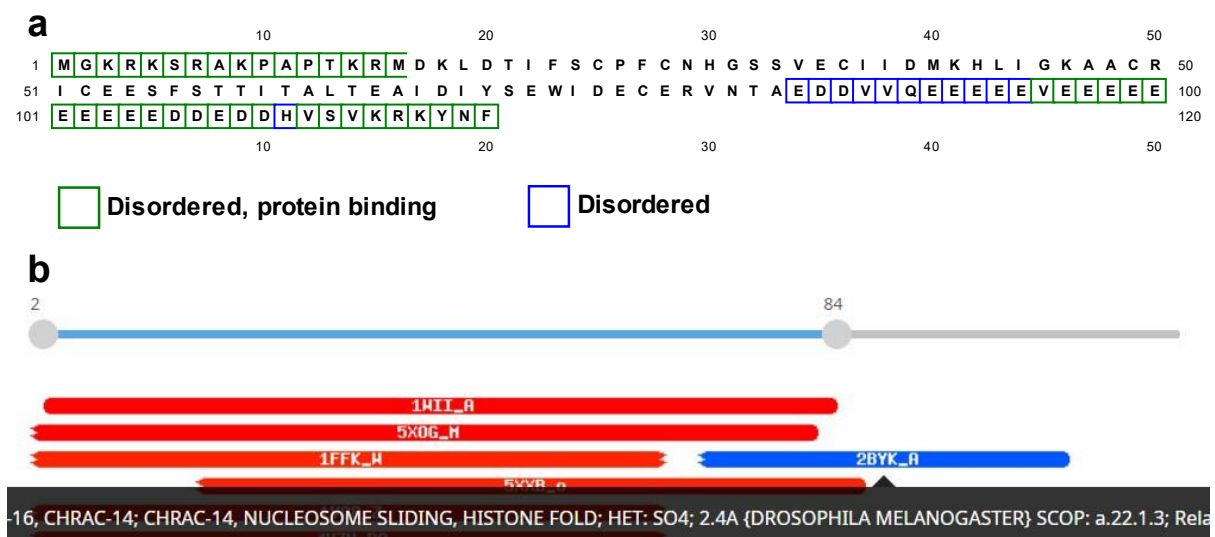


Figure 10 Bioinformatic analysis of ELF1 protein sequence (a) Analysis with DISOPRED3 (Jones and Cozzetto, 2015) shows that both N- an C-terminus are intrinsically disordered (green and blue frames), common for histone chaperones (Warren and Shechter, 2017) **(b)** Analysis with HHPRED (Zimmermann et al., 2018) reveals similarity of the acidic C-terminus with part of the PDB entry 2BYK_A (blue), the *drosophila* CHRAC-heterodimer which helps to facilitate nucleosome sliding (Hartlepp et al., 2005)

Bioinformatic evaluation with DISOPRED3 (Jones and Cozzetto, 2015) show that both the basic N- and the acidic C-terminus of ELF1 are disordered in *Arabidopsis* (**Figure 10a**) and thereby display flexible regions suitable for making transient contacts with both DNA and histones. With the N-terminus being basic and the C-terminus being acidic they will be termed BID (basic intrinsic disordered) and AID (acidic intrinsic disordered) from now on. Further

analysis with HHPRED (Zimmermann et al., 2018) shows, that the ELF1-AID (absent in cryo-EM structure) shows similarity with part of the *Drosophila* CHRAC14-16 heterodimer (**Figure 10b**), which has been shown to help in the process of nucleosome sliding (Hartlepp et al., 2005). With the Zn-Ribbon locked between RPB1 and 2 (Ehara et al., 2017), this places a protein which has its flexible charged intrinsic disordered regions in potential reach for the incoming, unwrapping nucleosome during transcription by Pol II.

2.3.1 ELF1-BID binds DNA

ELF1 completes the DNA entry tunnel by binding RPB1 and RPB2 (Ehara et al., 2017). The location on the TEC at the DNA entry site together with the intrinsically disordered basic N-terminus make it prone to bind to the DNA. To test this hypothesis a set of (truncated) ELF1 versions (ELF1-Full, Δ BID, Δ AID, Δ BID/ Δ AID, **Figure 11a**) was purified in *E. coli* to be tested in electrophoretic mobility shift assays (EMSAs). Prior purification of ELF1 has shown to be troublesome as the protein precipitated from solution (Marion Grasser, internal communication). To bypass this, the pET24b vector system was employed, which was modified by an additional GB1-tag to increase solubility (Cheng and Patel, 2004) and was obtained priorly by Stuart Wilson (Sheffield University). Proteins were expressed in BL21-CodonPlus(DE3)-RIL and purified via one step 6xHis affinity purification, which led to the relatively pure desired proteins (**Figure 11b**). Purified proteins were tested for their DNA binding affinity in electrophoretic mobility shift assays (EMSAs) with linear and bent DNA (4WJ-DNA). The cloning, protein purification and initial EMSAs with 4WJ DNA were realized together with Serena Herzinger in her 6 weeks Master's internship (Herzinger, 2018). EMSAs with linear DNA showed binding of ELF1 Δ AID, starting at concentration of around \sim 5 μ M. The shift disappeared when additionally, the BID (ELF1 Δ AID/ Δ BID) was removed. No shift was observed for full-length ELF1 and ELF1 Δ BID (**Figure 11c**, upper panel). It was concluded that the BID is responsible for DNA binding, however the AID seems to inhibit the BID, as no shift was observed for full-length ELF1. Interestingly the native form in e.g. *Drosophila melanogaster* to human does not contain an AID (Prather et al., 2005) and could potentially be reflected by the shifts of ELF1 Δ AID (**Figure 11c, d** third panels). Incubation of the respective variants with 4WJ DNA, which includes bent DNA fragments in the centre (Lilley and Clegg, 1993), increases the binding affinity to the high nM range for ELF1 Δ AID, while no shift was observed for the other variants (**Figure 11c**, lower panel). The increase in binding affinity for 4WJ DNA was assigned to the bent DNA, which potentially mimics the bent DNA at the borders of the nucleosome.

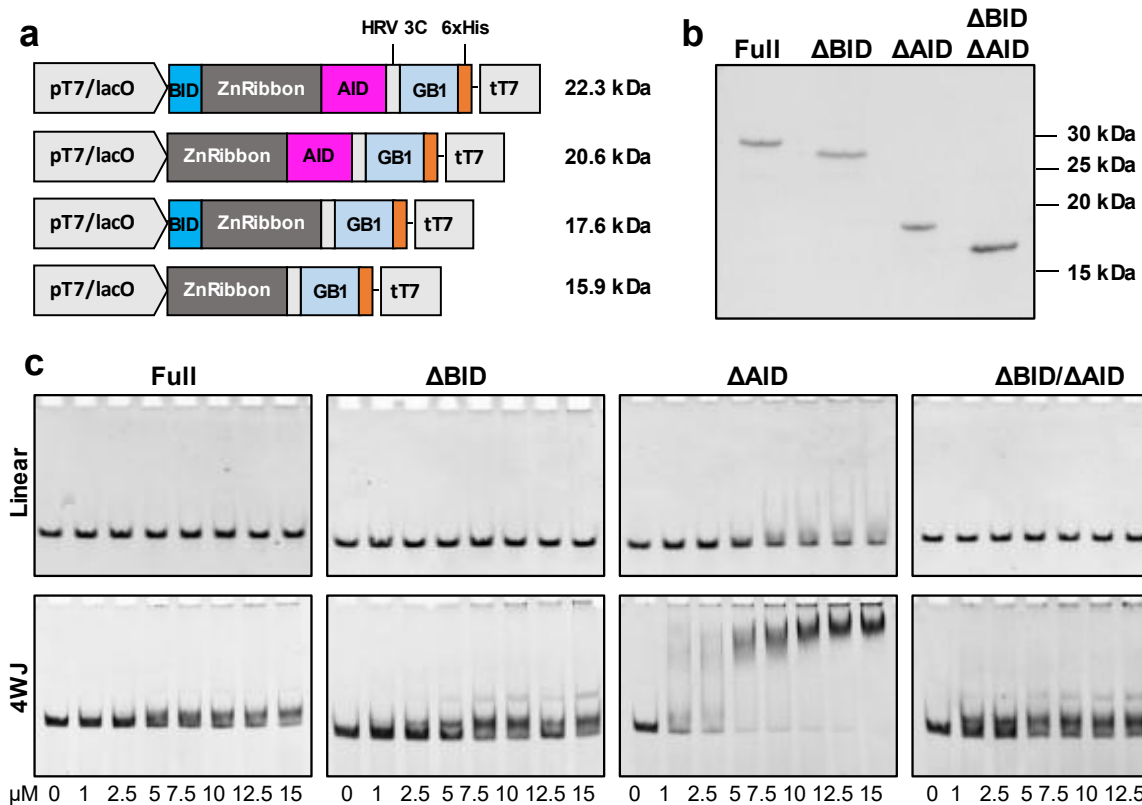


Figure 11 ELF1 binds to DNA with its N-terminus when the C-terminus is missing (a) Schematic illustration of the vectors driving the expression of the (truncated) ELF1 versions. From top to bottom: Full, Δ BID, Δ AID, Δ BID/ Δ AID. pT7/lacO = T7 promoter before the IPTG inducible lac Operon, BID in cyan, Zn-Ribbon in dark grey, AID in magenta. The tag includes a cleavage site for human rhinovirus 3C (HRV 3C, light grey), B1 domain of Streptococcal protein G (GB1, light blue) and a 6xHis affinity tag (6xHis, orange) (b) CBB stain of the end-products of one step affinity purifications (c) Electrophoretic mobility shift assays (EMSAs) of varying concentrations of GB1-tagged ELF1 versions with linear and Four-Way junction (4WJ)-DNA. Linear DNA includes the same sequences as 4WJ-DNA

2.3.2 Association of ELF1 with CK2 is independent of phosphorylation

Similar to other histone chaperones, the putative histone chaperone ELF1 showed strong association of ELF1 with CK2 (Table 4). To test if the acidic C-terminal gets phosphorylated by CK2 *in vitro*, like shown for yeast (Kubinski et al., 2006), a CK2 phosphorylation assay was performed with maize CK2 α (Krohn et al., 2003). To exclude unspecific phosphorylation of the GB1-tag, the intrinsic cleavage site for human rhinovirus 3C (HRV 3C) was employed to remove the GB1-tag (Figure 11a, Figure 12a). The prior identified CK2 substrate HMGB2 was used as a positive control, which is similar in size (Figure 12a) and shows 4 CK2 consensus phosphorylation sites (Stemmer et al., 2002). The CK2 consensus motive is S/T-x-x-E/D/pS and stretches of acidic aa have been shown to favour phosphorylation (St-Denis et al., 2015). However, no phosphorylation was observed in all technical replicates (Figure 12b). Sequence

alignment with Clustal Omega (Sievers et al., 2011) of *Arabidopsis* and yeast ELF1 (Figure 12c) show that the C-terminus is not conserved. Indeed, 9 putative sites are present in yeast (Kubinski et al., 2006), however only 2 putative CK2 sites are present in *Arabidopsis* (Figure 12c, yellow highlights). Interestingly, most of the putative sites present in yeast have been replaced by acidic aa in *Arabidopsis*, potentially abolishing the actual need for further charge modification.

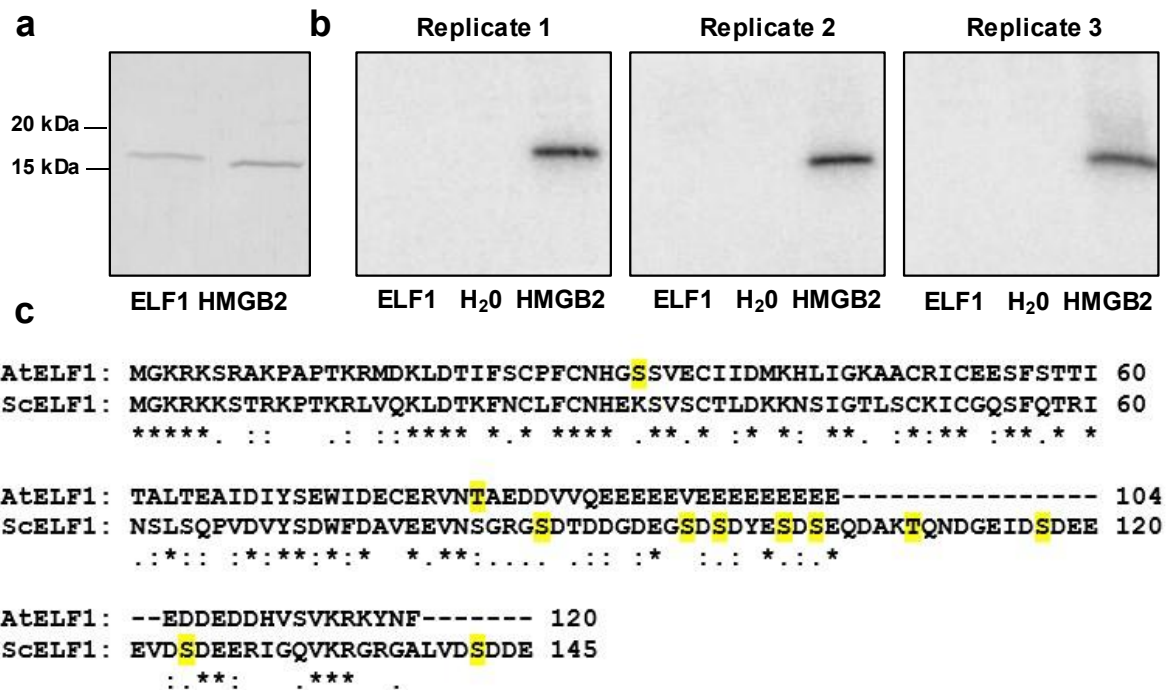


Figure 12 ELF1 is not phosphorylated by maize protein kinase CK2 α (a) CBB stain of ELF1 next to the positive control HMGB2 (Stemmer et al. 2002) (b) Autoradiography of ELF1, water or HMGB2 in 3 technical replicates. Substrates were incubated with radioactively labelled γ^{32} -ATP and maize CK2 α and separated by SDS-PAGE (c) Sequence alignment of *Arabidopsis thaliana* ELF1 and *Saccharomyces cerevisiae* ELF1. ScELF1 shows 9 putative CK2 phosphorylation sites (yellow, Kubinski et al. 2006) whereas AtELF1 shows only 2. Alignments were made with Clustal Omega (Sievers et al. 2011)

2.3.3 ELF1 binds to H2A-H2B; synergistic phenotypes with histone chaperones

From this point onward the project was handed over to master students Claudia Thorbecke (Thorbecke, 2019) and Hanna Markusch (Markusch, 2020) which were supervised during the course of this thesis. Relevant results are briefly summarized here:

The nucleosome at SHL-1 has a little less than half of the DNA unwrapped (Noe Gonzalez et al., 2020), exposing the proximal H3-H4 and H2A-H2B. Predictions of ELF1 anchored on the

TEC would put the acidic C-terminus facing H2A-H2B (**Figure 1**, Ehara et al., 2019), with H2B showing the biggest portion of potential interaction interface. GST-pulldown assays performed with full-length ELF1 with AtH2A-H2B displayed interaction of ELF1 with H2B. The GST-tag alone as well as ELF1 Δ AID did not lead to any detectable H2A-H2B signal, showing that the AID directly interacts with H2B (Thorbecke, 2019). This is in line with H2B ranking in each of the 3 technical AP-MS replicates third (**Table 3**), indicating that indeed ELF1 potentially binds the exposed octasome during transcript elongation.

While the here created CRISPR knockout line *Δelf1* showed no obvious alterations in development (**Figure 9b**), generation of double mutants of *Δelf1* with other histone chaperone mutants showed synergistic defects. The following transcript elongation complex factor single mutants were crossed with *Δelf1*, made homozygous and phenotypically analysed: T-DNA insertion lines *cdc73-2*, *tfIIs-1*, *spt16-1* and *ssrp1-2*. While only preliminary data is available it becomes apparent, that *Δelf1 tfIIs-1* and *Δelf1 cdc73-2* show no obvious additional defects. However, *Δelf1 spt16-1* and *Δelf1 ssrp1-2* display prior described defects (Lolas et al., 2010) in a more pronounced way, potentially indicating some interplay with other transcription associated histone chaperones (Markusch, 2020).

Further, the EMSAs with GB1-tagged ELF1 (**Figure 11**) were repeated with ELF1 versions where the GB1 tag was cleaved off, leading to comparable results. Binding to linear DNA, 4WJ-DNA and nucleosomes displayed binding when the BID was present and the AID missing, however absent in full-length ELF1, indicating a potential auto-inhibition of basic N-terminus and acidic C-terminus. This was followed up by EDC crosslinks, where carboxylic acid reacts with EDC and subsequently reacts with primary amines. There, intrinsic crosslinking was observed, dependent on the presence of the acidic C-terminus, pointing in the direction of auto-inhibition in the absence of other binding partners (Markusch, 2020).

In summary ELF1 shows properties which could assist in the disassembly of nucleosomes during transcript elongation. Synergistic effects with other transcript elongation factor mutants who display histone chaperone functions themselves and the high abundance of histones in the ELF1 AP-MS dataset further strengthen these findings.

2.4 Acetylation and Phosphorylation modulate the binding properties of the *Arabidopsis* Histone Chaperone FACT

The complex array of binding events upon nucleosome unwrapping and the subsequent release after e.g. Pol II progression could require a way to modulate FACT histone and DNA binding contacts. To detect PTMs on the FACT complex the Proteomics Department at the University of Southern Denmark was visited during my master's thesis. This led to the creation of a dataset, where transgenic *Arabidopsis* cell suspension culture (empty GS, GS-tagged SSRP1 and SPT16, compare **Figure 5**) was affinity purified in the presence of phosphatase inhibitors, in solution trypsin digested and subsequently analysed via LC-MS/MS in a label free quantitative way. Next to the putative interactome PTMs like acetylation, mono-, di- and tri- methylation and phosphorylation were included as variable modifications (Holzinger, 2015). The benzonase endonuclease digest was here not included to obtain a more chromatin prone interactome to potentially map the chromatin context of FACT (see section 3.3). As this introduces a second set of AP-MS datasets for FACT they will be termed SSRP1-GS PTM and SPT16-GS PTM, respectively.

Table 5 PTMs targeting FACT (Holzinger, 2015)

∅ =no high confidence spectra was detected, only low confidence

Modification	# Spectra	Domain	Protein
K539ac	5	BID/NLS	SSRP1
K549ac	17	BID/NLS	SSRP1
K594ac	12	HMGbox	SSRP1
K599ac	3	HMGBox	SSRP1
T1023p	∅	AID	SPT16
S1033p	39	AID	SPT16
S1035p	38	AID	SPT16

For SSRP1, K-acetylations in the BID and the HMGbox were found (**Table 5**, Holzinger, 2015), which will be discussed later (Section 2.5). For SPT16, S/T phosphorylation sites were detected in the C-terminal AID. Here, S1033p and S1035p were detected in plenty high confidence spectra (False discovery rate <1%, **Table 5**, Supplementary Data Table 11 and 12). Modifications occurring in only 1 high confidence spectra were not included. One exception was made: Lowering the threshold to obtain low confidence spectra (False discovery rate <10%) led to the detection of another phosphorylation site T1023p (Supplementary Data table 12). These 3 phosphorylation sites were also detected in other LC-MS/MS screens (Heazlewood et al., 2008) and hence all 3 of them were considered. As the AID is central for H2A-H2B

binding (Mayanagi et al., 2019; Tsunaka et al., 2016), phosphorylation could be a way of modulating the binding of AID to H2A-H2B. S/T-phosphorylation marks are reversible and increase the inherent negative charge of the AID. This might strengthen the affinity for the overall positively charged histones. This hypothesis was further evaluated here by studying the effects of SPT16-AID phosphorylation.

2.4.1 SPT16 AID is phosphorylated by CK2

All 3 detected phosphorylation sites display the CK2 consensus motif S/T-x-x-E/D/pS (**Figure 13a**) and the list of putative interactors from SPT16-GS PTM (Holzinger, 2015) shows strong association with all CK2 members (CKA1-4, CKB1-4, **Supplementary Table 1**), confirming the obtained hits for SPT16-GS (**Table 4**). This suggests, that CK2 is the respective writer of the phosphorylation. To confirm this, a CK2 phosphorylation assay was set up with truncated SPT16 AID (aa 955-1075, **Figure 13b, c**) and recombinant maize CK2 α (Stemmer et al., 2002). Please note, that proteins containing AIDs tend to show less mobility than expected during SDS-PAGE electrophoresis, as highly acidic patches can repel SDS electrostatically (Tiwari et al., 2019). The radioactive phosphorylation assay (**Figure 13d**) showed a single band, corresponding to the band of the purified protein determined in the CBB stain (**Figure 13c**). The increasing amount of protein correlated with increasing amount of signal, indicating that CK2 can indeed phosphorylate the AID of SPT16.

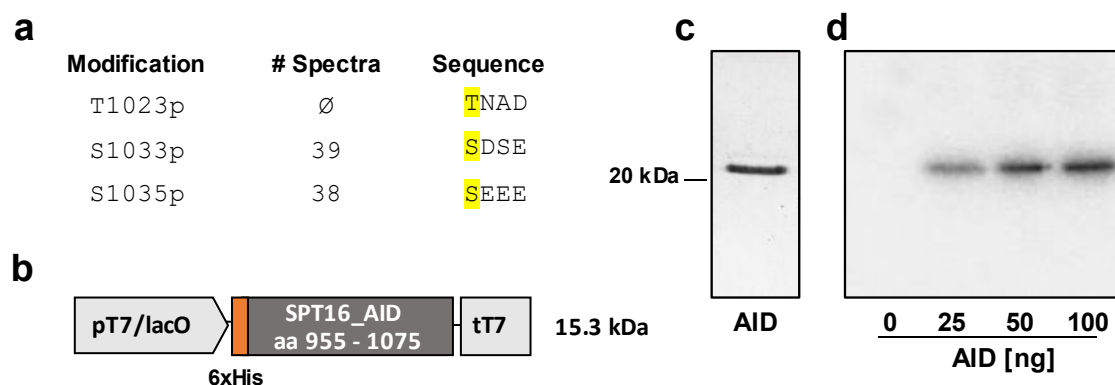


Figure 13 Protein kinase CK2 phosphorylates SPT16 AID (a) phosphorylation sites display the CK2 consensus motif S/T-x-x-E/D/pS (b) Schematic illustration of the vector driving SPT16-AID expression (c) CBB stain SPT16_AID one step 6xHis affinity purification (d) Autoradiography of recombinant maize CK2 α , γ 32-ATP and increasing amounts of SPT16_AID

To confirm the exact sites obtained from the *in vivo* cell culture analysis (**Table 5**), the *in vitro* assay was repeated with unlabelled ATP. Due to the small molecular weight of a single phosphorylation (~80 Da), quality control via SDS-PAGE and subsequent CBB staining leads

to no noticeable change in the migration pattern (**Figure 14a**). To bypass this, acetic acid urea PAGE (AU-PAGE) was utilised for quality control (Shechter et al., 2007). None of the unphosphorylated protein remained upon incubation with ATP and CK2 (**Figure 14b**). The experiment was in gel trypsin digested (compare **Figure 14a**) and analysed via shotgun-proteomics, including phosphorylation as variable modification. Indeed, this reciprocal *in vitro* analysis of the CK2 assay revealed the same spectra obtained by the *in vivo* analysis of the cell culture material (**Table 5**), showing that CK2 can phosphorylate the same sites. Additionally, one further site was detected in T1013 in low abundance (**Figure 14c**).

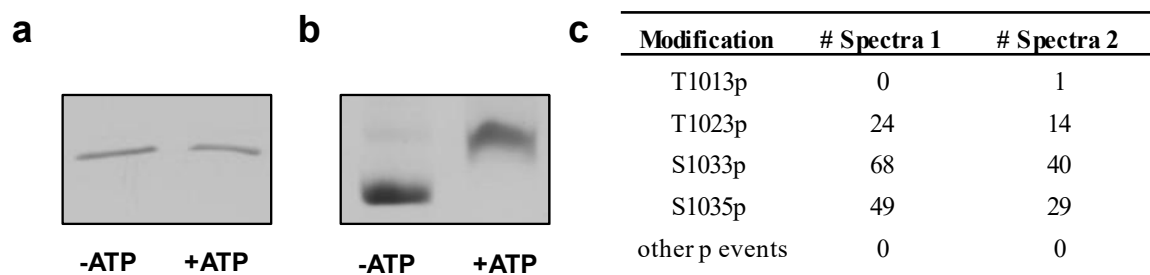


Figure 14 Unlabelled CK2 phosphorylation assay coupled to LC-MS/MS analysis leads to the detection of the same phosphorylation sites as detected *in vivo*. (a,b) CBB stain of SPT16 AID after the CK2 assay in presence or absence of ATP (a) by SDS-PAGE (b) by AU-PAGE (c) two replicates of (a) were subjected to in-gel trypsin digest and subsequently analysed via LC-MS/MS. Data analysis including phosphorylation and oxidation as fixed modifications leads to comparable phosphorylation events as determined *in vivo* (Table 5)

While the *in vitro* shotgun proteomics analysis of the CK2 assay is in line with the modifications observed *in vivo*, there is a total of 15 putative CK2 phospho-sites in the truncated SPT16 fragment (**Figure 15a**) and only the 3 most C-terminal sites were detected in the LC-MS/MS screen (**Figure 13a**). Trypsin cuts after arginine and lysine residues. This, together with the LC-MS/MS approach, which favours an optimal peptide length and little charge, leads to the same bias in both experiments. To bypass this, mutations for the 3 *in vivo* sites were introduced in the truncated protein (T1023V, S1033A, S1035A, compare **Figure 13b**), to mimic an unphosphorylated state (Dissmeyer and Schnittger, 2011), which is not a substrate of CK2 anymore. The protein was purified by one step 6x-His affinity purification (**Figure 15b**) and subjected in the CK2 assay next to the native AID. A signal reduction of ~ 36% was observed (**Figure 15c, d**) over 3 technical replicates. This confirms phosphorylation of the mutated sites and indicates that further sites are not mapped by the LC-MS/MS analysis. However, this assay containing purified truncated components has only limited validity for describing the situation *in vivo*. Additionally, an access of phospho-mimicking substitutions has been shown to abolish AID nucleosome contacts (Mayanagi et al., 2019). Hence, further experiments were continued

focusing on the three phospho-sites initially observed *in vivo* (**Table 5**). Mimicking fewer and the most C-terminal sites should leave properties of the AID, like e.g. flexibility, intact at the cost that potential effects could be weaker, compared to a fully phosphorylated or unphosphorylated state.

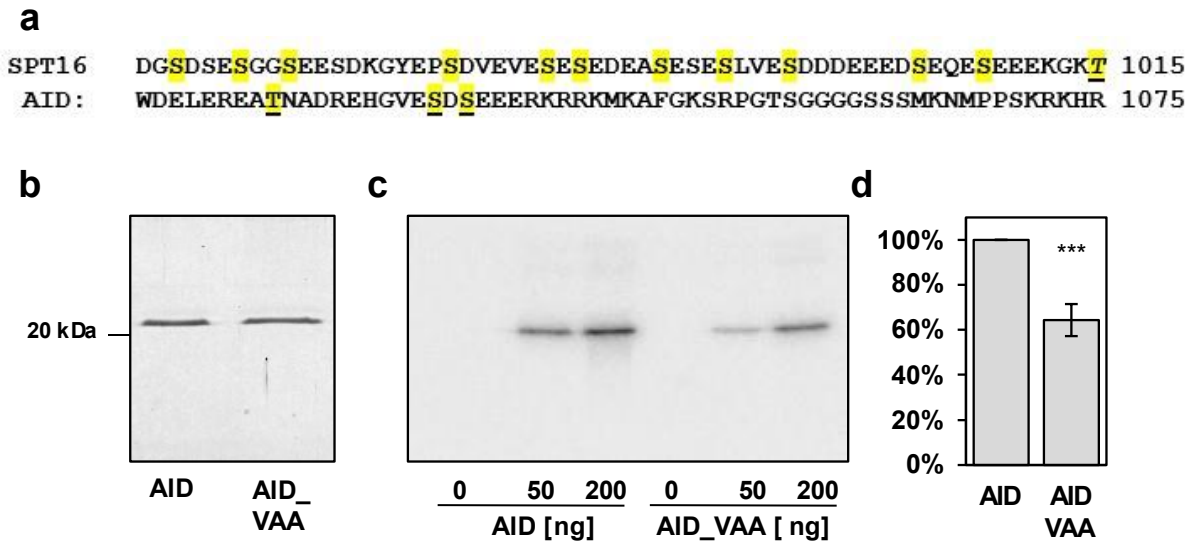


Figure 15 *In vitro* phosphorylation by CK2 is not limited to phosphorylation sites detected *in vivo* (a) SPT16 AID shows 15 putative CK2 sites (yellow highlight). Phosphosites verified are underlined, the phosphosites observed *in vitro* is underlined and in italics (b) CBB stain of AID (T1023, S1033, S1035) and AID_VAA (V1023, A1033, A1035) (c) Autoradiography of increasing amounts of AID or AID_VAA incubated with γ -³²P-ATP and maize CK2 α (d) Quantification of signal intensity with the software Image-J. Bars indicate mean values normalized to 200 ng AID [n=3], significance level has been determined by student's t-test: *** p = < 0.001

2.4.2 Direct interaction studies between CK2 and FACT by Y2H

An early dataset obtained in yeast by AP-MS of SPT16 detected histones, the PAF-Complex and CK2 (Krogan et al., 2002). A reciprocal approach in yeast pulling on CDC73 of the PAF-Complex or SPT16 led to a comparable result (Bedard et al., 2016). Here, SPT16 associated strongly in two independent shotgun proteomic datasets with CK2 (**Table 4, Supplementary Table 1**). To test for putative direct interactions a Y2H assay (Osman, 2004) was performed with either component of the CK2 complex or the FACT complex in both bait and prey orientations. All tested combinations were co-transformed into AH109 cells and selected on double dropout plates (DDO). Interaction was evaluated by growth on triple dropout (TDO) and quadruple dropout plates (QDO). No interaction was observed for either SPT16 with CKA1 and CKB1 (**Figure 16**, upper panel) or SSRP1 with CKA1 and CKB1 (**Figure 16**, lower panel) and vice versa. Interaction was observed for CKA1 and CKB1, the subunits of the

heterodimeric CK2 complex: In both bait and prey orientations on TDO and one orientation on QDO plates (**Figure 16**, upper and lower panel, first row).

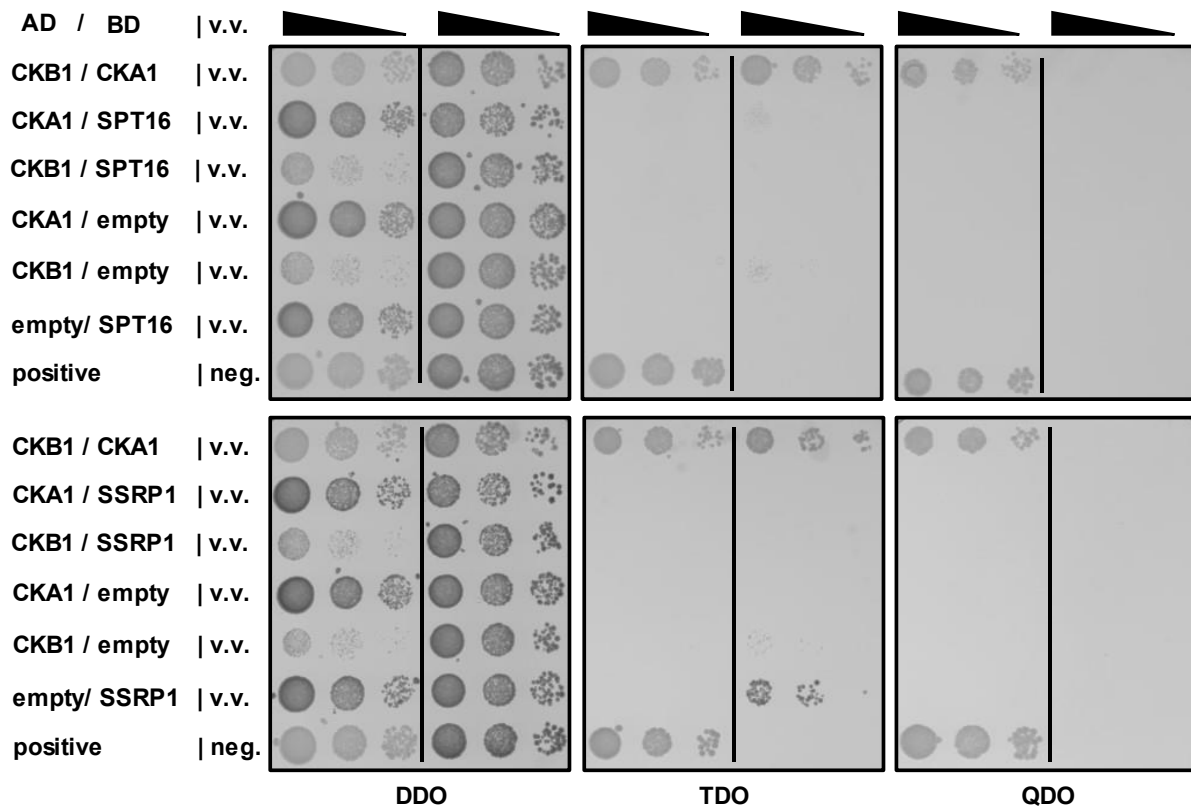


Figure 16 Y2H displays no direct interaction between FACT and CK2 components Different combinations of bait- (DNA-binding domain = BD) and prey- (activation domain = AD) fusion proteins were spotted on Synthetic Dropout plates (SD; double-dropout =DDO, triple = TDA; quadruple =QDO) of yeast AH109. No interaction was observed except for AD-CKB1/BD-CKA1 on TDO and QDO and BD-CKA1/AD-CKB1 on TDO. Spotted were serial dilutions (10^0 , 10^{-1} , 10^{-2}) on DDO- (SD/ -LEU -TRP), TDO-, (SD/- LEU -TRP -HIS) and QDO- plates (SD/ -LEU -TRP -HIS -ADE). v.v. = vice versa in respect to bait and prey combination

As a further positive control, the interaction of pGBKT7-SSRP1 and pGADT7-SPT16 and vice versa was spotted on dropout plates (**Figure 17**). No interaction for either combination was observed on QDO plates. Interactions observed on TDO plates by pGADT7-SSRP1 and pGBKT7-SPT16 can be explained by the respective unspecific interaction of pGADT7-SSRP1 with the empty pGBKT7 vector (**Figure 17**, right panel). This indicates that FACT subunits are potentially poor binding partners in Y2H, showing both a tendency for false negatives on QDO (**Figure 17**, left panel) and a tendency for false positives on triple dropout plates (**Figure 17**, right panel, TDO). It is unclear which subunit is affected by the fusion to DNA-binding and/or activation domain. This leaves some validity in testing FACT subunits, especially on quadruple dropout plates. However, negative results should be treated with extra care.

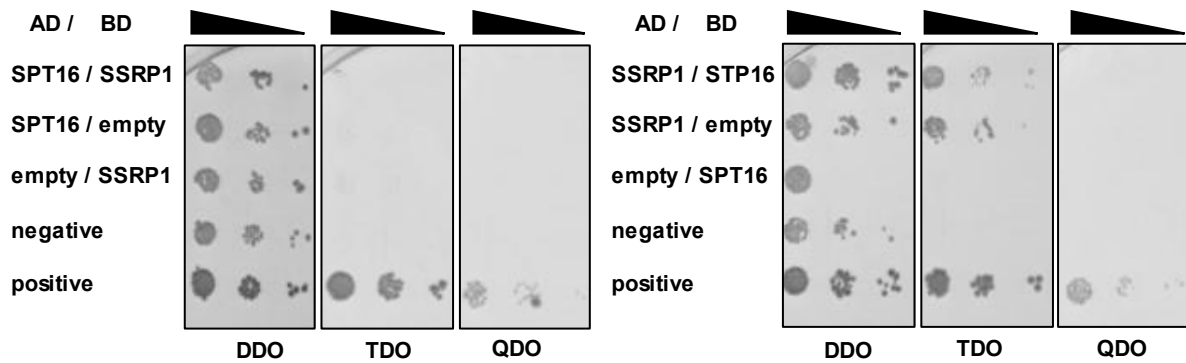


Figure 17 Y2H displays no direct interaction between SSRP1 and SPT16 Different combinations of bait- (DNA-binding domain = BD) and prey- (activation domain = AD) fusion proteins were spotted on dropout plates (DO) of yeast AH109 serial dilutions (10^0 , 10^{-1} , 10^{-2}). DDO (SD/ -LEU -TRP), TDO, (SD/- LEU -TRP -HIS)

2.4.3 Increase of H2A-H2B binding by phospho-mimetic SPT16_AID

To test for a possible H2A-H2B binding affinity change upon SPT16_AID phosphorylation, a GST protein binding assay was set-up. With the help of Prof. Dr. Gernot Längst and Elisabeth Silberhorn the purification assay of *Arabidopsis* H2A-H2B was designed, in a tag free manner, purifying the variants from inclusion bodies.

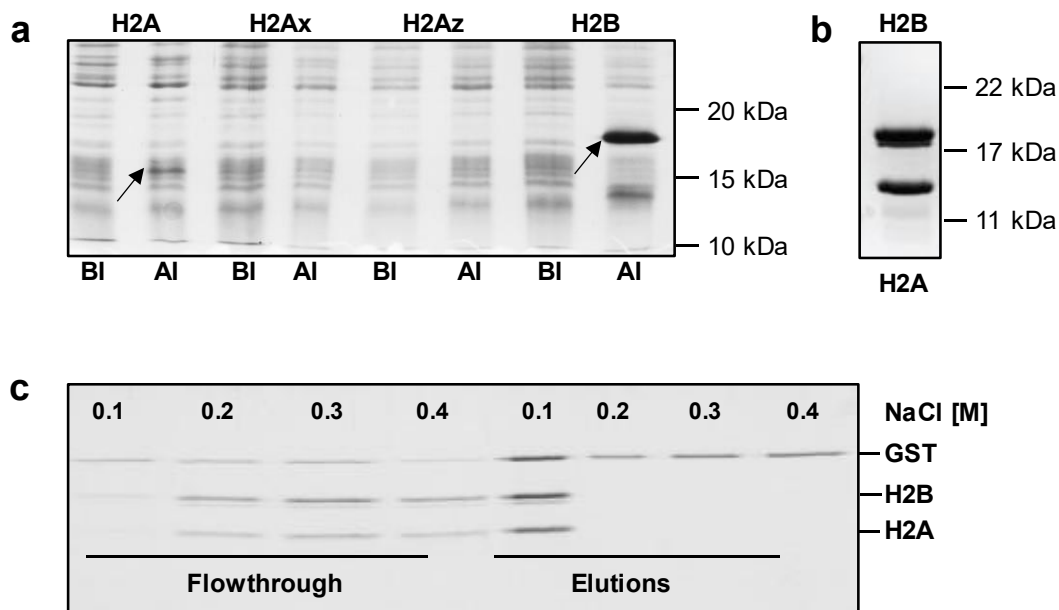


Figure 18 GST pull-down assay optimisation (a) CBB stain of AtH2A variants and AtH2B shown for 6h of induction at 28°C in the Rosetta expression strain. Several conditions and strains were tested, best results are shown here. BI = Before Induction, AI = After induction. **(b)** CBB stain of *Arabidopsis* H2A-H2B dimer obtained from Akihisa Osakabe. Picture was taken by Akihisa Osakabe **(c)** GST assay optimisation. CBB stain of GST Pull-down assay at different salt concentrations. The GST-tag shows unspecific binding towards *Arabidopsis* H2A-H2B at 100 mM NaCl. No more binding can be observed at 200 mM NaCl.

The sequences of H2A, H2A.X, H2A.Z and H2B were codon optimized for *E. coli* expression and expression was tested with a number of different T7 driven *E. Coli* expression strains (B121 RIL, B121 STAR, B121 pLys, Rosetta) at different conditions (37°C up to 6h; 28°C up to 6h; RT o/n). While induction worked well for H2B (**Figure 18a**, last lane), H2A was only poorly expressed, best with Rosetta 28°C for 6h (**Figure 18a**, second lane). No IPTG induction was detected for H2A.Z and H2A.X (**Figure 18a**, 4th and 6th lane). The poor induction was not sufficient to purify the proteins in an untagged, inclusion body dependent way. An alternative could be arranged by collaboration with Akihisa Osakabe from Frédéric Berger's laboratory who purified *Arabidopsis* H2A-H2B (**Figure 18b**) in a 6xHis-tag dependent manner which gets cleaved of afterwards (Osakabe et al., 2018). Next the GST-pulldown assay was established. Initial GST-pulldown assays in the standard 100 mM NaCl buffer led to unspecific interaction of the GST-tag with AtH2A-H2B. After optimisation of the set-up, increasing the salt concentration to 200 mM NaCl abolished this interaction, visible by the presence of H2A-H2B in the flowthrough- and the absence in the elution fractions (**Figure 18c**).

GST-tagged truncated SPT16_AID proteins were purified in wildtype or a phospho-mimetic variants by replacing the serine or threonine with either glutamic or aspartic acid (Dissmeyer and Schnittger, 2011), (**Figure 19a**, T1023E, S1033D, S1035D). Proteins were expressed in *E. coli* BL21 RIL cells and one step affinity purified using Glutathione Sepharose, leading to a pure protein (**Figure 19b**). The cloning and the affinity purification were performed together with Serena Herzinger in her 6 weeks Master's internship (Herzinger, 2018). Comparative GST-pulldown assays show, that both versions can bind to H2A-H2B at 200 mM NaCl (**Figure 19c**). With the GST-tag alone, no binding can be observed (**Figure 19c**, last lane and **Figure 19e**, left panel). However, the phospho-mimicking AID version binds with higher affinity to H2A-H2B, indicated by the increase in signal intensity of H2A and H2B (**Figure 19c**). Signal quantification with the software Image-J of the H2A- and H2B-signal at 200 mM NaCl, normalised to the respective AID signal, showed an increase of ~ 32% over 4 technical replicates (**Figure 19d**). Additionally, similar charged bovine Cytochrome C (Citterio et al., 2000), where 19% of aa are either arginine or lysine, compared to 16% for H2A and 24% for H2B (determined with the online tool ProtParam (EXPASy) ; Wilkins et al., 1999), was subjected to the GST-pulldown assay. No signal was detected on the CBB stain for AID and AID_EDD, indicating that the interaction is specific and independent of random charge interactions (**Figure 19e**, middle and right panel).

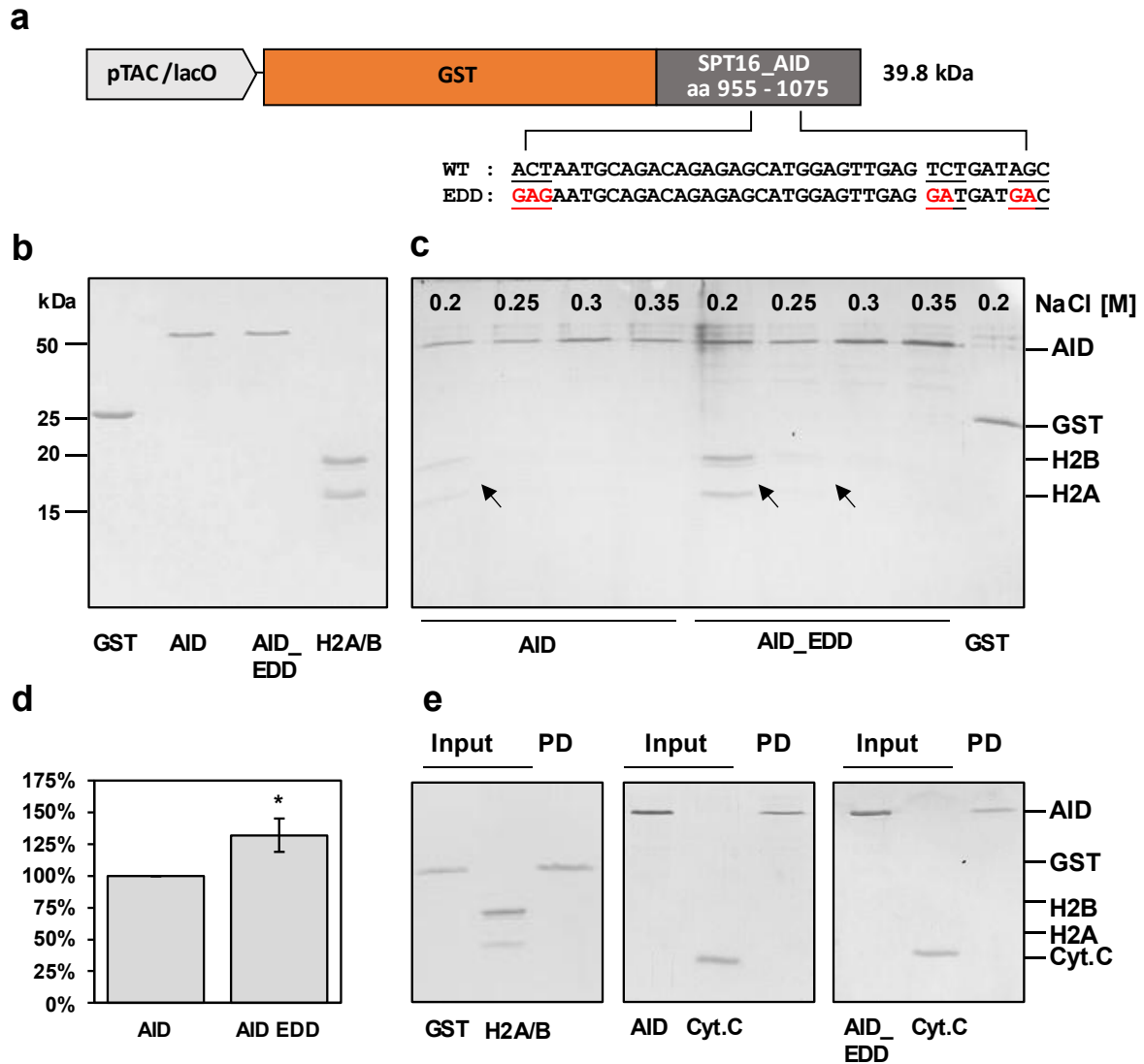


Figure 19 Phospho-mimetic SPT16 AID binds H2A-H2B with higher affinity than wildtype SPT16 AID

(a) Schematic illustration of GST-tagged SPT16 AIDs. Mutations (red) were initially introduced by overlap extension PCR (b) CBB stain of the final products of the one-step affinity purification of GST-tag, GST-SPT16_AID (=AID, T1023, S1033, S1035), GST-SPT16_AID_EDD (=AID_EDD, E1023, D1033, D1035). Additional AtH2A-H2B (H2A/B) is loaded (c) CBB stain of GST Pull-down assay at different salt concentrations comparing AID and AID_EDD. More H2A-H2B is detected in assays performed with AID_EDD (black arrows) (d) Signal of H2A and H2B at 200 mM NaCl normalized to the respective AID. Quantification of signal intensity with the software Image-J at 200 mM NaCl. Bars indicate mean values, normalized to SPT16_AID [n=4], significance level has been determined by student's t-test: * = $p < 0.05$ (e) CBB stain of GST Pull-down assays of controls at 200 mM NaCl. None of the controls shows unspecific binding. Proteins were separated by 18 % SDS-PAGE. The empty GST was available in the laboratory supply, AtH2A-H2B was obtained by Akihisa Osakabe. GST= Glutathione-S-Transferase.

2.4.4 Influence of Charge Alterations on Histone Immunoprecipitation

In vitro analysis showed that the phospho-mimetic AID binds with higher affinity to H2A-H2B compared to the WT variant. While this set-up might give insights into the respective affinity of the single components, the situation *in vivo* might not be accurately represented. To address this, the *Arabidopsis* cell-culture system was employed, where potentially all players are present (e.g. chromatin, Pol II, etc.). Hence, IgG affinity purifications were performed with full-length GS-tagged SPT16 variants under control of the native promoter (**Figure 20a**) to test the effects of natively phosphorylated (T1023, S1033, S1035), phosphorylation insensitive (V1023, A1033, A1035) and phospho-mimetic (E1023, D1033, D1035) variants.

PSB-D cells were transformed with the respective construct by *Agrobacteria*, selected and upscaled. Immunoprecipitation of the SPT16-GS variants under control of the native promoter (**Figure 20a**) led to a similar band pattern (**Figure 20b**) like observed before for SPT16-GS wildtype variant under control of the 35s promoter (**Figure 5b**) and was in most aspects comparable among the three SPT16 variants (**Figure 20b**). However, the signal for the putative histone band pattern (H) and the prior identified chloroplastic protein RecA (u, Supplementary data table 1, compare section 2.1.3) appeared weaker in the phospho-insensitive variant (**Figure 20b**, P0) which maintains the neutral charge (**Figure 20b**). The slight decrease of the putative histone bands in the phospho-mimicking variant (P+, **Figure 20b**) can be explained by the slightly uneven loading, visible by the decrease of the respective bait (**Figure 20b**, last lane). To confirm whether indeed histones are affected and to determine if the outer H2A-H2B dimers only or the whole nucleosome - including the inner H3-H4 tetrameric core - display this effect, immunoblot analysis of the affinity purifications was performed with α H2B, as a representative for H2A-H2B, and α H3, as a representative for the tetrameric H3-H4 core. Antibody binding was detected using HRP-coupled secondary antibody and chemiluminescence detection. 2,2,2-Trichloroethanol (TCE) staining of the respective gel subjected to western blot (**Figure 20c**) served as loading control. Please note that TCE selectively binds to tryptophan. Histones, due to their lack of tryptophan, are not visualized. The immunostaining revealed that the phospho-insensitive variant immunoprecipitated less H2B and H3 (**Figure 20b**, d). Two replicates were performed showing similar tendencies (**Supplementary Figure 1**). This indicates, that modifying the charge pattern of the very C-terminal CK2-phosphosites of SPT16 AID has an influence on the ability of SPT16 to interact with the entire nucleosome. The WT version (**Figure 20b**) is likely phosphorylated, like priorly detected in the initial screen (**Table 5**), in

line with enhanced binding properties upon charge modification in the GST-pulldown assay (Figure 19).

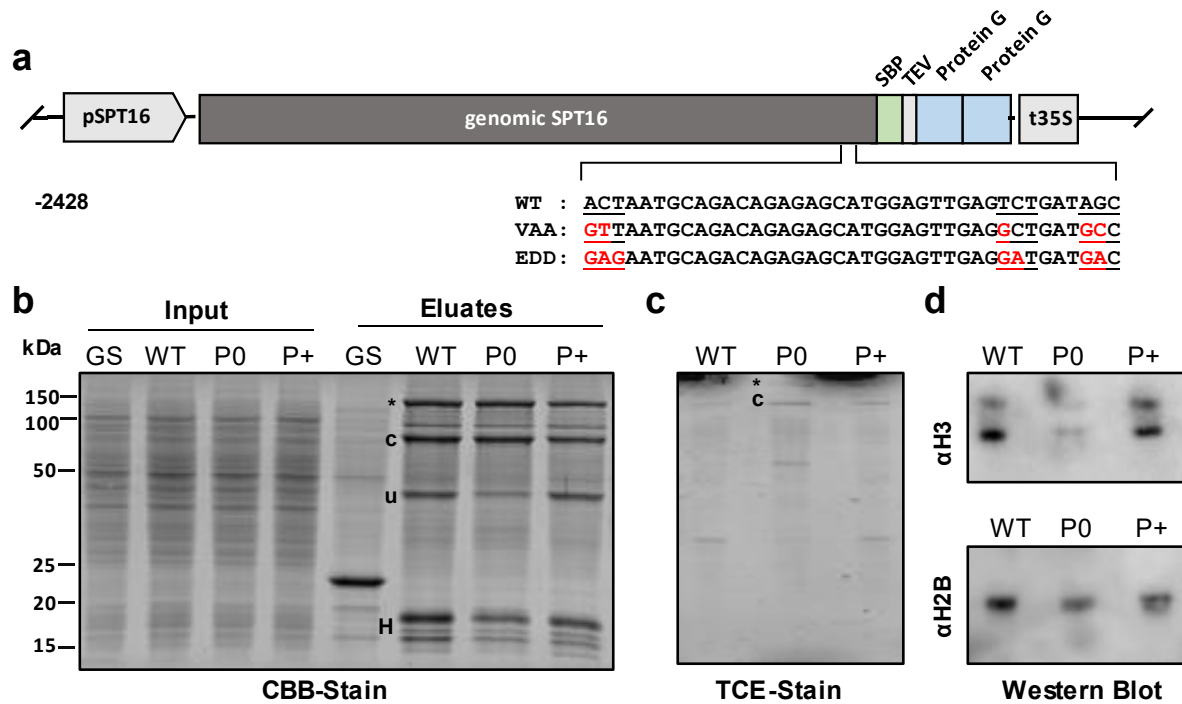


Figure 20 Phospho-insensitive SPT16 binds less H2B and H3 than phospho-mimetic and natively phosphorylated SPT16 (a) Schematic illustration of wildtype- (WT, T1023, S1033, S1035), phospho-insensitive- (P0 = VAA, V1023, A1033, A1035) and phospho-mimetic- (P+ = EDD; E1023, D1033, D1035) SPT16 bait proteins fused to a GS tag under control of the native promoter (introduced mutations in red, bait in dark grey, streptavidin-binding protein in green; TEV cleavage site in light grey; Protein G domains in light blue) (b) Input (0.01 % of total) next to Eluates (1/3 of total) of the one-step affinity purification using IgG coupled magnetic beads. The proteins were separated by 18 % SDS-PAGE and stained with CBB. * = bait, c = complex partner (here SSRP1), u = RecA (see section 2.1.1), H = putative histone band pattern (c) TCE stain corresponding to (d) Immunoblot with α H3 (upper panel) and α H2B (lower panel). TCE = 2,2,2-Trichlorethanol

2.4.5 Altering the charge pattern of SPT16 displays effects on plant development

Phospho-mimicking of the *in vivo* detected phosphorylation pattern of SPT16_AID (Section 2.4.1) led to an increase in H2A-H2B binding *in vitro* (section 2.4.3) and the inability to be phosphorylated in these sites led to a decrease in H2B and H3 affinity *in vivo* (section 2.4.4). To get more information about the effects of phosphorylation of the SPT16 acidic intrinsic disordered region, transgenes were created to complement *spt16-1* (Figure 21a), a T-DNA insertion knockdown mutant, reducing the transcript and protein level to ~ 60% (Lolas et al., 2010).

2.4.5.1 Line creation and validation

Transgenes contained the native promoter (*pSPT16*), a 5' *TagRFP* and the wildtype or phospho-variants of *SPT16* (**Figure 21a**; *wildtype* = *WT*, *phospho-insensitive* = *P0/VAA* or *phospho-mimetic* = *P+/EDD*). *Wildtype* and *phospho-mimetic* transgenes were directly introduced in the *spt16-1(-/-)* background by *Agrobacterium*-mediated transformation. Even after several tries, homozygous and heterozygous *spt16-1* mutants could not be transformed directly with the *phospho-insensitive* transgene. Hence, Col-0 was transformed first and crossed into the *spt16-1* background. For each transgene, three independent primary-transformants (T1) were selected on ½ MS plates containing hygromycin. The initial *wildtype* transgene and 3 descending independent transgenic lines were obtained by Alexander Pfab (unpublished). To obtain homozygous lines, segregating lines in the T3 generation were selected. The *spt16-1* T-DNA insertion in the 5'UTR, the respective locus in the native *SPT16* and the complementing construct were validated by genotyping PCR (**Figure 21b**, Primers **Figure 21a**). Additionally, in lines which were identified to be homozygous for *spt16-1* and the respective construct by selection, the segregation of 8 plantlets was monitored via genotyping PCR to reconfirm double-homozygosity (**Supplementary Figure 2**). This led to three independent transgene *spt16-1* rescue lines each: *WT* (#1, #2, #3), *VAA* (#1, #2, #5) and *EDD* (#1, #2, #3)

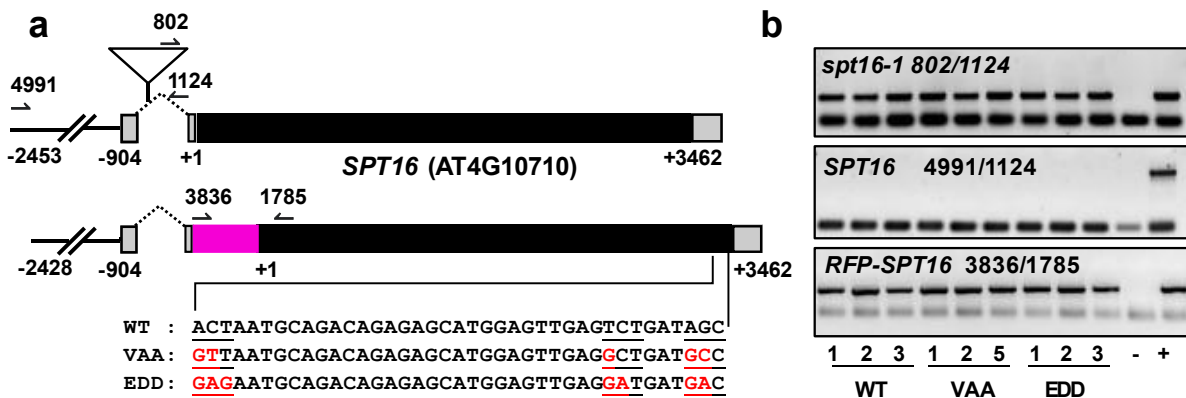


Figure 21 Generation of transgenic *Arabidopsis* cell lines expressing *SPT16* phospho-variants (a) Schematic illustration of *spt16-1* T-DNA insertion line and TagRFP-SPT16 variants: Wildtype (T1023, S1033, S1035), phospho-insensitive (V1023, A1033, A1035) and phospho-mimetic (E1023, D1033, D1035). The T-DNA insertion line *spt16-1* (SAIL_392_G06) is indicated as triangle. Primers for genotyping PCR are shown as arrows (Black bars = exons, dark grey bars = UTR, dotted lines = introns, red bars = TagRFP) (b) Genotyping PCR for T-DNA insertion *spt16-1* (upper panel), wild type *SPT16* (middle panel) and transgene (lower panel). Positive control (+): Upper panel = *spt16-1*; middle panel = Col-0; lower panel = transgene Plasmid. Negative control (-) = water

Next, the protein levels of the plasmid-derived TagRFP-SPT16 and the endogenous SPT16 were analysed in the generated *spt16-1* complementation lines with the priorly described SPT16 antibody (Duroux et al., 2004). Therefore, the nuclei of ~1g of 14-day old seedlings were isolated (**Figure 22**, upper panels). In agreement with prior work (Lolas et al., 2010), the downregulation of the endogenous protein in the *spt16-1* background can be observed (**Figure 22a**, lower panel, band e). In addition, a band with similar intensity than endogenous SPT16 in the Col-0 background appears, albeit with a slower migration pattern (**Figure 22a**, lower panel, band t). This is in line with the added molecular weight of the TagRFP and displays the good functionality of the added promoter. TagRFP-SPT16 protein expression could be observed in all 9 lines (**Figure 22b**, lower panel). Minor fluctuations can be explained by fluctuations in the loading of the nuclear protein extracts (**Figure 22b**, upper panel).

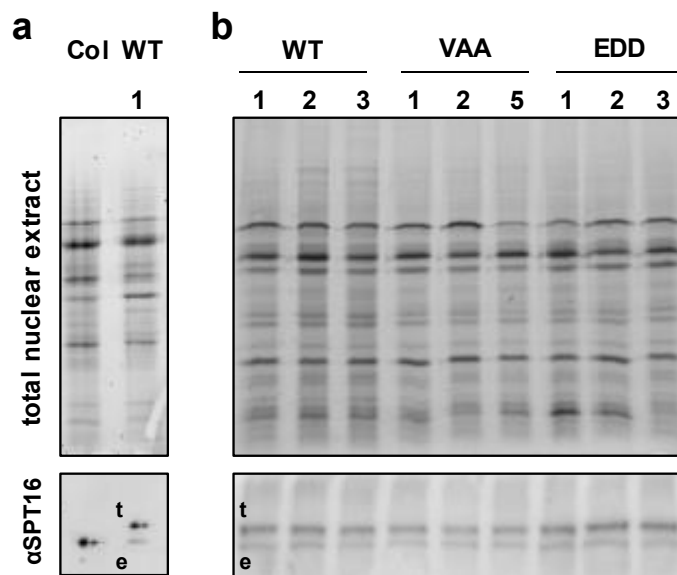


Figure 22 Immunoblot analysis of SPT16 phospho-variant complementation lines (a) Nuclear protein extracts of Col-0 and *spt16-1* TagRFP-SPT16_WT independent line 1 (b) Nuclear protein extracts of *spt16-1* TagRFP-SPT16 variants (Wildtype = WT, phospho-insensitive = VAA, phospho-mimetic = EDD). Total nuclear protein extracts are visualized with TCE stain (upper panel). α -SPT16 antibody with HRP-coupled secondary antibody and chemiluminescence detection reveals two distinct bands. e = endogenous SPT16; t = transgene SPT16 (lower panel). The difference in the migration pattern can be explained by the additional molecular weight of TagRFP. MW SPT16 = 120.6 kDa; TagRFP-SPT16 147.7 kDa

Transgene expression was confirmed by confocal microscopy (CLSM). Generally, the TagRFP signal was observable in nuclei over all tested tissues in all lines, here shown for roots (**Figure 23**, magenta). Next the validated lines were subjected to phenotypic analysis.

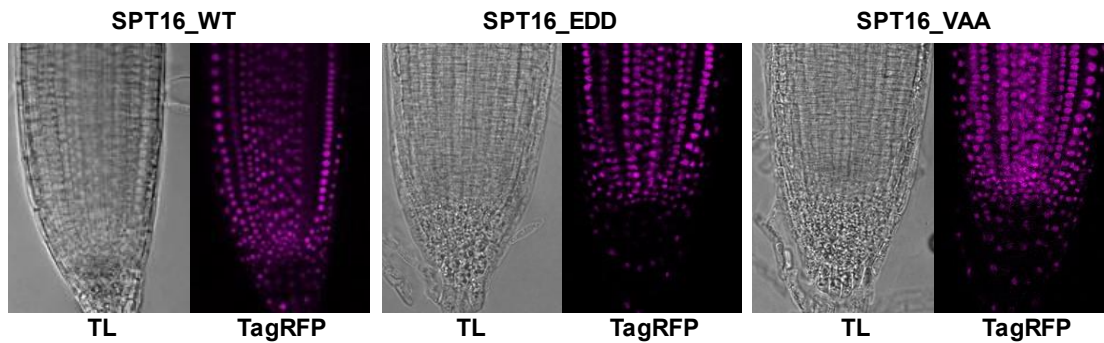


Figure 23 Different SPT16 phospho-variants localise to the nucleus. Root tips of one representative line *pSPT16:TagRFP-SPT16* of Wildtype (WT), phospho-mimetic (EDD) or phospho-insensitive (VAA) were subjected to confocal microscopy to investigate the TagRFP protein variants. Plants are 7 days old. Transmitting light (TL) next to TagRFP signal in cyan

2.4.5.2 Phenotypic analysis of SPT16 phospho-variants

spt16-1 is easily distinguishable from the wildtype (Col-0) by its phenotype: Its smaller in size, rosette leaves are uneven, it appears more bushy due to an increase of primary and secondary inflorescences and the seed set is severely decreased. This due to a huge number of aborted siliques. Siliques which are developed carry very little seeds. Additionally, the transition from vegetative to reproductive state happens early (Lolas et al., 2010).

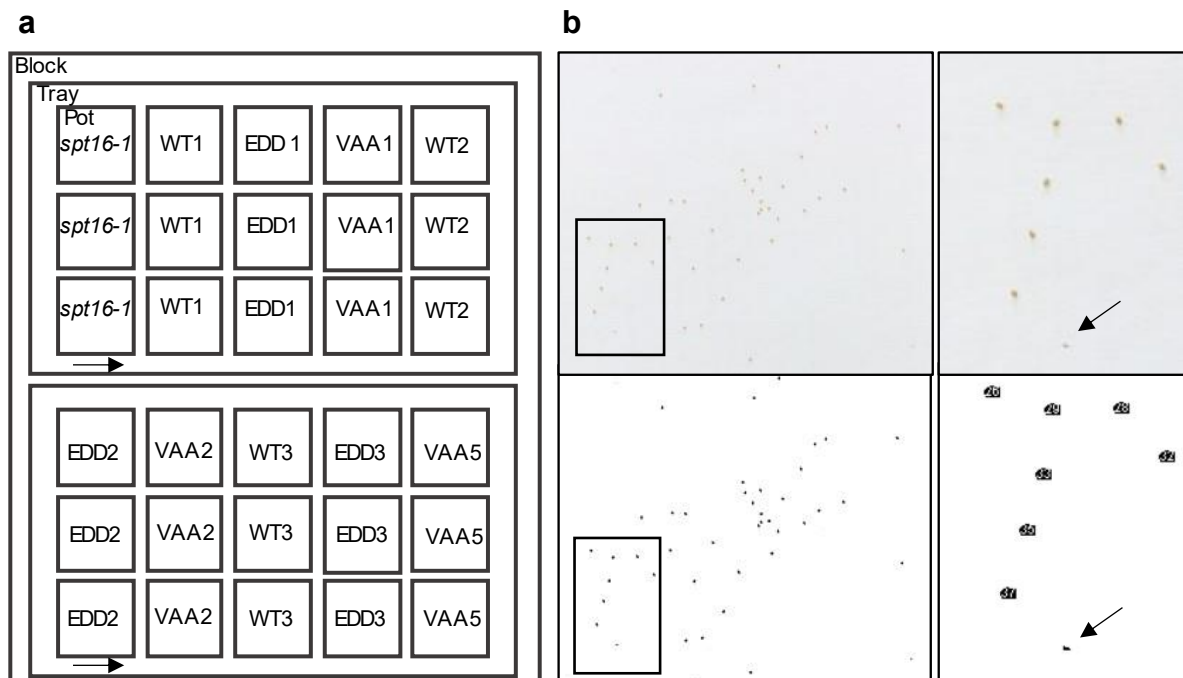


Figure 24 Experimental phenotyping setup (a) To avoid spatial influences (light, air circulation) during soil based phenotyping, the genotypes were arranged in 5 blocks, each containing 2 trays with 15 pots. Each block contained 10 genotypes (1x *spt16-1*, 3x3 *spt16-1* TagRFP-SPT16-variants) with 3 pots each. The respective

position of each genotype was varied by 1 position (black arrow) in the next block. Col-0 plants were grown on a separate tray (b) Macro development for automated seed counting with Image-J. Upper panel: Representative picture of seeds. Lower panel: Extraction of features. Right panels: Magnifications from left panel (rectangle). Impurities from seed purification are not counted (black arrow)

Here, plants were grown on soil under long day conditions to monitor these traits. To exclude any spatial influences like light or air circulation, the 3 independent lines for each SPT16 variant (*WT*, *VAA*, *EDD*) and *spt16-1* were arranged in 5 blocks (Figure 24a). The position of the respective genotype was varied in each block by 1 position and the blocks themselves were moved within the shelf every other day. For automated seed counting a macro was written in the software Image-J, counting seeds while excluding impurities (Figure 24b). The following measurements were carried out in three biological replicates (n=15) at timepoints where the respective trait would reach approximately its maxima (compare Boyes et al., 2001): Rosette diameter at day 21 after stratification (21 DAS; evaluation of vegetative growth), time of bolting and rosette diameter at bolting (transition from vegetative to reproductive state), height at day 42 and rosette diameter at day 42 (overall size), primary and secondary inflorescences at day 42 (bushiness), percentage of aborted siliques and number of seeds per pair of developed siliques (evaluation of seed set).

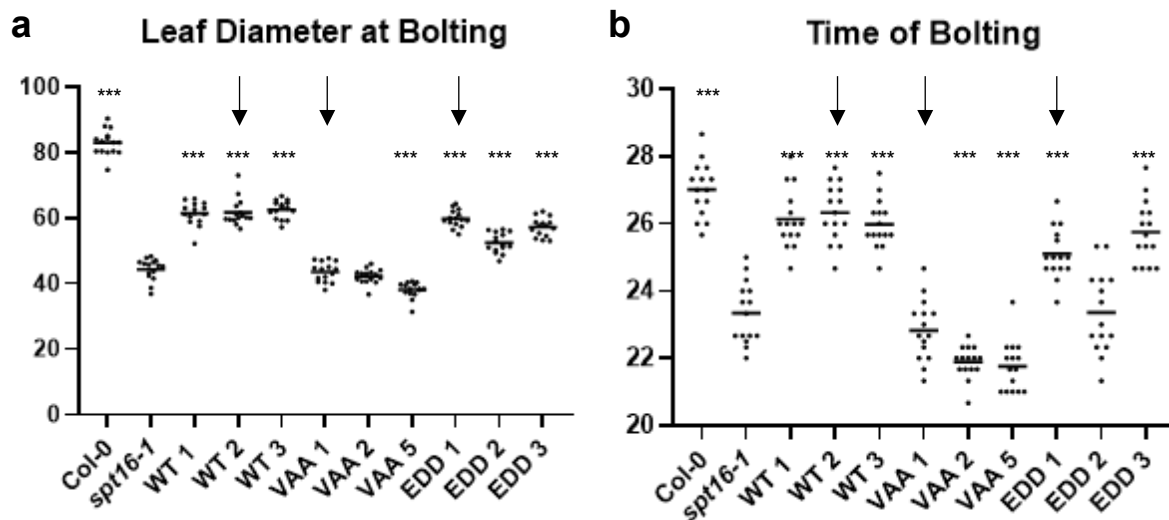


Figure 25 Phospho-insensitive SPT16 variants are unable to rescue the transition from vegetative to reproductive state. Plants were phenotypically analysed in comparison with Col-0 and *spt16-1* (a) leaf diameter at bolting [mm] (b) time of bolting (elongation of the first shoot) [d]. The data shown here comprises the measurements of 15 individual plants in three biological replicates. Data was analysed by one-way ANOVA and a multi comparisons Tukey's test comparing to *spt16-1* as a reference. The line in the scatterplot marks the average value. Asterisks indicate the outcome of the Tukey's test (p-value *** < 0.001)

The phenotypic analysis of *spt16-1* complementation lines revealed different degrees of growth defects in comparison with Col-0 and the *spt16-1* single mutant. Generally, all 3 lines of the respective phospho-variants group together, however some were slightly more affected than others (**Figure 25**), here shown at the example of bolting. To avoid false conclusions about the severity and to increase the readability, only the best rescuer in respect to Col-0 is shown from now on. The following lines were picked: *spt16-1 TagRFP-SPT16_WT* line 2 (= WT), *spt16-1 TagRFP-SPT16_VAA* line 1 (=Phos 0) *spt16-1 TagRFP-SPT16_EDD* line 1 (=Phos +) (**Figure 25**, arrows).

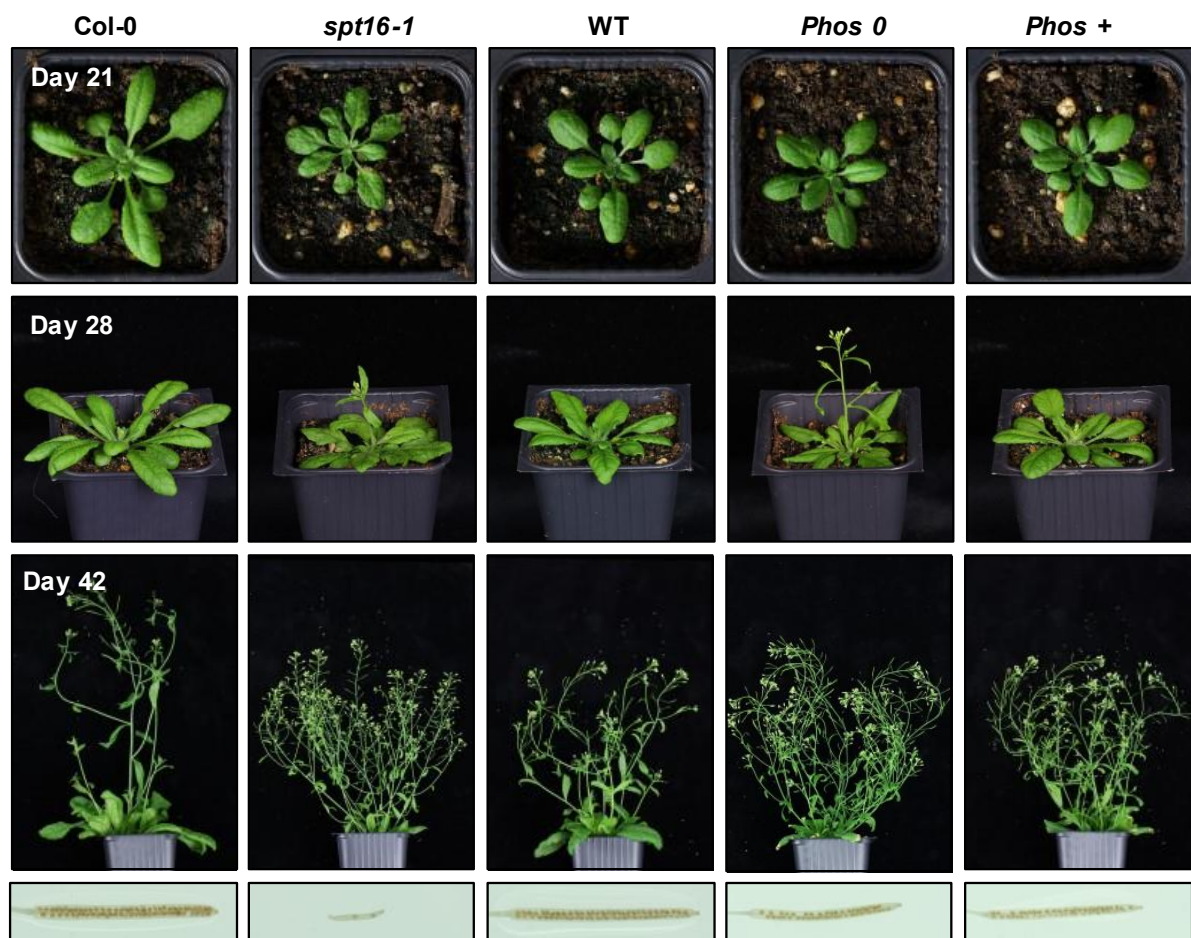


Figure 26 SPT16 Phospho-mutants display different degrees of defect. Phenotypical analysis of the *spt16-1* complementation lines in comparison to Col-0 and the single mutant *spt16-1*. Plants were grown under long day conditions. Representative individuals are shown at various developmental stages. Pictures were taken at 21 (upper panel), 28 (middle panel) and 42 (lower panel) days after stratification (DAS). Representative siliques were taken a 42 DAS (lowest panel). WT= *pSPT16::TagRFP-SPT16* line 2, Phos 0 = *pSPT16::TagRFP-SPT16_T1023V/S1033A/S1035A* line 1, Phos + = *pSPT16::TagRFP-SPT16_T1023E/S1033D/S1035D*

The WT-variant rescued the defects of *spt16-1* best, however vegetative traits like the rosette diameter at day 21 (**Figure 26** and **Figure 27a**) were still clearly affect compared to Col-0. In

consequence some reproductive traits like the diameter at bolting were also smaller (**Figure 25** and **Figure 26**). The time of bolting and the number of aborted siliques however were restored approximately to Col-0 levels (**Figure 25** and **Figure 27e**). The variant which mimicked an unphosphorylated state (*Phos 0*) was unable to rescue many of the defects observed in *spt16-1*. It had a tendency to bolt even earlier than *spt16-1* ((**Figure 25** and **Figure 26** second row) and did not rescue the final rosette diameter and the bushy appearance compared to *spt16-1* (**Figure 26** second row, **Figure 27d**).

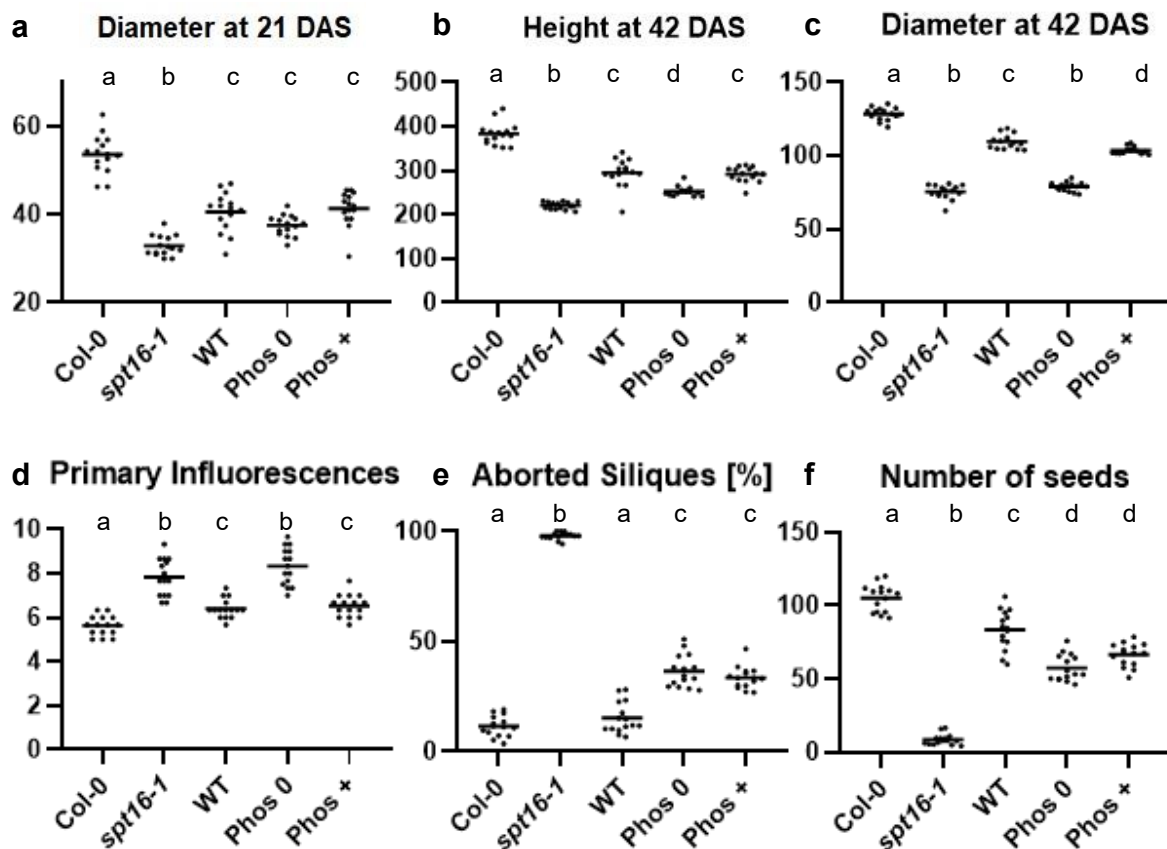


Figure 27 SPT16 Phospho-mutants display different degrees of defect. Plants were phenotypically analysed in comparison with Col-0 and *spt16-1* in the following parameters (a) Diameter [mm] 21 days after stratification (DAS) (b) Height [mm] at 42 [DAS] (c) Diameter [mm] at 42 DAS (d) number of primary inflorescences (e) Percentage of aborted siliques (f) Number of seeds in two representative, developed siliques. The data shown here comprises the measurements of 15 individual plants in three biological replicates. Data was analysed by one-way ANOVA and a multi comparisons Tukey's test. The line in the scatterplot marks the average value. Letters above the scatter indicate the outcome of the Tukey's test (p -value < 0.05)

In the phospho-mimetic variant (*Phos +*) many traits ranged intermediate between *WT* and *Phos 0*, however appeared more like the wildtype variant than *Phos 0* (**Figure 25-27**). All rescue constructs were able to restore the uneven leaves observed in *spt16-1* (**Figure 26**, first row) and

clearly reduce the percentage of aborted siliques (**Figure 27e**). The number of aborted siliques, and the actual number of seeds per silique were affected comparably in *Phos 0* and *Phos +* and restored best in the *WT* variant (**Figure 27f**). This phenotypic analysis shows that altering the SPT16 C-terminal charge change by phosphorylation has effects on the ability to rescue the *spt16-1* phenotype. The *WT* transgene, which can be either phosphorylated or unphosphorylated, rescued best, however could not restore Col-0 background appearance. Priorly, *spt16-1* rescued with untagged full-length SPT16 led to a similar, incomplete rescue of the phenotype (Lolas, 2008), indicating no major effects of the introduced *TagRFP*. *Phos +* shows similar effects as *WT* (although not as efficient) indicating that the interplay between phosphorylation and dephosphorylation is important. *Phos 0*, where no additional negative charge can be introduced via phosphorylation, generally rescues most traits worst. Additionally, it is incapable of rescuing the transition from vegetative to reproductive state, and even tends to increase the defect (**Figure 25**). Other defects, however like leaf architecture and silique development are partly compensated (**Figure 26**). In summary, the phenotypic analysis of the phospho-variants shows, that not all traits are affected equally. This might argue for a particular role of phosphorylation during certain aspects of transcription.

2.4.6 Phosphorylation of SPT16 plays a role in clearing nucleosome depleted regions

The absence of additional charge in the SPT16-AID had an impact on histone- (section 2.4.2) and nucleosome-interactions (section 2.4.3). Subsequently, the *Phos 0* variant rescues some of the defects of the *spt16-1* mutant poorly (section 2.4.4). The weaker histone interaction in *Phos 0* variant could lead to an accumulation of nucleosomes and a decrease of transcribing Pol II. In yeast it has been shown that H3, H4 and H2B display similar defects in a *spt16* knockout in ChIP-Seq experiments (Jeronimo et al., 2019). To have an indicator of nucleosome occupancy globally, H3 as a representative of the inner H3-H4 tetrameric core was subjected to ChIP-Seq experiments. Additionally, α -CTD-S2P, an antibody against the largest RNAPII subunit (NRPB1) phosphorylated at the CTD position Ser2, was ought to be included to map the influence of SPT16-AID phosphorylation on elongating Polymerase II. The obtained DNA was subject to Illumina Deep Sequencing. The experimental set-up was planned with the help of Uwe Schwartz (Computational Core Unit – Biology and Preclinical medicine).

Three biological replicates were grown on ½ MS plates, crosslinked with formaldehyde and quenched with glycine. Sonification lead to the desired fragment size between 100 and 300 bp (**Figure 28a**). Average ChIP efficiency over all genotypes (percentage of input) was ~ 4.2% for

H3, 0.3% for S2P and 0.1% for no antibody treatment (**Figure 28b**). PCR against an actively transcribed gene (*Actin8*) showed strong signal for H3 and the input. In line with measured ChIP efficiencies the PCR signal obtained for S2P was respectively smaller. Some signal, albeit less was observed for the mock control (**Figure 28c**). 20 ng of DNA were used for input and H3 libraries, <5 ng for S2P libraries. Adaptor ligated DNA was size selected and enriched via PCR. Quality control of the libraries via Bioanalyzer (**Figure 28d**) was performed at the Kompetenzzentrum Fluoreszente Bioanalytik (KFB) as well as Illumina Deep Sequencing.

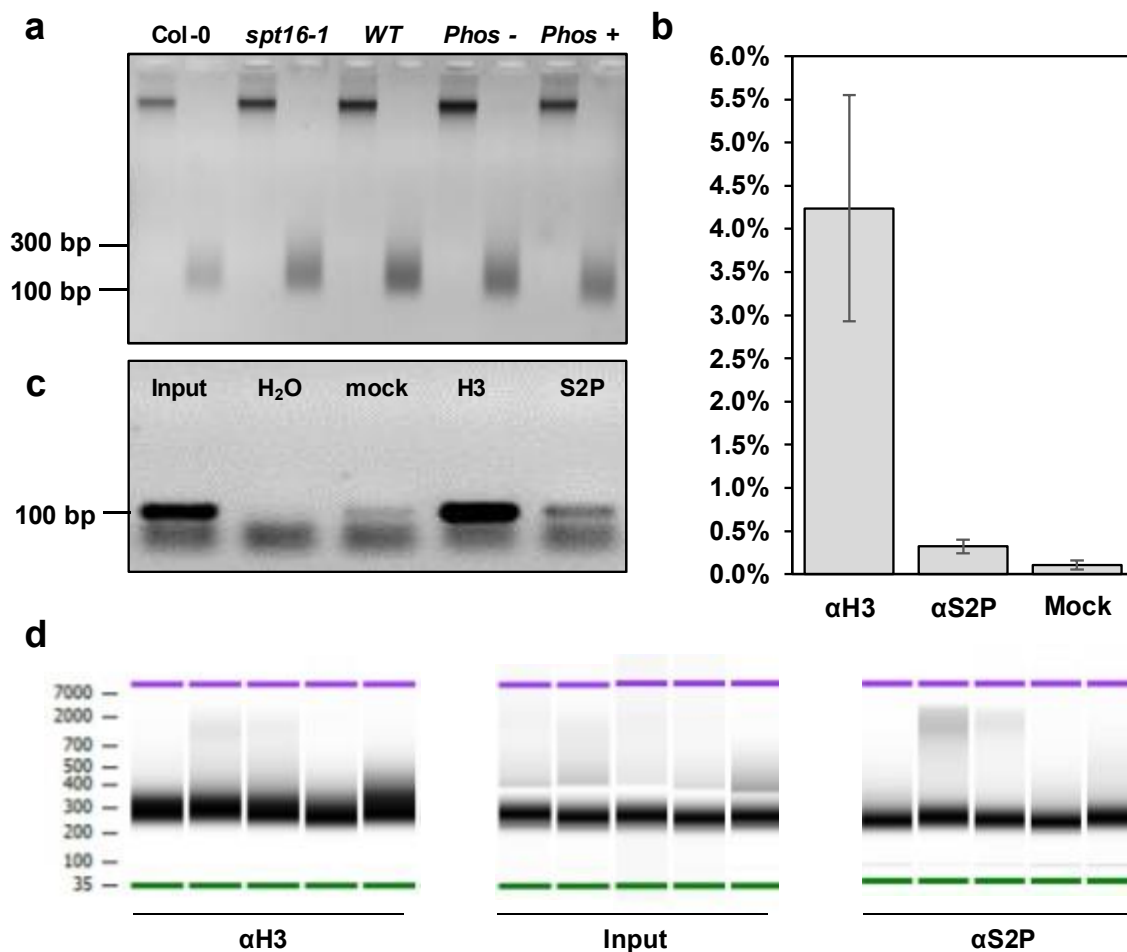


Figure 28 ChIP and Library Quality control (a) Shearing of genomic DNA. Before sonification and after sonification with 10 cycles 30''/30'' on/off cycle time next to each other (b) Average ChIP efficiency with α H3 (abcam ab1791), α S2P (abcam ab5095) and mock treatment (c) representative PCR targeting a Pol II transcribed gene: actin (*ACT8*). A 1/100 dilution of the input was used for PCR reaction (d) Gel like image of representative libraries (Bioanalyzer). Bioanalyzer runs were performed at the Kompetenzzentrum Fluoreszente Bioanalytik (KFB)

Depending on the quality of the size distribution of the bioanalyzer runs 3-5 libraries were sequenced per antibody and genotype. All bioinformatic analysis concerning ChIP Seq data was performed by Simon Obermeyer with support of Uwe Schwartz (Computational Core

Unit), focusing on 3 libraries per genotype. For differential analysis based on the gene expression level, the genome was divided into quartiles, determined by RNASeq of 6 day old Col-0 seedlings (Obermeyer unpublished). Unfortunately, the obtained dataset for S2P did not show the typical enrichment towards the transcription end site (compare Antosz et al., 2020, **Supplementary Figure 3**). Hence, this does not allow for global conclusions and all further analysis was discontinued for the S2P dataset. The general pattern of the obtained H3 ChIP-seq data was in line with published work (Zhang et al., 2015), showing nucleosome depleted region (NDRs) upstream of the transcription start site and stronger nucleosome positioning depending on the gene expression level (**Figure 29**). For quality control, a PCA analysis was performed. The respective replicates of the genotypes grouped together in a principal component analysis (**Supplementary Figure 4a**). Generally, the overall H3 pattern is intact in all genotypes (**Figure 29**), however clear differences appear when comparing the observed H3 occupancies normalized to H3 Col-0 reads (**Figure 30**)

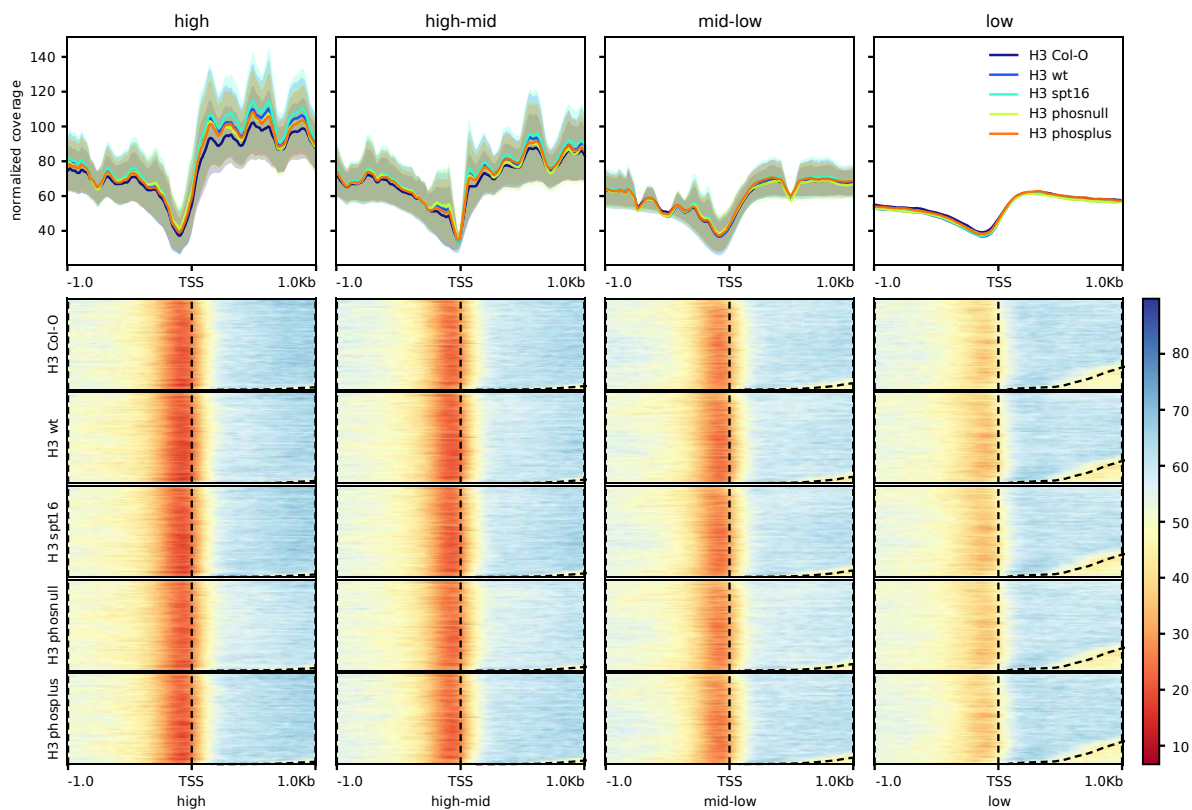


Figure 29 Average H3 distribution over Pol II expressed genes. Pol II transcribed genes were split in quartiles depending on their expression level: High, high-mid, mid-low and low expressed genes. The list was created by RNA seq of 6 day old seedlings (Obermeyer unpublished). Bioinformatic analysis was performed and figures were created by Simon Obermeyer. TSS = Transcription start site

No major differences can be observed between *spt16-1*, *spt16-1 pSPT16:SPT16-WT* and *spt16-1 pSPT16:SPT16-Phos +*. Slight differences could be interpreted as fluctuations around Col-0 levels (**Figure 30**, orange, light blue and dark blue). However, *spt16-1 pSPT16:SPT16-Phos 0* shows a clear increase of H3 levels at the nucleosome depleted region (NDR) upstream of the TSS and a decrease of H3 occupancies in the gene body (**Figure 30**, green, fourth row). These effect was present throughout all levels of gene expression, (**Figure 30**, row 1 and 4, panels left to right), however the higher the gene expression, the higher the average H3 accumulation at the NDR and the higher the decrease of H3 occupancies in the gene body. PCA restricted to the respective region in the NDR shows a clear effects depending on the respective genotype, with strongest deviations for *Phos 0* (**Supplementary Figure 4b**).

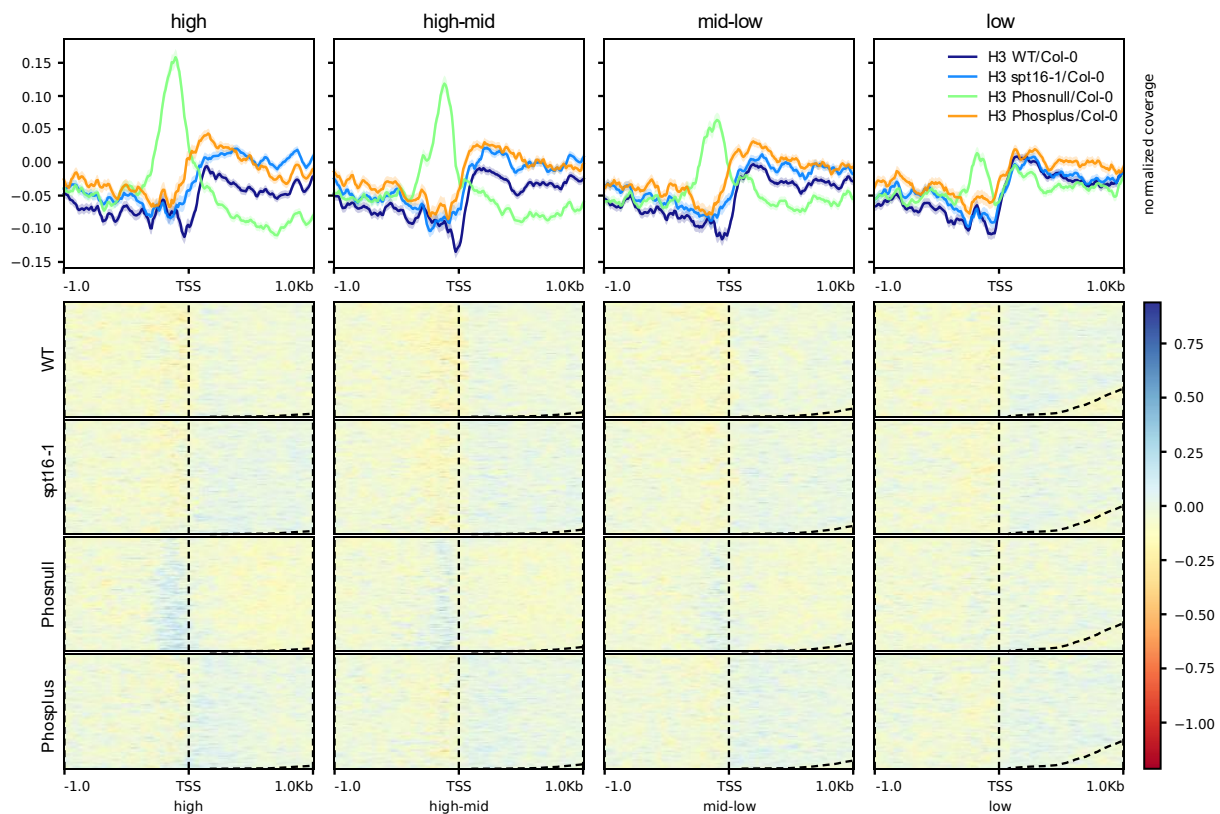


Figure 30 The SPT16 phosphorylation insensitive variant has an impact in clearing the nucleosome depleted region (NDR) Genome-wide occupancy profiling of H3 using ChIP-seq. Gene-averaged profiles for H3 around TSS normalized to Col-0. Pol II transcribed genes were split in quartiles depending on their expression level: High, high-mid, mid-low and low expressed genes. The list was created by RNA seq of 6 day old seedlings (Obermeyer unpublished). Bioinformatic analysis was performed and figures were created by Simon Obermeyer

In a yeast *spt16* knockout, other histone variants like H2B and H4 were comparatively regulated than H3 (Jeronimo et al., 2019) and hence, H3 shown here can be seen as a proxy for the nucleosome. Generally, genes with higher transcript level tend to have lower nucleosome occupancy in NDRs (Liu et al., 2015). Differential MNase digestion in *Arabidopsis* revealed a

labile -1 nucleosome upstream of the TSS nucleosome, which typically occurred in the lowest quartile of expressed genes (Pass et al., 2017). Here, the additional peak for H3 in a 300 bp window upstream of TSS could be in agreement with a potential fragile -1 nucleosome, however it is more pronounced with the strength of transcription, implicating that phosphorylation of SPT16-AID is also important for clearing the -1 nucleosome in highly transcribed genes.

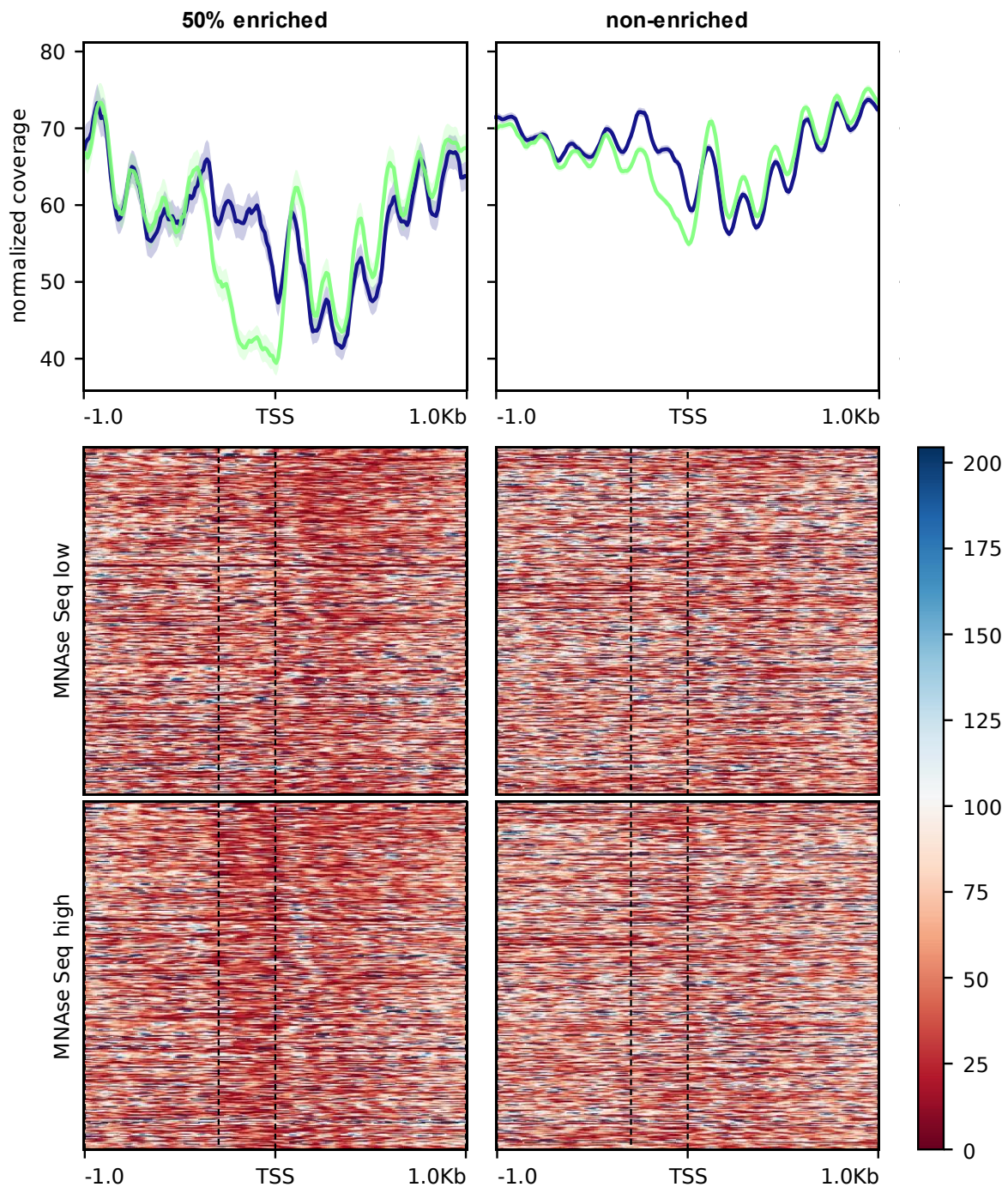


Figure 31 A subset of genes shows enriched H3 occupancy in the NDR and associates with a sensitive -1 nucleosome. Genes with enriched H3 signal in the NDR in *spt16-1 pSPT16:SPT16 Phos 0* show a differential

pattern depending on the type of MNase digest. **Upper Panel:** High MNase digest (green line) compared to low MNase digest (blue line) in strongest affected NDRs (left) compared to unaffected NDRs (right) **Middle Panel:** Low MNase digest. **Lower Panel:** High MNase digest. In genes with enriched H3 signal in the NDR, Low MNase digested chromatin displays no signal depletion in upstream of TSS, in contrast to highly MNase digested chromatin. This indicates the presence of sensitive, labile -1 nucleosome. To obtain differentially H3 occupied NDRs, the average value of *spt16-1 pSPT16:SPT16 Phos 0* H3 reads in the region upstream of TSS (-300 to 0) was normalized with the respective H3 reads in *spt16-1 pSPT16:SPT16 WT*. Significant hits ($p < 0.05$), which are at least 50% enriched ($Phos\ 0\text{-NDR} / WT\text{-NDR} \geq 150\%$; $n=648$) were compared to genes, which are not enriched in signal ($Phos\ 0\text{-NDR} / WT\text{-NDR} \leq 100\%$; $n=17156$). The lists of genes were used to perform cross-correlation with differential MNase digest (Pass et al. 2017). Bioinformatic analysis was performed and figures were created by Simon Obermeyer.

To address this further, the region 300 bp upstream of the transcription start site was analysed, by averaging the H3 signal obtained from -300 to 0 in respect to TSS and normalizing the obtained value to the WT transgene. A total 1593 genes showed > 50% increase of average H3 signal compared to the WT control sample. In contrast only 4 genes showed a < 50% depletion in respect to WT. 3 biological replicates were used to perform statistic evaluation. 648 genes remained showing a p-value <0.05 (Supplementary Data Table 14), displaying the most robust H3 enriched genes of *Phos 0* compared to the *WT* transgene. These 648 genes were cross-correlated with a dataset of differentially MNase digested chromatin in *Arabidopsis* cell culture.: A high digest level (**Figure 31**, upper panel, green line), extracting the most stable positionings and a low digest level (**Figure 31**, upper panel blue line), allowing the detection of sensitive features which are otherwise obscured, like fragile -1 nucleosomes (Pass et al., 2017). Genes which showed no enriched H3 signal ($Phos\ 0/WT$ signal ration <1) were used as a control (**Figure 31**, right panels). Comparing high and low MNase digested profiles, genes from the extracted list showed a bigger discrepancy in the profiles (**Figure 31**, left panels) compared to the control (**Figure 31**, right panels), and hence were also more likely to contain a sensitive, fragile nucleosome (**Figure 31**, first row).

Many regulatory elements are in the region upstream of TSS, like the TATA box (~-30 bp upstream of TSS) or proximal promoters (up to -150 bp upstream of TSS) (Hetzl et al., 2016). A fragile -1 nucleosome at highly transcribed genes could have regulatory functions, as generally, nucleosomes cover promoters and compete with transcription factors (Cairns, 2009). To address which proximal promoter elements are most affected, the gene-list of the most robust H3 enriched genes was used to perform motif enrichment with HOMER (Heinz et al., 2010). Particularly, the TCP/PCF motif (36.0% in NDR enriched genes vs 13.2% NDRs of all genes), the E-box (20.6% vs 10.5%) and “unknown” (11.2% vs 3.7%) were overrepresented

(**Figure 32a, Supplementary Figure 5**), compared with prior global promoter analysis (Hetzel et al., 2016). In line with the ChIP material (14-day-old seedlings) and a role in active gene transcription, proximal promoters TCP/PCF and E-Box are important during seedling development (Hetzel et al., 2016). Additionally, Gene Ontology (GO) analysis was performed (**Supplementary Figure 6**) with the tool AgriGO (Tian et al., 2017) to determine biological process which are particularly affected by the inability of AID phosphorylation. This resulted in the end-nodes: RNA metabolic process (GO:0016070; $p= 0.00025$), cofactor biosynthetic process (GO:0051188; 0.00014; node not shown) and response to temperature stimulus (GO:0009266; $p=0.0258$) (**Figure 32b**).

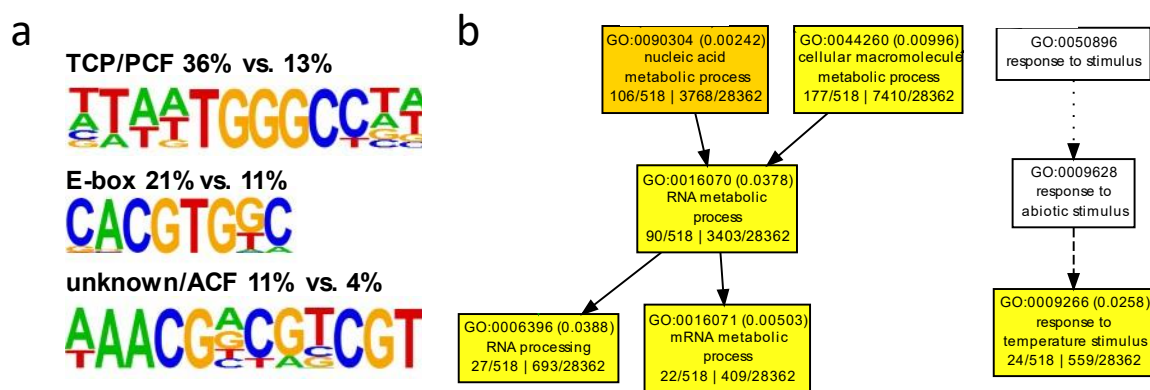


Figure 32 Motif-enrichment and GO analysis display broad regulatory functions and role in stress response for *Phos 0* affected genes (a) motif enrichment with homer (Heinz et al. 2010). Abundancy compared to motifs found in global promoter analysis: TCP/PCR and E-box are conserved among plants and important during seedling development. Unknown shows similarity to “Activator of Stress Genes 1” in yeast (Hetzel et al. 2016) (b) Gene Ontology (GO) analysis was performed using the single enrichment analysis (SEA) of AgriGO (Tian et al. 2017). Motif and GO-analysis was performed with 648 genes which were significantly ($p<0.05$) upregulated ($\geq 50\%$) in there H3 abundance in the NDR (-300 to 0 bp of TSS) of *spt16-1 pSPT16:SPT16 Phos 0* compared to *spt16-1 pSPT16:SPT16 WT*. Bioinformatic analysis of (a) was performed Simon Obermeyer. Only promoters discussed in Hetzel et al. 2016 and selective GO-terms are shown.

A closer look at the single genes level (**Figure 33**) shows, that particular affected genes can indeed be found from high to low expression level (**Figure 33**, panel left to right, RNAseq lane) and that the presence of the extra peak correlates with the presence of a sensitive -1 nucleosome (**Figure 33**, black arrows). This can be observed in mild MNase digest conditions, however is absent when treated with regular MNase digest conditions (**Figure 33**, light green vs. dark green) in agreement with the global analysis (**Figure 31**). This peak is present in the *phospho-insensitive* SPT16 variant (**Figure 33**, black) however absent in both the *WT* variant and the *Phos +* variant (**Figure 33**, blue and red), highlighting the important role of SPT16 AID

phosphorylation in clearing sensitive -1 nucleosomes. The potential role in heat stress response determined by GO-term enrichment (**Figure 32b**), can be seen by the first gene example (*AT5G02500*, **Figure 33** first panel), which displays *HSP70-1*. *HSP70* is a well-studied FACT dependent example in *drosophila*, where a role for FACT at the respective promoter has been shown (Saunders et al., 2003).

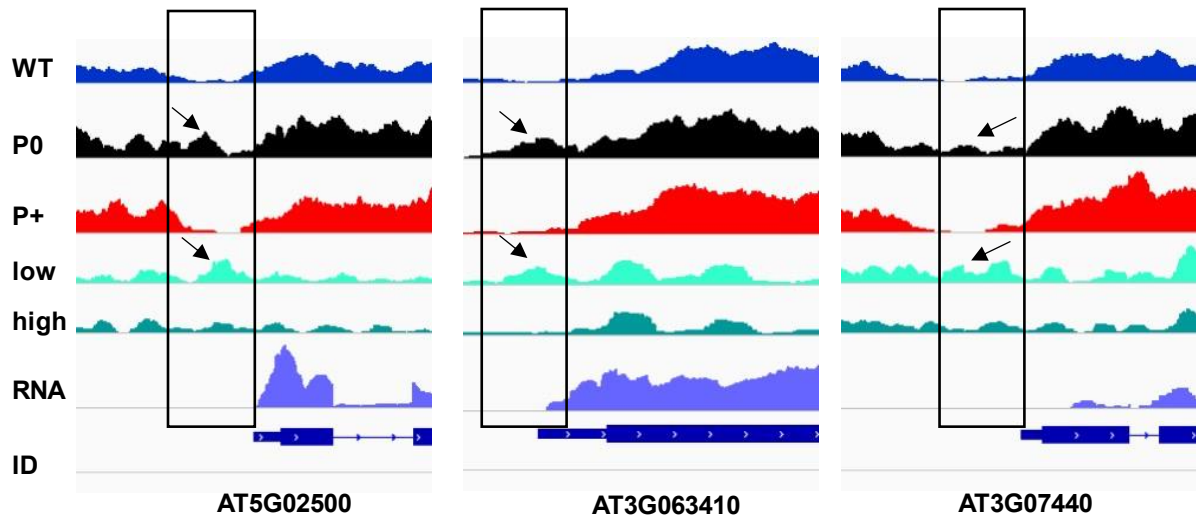


Figure 33 Impact of H3 occupancy at the single gene level in SPT16 phospho-variants. Differentially H3 occupancy shown at the region around TSS. Black Box indicates a 300 bp window upstream of TSS. Black arrows indicate an extra peak present in the phospho-insensitive mutant and the differentially low digested MNase-seq dataset obtained from cell culture (Pass et al. 2017). Reads are visualized by integrative Genomics Viewer (IGV). From top to bottom: H3 reads *spt16-1 pSPT16:SPT16-WT* (WT, blue), H3 reads *spt16-1 pSPT16:SPT16 Phos 0* (P0, black), H3 reads *spt16-1 pSPT16:SPT16 Phos +* (P+, red), differential MNase digest of *Arabidopsis* cell culture - mild conditions (low, bright green), differential MNase digest of *Arabidopsis* cell culture - normal conditions (high, dark green), RNASeq reads of 6 day old Col-0 seedlings (RNA, light blue), Gene Model (ID). RNAseq data was obtained from Simon Obermeyer (unpublished), Differential MNase-seq data was published in (Pass et al. 2017)

In summary: The SPT16 AID is modulated by phosphorylation to increase its respective binding properties. This plays an important role in clearing the NDRs of fragile -1 nucleosomes and subsequently reveal regulatory binding sites like proximal promoters. This, together with a slight decrease of H3 in gene body (**Figure 29**), shows that SPT16 and particularly phosphorylation of the SPT16 AID is needed for potentially linking initiation to elongation.

2.5 Acetylation of SSRP1 BID and HMGBbox

After taking a closer look on the role of the phosphorylation of SPT16-AID a second focus will be laid on the regulatory role of acetylation on the BID (K539Ac, K549Ac) and the HMGBbox of SSRP1 (K594Ac, K599Ac; **Table 6**, yellow highlights). The positively charged BID – containing the NLS – and the HMGBbox participate in the DNA binding mediated by SSRP1 (Aoki et al., 2020). To my knowledge, no study has focused on the role of acetylation of SSRP1. However, HMGB type proteins have been shown to be acetylated (Malarkey and Churchill, 2012), displaying various effects. For example acetylation of HMGB1 at two specific sites before the first alpha helix, led to a decrease in DNA binding (Assenberg et al., 2008). Additionally, it was shown that hyperacetylation of HMGB1 redirects its subcellular localisation from nuclear towards the secretory pathway (Bonaldi et al., 2003). NLS (nuclear localisation sequence) are typically of basic nature (Boulikas, 1994), which get neutralized by acetylation. K-acetylation might therefore have an impact on DNA binding and modifying the nuclear localisation. These hypotheses were evaluated here by studying the effects of SSRP1-BID- and SSRP1-HMGBbox- acetylation with an initial focus on potential writers and erasers of the acetylation

Table 6 PTMs modifying SSRP1

Modification	# Spectra	Sequence	Domain	Protein
K539ac	5	SKGLPPKRK K TVAADEGS	BID/NLS	SSRP1
K549ac	17	VAADEGSS K RKKPKKKK	BID/NLS	SSRP1
K594ac	12	GIAFGEV GK VLGDKWRQ	HMGBbox	SSRP1
K599ac	3	EVGKVL GDK WRQMSADD	HMGBBox	SSRP1

2.5.1 Putative KDACs

In *Arabidopsis* there are 18 KDACs (Lysine deacetylases) in 3 families: RPD3-like (11 members), HD-tuin (4 members) and sirtuin (2 members) (Hollender and Liu, 2008). Cross-referencing of the two independent AP-MS FACT datasets (Supplementary Data Table 6 and 7, section 2.1 and Supplementary Data Table 11, Holzinger 2015) showed hits for all 4 HD-tuin family members (**Table 7**). HDT1 and HDT2 were present in both datasets. Please note: Although HDT2 was on the empty GS list of the PTM datasets (Holzinger, 2015), it showed an average mascot score of 97 in compared to an average score of 282 in in the SSRP1 dataset and 385 in in the SPT16 dataset and will be considered here, due to the increase in mascot score in a more complex sample. Additionally, HDA19 -a RPD3 homologue – is present in the PTM datasets together with its adaptor SAP18 (**Table 7**).

Table 7 Putative KDACs found in Shotgun Proteomic FACT datasets \emptyset = no rank assigned; factor is present in the empty GS-list

SSRP1-GS		SPT16-GS		SSRP1-GS PTM		SPT16-GS PTM				
Rank	Score/#IPs	Rank	Score/#IPs	Rank	Score/#IPs	Rank	Score/#IPs			
		27	507/2	87	283/3	94	269/3	HDT1	AT3G44750	HDT
22	380/3	30	453/3	\emptyset	282/3	\emptyset	385/3	HDT2	AT5G22650	HDT
10	714/3	9	1178/3					HDT3	AT5G03740	HDT
25	330/3	14	878/3					HDT4	AT2G27840	HDT
						143	150/3	HDA19	AT4G38130	RPD3
				64	256/3	69	501/3	SAP18	AT2G45640	

The association of HDT1-4, HDA19 and SAP18 with SSRP1 was tested in Y2H and FRET experiments. SSRP1/HDT1-4, SSRP1/HDA19 and SSRP1/SAP18 combinations and vice versa were co-transformed into AH109 cells and selected on double dropout plates (DDO). Interaction was evaluated by growth on quadruple dropout plates (QDO). No growth was observed for all SSRP1/HDT1-4, SSRP1/HDA19 and SSRP1/SAP18 combinations (**Supplementary Figure 7**). Additionally, the protein-protein interactions of the detected KDACs and SSRP1 were validated by Förster Resonance Energy Transfer (FRET). FRET is a distance dependent process where energy is transferred from an excited fluorophore (the donor) to another fluorophore (the acceptor). This can be used to measure close proximity (<10 nm) between donor and acceptor and works best if both are positioned within a distance where half the excitation energy of the donor is transferred to the acceptor (=Förster radius) (Sekar and Periasamy, 2003). A common way to evaluate obtained data is hereby to look at the efficiency of the FRET experiment which has been used as a tool to estimate the distance between donor and acceptor (Tsien et al., 1993). Here, the donor was eGFP_SSRP1 and the acceptor was mCherry fused to the respective KDAC. A fusion protein containing eGFP-NLS_mCherry served as positive control; the donor (eGFP_SSRP1) together with mCherry-NLS was used as negative control. All constructs were under the control of the 35s promoter. The FRET assay was priorly optimized and plasmids driving the controls as well as eGFP_SSRP1 were readily available (Pfab, 2017). Positive, negative and donor acceptor pairs were transiently expressed in *N. benthamiana* leaves via *Agrobacterium*-mediated transformation. mCherry fusions HDT1-3 localized mainly to the nucleolus, while HDT4 localized to the nucleoplasm (**Figure 34a**), in line with priorly published work (Zhou et al., 2004). HDA19 localised to the nucleoplasm, excluding the nucleolus, like shown before (Chen et al., 2019b) similar to its adaptor SAP18 (**Figure 34a**). For eGFP-SSRP1 fusion proteins two different populations were observed. The by far biggest portion localised to the nucleus, excluding the nucleolus, in line

with its association with Pol II. On rare occasions, subcellular localisation of SSRP1 would change from the nucleoplasm to the nucleolus (**Figure 34a and b**). By bleaching of the acceptor, the positive control eGFP-NLS-mCherry showed an increase in donor signal (**Figure 34b**, first panel, yellow arrow), confirming the validity of the assay as well as the negative control, where the signal pre-bleach was comparable to the signal post bleach (**Figure 34b**, second panel). This is reflected in an average FRET efficiency of ~24% and 1.2%, respectively (**Figure 34c, d**)

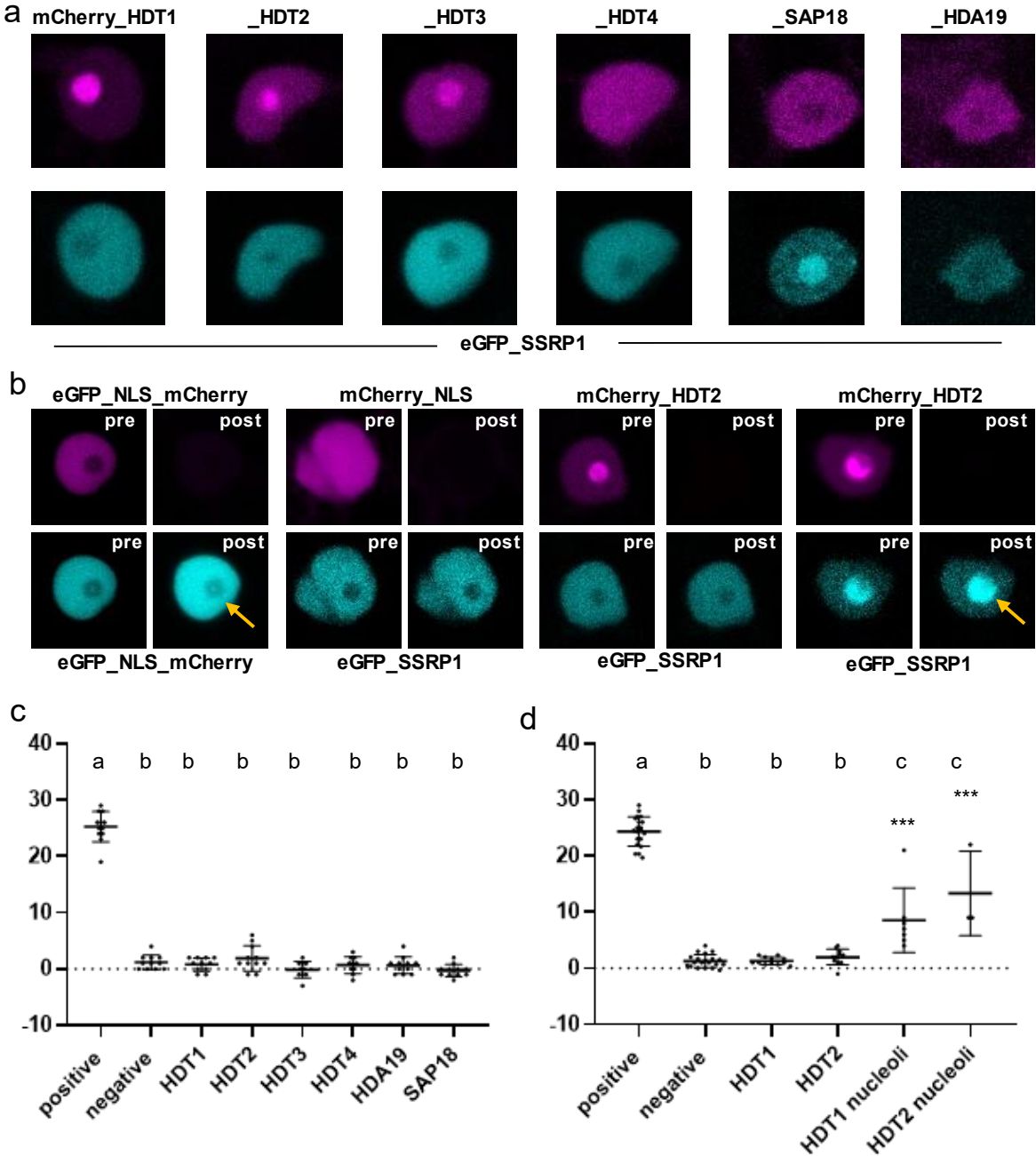


Figure 34 FRET of SSRP1 with KDACs (a) Transformed tobacco epidermal cells; Upper panel: Subcellular localisation mCherry-KDAC fusion proteins (magenta). Lower Panel: Corresponding eGFP-SSRP1 localisation (cyan) **(b)** Exemplary Acceptor-Photo Bleaching experiments pre- and post-bleach: Positive control

(eGFP-NLS_mCherry; first panel), negative control (eGFP_SSRP1/mCherry NLS; second panel). mCherry-HDT2/eGFP-SSRP1 (third and fourth panel). Representative examples are shown for both controls and the interaction. (c) FRET efficiencies [%] of ~10 nuclei each (d) FRET efficiencies [%] over 3 replicates. Data was analysed by one-way ANOVA and a multi comparisons Tukey's test. Letters above the scatter indicate the outcome (p-value < 0.05).

When eGFP_SSRP1 localized to the nucleoplasm, no FRET was observed for all KDACs (**Figure 34c**), exemplarily shown for HDT2 (**Figure 34b**, third panel,). In the rare occasions that SSRP1 localized to the nucleolus an increase of donor signal was observed for HDT1 and HDT2 (**Figure 34b**, fourth panel, **Figure 34d**). SSRP1 localized rarely to the nucleolus: Over 3 replicates only 7 nucleoli for HDT1 and 3 for HDT2 were observed where both, donor and acceptor colocalized in nucleoli. However, this led to a change in FRET efficiency from ~1.5% (1.2% for the negative control) to 8.7% for HDT1 and 13.3% for HDT2 (**Figure 34d**), showing that both fluorophores were in proximity when co-localising, indicating a possible direct interaction.

2.5.2 Putative KATs

In *Arabidopsis* there are 12 KATs (Lysine acetyl transferases) in 4 families (Pandey et al., 2002). Vice versa prediction of the *in vivo* detected acetylation sites (**Table 6**) with the tool ASEB (Wang et al., 2012), shows that in principal two families of KATs can account for all 4 detected acetylation sites: GNAT and CBP (GCN5-related N-acetyltransferases family; CREB-binding protein family). By cross-referencing the SSRP1 and SPT16 datasets derived by LC-MS/MS (Supplementary Data Table 6, 7 and 11) no members were found for CBP, however one SPT16 replicate showed GCN5, the defining member of the GNAT-family (Supplementary Data Table 11) making GCN5 a good candidate to write the respective acetylation. To evaluate a putative stable interaction of SSRP1 with GCN5, the proteins were tested by Y2H and FRET. No positive interaction was found in either assay (**Supplementary Figure 8**). Further subunits of the SAGA complex present (TAF10, TAF12, Supplementary Data Table 11, Holzinger 2015) were not tested. Next the potential effects of lysine acetylation were tested by introducing acetylation mimicking amino-acid substitutions and evaluate its DNA binding capacity.

2.5.3 Acetylation mimicking amino acid substitutions affect the binding of linear DNA

SSRP1 (Structure specific recognition protein 1) has been identified as a protein which specifically binds to distorted DNA (Bruhn et al., 1992). Ever since it has been widely established, that SSRP1 binds preferentially to bent or kinked DNA (Gurova et al., 2018). To

test the affinity of the SSRP1_ BID-HMGbox to linear and four-way junction DNA (4WJ) an electrophoretic mobility shift assay (EMSA) was set-up. The truncated BID-HMGbox domains (aa 516-630, **Figure 35b**) were purified via two step purification (**Figure 35a, c**) leading to a pure protein (**Figure 35c**). The desalted and concentrated protein was verified via MALDI-TOF (**Figure 35d**). The initial vector was modified via overlap extension PCR to mimic the priorly detected acetylations to either alanine or glutamine (Matsuzaki et al., 2005). While both substitutions are used to mimic acetylations, Alanine substitutions mimic the charge of acetyl-lysine, whereas Glutamine is ought to mimic charge as well as steric dimension (He et al., 2013). The following combinations were introduced to either mimic the acetylations in the BID (K539/K549A, K539Q/K549Q), the HMGbox (K594A/K599A, K594Q/K599Q) or both (4xA, 4xQ)

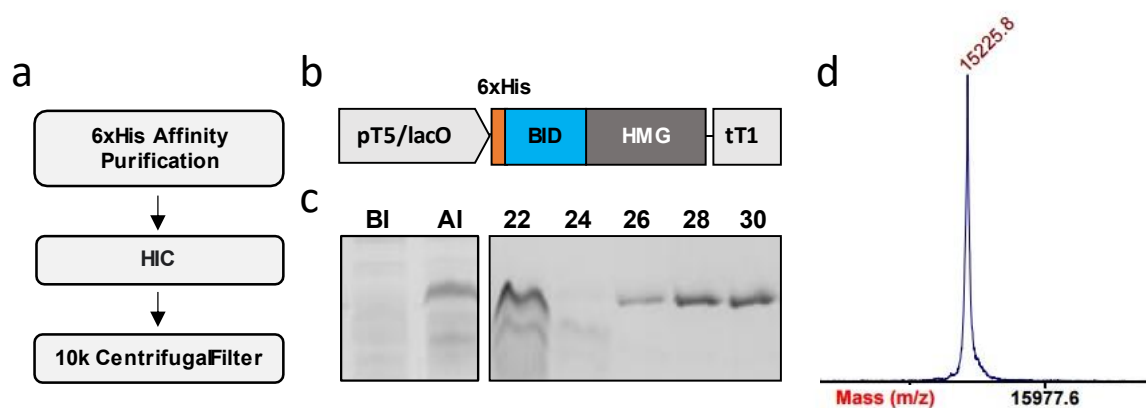


Figure 35 Two-step purification of recombinant 6xHis-BID-HMG proteins (a) Overview of the two-step chromatography with subsequent concentration and dialysis via centrifugal filter units. 6-His affinity purification was performed in batch mode, Hydrophobic interaction chromatography (HIC) on the column (b) Schematic illustration of the pQE9 vector driving SSRP1 BID-HMG expression. BID (blue aa 516-557), HMGbox (grey, aa 557-630) (c) Left panel: Before induction (BI) and after 4h of induction (AI) with 1 mM IPTG. Right panel: Fractions 22-30 of HIC (d) Quality control via MALDI-TOF: The expected MW is 15.226 Da

The respective combinations were purified as described above via two step affinity purification (**Figure 36 a, b**). Cloning and protein purification of some Lysine to Alanine variants were realized with the help of Clemens Kiefhaber in his Bachelor's thesis (Kiefhaber, 2016).

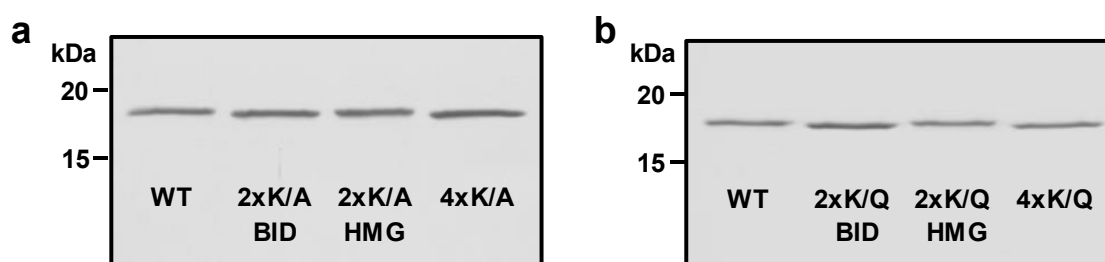


Figure 36 Final products of two step affinity purification of SSRP1_BID-HMGbox variants (a) Lysine to Alanine variants (b) Lysine to Glutamine variants. The different variants contained the following aa (-substitutions): WT (K539, K549, K594, K599), 2x K/A BID (K539A, K549A), 2x K/A HMG (K594A, K599A), 4xK/A (K539A, K549A, K594A, K599A), K/Q respectively

To test the binding of BID-HMG variants to DNA, increasing concentrations of the proteins (0-800 nM) were incubated with either the four-way junction DNA fragment or the linear control fragment, which contains the same sequence but can anneal to a double strand instead of a cruciform (**Figure 37a, b**, first panel). The formation of protein/DNA complexes was analysed by native gel electrophoresis and stained in 0.01% (v/v) ethidium bromide solution. Binding of BID-HMG to the DNA was observed for all variants and monitored via the disappearance of the unbound, free DNA band.

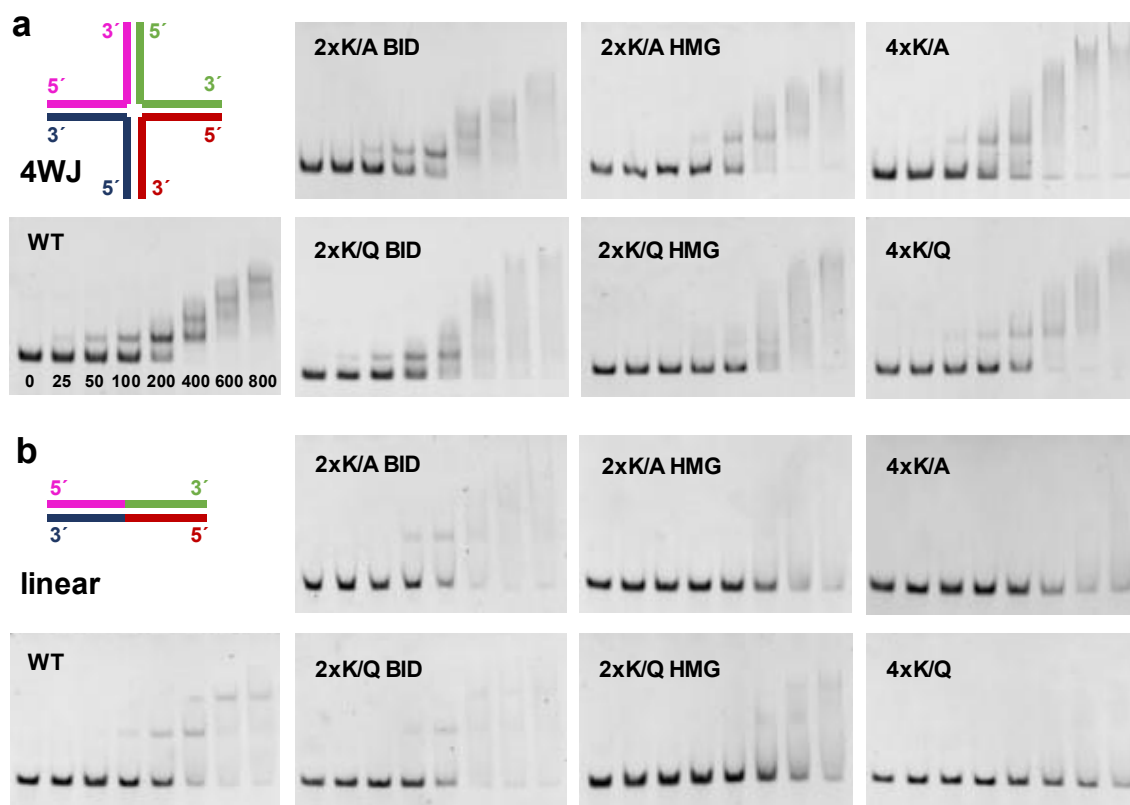


Figure 37 Acetylation mimetic amino acid substitutions in the HMGbox decrease binding of linear DNA EMSAs of different acetylation mimicking variants binding to (a) 4WJ DNA or (b) the linear control fragment.. EMSAs were performed with varying concentration of BID-HMG variants [nM]: 0, 25, 50, 100, 200, 400, 600, 800.

Two major observations can be made. First: The WT versions can bind 4WJ DNA, forming 4 distinct complexes (**Figure 37a**, second row, left panel). This argues for a distinct binding to certain features of the 4WJ DNA. Introducing mutations - especially in the HMGbox - lead to

the formation of one distinct and otherwise rather diffuse complex bands (**Figure 37a**), potentially abolishing the potentially ordered assembly on the 4WJ. Second: While the binding affinity for 4WJ DNA stays approximately constant when mutations are introduced in the HMGbox, the binding affinity for linear DNA decreases when mutations are present in the HMGBox (2xK/x HMG, 4xK/x, **Figure 37b**). This effect was observable for both acetylation-mimetic variants K/A and K/Q, suggesting that indeed the charge and not the steric dimension is the determining parameter (**Figure 37a, b**). Each shift for each variant was performed in duplicates. The altering factor for linear DNA binding are the mutations in the HMGbox, changing the concentration when half of the DNA is bound from ~200 nM to ~400 nM (**Figure 37b**).

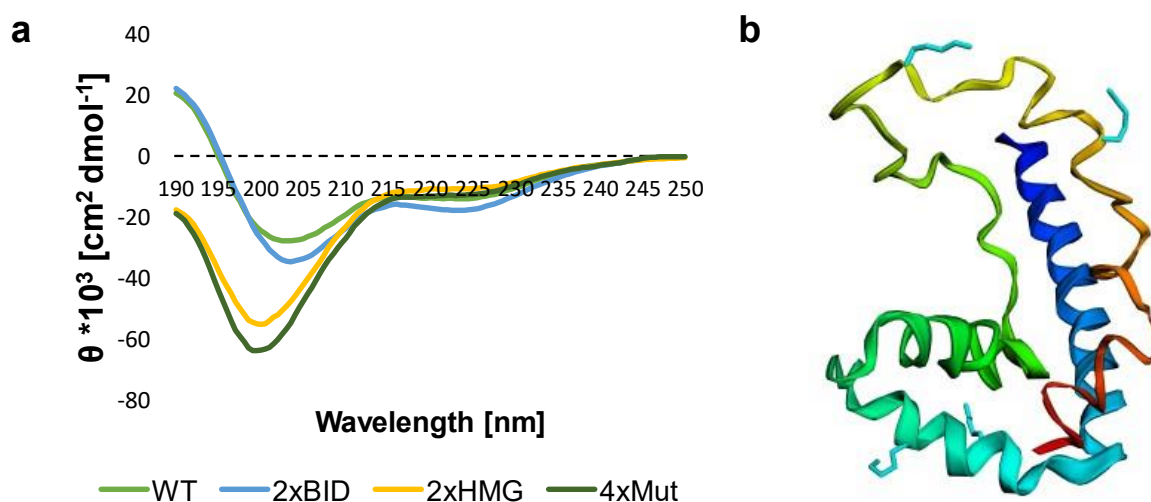


Figure 38 Secondary structure determination by CD spectroscopy and homology remodelling (a) CD spectroscopy of SSRP1 BID-HMG variants (aa 516-630). The graph displays the double minima typical for α -Helical proteins. These minima shift in HMGbox mutants, likely due to different degrees of random coil. θ = Mean residue ellipticity **(b)** Homology remodelling of SSRP1 BID-HMGbox. The BID is randomly coiled (red to green), the HMGbox consists of 3 α -helices (green to blue). Lysines which were found to be acetylated are displayed in cyan. Homology remodeling was performed with the online server I-TASSER (Roy et al., 2010). Protein structure visualisation was performed with the online tool EzMol (Reynolds et al., 2018). CD spectroscopy was performed with the help of Klaus Tiefenbach

To test if the tertiary structure of the protein is intact, CD spectroscopy was performed with the K/A variants. The WT spectra displayed two minima (**Figure 38a**, green), which is typical for α -helical proteins. These typical minima around 208 and 222 nm (Wei et al., 2014) were shifted towards lower wavelengths (**Figure 38a**). This can be explained by the huge portion of random coil (typical minimum at ~195 nm) present in the BID, combined with the alpha-helical portion of the HMGbox. Introducing mutations in the BID leads to similar spectra than in WT (**Figure**

38a, blue). Mutations in the HMGbox shift the minima further towards lower wavelengths, indicating an increase of random coil (**Figure 38a**, yellow and dark green). Homology remodelling with I-TASSER (Roy et al., 2010) and visualisation of the acetylated lysines with EzMol (Reynolds et al., 2018) show that the respective lysines are in the second alpha helix of the HMGbox (**Figure 38b**, cyan residues). This indicates that the increase in random coil could be due to an unfolding of the second alpha helix upon positive charge neutralization (**Figure 38b**, cyan helix).

2.5.4 Influences on Histone immunoprecipitation by SSRP1 acetylation variants

In a chromatin context, an acetylation mediated decrease in SSRP1 DNA binding affinity could mark the release of the FACT complex not only from DNA but ultimately from the nucleosome. This final release could be reflected in the efficiency to co-immunoprecipitate the single histones. To address this, the *Arabidopsis* cell-culture system was employed, to test the effects of native acetylation (K539, K549, K594, K599) acetylation insensitive (K539R, K549R, K594R, K599R) and acetylation-mimetic (K539Q, K549Q, K594Q, K599Q) full-length GS-tagged SSRP1 variants under control of the native promoter (**Figure 39a**). Immunoprecipitation of the SSRP1-GS variants (**Figure 39b**) led to a similar band pattern like observed before for SSRP1-GS wildtype variant under control of the 35s promoter (**Figure 5b**) and was in most aspects comparable among the three SSRP1 variants (**Figure 39b**), however the signal for the putative histone band pattern appeared stronger in the acetylation-insensitive (A0) variant, which maintains the positive charge, compared to the acetylation-mimicking (A+) variant, where the positive charge gets neutralized (**Figure 39b**). Immunoblot analysis of the AP was performed with α H2B, as a representative for H2A-H2B, and α H3, as representative for the inner H3-H4 tetrameric core. Antibody binding was detected using HRP-coupled secondary antibody and chemiluminescence detection. 2,2,2-Trichloroethanol (TCE) staining of the respective gel subjected to western blot served as loading control (**Figure 39c**). The experiment was repeated with independent pools of cells in two replicates (**Supplementary Figure 1b**) showing similar tendencies. The acetylation-insensitive variant (A0 or K/R) – hence preserving the native positive charge – showed an increased affinity for H2B and H3 compared to the WT variant. In contrast, the acetylation mimicking variant pulled down slightly less histones, comparable to the WT variant (**Figure 39b, d**). This indicates that the WT variant is at least partly acetylated, in line with the observation of the initial screen (**Table 6**). Overall, this shows that modifying the charge pattern of the HMGbox indirectly modulates the interaction with the

nucleosome, by neutralizing the positive charge of the respective lysines, thereby potentially weakening the tethering of the nucleosome to FACT.

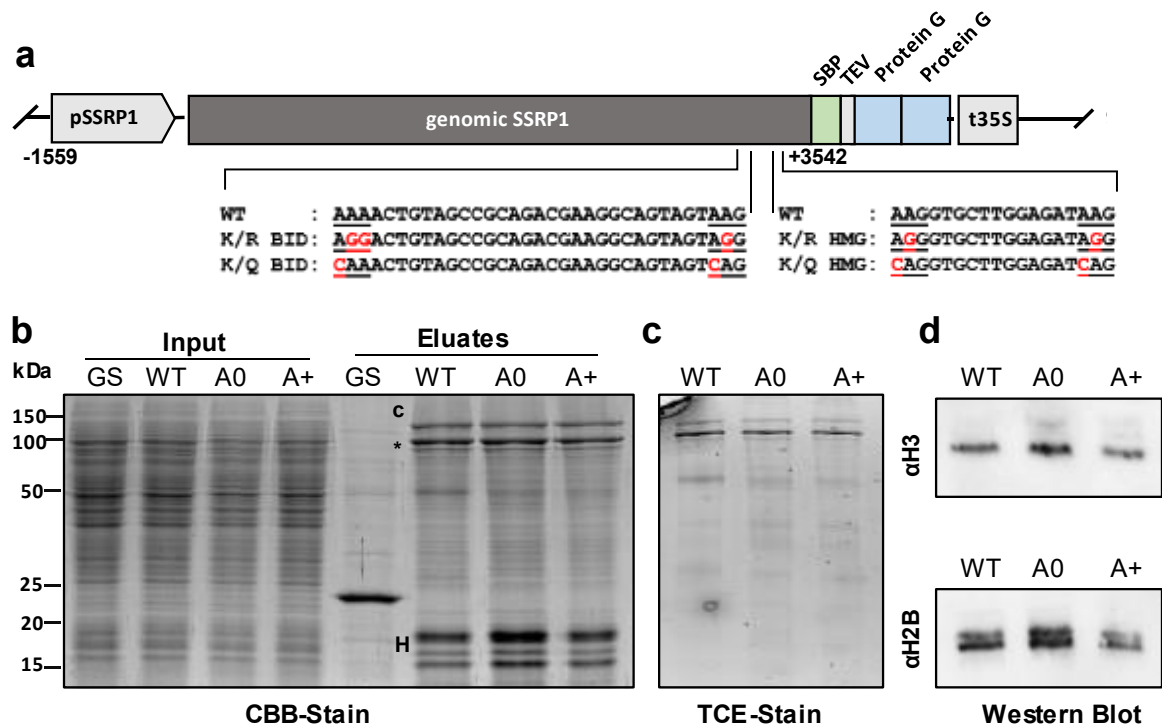


Figure 39 H2B and H3 Immunoblot analysis of SSRP1 AP. The Acetylation insensitive variant, preserving the positive charge, immuno-precipitates more H3 and H2B (a) Schematic illustration of wildtype- (WT, K539, K549, K594, K599), Acetylation-insensitive (A0/4xR, K539R, K549R, K594R, K599R) and Acetylation-mimetic (A+/4xQ; K539Q, K549Q, K594Q, K599Q) -SSRP1 bait proteins fused to a GS tag under control of the native promoter (bait in dark grey, streptavidin-binding protein in green; TEV cleavage site in light grey; Protein G domains in light blue, introduced mutations in red) **(b)** Input (0.01 % of total) next to Eluates (1/3 of total) of the one-step affinity purifications using IgG coupled magnetic beads. The proteins were separated by 18 % SDS-PAGE and stained with CBB. * = bait, c= complex partner (here SPT16), H = putative histone band pattern **(c)** TCE stain corresponding to **(d)** Immunoblot with α H3 (upper panel) and α H2B (lower panel). TCE = 2,2,2-Trichloroethanol

2.5.5 No obvious defect on subcellular localisation

Acetylation of the NLS of HMGB1 has been shown to redirect its subcellular localisation from the nucleus towards the secretory pathway (Bonaldi et al., 2003; Wang et al., 2019). The maize SSRP1 NLS has been mapped before to the basic region next to the HMGbox (Röttgers et al., 2000), containing two of the detected acetylation sites (**Figure 40a**, NLS underlined, acetylated Lysine cyan). To test whether this influences subcellular localisation, eGFP-SSRP1 acetylation mimetic and wildtype variants under control of the native promoter (**Figure 40b**) were introduced into the Col-0 background by *Agrobacterium* mediated transformation. Plants were

selected on hygromycin and the transgene were confirmed by genotyping PCR (**Figure 40c**). EGFP expression of T1 plants was confirmed by confocal microscopy (CLSM). Both, the EGFP-SSRP1 WT variant and the EGFP-SSRP1-4xQ variant showed nuclear localisation (**Figure 40d**). Hence, no obvious localisation change was observed upon acetylation-mimicking.

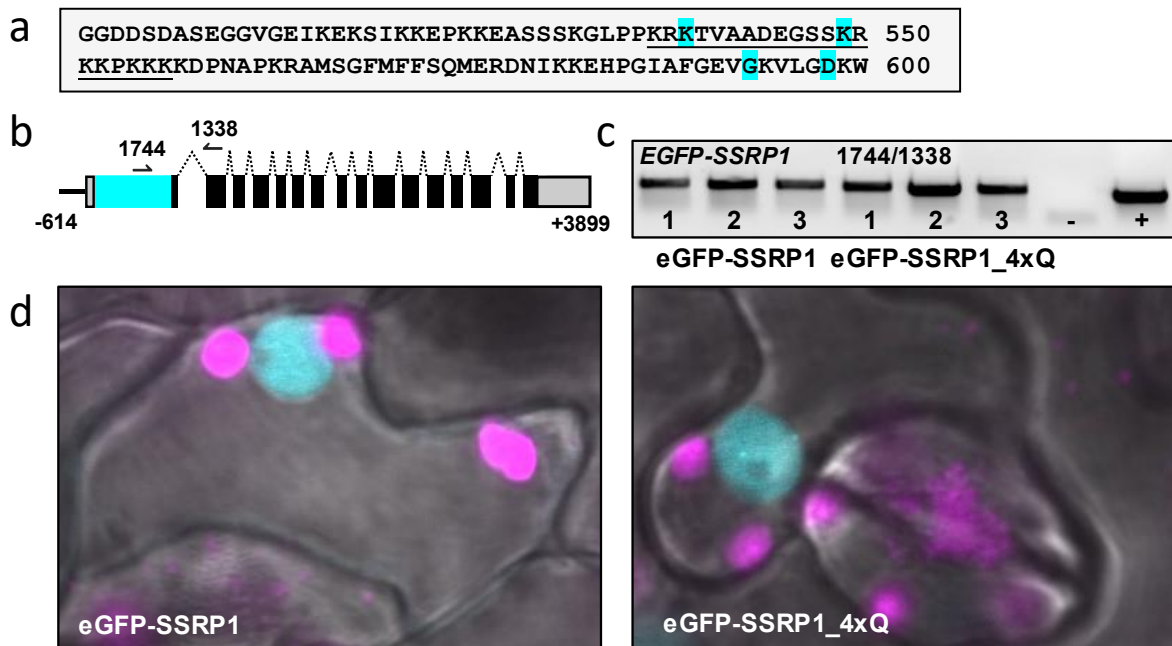


Figure 40 The Acetylation mimetic variant shows no obvious subcellular localisation change (a) Two of the four detected acetylations (cyan) are located in the NLS (underlined, Röttgers et al., 2000) (b) Schematic illustration of the wildtype- (WT, K539, K549, K594, K599), transgene under control of the native promoter. Primers for the genotyping PCR are shown as arrows (Black bars = exons, dark grey bars = UTR, dotted lines = introns, cyan bar = TagRFP) (c) Genotyping PCR for independent T1 eGFP-SSRP1 transgenes. Positive control (+) = Plasmid; Negative control (-) = water (d) eGFP-SSRP1 and eGFP-SSRP1_4xK/Q both localize to the nucleoplasm. *Arabidopsis* leaf cells expressing the eGFP fusion proteins were analyzed by CLSM and merges of bright field and eGFP fluorescence (cyan) and chlorophyll (magenta) are shown

2.5.6 Acetylation-mimicking in SSRP1 leads to no severe defects on plant development

Acetylation-mimicking of the *in vivo* detected acetylation pattern of SSRP1_BID-HMGbox (Section 2.5) led to a decrease of linear DNA binding *in vitro* (section 2.5.3). The inability to get acetylated, preserving the positive charge in the respective sites, led to the immunoprecipitation of more H2B and H3 *in vivo* (section 2.5.4). To get more insights in the effects of acetylation of the SSRP1 basic intrinsic disordered region and its neighbouring HMGbox, transgenes mimicking the unacetylated state (K to R) and the acetylated state (K to

Q) were created to complement *ssrp1-1* (**Figure 41a**). *ssrp1-1* is a T-DNA insertion knockout mutant in the Landsberg erecta background *Ler* (Lolas et al., 2010). While both variants were located in the nucleoplasm (section 2.5.5) certain developmental processes or certain tissues might be (transiently) deregulated. To exclude any effect of subcellular localisation a C-terminal NLS was included in the respective transgenes (WT, 4xR, 4xQ).

2.5.6.1 Line creation and validation

The transgenes containing the genomic sequences of the native promoter (1600 bp upstream of TSS), the wildtype or acetylation-variants of SSRP1 together with an additional NLS (**Figure 41a**; *pSSRP1:SSRP1-NLS* ; *Wildtype* = WT, *Acetylation-insensitive* = 4xR or *Acetylation-mimetic* =4xQ;) were introduced directly in the heterozygous *ssrp1-1* background by *Agrobacterium*-mediated transformation. For each transgene, several independent primary-transformants (T1) were picked on ½ MS plates containing hygromycin. To obtain homozygous lines, segregating lines in the T3 generation were selected. The *ssrp1-1* T-DNA insertion in the first exon, the respective locus in *SSRP1* and the construct complementing were validated by genotyping PCR (**Figure 41b**, Primers **Figure 41a**).

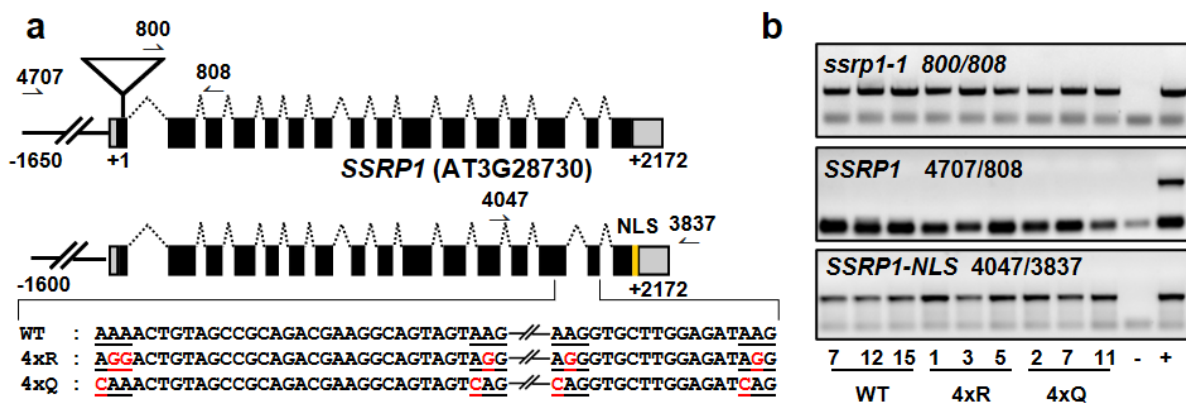


Figure 41 Generation of transgenic *Arabidopsis* cell lines expressing SSRP1-NLS acetylation variants (a) Schematic illustration of *ssrp1-1* T-DNA insertion line and SSRP1-NLS variants: *Wildtype* (=WT; K539, K549, K594, K599), *Acetylation-insensitive* (=A0/4xR; K539R, K549R, K594R, K599R) and *Acetylation-mimetic* (=A+/4xQ; K539Q, K549Q, K594Q, K599Q). The T-DNA insertion line for *ssrp1-1* (GT7431) is indicated as triangle. Primers for genotyping PCR are shown as arrows (Black bars = exons, dark grey bars = UTR, dotted lines = introns, yellow bar = NLS) (b) Genotyping PCR for T-DNA insertion *ssrp1-1* (upper panel), wild type *SSRP1* (middle panel) and transgene (lower panel). Positive control (+): Upper panel = *ssrp1-1*; middle panel = Col-0; lower panel = Plasmid (Stock ID 1217). Negative control (-) = water

Additionally, in lines which were identified to be homozygous for *ssrp1-1* and the respective construct by selection, the segregation of 8 plantlets was monitored via genotyping PCR to

reconfirm double-homozygosity (**Supplementary Figure 9**). This confirmed 3 independent lines for WT (#7, #12, #15), 4xR (#1, #3, #5) and 4xQ (#2, #7, #11). Next, the protein levels of plasmid-derived SSRP1-NLS was analysed in the generated *ssrp1-1* complementation lines with the priorly described SSRP1 antibody (Duroux et al., 2004). Therefore, the nuclei of ~1g of 14-day old seedlings were isolated (**Figure 42a**). SSRP1 protein levels were approximately comparable to *Ler* (**Figure 42b**, upper band). Each line shows the presence of full-length SSRP1-NLS, indicating transgene expression. A second unspecific band can be observed here (**Figure 42b**, lower band) and in other experiments (Pfab et al., 2018b). Band identity can be assigned to SSRP1 due to the shift in migration pattern in truncated SSRP1 (**Supplementary Figure 14, Supplementary Figure 15**). Next the validated lines were subjected to phenotypic analysis.

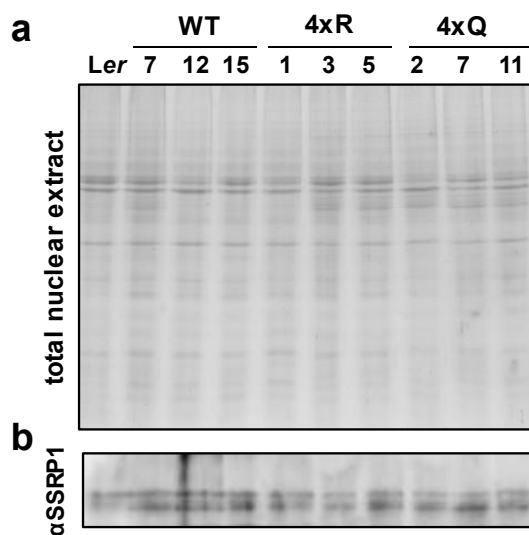


Figure 42 Immunoblot analysis of SSRP1-NLS complementation lines (a) CBB stain of nuclear protein extracts of *Ler*, *ssrp1-1* (-/-) SSRP1-NLS (+/+) variants (Wildtype = WT, *Acetyl0* = 4xR, *Acetyl+* = 4xQ) **(b)** α -SSRP1 Immunostaining. SSRP1 antibody with HRP-coupled secondary antibody and chemiluminescence detection. MW SSRP1 = 71.7 kDa; SSRP1-NLS 72.5 kDa

2.5.6.2 Phenotypic analysis of SSRP1 acetyl-variants

During phenotypic analysis plants were grown on soil under long day conditions. The set-up contained *Ler*, as a background control, and 3 independent *ssrp1-1* complementation lines each (*ssrp1-1 pSSRP1:SSRP1-WT*, *ssrp1-1 pSSRP1:SSRP1-4xR* and *ssrp1-1 pSSRP1:SSRP1-4xQ*). Priorly, it was shown that homozygous *ssrp1-1* (-/-) is lethal and that heterozygous *ssrp1-1* (+/-) does not show a phenotype (Lolas et al., 2010) and were therefore not included. During the course of obtaining double-homozygous lines it became apparent that no severe defects were to be expected. To quantify growth phenotypes and potentially better evaluate minor

differences, the software Leaf-GP (Zhou et al., 2017) was employed with a fixed set-up (**Figure 43a**) for automated feature extraction, like e.g. leaf perimeter and leaf area (**Figure 43b**).

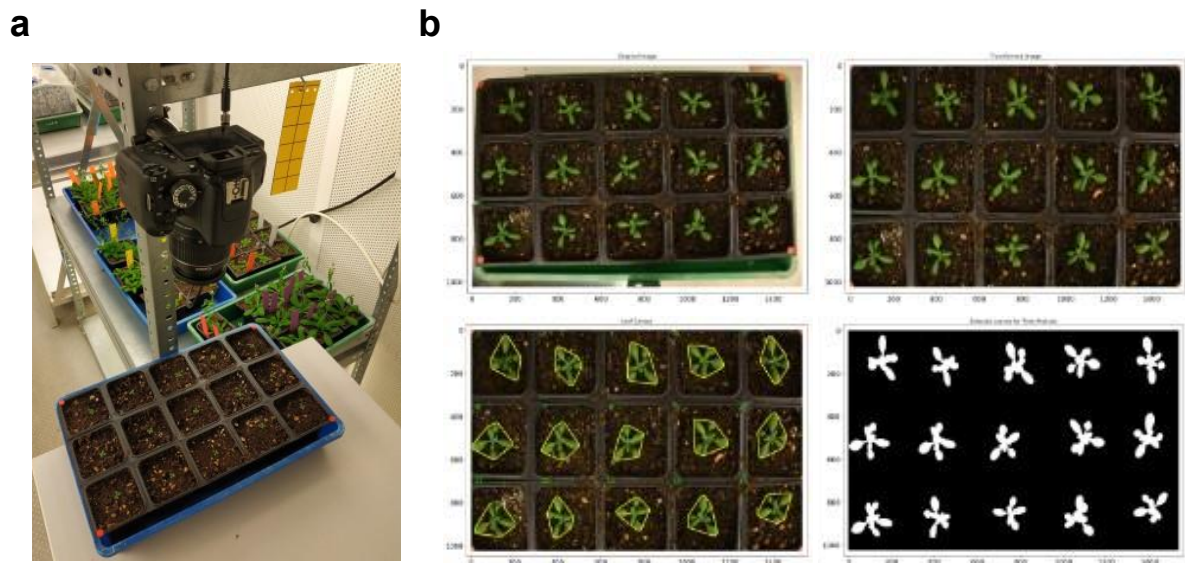


Figure 43 Automated feature extraction with Leaf-GP (a) Fixed camera Set-up in the plant chamber **(b)** Exemplarily image processing steps with the Software Leaf-GP (Zhou et al. 2017). Upper row: From raw to cropped picture. Lower row: Feature extraction Perimeter and Leaf Area

The following measurements were carried out in three biological replicates (n=15): Leaf area at 21 days after stratification (DAS; evaluation of vegetative growth), time of bolting and rosette perimeter and area at bolting (transition from vegetative to reproductive state), height at 42 DAS and rosette diameter at 42 DAS (overall size).

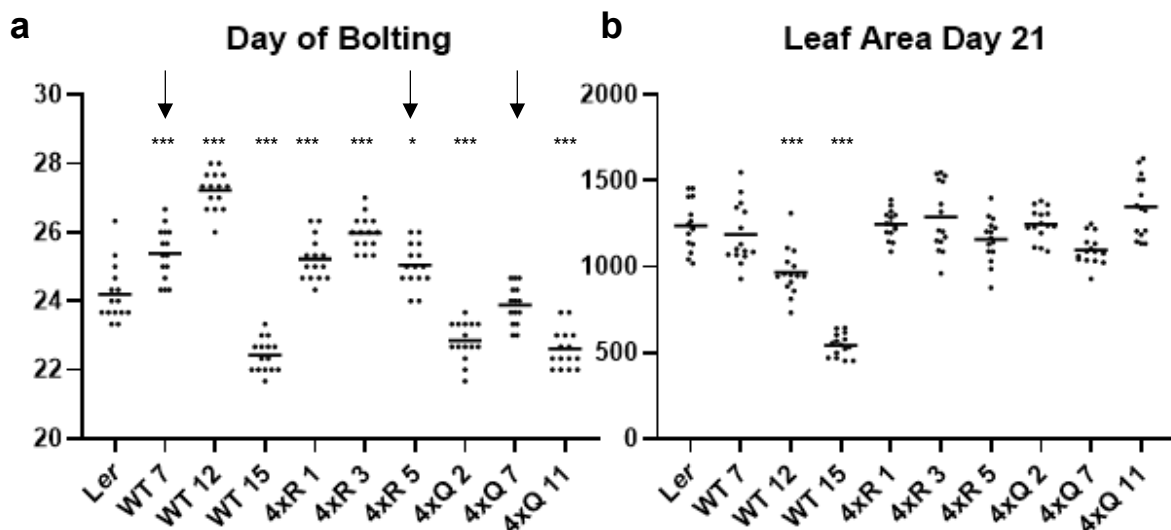


Figure 44 Acetylation-mimetic (4xQ) variants show a tendency to bolt earlier compared to Acetylation-insensitive variants (4xR). Plants were phenotypically analysed in comparison with the genetic background *Ler* **(a)** time of bolting (elongation of the first shoot) [d] **(b)** Leaf area 21 Days after stratification (DAS) [mm²]. Data

was analysed by one-way ANOVA and a multi comparisons Tukey's test, comparing to *Ler* as a reference. The line in the scatterplot marks the average value. Asterisks indicate the outcome of the Tukey's test (p -value $* < 0.05$, $*** < 0.001$). Arrows mark lines which will be shown in all further analysis.

The phenotypic analysis of *ssrp1-1* complementation lines revealed minor differences. Generally, all 3 lines of the respective acetyl-variants group together (**Figure 44a,b**): Independent acetylation-mimetic lines (*4xQ*) bolt earlier than acetylation-insensitive (*4xR*) lines. However, wildtype rescues showed a non-uniform pattern. While line 7 and 12 bolt later than acetylation-mimicking variants, line 15 bolts earlier (**Figure 44a**). A closer look on leaf area at day 21 shows, that in both line 15 and slightly in line 12, the overall area is decreased (**Figure 44b**) and potential secondary effects could affect vegetative traits.

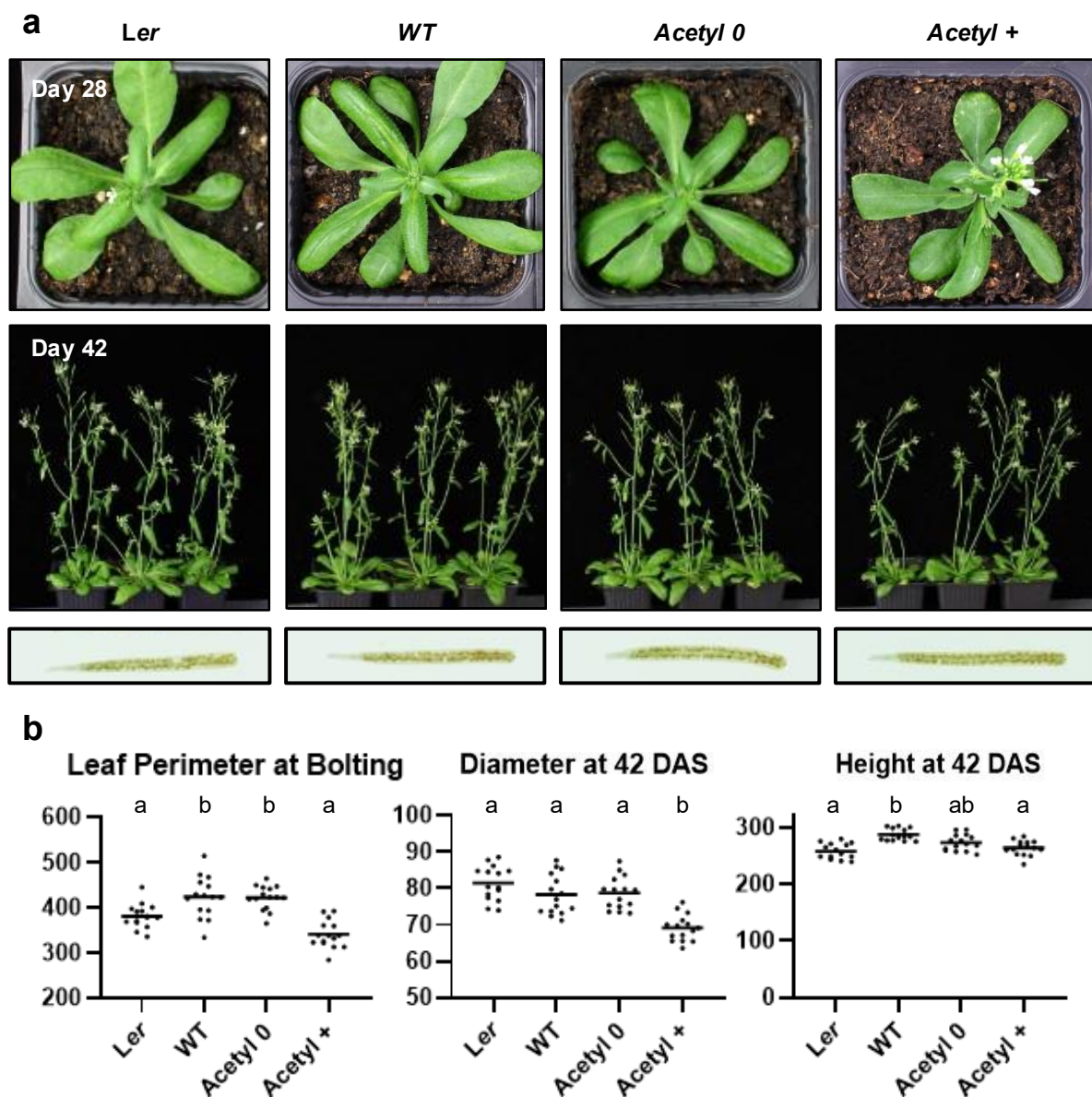


Figure 45 *SSRP1-Acetyl+* variants are slightly smaller compared to *Acetyl-0* and *WT-variants*. Phenotypical analysis of the *ssrp1-1* complementation lines in comparison to wild type *Ler*. Plants were grown under long day

conditions. (a) Representative individuals are shown at various developmental stages. Pictures were taken at 28 (upper panel) and 42 days after stratification (DAS) (middle panel). Representative siliques were taken at 42 DAS (lowest panel) (b) Quantification of Leaf Perimeter at Bolting [mm], Diameter at 42 DAS [mm], Height at 42 DAS [mm]. The data shown here comprises the measurements of 15 individual plants in three biological replicates. Data was analysed by one-way ANOVA and a multi comparisons Tukey's test. The line in the scatterplot marks the average value. Letters above the scatter indicate the outcome of the Tukey's test (p -value < 0.05). *WT* = *pSSRP1::SSRP1-NLS* line 7, *Acetyl0* = *pSSRP1::SSRP1-NLS_K539R/K549R/K594R/K599R* line 5, *Acetyl+* = *pSSRP1::SSRP1-NLS_K539Q/K549Q/K594Q/K599Q* line 7

To exclude any over-interpretation of results and to simplify readability, the best rescuer in respect to *Ler* is shown from now on. The following lines were picked: *SSRP1-NLS_4xR* line 7 (= *Acetyl0*), *SSRP1-NLS_4xQ* line 7 (= *Acetyl+*) (**Figure 44a**, arrows). In line with a slightly earlier shift from vegetative to reproductive state compared to *Acetyl0*, the *Acetyl+* variants show a decrease in rosette size at bolting (**Figure 45a**, first row, **Figure 45**, first panel). The slightly smaller size continuous throughout the life cycle (**Figure 45b**, diameter 42 DAS) in contrast to *WT*- and *Acetyl0* variants. Generally, measured deviations were minor, e.g. $\sim 1.5 - 2$ Days in respect to bolting (**Figure 45**) or 1 cm leaf diameter 42 DAS (**Figure 45b**). The overall appearance of the different variants in later stages is quite similar (**Figure 45a**, second row) and no severe disadvantage of the respective line in respect to the seed set (**Figure 45a**, third row) was observed. As the observed effects were small, the plants were additionally stressed to further increase potential negative effects. Cold-, heat-, salt- and highlight stress was applied like described before (Andrés-Barrao et al., 2017; Dong et al., 2006; Pfab et al., 2018a; Wu et al., 2010). No treatment revealed a pronounced decrease in size (**Figure 46a, b, c**) or an altered accumulation of anthocyanins (**Figure 46d**). Detailed comparisons to untreated plants and quantifications can be found in **Supplementary Figure 10-13**. This indicates that vegetative growth is unaffected by charge alterations in BID-HMG under stress conditions.

Mimicking the acetylations detected in the BID and HMGbox of *SSRP1* (2.5) altered the DNA binding ability to linear DNA (2.5.3). The acetylation insensitive variant led to an increase the number of histones pulled down (2.5.4). Rescuing the lethal *ssrp1-1* T-DNA knockout showed minor influences in the transition from vegetative to reproductive state (2.5.6). While modifications to the BID and the HMGbox showed only mild effects, the overall role of the *SSRP1* HMGbox were studied by former colleague Alexander Pfab. Small contributions were made to his study and are briefly summarized next, particular to put the mild defects of *SSRP1* BID-HMGbox modulation into perspective.

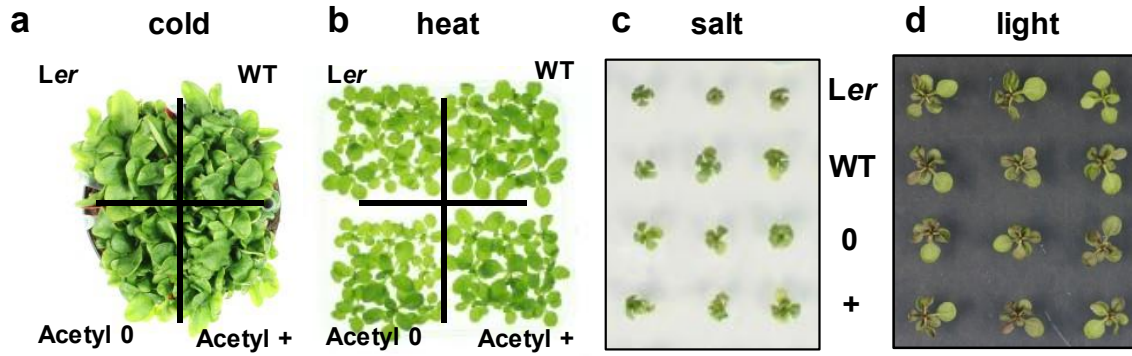


Figure 46 *ssrp1-1* plants rescued with *pSSRP1:SSRP1* acetyl-variants show no defect when subjected to stress (a) 14-day-old plantlets grown on soil were switched to cold treatment for 40 days at 4°C (compare Dong et al. 2006) (b) 7-day-old plantlets were heat treated for 3 days at 37°C, Picture shows 14 days after heat treatment (compare Wu et al. 2010) (c) 3-day-old plantlets were transferred to plates containing 100 mM salt (compare Andrés-Barrao et al. 2017) (d) 14-day-old plantlets were grown on plates containing 2% sucrose at lowlight (60 $\mu\text{mol m}^{-2} \text{s}^{-1}$) and switched to highlight for 7 days (600 $\mu\text{mol m}^{-2} \text{s}^{-1}$) (compare Pfab et al. 2018). If not indicated otherwise plants were grown on $\frac{1}{2}$ MS plates containing 1% sucrose, 16h light 8 h dark cycle at 21°C

2.6 The *Arabidopsis* Histone Chaperone FACT: Role of the HMG-Box Domain of SSRP1

Disclaimer: The figures in this chapter were published in JMB (Pfab et al., 2018b). Philipp Michl-Holzinger contributed by performing major revisions. These revisions included a more detailed look on the phenotypic aspects leaf and flower morphology and a validation of SSRP1 and SSRP1 Δ HMG protein levels in the *ssrp1-1* knockout background under control of the native or the 35s promoter via western blot and subsequent signal quantification (compare Figure S6, Figure S4, Figure S7 D-F in Pfab et al., 2018b).

In this study full-length SSRP1 and SSRP1 without the HMGbox was analysed (SSRP1 Δ HMG). In *in vitro* experiments, the deletion of the HMGbox led to reduced binding of DNA and a reduced interaction with nucleosomes. Plant lines expressing SSRP1 Δ HMG in the *ssrp1-1* background showed normal growth and development, comparable to full-length SSRP1 and *Ler*. The respective constructs were under control of either the native or the 35s promoter. In line with the general phenotypic analysis performed by Alexander Pfab, neither flowers nor leaves displayed any obvious abnormalities (**Figure 47**). Protein levels of SSRP1 or SSRP1 Δ HMG under control of the native promoter were comparable to those of the background *Ler* (**Supplementary Figure 14**). While the 35s promoter led to a severe increase in transcript (10-50 fold enrichment), protein levels stayed rather constant in most cases around native SSRP1 levels in *Ler* (**Supplementary Figure 15**), in agreement with no phenotypic

alterations. These findings indicate that SSRP1 HMGbox is not critical in *Arabidopsis* and that SSRP1 protein levels are tightly controlled. This potentially explains the minor defects upon HMG-box modulation by acetylation-mimicking substitutions (Section 2.5.6).

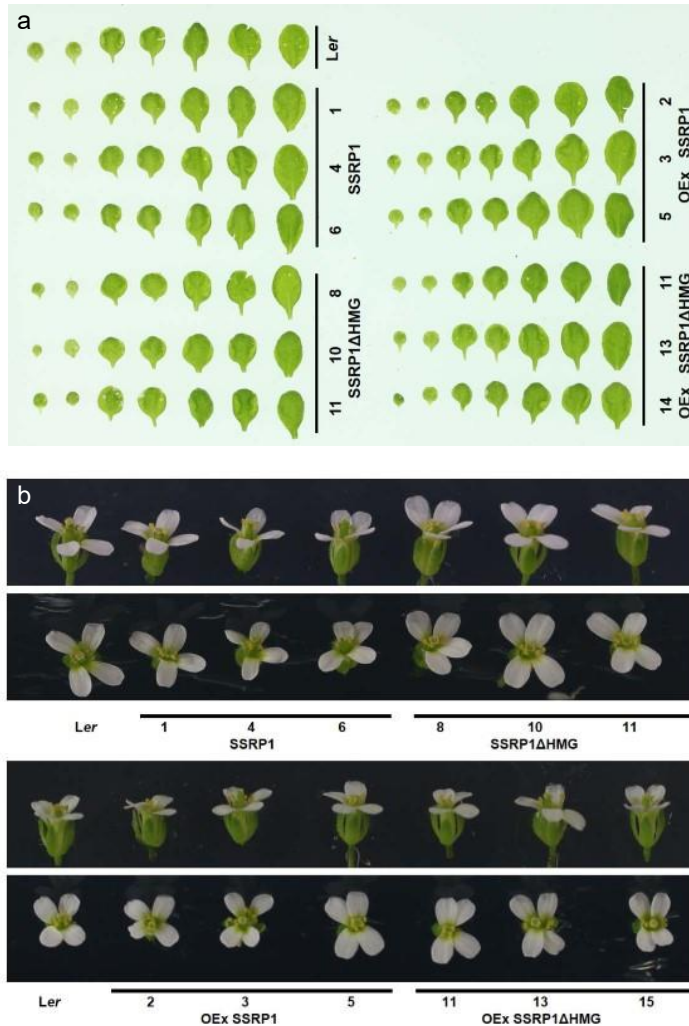


Figure 47 Leaf and flower morphology are not affected by deletion of the SSRP1 HMGbox (a) Representative images of *ssrp1-1* SSRP1Full and SSRP1ΔHMG complementation lines (left) and overexpression lines (OEx; right) plants (21 DAS). (b) Flowers of *ssrp1-1* complementation (top) and overexpression (bottom) plants.

2.7 The SSRP1 subunit of the histone chaperone FACT is required for seed dormancy in *Arabidopsis*

Seed dormancy determines when a seed is able to germinate and thereby ensures that the later stages, which are more vulnerable to environmental conditions than the seed itself, happen during favourable seasonal and environmental conditions (Bewley, 1997). One main factor of seed dormancy regulation is the antagonism between abscisic acid and gibberellic acid:

Abscisic acid is important to establish dormancy and maintenance; gibberellic acid helps to leave dormancy via germination. The ratio between the hormones is regulated by environmental signals which alter the expression of biosynthesis and degradation (Finkelstein et al., 2008). In *Arabidopsis* several seed dormancy-specific quantitative trait loci have been identified which have been termed *Delay of Germination (DOG)* genes (Alonso-Blanco et al., 2003). Since then one *DOG* gene has been found to be especially interesting, as loss of function leads to loss of seed dormancy: *DOG1* (Bentsink et al., 2006). While molecular function of *DOG1* is still elusive, transcriptional control of the *DOG1* gene is heavily regulated by antisense transcription, alternative polyadenylation and alternative splicing (Carrillo-Barral et al., 2020). This heavy regulation might indicate why *DOG1* can be used as a marker, in e.g. the transcript elongation factor mutants *tfIIs*, which is otherwise only mildly affected (Grasser et al., 2009; Mortensen and Grasser, 2014; Mortensen et al., 2011): A spatially, temporally and highly expressed transcript, demanding for a fine-tuned transcription machinery, which in case of alterations directly translates into a phenotype.

Disclaimer: The following part was published in Journal of Plant Physiology (Michl-Holzinger et al., 2019) All experimental work was performed by Philipp Michl-Holzinger, except: Initial observations were made by Simon Arnold Mortensen (Mortensen, 2012); T₀ seeds of of *ssrp1-2* mutants with an additional copy of *DOG1* were obtained from Marcel Kaljanac (Kaljanac, 2014).

In view of the emerging role of RNAPII-mediated transcriptional elongation in the regulation of seed dormancy (Nonogaki, 2014) we analysed here whether FACT plays a role thereby. TFIIIS and PAF1c are involved in seed dormancy (Grasser et al., 2009; Liu et al., 2011) and both co-purified with FACT and elongating RNAPII (Antosz et al., 2017). In addition, genetic interactions were observed between the genes encoding FACT, PAF1C and TFIIIS (Antosz et al., 2017). Since both *ssrp1-2* and *spt16-1/2* mutants have a strongly reduced seed set but *ssrp1-2* is less affected regarding this phenotype (Lolas et al., 2010) we decided to use the *ssrp1-2* mutant line for our experiments. Initially, we tested whether *ssrp1-2* seeds show altered seed dormancy, when compared with the wild type Col-0. Siliques of *ssrp1-2* and Col-0 freshly picked 14 days after flowering (14 DAF) were used for germination assays either with or without prior stratification (**Figure 48a**). Following stratification, almost all seeds of both genotypes germinated after seven days, as evident from the growing seedlings. In contrast, without stratification only approximately half of the Col-0 seeds germinated, whereas the *ssrp1-2* seeds germinated efficiently (**Figure 48b**). To evaluate this observation further, a larger

number of seeds was analysed and we included *tfIIs-1* seeds for comparison that were previously found to show reduced seed dormancy (Grasser et al., 2009; Liu et al., 2011; Mortensen and Grasser, 2014). In these experiments ~45% of the freshly harvested Col-0 seeds germinated, while 93% and 84% of the *ssrp1-2* and *tfIIs-1* seeds germinated, respectively (**Figure 48c**), indicating reduced dormancy with *ssrp1-2* (and *tfIIs-1*). In case of *tfIIs* mutant seeds, the effect on dormancy was mediated by decreased expression of DOG1 (Mortensen and Grasser, 2014). Therefore, we comparatively analysed the DOG1 transcript levels of *ssrp1-2* and *Col-0*. Using qRT-PCR we determined that the transcript level of DOG1 in *ssrp1-2* seeds is reduced by ~28% (**Figure 48d**) suggesting that decreased amount of DOG1 mRNA mediates the weaker seed dormancy.

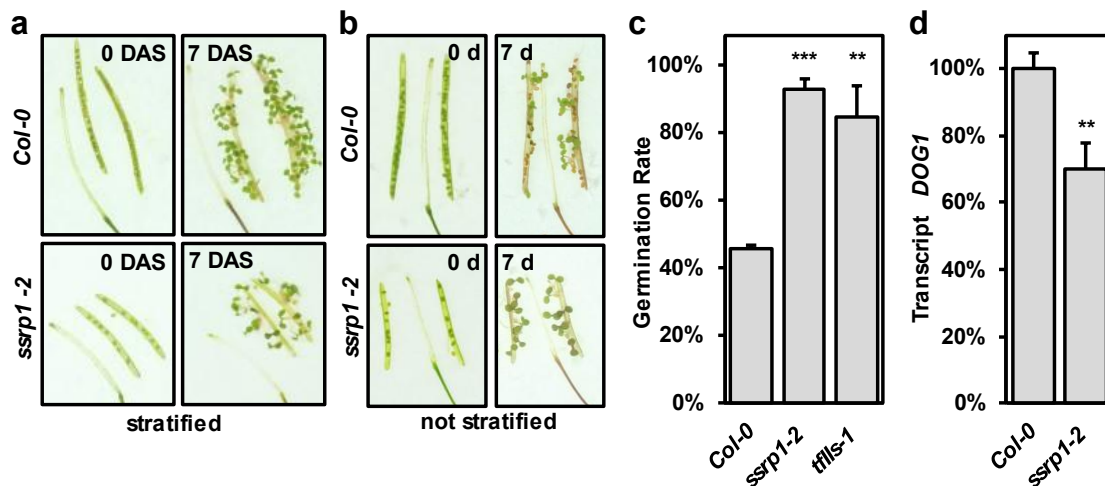


Figure 48 Germination assays of Col-0 and *ssrp1-2* seeds. Representative, opened siliques harvested 14 days after flowering (DAF) were used for germination analysis with or without stratification. Each image depicts the valves next to the septum. Note that the siliques of *ssrp1-2* are shorter and have a clearly reduced seed set when compared to those of Col-0; compare left top and bottom panels in (a) and (b). **(a)** Siliques before and after stratification. **(b)** Siliques incubated for 0 or 7 days without stratification. **(c)** Seed germination rates of Col-0, *ssrp1-2* and *tfIIs-1*. Freshly harvested seeds without stratification (~60-150 seeds were used per genotype in three independent biological replicates) were sown and germination rates were scored after seven days. **(d)** Quantification of the DOG1 transcript level by RT- qPCR. RNA isolated from pools of freshly harvested seeds and transcript levels were normalised to Col-0. Relative quantities are shown (three biological and three technical replicates). Error bars indicate standard deviation of the mean. Significance compared to Col-0 was analysed by Student's t-test (**p < 0.01 and ***p < 0.001).

Since the transcript levels of TFIIIS and of the genes encoding PAF1C subunits (e.g. ELF7, ELF8) were upregulated during seed maturation (Liu et al., 2011), we tested whether this applies also to SSRP1. As examined by qRT-PCR the SSRP1 transcript level increased by ~70% during seed development (9–19 DAF) (**Figure 49a**). Upregulation of SSRP1 during seed

maturation may reflect an increased requirement for FACT (and other TEFs) to maintain gene expression in a situation with increased chromatin condensation in the ripening seed (Van Zanten et al., 2011). We also analysed the transcript level of *DOG1* over the same period of seed development. Consistent with global gene expression analyses (Schmid et al., 2005), we observed a peak of the *DOG1* transcript during seed maturation under our experimental conditions (**Figure 49b**). Therefore, the rise in *DOG1* expression is associated by increased *SSRP1* transcript levels, but towards the end of maturation the transcript levels diverge, which is in line with the fact that *DOG1* expression is regulated by multiple factors (Nonogaki, 2014) and FACT performs various chromatin-related functions (Formosa, 2012; Gurova et al., 2018).

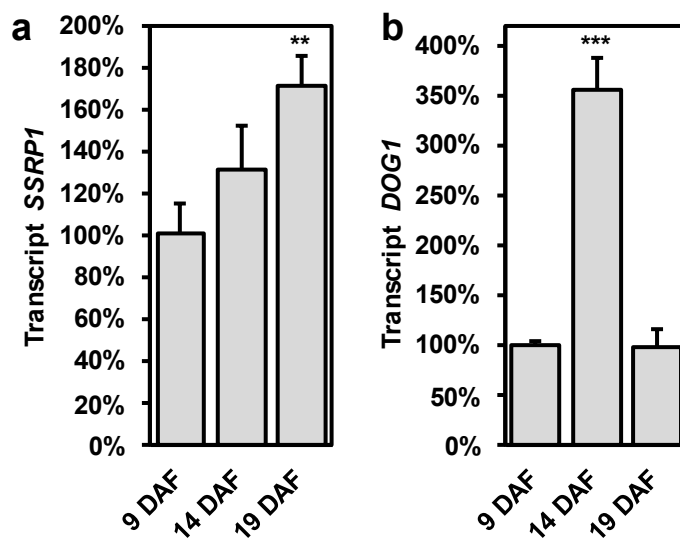


Figure 49 Quantification of *SSRP1* and *DOG1* transcript levels of Col-0 seeds. RNA isolated of seeds 9, 14 and 19 days after flowering (of three independent pools of seeds) was analysed by qRT-PCR (in three technical replicates) to determine the *SSRP1* transcript (**a**) and the *DOG1* transcript (**b**). Error bars indicate standard deviation of the mean. Significance compared to 9 DAF was analysed by Student's t test (** $p < 0.01$ and *** $p < 0.001$).

To examine whether the effect of *SSRP1* on seed dormancy is indeed mediated by reduced *DOG1* expression, we employed a strategy that we have used before to examine the role of TFIIS in dormancy (Mortensen and Grasser, 2014). We introduced an additional copy of the *DOG1* gene into *ssrp1-2* mutant background to analyse whether elevated transcript levels can reduce the germination rates of *ssrp1-2* seeds. To that end a vector containing the genomic sequence of *DOG1* was transformed into *ssrp1-2* plants. Plants harbouring the *DOG1* construct (termed *ssrp1-2 DOG1*) were selected and characterised by PCR-based genotyping. We further analysed three independent plant lines homozygous for the *DOG1*-transgene in *ssrp1-2* background, which were phenotypically indistinguishable from *ssrp1-2* including comparable

seed set. Initial germination tests using complete siliques revealed that after stratification the seeds germinated efficiently (**Figure 50a**). Without stratification the germination of *ssrp1-2 DOG1* was clearly reduced (**Figure 50a**) when compared with *ssrp1* seeds (**Figure 48b**), indicating increased dormancy. Germination analyses of three *ssrp1-2 DOG1* lines in comparison to *ssrp1-2* and Col-0 demonstrated that the germination rate of the three *ssrp1-2 DOG1* lines was markedly lower than that of *ssrp1-2* and was even lower than that of Col-0 (**Figure 50b**). Measuring the *DOG1* transcript levels of these seeds revealed that the transcript levels of the *ssrp1-2 DOG1* lines were increased relative to *ssrp1-2* and they were also higher than that of Col-0 (**Figure 50c**). The correlation of germination efficiency and *DOG1* transcript levels suggest that seed dormancy is controlled by SSRP1-mediated regulation of *DOG1* expression. Hence, the dormancy phenotype of the *ssrp1-2* mutant likely is caused by reduced *DOG1* transcript levels during seed maturation.

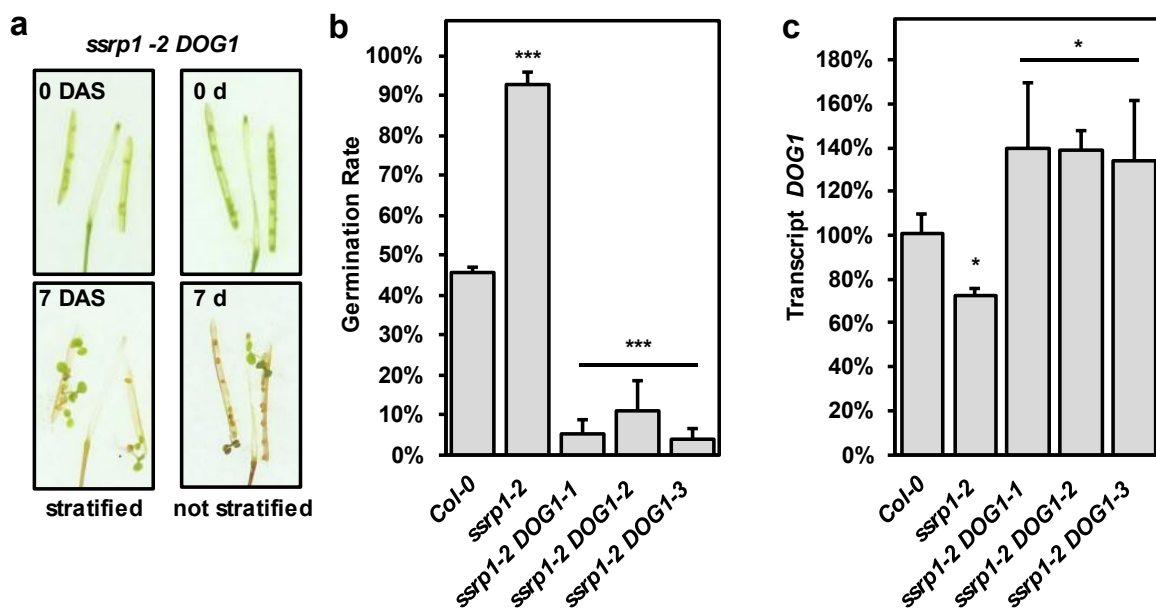


Figure 50 Germination assays of *ssrp1-2* harbouring an additional copy of *DOG1*. (a) Freshly harvested, opened siliques 14 days after flowering (DAF) at day 0 and day 7 after stratification (left panel) and without stratification (0 d and 7 d; right panel) (b) Seed germination rates of Col-0, *ssrp1-2* and 3 independent lines of *ssrp1-2* harbouring an additional copy of *DOG1* (*ssrp1-2 DOG1 1-3*). Freshly harvested seeds without stratification (~60-150 seeds) were used per genotype in three independent biological replicates and germination rates were re- corded after seven days. (c) Quantification of the *DOG1* transcript level by qRT-PCR. RNA isolated from three independent pools of seeds were used and normalised relative quantities are shown (three technical replicates). Error bars indicate standard deviation of the mean. Significance compared to Col-0 was analysed by Student's t-test (* $p < 0.05$ and *** $p < 0.001$).

3 Discussion

3.1 The Transcript Elongation Histone Chaperone Complex

Here AP-MS datasets were raised for SSRP1, SPT16, ELF1 and SPT61. All of them contain acidic intrinsic disordered (AID) regions in their N- or C-terminus and are thereby presumed to interact with histones/nucleosomes in the process of transcription (Ehara et al., 2019). Indeed, AP-MS analysis showed strong association with H2A and H2B variants for all factors (**Table 3**), including ELF1 which has been only hypothesized to interact with histones so far (Ehara et al., 2019). Affinity purification coupled to mass-spectrometry (AP-MS) of these factors in *Arabidopsis* cell culture (**Figure 5**) shows particularly validity in the time of cryo-EM: Due to their high flexibility, acidic intrinsic disordered regions are typically not resolved. However, hypothesis drawn from those structures can be validated *in vivo* in a context where potentially all factors are present. Although histones are highly abundant in the nucleus and are sometimes co-purified in AP-MS approaches (Van Leene et al., 2015), the affinity purifications here show a band patterning on the CBB stain displaying numerous prominent bands in the range from 15-20 kDa (**Figure 5b**). This strong band patterning on the CBB stain of the respective factors vs. the empty tag excludes unspecific interactions and makes histones the prime candidate for potential direct interactors. Although each protein has its own bias (for details see Section 2.1.2), the comparison between datasets of similar complexity will lead to individual proteins being more pronounced in one dataset compared to the next dataset and give some additional informative value, for example here shown for histone variants (**Table 3**). While H2As and H2Bs were found in all histone chaperones, including H2A.Z, a mark for active transcription usually limited to +1 nucleosomes. However, H2A.X a marker for DNA damage (Lei and Berger, 2020), was only found in the two members of the FACT complex, SSRP1 and SPT16 (**Table 3**). This is in good agreement with FACT's association in all kinds of chromatin transactions, here DNA repair (Heo et al., 2008). Similarly, the linker histone H1 was solely found in the SPT16-GS AP-MS dataset (**Table 3**) and occurred strongly in the SSRP1-GS PTM and SPT16-GS PTM datasets (Holzinger, 2015), which will be discussed later (**Table 8**). While H1 has distinct roles in both hetero- and euchromatin (Rutowicz et al., 2019) interplay of FACT with DEMETER in *Arabidopsis* was only present dependent on H1 and heterochromatin marks (Frost et al., 2018), indicating additional roles for FACT in heterochromatin, like shown for other organisms (Formosa and Winston, 2020; Gurova et al., 2018)

Generally, the obtained data fits to direct interactions observed in recent cryo-EM structures (Ehara et al., 2017, 2019; Vos et al., 2018, 2020), which were represented in high scores within the datasets (**Table 1** and **Table 2**), e.g. direct interaction of ELF1 with NRPB1, NRPB2, SPT5 or direct interaction of SPT6 with NRPB1 and SPT5. The FACT complex has been crystallized on the nucleosome (Liu et al., 2020) and its entry point on the transcript elongation complex has been shown recently (Farnung et al., 2021), confirming that SPT16 targets the proximal H2A-H2B and SSRP1 the distal H2A-H2B (Ramachandran et al., 2017). This puts an orientation on the FACT complex, with SPT16 facing the DNA entry, which is reflected in the datasets by the high score of SPT16 in the ELF1 affinity purification (**Table 1**). Especially at the unwinding nucleosome at SHL -5, ELF1 (Ehara et al., 2019) and SPT16 should be directly facing each other (Liu et al., 2020) (**Figure 51b, c**) explaining the high score for SPT16 observed in the ELF1 dataset.

CK2 was associated with all histone chaperones tested (**Table 4**), in good agreement with the published landscape: SPT6 was shown to be regulated by CK2 phosphorylation in yeast, repressing spurious transcription (Gouot et al., 2018). SSRP1 is phosphorylated in *drosophila* (Tsunaka et al., 2009) and *maize* (Krohn et al., 2003). Early data in yeast associated SPT16 with histones, the PAF-Complex and CK2 (Krogan et al., 2002) and in human direct interaction of CK2 with both SSRP1 and SPT16 has been shown in GST-pulldown assays (Keller and Lu, 2002). The PAF-Complex has been shown to be phosphorylated by CK2 in yeast (Bedard et al., 2016). Functional analysis showed that phosphorylation of SPT16 by CK2 plays an important role in nucleosome binding (Mayanagi et al., 2019). The AID of yeast ELF1 is as well phosphorylated by CK2 *in vitro* (Kubinski et al., 2006). In good agreement with all these observations, ChIP in yeast showed that CK2 is present along the transcribed gene and shows a second strong peak prior to the TSS (Basnet et al., 2014), indicating a role both for transcript elongation and initiation. Further histone turnover was increased in yeast *ck2^{ts}* mutants, which was attributed to a loss of histones during transcription. This was only partially explained by SPT6 phosphorylation (Gouot et al., 2018). In the datasets presented here, ELF1 shows very high association with CK2, compared to the other dataset (**Table 4**) and direct interaction with ELF1 has been shown by GST pulldowns for both CK α and CK β in yeast (Kubinski et al., 2006).

Here, ELF1 itself was not phosphorylated by CK2 (**Figure 12a**) and all of the CK2 sites present in yeast (Kubinski et al., 2006) are absent (**Figure 12b**). Even though two potential new sites arise, the replacement of serine or threonine with either aspartic or glutamic acid in *Arabidopsis*

compared to yeast eliminate the actual need of the ELF1-AID to be phosphorylated (**Figure 12b**). This makes the strong association of ELF1 with CK2 (**Table 4**) in absence of enzyme substrate interaction more interesting, as an alternative explanation for their association is needed, for example close proximity in a complex. While CK2 has been attributed to numerous substrates (Meggio and Pinna, 2003) a distinct role during transcription seems likely. Indeed, GST-pulldown assays displayed direct interaction of CK β with Pol II in human (Cabrejos et al., 2004). In yeast, RNA polymerase II coimmunoprecipitated with both CK α and CK β indicating that CK2 interacts with RNA polymerase II *in vivo* (Tripodi et al., 2013). A stable interaction of ELF1 and Pol II with the CK2 complex would be spatially in a good place (preferably located in the gap between the PAF-Complex and ELF1), as all except one AID are potentially in close proximity to be activated by phosphorylation: SPT6 and CTR9 (**Figure 51a**, dotted lines), ELF1 and SPT5 (**Figure 51b**, dotted lines). Additionally, SPT16 invades the nucleosome during transcription, in proximity to the emerging H2A-H2B DNA binding site (Farnung et al., 2018; Liu et al., 2020) (**Figure 51c**).

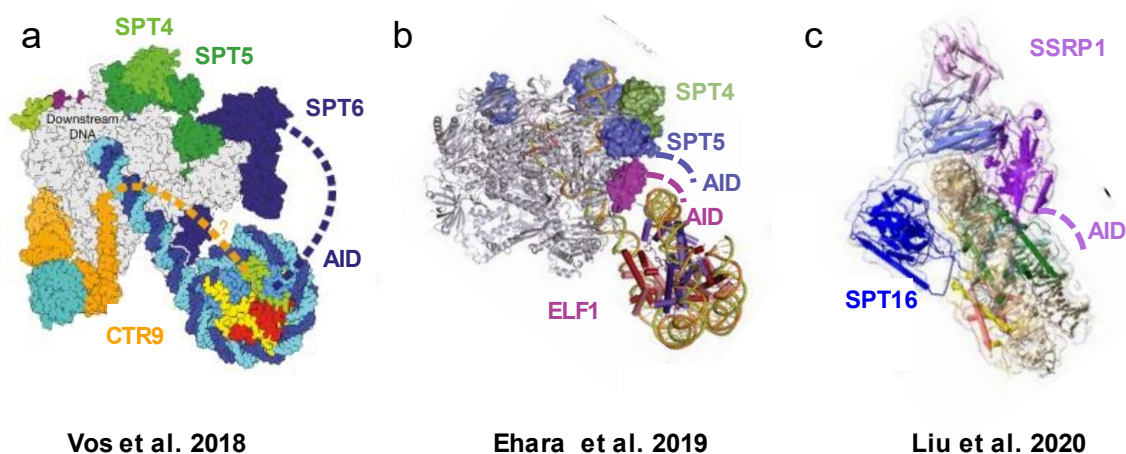


Figure 51 AIDs of TEFs potentially extend to the incoming nucleosome. Due to their high flexibility acidic intrinsic disordered regions are typically not resolved in crystal structures. However, their location on Pol II potentially allow **(a)** the N-terminus of SPT6 (blue) and the C-terminal of CTR9 (orange) to extend to the incoming nucleosome. Figure is modified from Vos et al. 2018. **(b)** The N-terminus of SPT5 (blue) and the C-terminus of ELF1 to extend to the incoming nucleosome (magenta). Figure is modified from Ehara et al. 2019. **(c)** The AID of SPT16 binds to the exposed DNA binding surfaces of H2A-H2B (Liu et al. 2020). The AID of SSRP1 potentially extends to the other H2A-H2B dimer (Mayanagi et al. 2019). Figure is modified from Liu et al. 2020

The AIDs of these TEFs have been implicated to cooperate for the nucleosome reassembly during transcript elongation complex passage (Ehara et al., 2019). The only AID, which has been shown to be phosphorylated by CK2 and is not in direct proximity is in SSRP1. SSRP1-

AID has been implicated in binding the proximal H2A-H2B (Mayanagi et al., 2019). Imagining the unwinding process during transcription further, at SHL-1 ~ half of the DNA is peeled of (Zhou et al., 2019). SPT16 sits at the dyad (SHL 0) and tethers the proximal H2A-H2B and the proximal H3-H4 (Liu et al., 2020). SPT16 would have to be released from the dyad to allow progression of Pol II (Farnung et al., 2021; Zhou et al., 2020). At the same time, the BID and the HMGbox of SSRP1 tether the nucleosome to the most distal linker DNA (Winkler et al., 2011) while the rest of the FACT complex tethers the histone octamer core and the polymerase transcribes further, progressing from SHL +1 to SHL +7 (Zhou et al., 2020). There would be the point where the SSRP1 AID is potentially in close proximity to the DNA entry tunnel (RPB1 and RPB2), the bound ELF1 and a hypothetically docked CK2. Indeed, high scores were obtained for NRPB1 and NRPB2 in SSRP1-GS affinity purifications (rank 6 and 8, **Table 2**) and SSRP1 in ELF1 affinity purification (rank 17, **Table 1**). Interestingly, it has been shown that increasing phosphorylation of the SSRP1 AID leads to an ultrasensitive answer: The AID and the BID, which are connected by a hinge, bind to each other abolishing DNA binding of SSRP1 (Aoki et al., 2020). While this has not been tested in the presence of the nucleosome or histones, it could play a role in releasing DNA from the nucleosome when transcription has already progressed and peeled of huge parts of DNA from the nucleosome. This could assist in depositing the nucleosome upstream of Pol II.

Further, RTF1, which is labile associated with the PAF-complex in organisms other than yeast, has been shown to sit at the DNA exit tunnel and is proposed to mediate histone modifications after Pol II passage (Vos et al., 2020). RTF1 is present with a high score in both FACT AP-MS datasets. Especially in SSRP1 it ranks on position 5th (1st being SSRP1, 2nd SPT16, 3 and 4 being histones). This is in agreement with affinity purifications where Pob3 (the yeast SSRP1 orthologue) co-purified near-stoichiometric with RTF1 (Krogan et al., 2002). Additionally, synthetic lethality was observed when *rtf1Δ* and *pob3* were combined (Costa and Arndt, 2000). For FACT however this could imply, that it is not only present at the DNA entry (shown by high scores for NRPB1, NRPB2, and CTR9 in SPT16 AP, and high scores for SPT16 in ELF1-AP, **Table 1**, **Table 2**) but also at the DNA exit, potentially travelling along with the looping nucleosome. Recent ChIP-Exo studies of SPT16 display a nucleosome like pattern over transcribed genes, in contrast to SPT5 or ELF1 (Badjatia et al., 2021), strengthen this notion that FACT is rather associated with nucleosomes than PolII. In the SPT6 AP-MS dataset, RTF1 ranked on 360th place in and was present in 1/3 replicates. Interestingly, for SPT6 it was shown that RTF1-dependent stimulation is independent of SPT6 (Vos et al., 2020), potentially

indicating that there could be different combinations of the transcript elongation complex and SPT6 and RTF1 might not necessarily occur together.

Surprisingly, ELF1 could not be found in any pulldowns such as NRPB1, SPT16, SSRP1, SPT4, TFIIIS (and others) (Antosz et al., 2017). While this might reflect that complexes are very dynamic, it is puzzling why there are such clear indications for association of ELF1 with the transcript elongation complex in LC-MS/MS experiments (**Table 1-4**), however it is absent *vice versa*. To address this, the mentioned datasets were re-evaluated to test if ELF1 was missed as an interactor due to cut off scores. However, no MS/MS spectra were found for ELF1. Further MS1 spectra were manually checked for the two highest ranking factors with available datasets: NRPB1 and SPT16 (**Table 1**). The most likely peptide obtained in ELF1-GS analysis (**Supplementary Figure 16a**, third row, **Supplementary Figure 16b**) was found in a single spectra (**Supplementary Figure 16c**) in one out of 3 replicates in NRPB1 AP-MS which *could* belong to ELF1 (similar retention time, correct m/z ratio). However, this peptide was so low abundant that it was not analysed further by fragmentation resulting in a MS2 spectra. This still raises the question why ELF1 is so hardly detectable by LC-MS/MS. While purifying ELF1, former team members faced the trouble that 6xHis-ELF1 would precipitate easily and would be found in the pellet. To bypass this, ELF1 was tagged with a GB1-tag (Cheng and Patel, 2004) (**Figure 11**) which was cleaved of later on in a very controlled manner (Markusch, 2018, 2020; Thorbecke, 2019). The GS-tagged ELF1 version used for AP-MS experiments (**Figure 5a**) is also stabilized via the tag, as the GB tag and the GS-tag are partly overlapping, with the GB tag containing part of protein G (Cheng and Patel, 2004). Hence tagged ELF1 can be detected in ELF1-GS pulldowns, however vice versa the untagged ELF1 might precipitate out of solution somewhere along the way when subjected to the steps of affinity purification. While *Arabidopsis ELF1* is highly expressed in all tissues (Schmid et al., 2005; Waese et al., 2017), mass-spec approaches targeting extensively the *Arabidopsis* nucleus in (Goto et al., 2019) or chromatin-associated proteins (Bigeard et al., 2014) run short of detecting ELF1, showing its elusiveness in shotgun proteomics.

3.2 The histone chaperone ELF1

ELF1 contains a basic N-terminus, a defined Zn-Ribbon in the middle and an optional acidic C-terminus (Prather et al., 2005). The presence of the acidic C-terminus in plants is a unique feature in higher eukaryotes and make it a desirable candidate to study. So far ELF1 was not studied in plants and hence, a starting point to study ELF1 in the model organism *Arabidopsis* was created here. This included an AP-MS dataset (Section 2.1) and an ELF1 CRISPR knockout

line (Section 2.2) This was complimented with biochemical studies. The ELF1 AP-MS dataset has been discussed above (**Table 1-4**, Supplementary Data Table 8) and is in good agreement with published datasets: interaction with SPT5, NRPB1, NRPB2 (Ehara et al., 2017), association with CK2 (Kubinski et al., 2006) and the strong association with histones, gives insights into a priorly proposed hypothesis by Ehara et al., 2019: The spatial arrangement on Pol II makes ELF1 acidic region prone to interact with histones. Indeed, GST-pulldown assays showed an acidic C-terminus dependent pulldown of H2B (Thorbecke, 2019). On the other end, ELF1 contains a basic N-terminus. It was hypothesized that this would bind DNA (Ehara et al., 2017). EMSAs showed N-terminus dependent DNA binding in the low μM range (**Figure 11**). This effect was increased by 4WJ DNA, indicating that potentially bent DNA is preferred, similar to the bent DNA obtained in nucleosomes. This effect persisted even in the absence of the GB1-tag (Markusch, 2020), excluding unspecific interaction of the tag. Further, nucleosomes containing linker DNA, as well as nucleosome containing no linker DNA were bound by the basic N-terminus of ELF1 (Markusch, 2020). Intriguingly, all binding events would occur when the C-terminus is absent. As both, the N- and the C-terminus are intrinsically disordered (**Figure 10**, Ehara et al., 2017, 2019) and should therefore show high flexibility, the hypothesis was proposed that the C-terminus might bind and thereby inhibit the N-terminus. This was confirmed by EDC crosslinking experiments (Markusch, 2020). The C-terminal deletion constructs do resemble e.g. human ELF1 (Prather et al., 2005), where the acidic C-terminus is missing. It can therefore be assumed that human ELF1 has DNA binding properties and no histone binding properties. At the same time this raises the question why there is a need for an acidic C-terminus in *Arabidopsis* and yeast, which has yet to be answered.

Another open question is, how the actual autoinhibition of ELF1 might be released as completely wrapped nucleosomes were not bound by full-length ELF1 (Markusch, 2020). The gradual unwrapping of DNA by Pol II progression (Farnung et al., 2018) could provide the force to dissociate DNA H2A-H2B binding sites. Hence, the ELF1-AID could bind to H2B and release the ELF1-BID to bind to the free DNA. A putative way to test this hypothesis could be to perform EMSAs with full-length ELF1 and a 112 bp octasome, lacking a 33bp DNA fragment typically bound by H2A-H2B (Mayanagi et al., 2019).

In the ELF1-GS AP-MS dataset high scores were detected for both SPT16, SSRP1, SPT6l and SPT5. Further TEC components like TFIIS and SPT4 were barely detectable (**Table 1**). The created CRISPR knockout mutant $\Delta elf1$ alone showed no apparent phenotype (**Figure 9**) (Markusch, 2018). However the double mutants $\Delta elf1, ssrp1-2$ and $\Delta elf1, spt16-1$ showed clear

synergistic effects (Markusch, 2020) and an increase of the priorly attributed defects of the T-DNA single mutants *spt16-1* and *ssrp1-2* (Lolas et al., 2010). Similarly, a synthetic *Spt*-phenotype has been described before for *spt16 elf1* combinations in yeast (Prather et al., 2005). This is in line with a potential concerted effort of AID containing transcript elongation factors to tether and hand over the unwrapping nucleosome during transcription. While the lack of one AID in *Δelf1* might not be detrimental, an already impaired *ssrp1-2* or *spt16-1* mutant is further handicapped by the loss of ELF1 and its tethering AID. The strong association of ELF1 with CK2 (**Table 4**) in the absence of enzyme/substrate interaction (**Figure 12**) has been discussed before (Section 3.1). While phosphorylation of its AID might not be necessary for ELF1, phosphorylation of SPT16 AID seems to play an important role and will be discussed next.

3.3 Phosphorylation of SPT16 AID

Via affinity purification in presence of phosphatase inhibitors and a subsequent LC-MS/MS analysis many modifications were detected (Holzinger, 2015). Due to the high abundance of histones in FACT affinity purifications (compare **Figure 5**) many histone marks (Supplementary Data Table 11) were among them (**Table 8**).

Table 8 Histones and Histone Modifications in FACT AP-MS (Holzinger 2015)

SPT16		SSRP1		PTMs	Interactor	AGI	UNIPROT
Rank	Score/#IPs	Rank	Score/#IPs				
25	1384/3	13	1616/3	K150ac	H1.1	AT1G06760	P26568
8	2015/3	6	2370/3	K156ac	H1.2	AT2G30620	P26569
20	1564/3			K5ac	H2A.1	AT5G54640	Q9LD28
9	2008/3	8	1894/3	K5ac	H2A.10	AT1G51060	Q9C681
22	1434/3	18	1388/3	K5ac, K119me	H2A.13	AT3G20670	Q9LHQ5
17	1608/3	12	1712/2	K5ac	H2A.2	AT4G27230	O81826
61	575/3	47	760/3	K5ac, K140ac, K144ac	H2A.W.6	AT5G59870	Q9FJE8
18	1585/3	9	1888/3		H2A.W.7	AT5G27670	Q94F49
15	1683/3	14	1501/3		H2A.X.3	AT1G54690	Q9S9K7
		10	1857/2		H2A.X.5	AT1G08880	O04848
32	1105/3	21	1334/3	K3ac, K6ac, K12ac	H2A.Z.8	AT2G38810	Q9SII0
31	1108/2	29	1116/3	K3ac, K6ac	H2A.Z.9	AT1G52740	Q9C944
5	3458/3	4	3302/3	K3me3, K6ac, K11ac, K27ac, K39ac, K40ac	H2B.11	AT5G59910	P40283
14	1689/2				H2B.4	AT2G37470	Q9ZUS0
4	3523/3	3	3455/3	K6ac, K11ac	H2B.6	AT3G45980	O23629
6	3126/3	5	2970/3	K3me3, K6ac, K11ac, K22ac, K27ac	H2B.7	AT3G46030	Q9LZT0
79	370/3	80	374/3	K9ac, K14ac, K18ac, K24ac, K9me1, K9me2, K27me1, K27me2, K27me3, K36me3	H3.1	AT1G09200	P59226
29	1126/3	27	1134/3	K12ac, K16ac	H4	AT1G07660	P59259

A more detailed evaluation of the datasets raised in my master's thesis (Holzinger, 2015) shows that co-immunoprecipitated histones and histone marks show association of the FACT complex with both hetero- and euchromatin (**Table 8**). In line with FACTs role in transcription, many histone marks associated with transcript elongation were found, like e.g. H2Aac, H2Bac, H3ac and H4ac, H3K36me3 (Leng et al., 2020). Most striking however was the presence of the determining histone modifications present in heterochromatin, H3K9me2 and H3K27me1 (Roudier et al., 2011; Sequeira-Mendes et al., 2014), confirming the broad role for FACT overall, here in heterochromatin. The association with heterochromatin is potentially shown by the high scores obtained for linker histone H1 (**Table 8**), which has been observed before exclusively in the second SPT16 AP-MS dataset (**Table 3**). FACT has been shown to bind directly to H1 (Kalashnikova et al., 2013) and SSRP1 has been implicated in the eviction of H1 (Falbo et al., 2020). In *Arabidopsis* FACT was required for proper DEMETER function, a DNA glycosylase which catalyses genome-wide DNA demethylation. Intriguingly, not all DEMETER targets were affected but those who were enriched with H3K9me2 and H3K27me1 and associated with linker histone H1 (Frost et al., 2018). The strong immunoprecipitation of heterochromatin- as well as euchromatin- (H2A.Z) and repair marks (H2A.X) show that FACT is important for many chromatin processes and is not limited to Pol II transcript elongation.

SPT16 phosphorylation has been shown to be crucial *in vitro* for the binding of SPT16-AID to the 112bp octasome (Mayanagi et al., 2019). Here it was shown that phosphorylation is mediated by CK2 (**Figure 13**) and that phospho-mimicking, albeit potentially not all sites were targeted (**Figure 15**), leads to a slight increase in H2A-H2B binding affinity in GST-pulldown assays (**Figure 19**). In line with this, cell culture affinity purifications with phospho-mimicking and phospho-insensitive SPT16 variants showed a decrease in H2B and H3 affinity when phosphorylation is averted (**Figure 20b**). The WT-variant (being natively phosphorylated) shows a histone pulldown efficiency comparable to the phospho-mimetic variant, indicating that the phosphorylated SPT16-AID is the default state (**Figure 20b**). In line, in an *in vitro* set-up with the 112 bp nucleosome and truncated SPT16 AID, the phosphorylated AID bound to H2A-H2B DNA binding sites. In the absence of phosphorylation no binding was observed with AID and 112 bp nucleosome (Mayanagi et al., 2019). Indeed, the rescue-ability of the respective transgenes for the *spt16-1* T-DNA insertion line differed in almost all tested traits (**Figure 25- Figure 27**). The *spt16-1 pSPT16:TagRFP-SPT16-WT*-variant rescued best, still showing some impairment compared to the Col-0 background, like observed before for an untagged construct (Lolas, 2008). The Phospho-mimicking variant rescued all traits, however not as efficiently as the WT-variant, showing that the switch between phosphorylated and an unphosphorylated

states are important for proper function. The Phospho-insensitive variant rescued most traits worst showing that phosphorylation of the AID is part of SPT16 function. While some traits were rescued and restored comparable to the Phospho-mimetic variant, e.g. leaf shape and number of seeds (**Figure 26**, **Figure 27**), some defects of *spt16-1* were slightly increased, like the time of bolting and subsequently the leaf diameter at bolting (**Figure 25**, **Figure 26**). Altering the timing of reproduction is often a response to stress to finish the lifecycle in a shortened timeframe (Zhou et al., 2017), potentially indicating an increased negative effect when the Phospho-insensitive transgene is introduced. Initial problems with direct transformation of *spt16-1* *-/-* and *spt16-1* *+/-* strengthen this notion.

H3 ChIP-seq analysis comparing Col-0, *spt16-1*, *spt16-1 pSPT16:SPT16-WT/Phos 0/Phos +* show a pronounced defect for the Phospho-insensitive variant. While the overall H3 occupancy is intact (**Figure 29**), normalization to Col-0 (**Figure 30**) displayed a distinct peak in the region upstream of transcription start site (TSS) in the otherwise nucleosome depleted region (Zhang et al., 2015). This peak was present from high- to low expressed genes, however most pronounced in the quartile of highest expressed genes and absent in any other genotype, including *spt16-1* *-/-*. Recent differential MNase seq datasets showed the presence of a fragile -1 nucleosome upstream of the TSS, particularly in low transcribed genes (Pass et al., 2017). As not all genes were affected, a list was extracted which showed >50% enriched NDR H3-signals in *Phos 0*. This list was cross-correlated with the differential MNase seq data (Pass et al., 2017), displaying a clear discrepancy between high and low MNase digests which can be explained by the presence of a sensitive -1 nucleosome in some of the genes (**Figure 31**). This shows that that indeed phosphorylation of SPT16-AID is important in clearing the region upstream of TSS. Generally, binding of H2A-H2B by AID leads to steric collisions with H3-H4, displacing the H2A-H2B dimer and thereby enables the SPT16 middle domain to bind to H3-H4 and hence to a proposed opening up of the nucleosome (Liu et al., 2020). The here shown lack of negative charge in the three respective sites in the phospho-insensitive variant might therefore impair the initial invasion step, leading to diminished nucleosome binding by FACT and a possible impaired nucleosome removal at NDRs.

Generally, miss-localisation of H3 was present in *spt16-1 pSPT16:SPT16 Phos 0* and showed no obvious defects in *spt16-1*. In yeast the temperature sensitive strain *spt16-197* leads to a full knockdown when shifted to non-permissive temperatures. H3-ChIP seq analysis (Jeronimo et al., 2019; True et al., 2016) shows a similar, more severe pattern than *Phos 0* (**Figure 52a**, arrow) with enriched signals in the NDR and a decrease over the gene body (however not

normalized to wildtype but to the input). H4 and H2B ChIP-seq experiments showed similar patterns (Jeronimo et al., 2019), indicating that H3 is a good proxy for the entire nucleosome. The T-DNA insertion line *spt16-1* is a knockdown allele, reducing the transcript level by ~ 40% and comparatively the protein level (Lolas et al., 2010). The absence of the described pattern in *spt16-1* (**Figure 30**) could be due to the remaining FACT activity which prevents accumulation of histones/nucleosomes in the NDR. Hence, it would have been interesting to see if the here introduced mutations are viable in a full knockout background like e.g. *spt16-3* (Frost et al., 2018). The here observed H3 enrichment in the NDR in the *spt16-1 pSPT16:SPT16 Phos 0* line might also be partially rescued by normal SPT16 function. The remaining accumulation observed in *spt16-1 pSPT16:SPT16 Phos 0* not being rescued by the remaining FACT activity, could be explained by acetylation-insensitive SPT16 occupying the gene and blocking it for native SPT16 function, thereby leading to decelerated clearing of the NDR. Next to the defects in the NDR, a reduction of H3 over the gene was observed in the *Phos 0* mutant (**Figure 30**), showing that AID phosphorylation might also be important during transcript elongation.

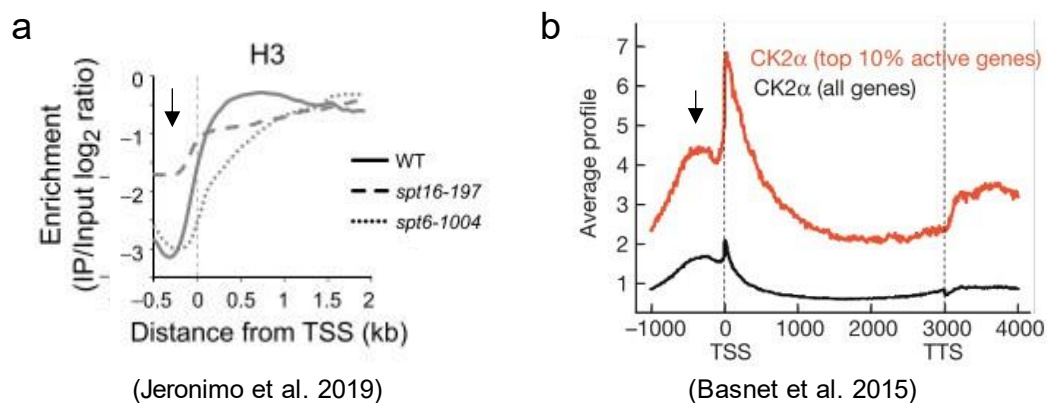


Figure 52 H3 and CK2 α ChIP-Seq analysis in yeast show a role in the region upstream of TSS (a) H3 Signal is misslocalised in *spt16* and *spt6* mutants. *spt16* displays increased H3 signal in the region upstream of TSS compared to the WT control (black arrow) (b) CK2 α binds across the actively transcribed genes globally and in enhancer elements upstream of TSS. Panel (a) is taken from Jeronimo et al. 2019, Panel (b) from Basnet et al. 2015

The here shown defect was mediated by replacing serine or threonine with either valine or alanine, to obtain a CK2 insensitive substrate in the respective sites. In line with an important role for CK2 mediated activation of SPT16 in the process of -1 nucleosome eviction, CK α ChIP-Seq in yeast showed a second peak upstream of the TSS (**Figure 52b**, arrow). This peak was particularly pronounced in highest transcribed genes, potentially indicating - similar to the H3 ChIP seq data of *Phos 0* (**Figure 30**) - that highest transcribed genes are equally occupied

by sensitive -1 nucleosomes, however rapidly removed. In line with this, H3 ChIP-Seq in a *ck2* temperature sensitive mutant showed an enrichment of H3 signal in the region upstream of the TSS (Gouot et al., 2018).

The presence of a sensitive -1 nucleosome has regulatory implications, as proximal promoters are covered in its presence. Indeed promoter motif enrichment (**Figure 32**) of particularly affected genes (>50% enriched, $p < 0.05$) shows a clear enrichment of certain motifs like e.g. E-box and TCP, which are critical for development especially during seedling development (Hetzl et al., 2016). This is in line with the 14-day old seedlings used for ChIP analysis and highlights the strong need for FACT activity during these stages which is further highlighted by ubiquitous SPT16 promoter expression shown by promoter GUS fusion constructs in 14-day old seedlings (Pfab et al., 2018a).

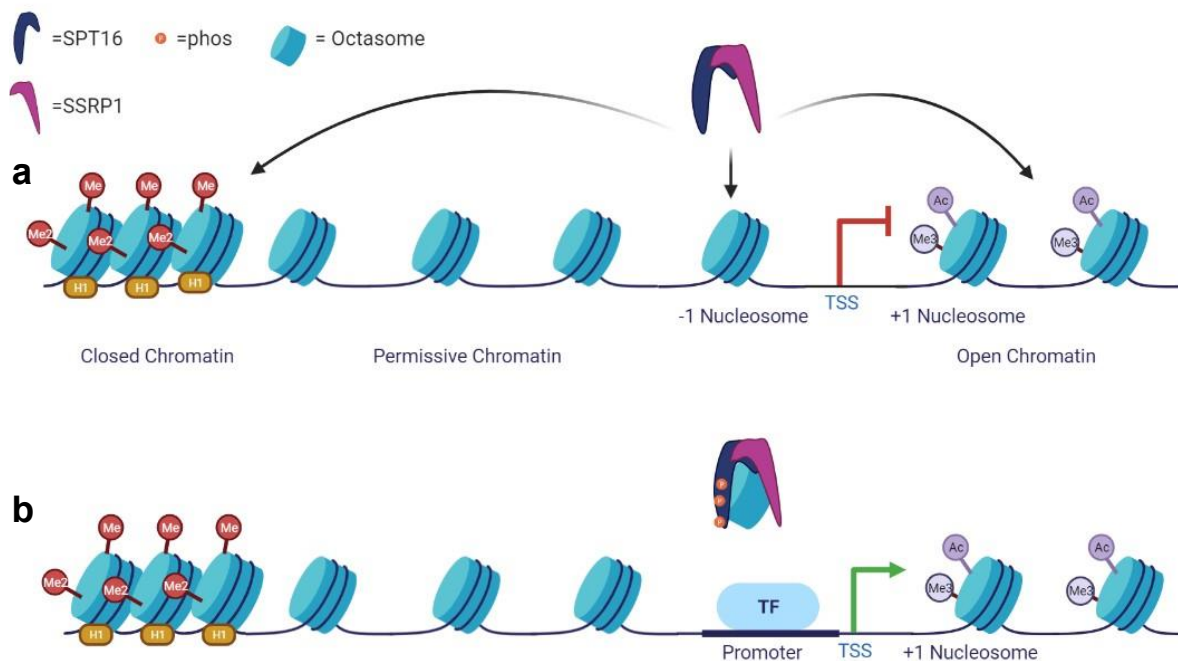


Figure 53 The FACT-complex removes the -1 nucleosome to facilitate transcription (a) FACT potentially associates with closed, permissive and open chromatin. Genes with covered promoters are not transcribed **(b)** Phosphorylation of SPT16 enables the removal of the fragile -1 nucleosome in a subset of genes and reveals covered promoters which enables transcription factors (TF) to bind and initiate transcription. Dark blue: SPT16, Magenta: SSRP1, orange Me circles: H3K27me1, orange Me2 circles: H3K9me2, Blue Ac and Me circles: active chromatin methylation and acetylation marks. Figure was created with BioRender.com

To propose a model: The strong presence of active chromatin marks like H3-, H4-, H2B-, H2A-Ac and H3K36me3, as well as the determining histone modifications of heterochromatin, H3K9me2 and H3K27me1 (**Table 8**) and the strong association with linker histone H1 suggest

a broad role for FACT in all chromatin states (**Figure 53a**). During initiation, the phosphorylation of SPT16-AID shows a particular role for FACT in proximal promoter clearing. This could activate transcription factor binding and the start of the transcription machinery (**Figure 53b**). This is in line with studies which show that FACT binding at certain promoters precedes nucleosome eviction and hence gene expression (Takahata et al., 2009)

This model lacks how FACT is recruited to histones and how DNA is loosened from the nucleosome for FACT to invade. Recent ChIP-Exo studies in the absence of stress depict a regular patterning, potentially overlapping with nucleosomes along transcribed genes (Badjatia et al., 2021). Indeed, FACT is very abundant, estimated at approximately one complex per three nucleosomes. In consequence enough molecules would be readily available without prior recruiting it to specific sites (Formosa, 2012). Indeed, upon heat shock FACT levels at promoters stayed constant and got enriched at the CDS (Saunders et al., 2003), indicating that FACT might steadily sit at some nucleosomes.

The driving force for nucleosome invasion might arise when the SWI/SNF family functions in NDR formation. *In vitro* the ATP-dependent chromatin remodelling complex SWI/SNF mediates disassembly of nucleosomes, which leads to loss of DNA contacts at H2A-H2B which can promote the dissociation of one H2A-H2B dimer and eventually leads to the complete loss of the nucleosome (Dechassa et al., 2010). The dissociation of DNA from H2A-H2B mediated by SWI/SNF might be the start point for invasion. Phosphorylation of SPT16-AID might hereby also be required (compare Mayanagi et al., 2019) and play a role in tethering first the H2A-H2B dimer and later the whole nucleosome, thereby preventing the loss and uncoordinated exposure of histones to DNA. By shielding the charge interface of the histones and DNA with the AID of SPT16, this process might become energetically more favorable. Indeed, AP-MS data (**Table 9**, Holzinger, 2015) shows some indications for co-occurrence of the SWI/SNF-complex and FACT, linking the two promoter clearance events.

Table 9 Association of SPT16 with Swi/Snf-Complex

SPT16 - SDU		Interactor	AGI	Uniprot
Rank	Score/#IPs			
155	131/2	SNF5	AT3G17590	P93045
112	210/3	SNF12	AT5G14170	Q9FMT4
170	113/2	SWI3D	AT4G34430	Q8VY05

Requirements for SWI/SNF binding were a DNA linker length between two nucleosomes of 40–50 bp (Wagner et al., 2020). Binding of SPT16-AID to H2A-H2B, thereby freeing the histone bound DNA (Mayanagi et al., 2019), might help to establish the necessary DNA linker length for SWI/SNF action. Fittingly, in yeast Swi2/Snf2 ATPase MOT1 has been shown to co-regulate transcription with SPT16 and alter nucleosome assembly upstream of TSS (True et al., 2016).

3.4 Acetylation of SSRP1 BID and HMGbox

Next to the phosphorylation of SPT16-AID, acetylations in the basic intrinsic disordered region of SSRP1 and its neighbouring HMGbox were analysed. In line with a regulatory role of the acetylations, the DNA binding affinity towards linear DNA in EMSAs was decreased when the *in vivo* acetylated lysines (**Table 6**) were substituted for acetylation mimicking amino acids (**Figure 37**). *In vivo*, in *Arabidopsis* cell culture The insensitivity to acetylation in the respective sites led to an increase in H3 and H2B pulldown efficiency compared to the wildtype SSRP1 variant (**Figure 39**). This correlates with the positive charge provided by lysine, potentially binding to DNA forming an electrostatic interaction which gets neutralized by acetylation. In the WT variant, pulldown efficiency is similar to the acetylation-mimetic version (**Figure 39**), indicating a regulatory effect on DNA binding by acetylation. Due to the role of the HMGbox in tethering the nucleosome to the DNA (Chen et al., 2018) this indicates that ultimately the release of SSRP1 from DNA and the nucleosomes could be regulated.

The rescue-ability of the respective transgenes for the *ssrp1-1* T-DNA insertion line differed slightly. All *pSSRP1:SSRP1-NLS*-variants were able to complement the absence of native SSRP1. The acetylation-mimetic variant bolted slightly but significantly earlier than wildtype and acetylation-insensitive SSRP1 variants (**Figure 44**). In agreement the final rosette diameter was smaller compared to *Ler*, *WT* and *Acetylo* (**Figure 45**), indicating some mild adverse effects in the later stages. The distortion in charge leads to a secondary structure change in the HMGbox, increasing the random coil (**Figure 38**) and at the same time decreases the DNA binding affinity (**Figure 37**). While this might not abolish DNA binding altogether it reduces the functionality of the HMGbox. When the HMGbox is completely missing, alternative small HMGB proteins might compensate its function (Pfab et al., 2018b). With the presence of an impaired HMGbox this compensation might be obscured, hence explaining the mild defects compared to *ssrp1-1* SSRP1 Δ HMG rescues (Pfab et al., 2018b). In yeast SSRP1 is split into POB3 and the HMGbox containing NHP6. Similarly, a construct expressing POB3 fused to 3 NHP6 molecules, would lead to general toxicity and would be insufficient in rescuing a *pob3*

deletion strain (McCullough et al., 2018), indicating a general sensitivity towards altering the DNA binding functions of the HMGbox of SSRP1.

The increased FRET efficiency of SSRP1 with HDT1 and HDT2 in nucleoli (**Figure 34**) must be interpreted with care. The interaction occurred rarely and in tobacco leaf epidermis cells under control of the 35s promoter and one possibility would be the observation of artefacts due to overexpression. However, high scores in two independent AP-MS datasets point in the direction of biological relevance (**Table 7**). HDT1-3 were localised in the nucleolus (**Figure 34a**) in line with prior work (Zhou et al., 2004). Rare subcellular localisation of SSRP1 in the nucleolus (**Figure 34a and b**) is in line with two independent proteomic approaches analysing the nucleolus (Montacié et al., 2017; Pendle et al., 2005) and prior analysis of eGFP_SSRP1 in cell culture by former team colleague Alexander Pfab showed an enrichment in a ring like structure at the nucleolus (Pfab, 2017). Next to its role in histone deacetylation (Li et al., 2017) HD-tuins have been suggested to serve as nucleoplasmins in *Arabidopsis* and hence store and transport histones during nucleosome assembly (Kumar and Vasudevan, 2020). FACT has been implicated also in the deposition of nucleosomes (Johnson et al., 2013; Yang et al., 2016) and particularly the SSRP1 HMGbox has been proposed to overcome the inherent stiffness of DNA and mediate bend formation during nucleosome assembly (Formosa and Winston, 2020; McCullough et al., 2018). Hence, nucleosome assembly mediated by FACT could require full SSRP1-HMGbox functionality and therefore prior deacetylation by the HD-tuin family of histone storage proteins.

No direct interaction of SSRP1 with GCN5 was displayed in Y2H and FRET (**Supplementary Figure 8**), however here, for enzyme substrate interaction a transient indirect interaction might be sufficient. A study in human profiling GCN5 and P300 substrates showed that SSRP1 is a shared substrate of both (Chen et al., 2017). Further, the invasion of the nucleosome by the phosphorylated SPT16 AID enhances the ability of GCN5 to acetylate lysines in the H3 N-termini by exposing them and making them more accessible (Tsunaka et al., 2020). GCN5 ChIP in *Arabidopsis* shows association along both promoters and transcribed genes correlating with the strength of transcription (Kim et al., 2020). Surprisingly, nucleosome promoter occupancy was not altered upon stimulus in a *gcn5* knockout in fission yeast, however nucleosomes downstream of Pol II were not evicted (Sansó et al., 2011). This indicates a role for GCN5 in Pol II progression especially during transcript elongation, particularly in early stages where acetylation marks are most enriched (Leng et al., 2020).

While SPT16 phosphorylation and SSRP1 acetylation do not necessarily occur together, combining the two processes could lead to a regulatory cascade: Pol II transcribes, leading to a loss of histone-DNA contacts (Farnung et al., 2018; Kujirai et al., 2018) and SPT16 phosphorylated in its AID invades (Mayanagi et al., 2019). The binding of SPT16 AID at the H2A-H2B binding sites make the H3 N-terminus on the SPT16-AID side more accessible for GCN5 acetylation and additionally increases accessibility of the H3-N-terminus on the other DNA side (Tsunaka et al., 2020). Acetylated N-termini loosen histone DNA contacts thereby enhancing Pol II progression rate. During the acetylation of histone N-termini, acetylation of SSRP1 BID and SSRP1 HMGbox could co-occur thereby loosening the association of FACT to the nucleosome. Following this line of logic, the acetylation in SSRP1 BID and HMGbox occurs at a time point where a) DNA is already (partly) peeled of the nucleosome and bound by SPT16; b) histone DNA contacts have already been weakened by H3 N-termini acetylation c) Pol II can unwrap the protected octasome/nucleosome further. This could be a good timepoint to loosen FACT DNA contacts to reposition the nucleosome upstream of Pol II.

3.5 A role for SSRP1 in seed dormancy

3.5.1 The SSRP1 subunit of the histone chaperone FACT is required for seed dormancy in *Arabidopsis*

Disclaimer: This chapter was published in Journal of Plant Physiology (Michl-Holzinger et al., 2019)

DOG1, a QTL which is transiently highly expressed, is affected by knockdown of SSRP1 in the *ssrp1-2* mutant (section 2.7). Comparative, genome-wide transcript profiling of *Arabidopsis ssrp1-2* and *spt16-1* relative to Col-0 seedlings demonstrated that a very similar and relatively small subset of genes is differentially expressed in both mutants (Pfab et al., 2018a). The differential expression of only relatively few genes is in agreement with the observation that the transcription of some genes is more sensitive to the absence of certain TEFs (Van Lijsebettens and Grasser, 2014). Transcription of DOG1 appears to be particularly susceptible to chromatin-mediated regulation as its expression is dependent on RNAPII-associated TEFs including SSRP1 (section 2.7) and TFIIS (Mortensen and Grasser, 2014) as well as on certain histone modifications including H2B-monoubiquitination and H3-methylation (Liu et al., 2007; Molitor et al., 2014; Zheng et al., 2012). Thus, FACT (in combination with other TEFs) may promote DOG1 transcription during seed maturation by destabilising nucleosomes in the path of RNAPII. Interestingly, there is genetic interaction between the gene encoding the histone

H2B-monoubiquitinase HUB1 and the genes encoding the FACT subunits SSRP1 and SPT16, for instance, regarding *Arabidopsis* leaf vein patterning or silique development (Lolas et al., 2010). Therefore, it appears likely that proper transcription of *DOG1* during seed maturation requires the concerted action histone modifiers and RNAPII-associated TEFs including FACT to achieve appropriate levels of seed dormancy.

3.5.2 General Discussion

The expression of *DOG1* was particularly sensitive to *SSRP1* downregulation in the *ssrp1-2* mutant (**Figure 48**) and similar tendencies have been observed for *spt16-1* (Mortensen, 2012). The here shown regulatory effects of PTMs of FACT might also be valid here: Phosphorylation of the AID could lead to promoter clearance promoting *DOG1* expression. Indeed, the regulation of *DOG1* by *SSRP1* and its regulation of seed dormancy shown here, has been cited as a potential example for the role of FACT in the “expression of key proteins that are repressed in heterochromatin” (Tsunaka et al., 2020). Although only slightly miss-regulated, the expression level of *DOG1* directly translated into a phenotype (**Figure 50**): 30 % reduction, leading to early germination and 40% increase leading to delayed germination. This makes it a sensitive marker which can be employed in other transcript elongation factor mutants which otherwise display little phenotype, like shown before for the *tfl1s* knockout mutant (Mortensen et al., 2011).

4 Summary

The landscape of transcript elongation factors associated with transcribing Pol II contains multiple factors with AIDs which potentially interact with the basic interface of the unwinding nucleosome: ELF1, SPT5, CTR9, SSRP1, SPT16 and SPT6 (Ehara et al., 2019). Here, four of those factors have been targeted by AP-MS approaches (ELF1, SPT6l, SSRP1 and SPT16) in the *Arabidopsis* cell culture system. Indeed, each dataset contained histones, Pol II and other transcript elongation factors. In line, direct interaction of ELF1 with both DNA and histones was shown here and/or by students supervised in this thesis (Markusch, 2020; Thorbecke, 2019). Transient binding of histone and subsequent release qualify ELF1 as a histone chaperone. Concomitantly, double mutant analysis of ELF1 with other histone chaperones showed synergistic effects (Markusch, 2020), potentially indicating a concerted action in tethering the nucleosome in the process of transcription. Additionally, it was shown that histone chaperone function of the FACT complex is regulated by post-translational modifications. Prior to this work, post-translational modifications of FACT were detected by a shotgun proteomics approach (Holzinger, 2015), leading to the detection of phosphorylations in the acidic region of SPT16 and acetylations in the DNA binding region of SSRP1. For SPT16 phospho-insensitive/unphosphorylated variants led to a decrease, phospho-mimetic variants however led to an increase in histone binding affinity, both *in vivo* and *in vitro*. Creation of phospho-insensitive and phospho-mimetic SPT16 transgenes complementing *spt16-1* showed that altering the charge has an impact on the rescue-ability of the respective transgene. Particularly the phospho-insensitive variant was affected. H3 ChIP-Seq analysis revealed altered H3 occupancy for the phospho-insensitive variant, highlighting the need of SPT16 phosphorylation. Particularly the region upstream of TSS containing the fragile -1 nucleosome was affected, indicating a role for clearing the nucleosome depleted region. Changing the acetylation pattern in SSRP1, led to a loosening of chaperone/DNA contacts for acetylation-mimetic variants, which translated into a reduction of histone pulldown efficiency compared to the fully charged variant. Acetylation-insensitive and acetylation-mimetic SSRP1 transgenes complementing *ssrp1-1* led to only mild phenotypic alterations. Finally, DOG1, the quantitative trait locus for seed dormancy was shown to be particularly affected by FACT function in the *ssrp1-2* mutant.

5 Materials

5.1 Instruments

Table 10 Instruments used in this study

Instrument	Model (Manufacturer)
Immunoblotting system	Semi-dry Blotting System (Carl Roth)
Centrifuges	Sorvall LYNX 4000 equipped with SLA1500 or SS34 rotor (Thermo Fisher Scientific), Centrifuge 5417R and 5804R (Eppendorf)
Digital camera	EOS 600D: Macro lens EF-S 60 mm 1:2.8 USM; ETS 18-55 mm objective (Canon)
FPLC System	Gradient Programmer GP250 (Pharmacia Biotech)
Fluorometer	Qubit (Thermo Fisher Scientific)
Homogenizer	TissueLyser II (Quiagen)
Imager	BioDocAnalyze System (Biometra), ChemiDoc MP (Bio-Rad), Multimage TM FluorChem FC2 (Alpha Innotech), Typhoon FLA 9500 (GE Healthcare)
Microscopes	TCS SP8 (Leica)
Phosphoscreen	Cyclone Storage Phospho Screen (Packard Instruments Co.)
Phosphor imager	Cyclone Storage phosphor imager (Canberra Packard)
Plant incubator	Plant incubator (Percival Scientific)
qPCR cycler	Mastercycler ep RealPlex (Eppendorf)
Shaking Incubator	Multitron Standart (Infors HT)
Sonicator	Bioruptor Pico (Diagenode), UW2070 MS73 (Bandelin electronic)
Spectrophotometer	NanoDrop ND-1000 (Peqlab)
Thermocycler	T3000 and T Gradient thermocyclers (Biometra)

5.2 Chemicals and Enzymes

Laboratory grade chemicals and reagents were purchased from AppliChem (Germany), Carl Roth (Germany), Duchefa (Netherlands), Eurogentec (Belgium), Merck (Germany), Sigma Aldrich (Germany), TAKARA BIO (Japan), US Biological (USA) and VWR (USA). Enzymes were purchased from New England Biolabs (USA), PEQLAB/VWR (USA) and Thermo Fisher Scientific (USA). [γ -³²P]ATP was obtained from Hartman Analytic (Germany)

5.2 Oligonucleotides

Table 11 List of Oligonucleotides. ID = Internal lab identifier; S. = Source: * = from this study, L = from lab collection).

ID	Sequence 5'-3'	Description	S.
2467	AATGGGCCTTAAATACTTGGAA	Genotyping ELF1	L
2445	ACCAATCAGATGCTTCATATCA	Genotyping ELF1	L
802	GCCTTTTCAGAAATGGATAAATAGCCTTGCTTCC	Genotyping spt16-1	L
1124	TACTTGTCTAACGCAGCGAAATC	Genotyping SPT16/spt16-1	L
4991	GTAGCTACGATCAATCTTGGATCCA	Genotyping SPT16	L
3836	AAGTGATCGCGAATGGTGTCTAAGGGCGAA	Genotyping TagRFP-SPT16	L
1785	GAGGGGCTCGGGCATTACCAT	Genotyping TagRFP-SPT16	L

800	ACCCGACCGGATCGTATCGGT	Genotyping <i>ssrp1-1</i>	L
808	GATAATTGCTTCTCATCCGGTGT	Genotyping <i>ssrp1-1/SSRP1</i>	L
4707	GGATGAAGCTGAGAGTGGTG	Genotyping SSRP1	L
4047	TGGTTCACCAACTGATGATTCT	Genotyping <u>SSRP1</u> -NLS	L
3837	TTCCTAGGATCCCAATTGCC	Genotyping SSRP1-NLS <u>BB</u>	L
812	GTTGCCCGTCTCACTGGTGA	Genotyping <i>ssrp1-2</i>	L
810	CCCTCATCTTACGCGTATCAGA	Genotyping <i>ssrp1-2/SSRP1</i>	L
874	GAAACACGACGATCTGTTTTGTTGCT	Genotyping SSRP1	L
1744	AACGAGAAGCGCGATCACAT	Genotyping SSRP1- <u>EGFP</u>	L
1338	TGATCTCGAAATCCAACGAATTGT	Genotyping <u>SSRP1</u> -EGFP	L
2368	ATTTTGCCGATTTCCGGAAC	Genotyping <i>tflls-1</i>	L
1185	TTTCCTCTTGTCACTTGCCAT	Genotyping <i>tflls-1/TFIIS</i>	L
1184	ATCCTCTGGAATGTTGATAGT	Genotyping TFIIS	L
2511	CATGTACAACGTGAATAGTGG	Genotyping <u>DOG1</u> transgene	L
1939	ATTTGTAGAGAGAGACTGGTG	Genotyping DOG1 <u>transgene</u>	L
4664	TGAAAACGACCATGAACATCTG	qRT-PCR SSRP1	L
4665	CATTATCCCCAAGAAGCAGCAG	qRT-PCR SSRP1	L
4917	GACGGCTACGAATCTTCAGGTG	qRT-PCR DOG1	*
4918	TGCGTCTTCTGTAGGCTTGAGAC	qRT-PCR DOG1	*
4921	GAGGCTTGTTCACTCATTCTCG	qRT-PCR AT4G12590	*
4922	CCTTCTCTGCACCCAGACTCTTTG	qRT-PCR AT4G12590	*
4919	AGCCTACGCAGCATCCAACCTC	qRT-PCR AT4G02080	*
4920	TAGACCACAGCGTCCACCTTAG	qRT-PCR AT4G02080	*
4667	ATTGTAGACCCGTGATTGCAGAA	Cloning Plasmid ID 1234	*
4668	AACTTCTGCAATCACGGGTCTA	Cloning Plasmid ID 1234	*
4063	CAGTCCATGGCAAATTCAAAAAGAGGCAGTATAAGC	Cloning Plasmid ID 977	*
4065	GCTCTAGAGCTGGCGGATTTTCATCATC	Cloning Plasmid ID 976	*
4062	GCCCTCGAGGCTGGCGGATTTTCATCATC	Cloning Plasmid ID 977	*
4064	CGGGATCCAAATTCAAAAAGAGGCAGTATAAGC	Cloning Plasmid ID 976	*
4364	AGAAGGAGATATACATATGGCC	Cloning Plasmid ID 1116, 1118, 1119	*
4365	GGAGCTCGAATTCGGATC	Cloning Plasmid ID 1116-1119	*
4366	ATACATATGAGTTCTGGTGCC	Cloning Plasmid ID 1117	*
4937	TCTGGATCCGTATGGGAAAGAGGAAATCAAGAGC	Cloning Plasmid ID 1393, 1394	*
4938	AGTTCTCGAGTCAGGTATTAACCCTCTCGCAC	Cloning Plasmid ID 1394	*
1253	ATACTCGAGTCAGAAGTTATACTTCTTTTTG	Cloning Plasmid ID 1393	L
4697	GGA CAT ATG GGA AAG AGG AAA TCA AGA G	Cloning Plasmid ID 1246, 1248	*
4698	CGA CAT ATG GAT AAG CTT GAC ACA ATC T	Cloning Plasmid ID 1247, 1249	*
4699	GGC ACT CGA GGA AGT TAT ACT TCC TTT TGACAG AGA CAT	Cloning Plasmid ID 1246, 1247	*
4700	AGT TCT CGA GGG TAT TAA CCC TCT CGC ACT C	Cloning Plasmid ID 1248, 1249	*
4695	AGTTTAAACACTCCAGATGAGATCGT	Cloning Plasmid ID 1250	*
4696	GAGGGATCCGAAGTTATACTTCTTTTTGACAGAGAC	Cloning Plasmid ID 1250	*
4908	CCGGAATTCGACGAGTGTTTTATCGAAAATC	Cloning Plasmid ID 1392	*
4909	CCGGAATTCGGTTGTAATAAAATGTATGGATTGG	Cloning Plasmid ID 1392	*
4122	TTAGAGCTCCGACGGAAGCGATTCCAG	Cloning Plasmid ID 980, 1078, 1079	*
3180	AAATCTAGAATGGAGGAGACGACGATTCCTTTCAA	Cloning Plasmid ID 980, 1078, 1079	L
4947	GCCCATATGTATAGAGACAGAGGAACGGTG	Cloning Plasmid ID 1353	*
4948	CCGGGATCCTCACGGTTTGTGTAATTTGAACC	Cloning Plasmid ID 1353	*
4211	TTACTGCAGCAATGGCGGACGG	Cloning Plasmid ID 1006	*

4166	GCGGCCGCTAGTTACTATCGGAATCG	Cloning Plasmid ID 1006	*
2683	AATTGTGCACTCATGGCAGACTCTCGGAATGGTAAT	Cloning Plasmid ID 1007	*
4212	GA CTGCAGTCACCTGTGCTTGC GTTTAGAT	Cloning Plasmid ID 1007, 1236, 1237	*
4694	CGCGGATCCTGGACGGAAGCGATTCA	Cloning Plasmid ID 1236, 1237	*
4017	CGCCAATTGGCGGCCGCACCTAACACCACAATGGGACATTA	Cloning Plasmid ID 1008, 1009	*
3667	CGGGAGCTCCCCGGGATGGCAGACTCTCGGAATGGTAA	Cloning Plasmid ID 1008, 1009	L
4283	CCTCGGCATCAGCCTCAACTCCATGCTCTGTCTGCATTAACAGC TTCTCTCCAGTTCATCCCAAG	Cloning Plasmid ID 1008	*
4284	CCTCGTCATCATCCTCAACTCCATGCTCTGTCTGCATTCTCAGCT TCTCTCCAGTTCATCCCAAGT	Cloning Plasmid ID 1009	*
4285	GCTGTTAATGCAGACAGAGCATGGAGTTGAGGCTGATGCCGAG GAAGAGAGGAAGAGAAGAAAG	Cloning Plasmid ID 1008	*
4286	GAAGCTGAGAATGCAGACAGAGCATGGAGTTGAGGATGATGAC GAGGAAGAGAGGAAGAGAAGAAAG	Cloning Plasmid ID 1009	*
4176	GGGCATATGATGGAGTTCTGGGGAATTG	Cloning Plasmid ID 1071	*
4177	TATGGATCCTCACTTGGCAGCAGCG	Cloning Plasmid ID 1071	*
4178	GCACATATGATGGAGTTCTGGGAGTTGC	Cloning Plasmid ID 1072	*
4179	GCAGGATCCTTAAGCTCTACCCTTTCCCTTG	Cloning Plasmid ID 1072	*
4180	GGGCATATGATGGAGTTCTGGGGTGTGAAG	Cloning Plasmid ID 1073	*
4181	TAGGGATCCTCAAGCAGCTGCACTGTGTT	Cloning Plasmid ID 1073	*
4182	CGGCATATGATGGAGTTTTGGGGTATCGAG	Cloning Plasmid ID 1074	*
4183	CGCGGATCCCTACTTTTTGCAAGAGGGACCAC	Cloning Plasmid ID 1074	*
4654	GCTGCTATTAATATGGATACTGGCGCAATTCCG	Cloning Plasmid ID 1224, 1380, 1385	*
4655	AGAGTCGACCTAGGTTATGTTTTAGGAGGAAACGCCTGCTCC	Cloning Plasmid ID 1224, 1380, 1385	*
4656	GCTCATATGGCTGAAGCAGCGAGAAG	Cloning Plasmid ID 1226, 1219	*
4657	ACCCGGGCTAGTAAATTGCCACATCCAGATAATCTCCA	Cloning Plasmid ID 1226, 1219	*
4658	GCTGCTATTAATATGGACTCTCACTTTCCACC	Cloning Plasmid ID 1225, 1382, 1223	*
4659	GACCCGGGCTATTGAGATTTAGCACCAGATTGGAGACC	Cloning Plasmid ID 1225, 1382, 1223	*
4061	AACTGCAGAAAGAGAAATCTATCAAGAAGGAACCT	Cloning Plasmid ID 973-975, 1066-1069, 1131, 1132	*
3827	CCAAGCTTGTAATCACTGATCTCATCCTTGATC	Cloning Plasmid ID 973-975, 1066-1069, 1131, 1132	*
3828	TGGGAGCGGTGCTTGGAGATAAGTGGCGTCAAATGTCT	Cloning Plasmid ID 974	*
3829	ATCTCCAAGCACCGCTCCACCTCTCCAAATGCTATTCC	Cloning Plasmid ID 974	*
3830	ATGTCTGCTGATGATAAAGAGCC	Cloning Plasmid ID 975	*
3831	TTTGACGCCACGCATCTCCAAGCACCTTTCCACCTC	Cloning Plasmid ID 975	*
4160	CTCCTAAGAGGGCAACTGTAGCCGCAGACGAAGGCAGTAGT	Cloning Plasmid ID 1066	*
4161	GGCTACAGTTGCCCTCTTAGGAGGCAATCCTTTGATGACG	Cloning Plasmid ID 1066	*
4162	CAGTAGTGCAAGGAAGAAGCCGAAGAAGAAGGATCCCAACGC	Cloning Plasmid ID 1067	*
4163	CGGCTTCTCCTGCTACTACTGCCTTCGTCTGCGGCTACAGT	Cloning Plasmid ID 1067	*
4461	AGAGGGCAACTGTAGCCGCAGACGAAGGCAGTAGTGCGAGGAAGA AGCCGAAGAAGAAGA	Cloning Plasmid ID 1068	*
4462	TTCTCGCACTACTGCCTTCGTCTGCGGCTACAGTTGCCCTCTTAG GAGGCAATCCTTTC	Cloning Plasmid ID 1068	*
4471	GGTGGGAGCGGTGCTTGGAGATGCGTGGCGTCAAATGTCTG	Cloning Plasmid ID 1069	*
4472	GCCACGCATCTCCAAGCACCGCTCCACCTCTCCAAATGCTATTCC TG	Cloning Plasmid ID 1069	*
4463	AGAGGCAAACCTGTAGCCGCAGACGAAGGCAGTAGTCAGAGGAAGA AGCCGAAGAAGAAGA	Cloning Plasmid ID 1131, 1138	*
4464	TCCTCTGACTACTGCCTTCGTCTGCGGCTACAGTTTGCCTCTTAGG AGGCAATCCTTTCG	Cloning Plasmid ID 1131, 1138	*
4467	GGTGGGACAGGTGCTTGGAGATCAGTGGCGTCAAATGTCTG	Cloning Plasmid ID 1132	*
4468	GGTGGGAAGGGTGCTTGGAGATAGTGGCGTCAAATGTCTG	Cloning Plasmid ID 1132	*
4367	ATAAGAGAGCGGCCGCTCGTTTTGCGGTATCTCGTGGG	Cloning Plasmid ID 1123	*
4368	GCGAGCTCGAACCACAATGCGAAAAGCTACATCG	Cloning Plasmid ID 1123, 1133, 1134, 1137, 1138	*

810	CCCTCATCTTACGCGTATCAGA	Cloning Plasmid ID 1133, 1134, 1137, 1138	L
4467	CACTGATCTCCAAGCACCTGTCCCACCTCTCCAAATGCTATTCTG	Cloning Plasmid ID 1133	*
4468	CACCTATCTCCAAGCACCTTCCCACCTCTCCAAATGCTATTCTG	Cloning Plasmid ID 1134	*
4465	AGAGGAGAACTGTAGCCGACAGCAAGGCAGTAGTAGAAGGAAGA AGCCGAAGAAGAAGA	Cloning Plasmid ID 1137	*
4466	TTCCTTCTACTACTGCCTTCGCTGCGGCTACAGTTCTCCTTTAGG AGGCAATCCTTT	Cloning Plasmid ID 1137	*
4627	TCAGCCGATGAATGTGGACTCAGGAAACGATTCCGATAGTAACCCA AAAAAGAAGAGAAAGGTCTAACTTTGATTCTCCAACATTCTCTA	Cloning Plasmid ID 1210	*
4628	CTAGTAGAGAATGTTGGAGAATCAAAGTTAGACCTTTCTCTCTTT TTTGGTTACTATCGGAATCGTTTCTGAGTCCACATTTCATCGGC	Cloning Plasmid ID 1210	*

5.4 Plasmids

Table 12 List of Plasmids. (ID = Internal lab identifier; R. sites = Restriction sites; Exp. = Use for the following experiments: AP = Affinity Purification, I = Intermediate; Comp = Complementation studies S. = Source: * = from this study, L = from lab collection). For a more detailed guide see **Supplementary Data Table 15**

ID	Plasmid	R.Sites	Exp.	S.
728	pCambia2300_35s_GS		AP	L
821	pCambia2300_35s_SPT16-GS		AP	L
822	pCambia2300_35s_SSRP1-GS		AP	L
949	pCambia2300_35s_ELF1-GS		AP	L
1140	pCambia2300_35s_GS-SPT6I	Sall/SmaI	AP	*
1234	pHEE401E ELF1 CRISPR	BsaI	CRISPR	*
976	pFGC5941 SPT6 sense	BamHI/XbaI	I	*
977	pFGC5941 SPT6 antisense	XhoI/NcoI	I	*
978	pENTR dsRNAi SPT6	XhoI/XbaI	I	*
979	pGII B-estradiol ind. XVE-LexA dsRNAi SPT6	Gateway	RNAi	*
1116	pET21a atH2A	NdeI/BamHI	AP	*
1117	pET21a atH2Ax	NdeI/BamHI	AP	*
1118	pET21a atH2Az	NdeI/BamHI	AP	*
1119	pET21a atH2B	NdeI/BamHI	AP	*
1393	pGex5x-1_GST_ELF1 full	BamHI/XhoI	AP	*
1394	pGex5x-1_GST_ELF1ΔAID	BamHI/XhoI	AP	*
1246	pET24b_ELF1-Full_gb	NdeI/XhoI	AP	*
1247	pET24b_ELF1_ΔBID_gb	NdeI/XhoI	AP	*
1248	pET24b_ELF1_ΔAID_gb	NdeI/XhoI	AP	*
1249	pET24b_ELF1_ΔAID/ΔBID_gb	NdeI/XhoI	AP	*
1250	pCambia2300_pELF1(1kb)_gELF1-3'eGFP	BamHI/PmeI	CLSM	*
	pCambia2300_pELF1(4kb)_gELF1_EGFP	BamHI/PmeI	I	*
1392	pCambia2300_pELF1(4kb)_gELF1_EGFP_3'UTR	EcoRI	CLSM	*
980	pRSF Duet 6xHis SPT16_AID	SacI/HindIII	AP	*
1078	pRSF Duet 6xHis SPT16_AID V1023/A1033/A1035	SacI/HindIII	AP	*
1079	pRSF Duet 6xHis SPT16_AID E1023/D1033/D1035	SacI/HindIII	AP	*
1352	pGADT7 CKA1	NdeI/BamHI	Y2H	*
1353	pGADT7 CKB1	NdeI/BamHI	Y2H	*
1354	pGBKT7 CKA1	NdeI/BamHI	Y2H	*
1355	pGBKT7 CKB1	NdeI/BamHI	Y2H	*
819	pGADT7-SPT16		Y2H	L

820	pGADT7-SSRP1		Y2H	L
1006	pGBKT7 SSRP1	PstI/NotI	Y2H	*
1007	pGBKT7 SPT16	Sall/PstI	Y2H	*
1236	pGex-5x-1 SPT16 AID	BamHI/PstI	AP	*
1237	pGex-5x-1 SPT16 AID_EDD	BamHI/PstI	AP	*
1317	pCambia2300-35S:SPT16-GS_V1023/A1033/A1035	BamHI/NruI	I	*
1318	pCambia2300-35S:SPT16-GS E1023/D1033/D1035	BamHI/NruI	I	*
1372	pCambia2300-pSPT16:GS	PmeI/XbaI	AP	*
1373	pCambia2300-pSPT16:SPT16-GS	PmeI/XbaI	AP	*
1374	pCambia2300-pSPT16:SPT16_VAA_GS	PmeI/XbaI	AP	*
1375	pCambia2300-pSPT16:SPT16_EDD-GS	PmeI/XbaI	AP	*
965	pGreen0179_pSPT16::5'TagRFP-gSPT16	SacI/MfeI	Comp	L
1008	pGreen0179_pSPT16::5'TagRFP-gSPT16_V1023/A1033/A1035	SacI/MfeI	Comp	*
1009	pGreen0179_pSPT16::5'TagRFP-gSPT16_E1023/D1033/D1035	SacI/MfeI	Comp	*
1071	pGBKT7-HDT1	NdeI/BamHI	Y2H	*
1072	pGBKT7-HDT2	NdeI/BamHI	Y2H	*
1073	pGBKT7-HDT3	NdeI/BamHI	Y2H	*
1074	pGBKT7-HDT4	NdeI/BamHI	Y2H	*
1348	pGADT7 HDT1	NdeI/BamHI	Y2H	*
1349	pGADT7 HDT2	NdeI/BamHI	Y2H	*
1350	pGADT7 HDT3	NdeI/BamHI	Y2H	*
1351	pGADT7 HDT4	NdeI/BamHI	Y2H	*
1212	pGreen0229 35s 5'mCherry HDT1	NdeI/BamHI	FRET	*
1213	pGreen0229 35s 5'mCherry HDT2	NdeI/BamHI	FRET	*
1214	pGreen0229 35s 5'mCherry HDT3	NdeI/BamHI	FRET	*
1215	pGreen0229 35s 5'mCherry HDT4	NdeI/BamHI	FRET	*
1380	pGADT7 HDA19	Asel-NdeI/Sall	Y2H	*
1381	pGADT7 SAP18	NdeI/XmaI	Y2H	*
1385	pGBKT7 HDA19	Asel-NdeI/Sall	Y2H	*
1226	pGBKT7 SAP18	NdeI XmaI	Y2H	*
966	pCambia2300_p35S::eGFP-NLS-mCherry		FRET	L
921	pGreen0179_p35S::mCherry-NLS		FRET	L
827	pCambia2300-p35S:EGFP-SSRP1		FRET	L
1219	pGreen0229 35s 5'mCherry SAP18	NdeI XmaI	FRET	*
1224	pGreen0229 35s 5'mCherry HDA19	Asel-NdeI/AvrIIAvrII	FRET	*
1225	pGBKT7 GCN5	Asel-NdeI/XmaI	Y2H	*
1382	pGADT7 GCN5	Asel-NdeI/XmaI	Y2H	*
1223	pGreen0229 35s 5'mCherry GCN5	Asel-NdeI/XmaI	FRET	*
973	pQE9-SSRP1_basicHMGbox-WT	PstI/HindIII	AP	*
974	pQE9-SSRP1_basicHMGbox_K594A	PstI/HindIII	AP	*
975	pQE9-SSRP1_basicHMGbox_K599A	PstI/HindIII	AP	*
1066	pQE9-SSRP1_basicHMGbox-K539A	PstI/HindIII	AP	*
1067	pQE9-SSRP1_basicHMGbox-K549A	PstI/HindIII	AP	*
1068	pQE9-SSRP1_basicHMGbox-K539A/K549A	PstI/HindIII	AP	*
1069	pQE9-SSRP1_basicHMGbox-K594A/K599A	PstI/HindIII	AP	*
1070	pQE9-SSRP1_basicHMGbox-K539A/K549A/K594A/K599A	BamHI	AP	*
1131	pQE9 basicHMGbox K539/549Q	PstI/HindIII	AP	*
1132	pQE9 basicHMGbox K595/599Q	PstI/HindIII	AP	*
1135	pQE9 basicHMGbox K539/549Q/K595/599Q	BamHI	AP	*

1123	pGreen0179_pSSRP1(1.6 kb)_gSSRP1_3'UTR	NotI/SacI	I	*
1133	pGreen0179_pSSRP1(1.6 kb)_gSSRP1-R595/R599_3'UTR	NotI/SacI	I	*
1134	pGreen0179_pSSRP1(1.6 kb)_gSSRP1-Q595/599_3'UTR	NotI/SacI	I	*
1137	pGreen0179_pSSRP1(1.6 kb)_gSSRP1-4xR_3'UTR	MluI/SacI	I	*
1138	pGreen0179_pSSRP1(1.6 kb)_gSSRP1-4xQ_3'UTR	Sall/Smal	I	*
1186	pCambia(hygro)_pSSRP1_EGFP_gSSRP1_3'UTR	MluI/AvrII	CLSM	*
1156	pCambia(hygro)_pSSRP1_EGFP_gSSRP1-4xQ_3'UTR	MluI/AvrII	CLSM	*
1200	pCambia(hygro)_pSSRP1_EGFP_gSSRP1-4xR_3'UTR	MluI/AvrII	CLSM	*
1376	pCambia2300-pSSRP1:GS	PmeI/XbaI	AP	*
1377	pCambia2300-pSSRP1:SSRP1-GS	BstZ17I-PmeI/Sall	AP	*
1378	pCambia2300-pSSRP1:SSRP1_KR-GS	BstZ17I-PmeI/Sall	AP	*
1379	pCambia2300-pSSRP1:SSRP1_KQ-GS	BstZ17I-PmeI/Sall	AP	*
923	pCambia2300_p35S::eGFP-NLS		CLSM	L
1210	pCambia(hygro)_pSSRP1_EGFP_gSSRP1_4xR-NLS_3'UTR	BbvCI/Spel	I	*
1216	pGreen0179_pSSRP1(1.6 kb)_gSSRP1_4xR-NLS_3'UTR	MluI/AvrII	Comp	*
1217	pGreen0179_pSSRP1(1.6 kb)_gSSRP1-WT-NLS_3'UTR	Sall	Comp	*
1218	pGreen0179_pSSRP1(1.6 kb)_gSSRP1-4xQ-NLS_3'UTR	Sall	Comp	*

5.5 T-DNA insertion lines

All mutant lines within this thesis were homozygous, if not indicated otherwise (+/-).

Table 13 List of T-DNA insertion lines

Name	Locus	Insertion	Reference
<i>spt16-1</i>	AT4G10710	SAIL_392_G06	(Lolas et al., 2010)
<i>ssrp1-1</i> (+/-)	AT3G28730	GT7431	(Lolas et al., 2010)
<i>ssrp1-2</i>	AT3G28730	SALK_001283	(Lolas et al., 2010)
<i>tflls-1</i>	AT2G38560	SALK_056755	(Grasser et al., 2009)

5.6 Bacteria and yeast strains

Table 14 List of bacteria and yeast strains

Organism	Name	Selection	Purpose	Company
<i>A. tumefaciens</i>	GV3101::pMP90 + pSoup	Gentamycin, Rifampicin, Tetracycline	Transformation of plants	DSMZ
<i>E. coli</i>	BL21-CodonPlus(DE3)-RIL	Tetracycline, Chloramphenicol	Protein expression	Novagen
<i>E. coli</i>	BL21 (DE3) pLysS	Chloramphenicol	Protein expression	Novagen
<i>E. coli</i>	BL21 Star (DE3) + pRARE	Chloramphenicol	Protein expression	Invitrogen
<i>E. coli</i>	M15	Kanamycin	Protein expression	Qiagen
<i>E. coli</i>	Rosetta	Chloramphenicol	Protein expression	Novagen
<i>E. coli</i>	XL1-Blue	Tetracycline	Plasmid amplification	Stratagen
<i>S. cerevisiae</i>	AH109	-Ade -His -Leu -Trp	Y2H	Clontech

5.7 Databases, Online Tools and Software

Table 15 List of Databases, Online Tools and Software

Tool	Link
ClustalOmega	https://www.ebi.ac.uk/Tools/msa/clustalo/
DISOPRED3	http://bioinf.cs.ucl.ac.uk/psipred/
EasyFRAP	https://easyfrap.vynet.upatras.gr/GettingStarted/?AspxAutoDetectCookieSupport=1
ePlant	http://bar.utoronto.ca/eplant/
EzMol	http://www.sbg.bio.ic.ac.uk/ezmol/
Fiji	https://imagej.net/Fiji/Downloads
HHpred	https://toolkit.tuebingen.mpg.de/tools/hhpred
HOMER	http://homer.ucsd.edu/homer/introduction/basics.html
IDT codon optimization tool	https://eu.idtdna.com/CodonOpt
Inkscape	https://inkscape.org/de/
Integrative Genomics Viewer	https://software.broadinstitute.org/software/igv/
I-TASSER	https://zhanglab.ccmb.med.umich.edu/I-TASSER/
Leaf-GP	https://www.quantitative-plant.org/software/leaf-gp
Leica Application Suite X	https://www.leica-microsystems.com/de/produkte/mikroskop-software/p/leica-las-x-ls/
Mendeley	https://www.mendeley.com/?interaction_required=true
Microsoft Office 365	https://www.office.com/
OligoCalc	http://biotools.nubic.northwestern.edu/OligoCalc.html
PeptideCutter (EXPASy)	https://web.expasy.org/peptide_cutter/
PhosPhAt	http://phosphat.uni-hohenheim.de/phosphat.html
Phytozome	https://phytozome.jgi.doe.gov/pz/portal.html#
ProtParam (EXPASy)	https://web.expasy.org/protparam/
QuantPrime	https://quantprime.mpimp-golm.mpg.de/main.php
SnapGene	https://www.snapgene.com/
The <i>Arabidopsis</i> Information Resource v10	https://www.arabidopsis.org/
UniProt	https://www.uniprot.org/

6 Methods

6.1 Plant based Methods

6.1.1 Cultivation of *A. thaliana* on soil

Suitable pots were filled with soil and soaked with water containing 200 mg/L of the insecticide Confidor WG 70 and 1.5 mL/L of the fungicide Previcur Energy. *Arabidopsis thaliana* seeds were sown out and subsequently stratified for 48-72 hours at 4 °C in darkness. The pots were transferred into a growth chamber and grown during long-day conditions (16 h light, ~7000 lux at 21 °C). Depending on the age, plants were watered 1-2 times weekly for several minutes from the bottom.

6.1.2 Surface sterilisation of seeds and cultivation of *A. thaliana* on MS-media

Small amounts of *A. thaliana* seeds were filled into micro tubes and the open tubes were placed into a desiccator. Chloric gas production was started by adding 2 mL 37% (v/v) HCl into a beaker containing 50 mL of 12% (v/v) sodium hypochlorite. The desiccator was sealed immediately, and the seeds are incubated in the emerging chlorine gas for at least 2 hours. The surface sterile seeds were sown out on solid ½ MS-agar plates (2.2 g/L Murashige and Skoog media including vitamins, 1% sucrose, 0.8% phyto-agar (w/v); adjusted to pH 5.8) under the sterile bench. Plates were sealed with micropore tape and stratified for 48-72 hours at 4 °C in darkness and placed in a plant incubator and grown during long-day conditions (16h light at 21°C and ~7000 lux).

6.1.3 Crossing of *A. thaliana*

Plants used for crossing were grown on soil until a height was reached which allowed convenient work with the flowers using the binocular microscope. First mature siliques, open flowers and small buds were removed. From the remaining unopened flowers sepals, petals and stamens were gently removed, only leaving the carpel. Pollen from an open flower was applied to the female stigma and the plants were moved back the plant growth chamber to develop siliques.

6.1.4 Stable transformation of *A. thaliana*

For stable transformation of *A. thaliana* (Clough and Bent, 1998) 6 big pots (12 x 12 cm) of the host line were grown until a height of ~5-15 cm was reached. In the meanwhile, *A. tumefaciens* was transformed with the desired plasmid and colonies were tested by PCR. A colony, positive for the transformed vector, was grown for 16 h in 5 mL LB media with appropriate selection at 28 °C and 200 rpm. The following day 500 mL of selective LB medium was inoculated with 500 µL of starter culture and incubated o/n at 28 °C. The cells were harvested (4000 rcf, 15 min, 4 °C) and the pellet was re-dissolved in 500 mL of infiltration medium (5% sucrose, 10mM MgCl₂, 0.02% Silwet L-77 and 10 µM acetosyringone). The stems and flowers were dipped in the *agrobacteria* suspension for 1 min, slightly moving the plant up and down. Dipped plants were covered in plastic wrap and left o/n at RT. The plants were transferred back to a phytochamber and grown to maturity.

6.1.5 Selection of transgenic lines

Plants transformed with constructs carrying BASTA resistance were sown out on soil and 7 days after stratification (DAS) the plant were sprayed with the BASTA spray solution (100 mg/L BASTA and 200 µL/L Silwet-77) with a repetition of the treatment 2 days later. For selection of transgenic plants carrying hygromycin or kanamycin resistance markers, plants were grown on 0.5x MS (2.2 g/L Murashige and Skoog media including vitamins, 1% sucrose, 0.8% phyto-agar (w/v); adjusted to pH 5.8) supplemented with 30 µg/mL hygromycin B or 50 µg/mL kanamycin, respectively. Plants that survived selection were transferred to soil and grown to maturity. Seedlings were verified by PCR-based genotyping.

6.1.6 Soil based phenotypic analysis

For phenotypic analysis, the plants were grown like described in section 6.1.1. The trays were rotated every other day on the shelf to avoid positional effects. Parameters were measured when the respective trait reached approximately its maximum (Boyes et al., 2001) and varied depending on the characteristics of the respective phenotype. Parameters as well as the experimental set-up are listed in section 2.4.6 and 2.5.6. For phenotypic analysis from 21 – 28 DAS in section 2.5.6 the software LeafGP was used (Zhou et al., 2017). Pictures were taken with a Canon EOS 550D. For automated seed counting a macro was written for the software Image-J/Fiji:

```
run("8-bit");
setAutoThreshold("Default");
//run("Threshold...");
//setThreshold(0, 200);
setOption("BlackBackground", false);
run("Convert to Mask");
run("Watershed");
run("Analyze Particles...", "size=25-Infinity circularity=0.60-1.00 exclude clear summarize add");
```

6.1.7 Abiotic stress treatment

Cold-, heat-, salt- and highlight stress was applied like described before (Andrés-Barrao et al., 2017; Dong et al., 2006; Pfab et al., 2018a; Wu et al., 2010). All experiments, if not indicated otherwise were performed on ½ MS plates (2.2 g/L Murashige and Skoog media including vitamins, 1% sucrose, 0.8% phyto-agar (w/v); adjusted to pH 5.8). For salt stress plates were supplemented with 100 mM NaCl, for highlight stress with an additional 1% (w/v) sucrose. To

exclude bias due to different germination speeds, 3-day old seedlings showing comparable growth were transformed to a new plate. There, the square plate was divided into quartiles and seedlings were arranged accordingly to exclude positional effects.

6.1.8 Photometric determination of anthocyanins

Anthocyanins were extracted from *Arabidopsis* aerial parts like described before (Pfab et al., 2018a; Yin et al., 2012). Pools of highlight treated *Arabidopsis* plantlets were frozen in liquid nitrogen and disrupted for 60s in a Qiagen TissueLyser II homogeniser. 500 µL extraction buffer (acidic methanol, 1 % HCl (v/v)) was added to 20 mg of ground plant material. Samples were mixed for 15 minutes at 4 °C in the dark. The homogenate was clarified by centrifugation (full speed; 20800 rcf) and the supernatant was used for photometric measurements. The anthocyanin content was quantified by the following equation (Mehrtens et al., 2005): $Q_{\text{Anthocyanins}} = (A_{530} - 0.25 \times A_{657}) \times M^{-1}$, where $Q_{\text{Anthocyanins}}$ is the amount of anthocyanins, A_{530} and A_{657} is the absorption at the indicated wavelengths and M is the weight of the plant material used for extraction [g].

6.1.9 Germination assays

Disclaimer: This chapter was published in Journal of Plant Physiology (Michl-Holzinger et al., 2019)

All germination experiments were performed in Petri dishes on disks of Whatman 3M paper that were soaked with water. The assays were carried out either with freshly picked siliques or freshly harvested, fully developed seeds (early stage 17B, according to (Roeder and Yanofsky, 2006)), either with stratification (48 h at 4 °C in darkness) or without. The germination rate was determined after 7 d of incubation in a plant incubator (Percival Scientific) at 20 °C at 16 h of light (~7000 lx) in three biological replicates (n ~60-150 seeds).

6.1.10 Transient transformation of *N. benthamiana*

For transient expression of proteins in tobacco *Agrobacterium*-mediated infiltration was used (Romeis et al., 2001). A colony, positively selected for the vector, was grown for 16h in 15 mL LB media with appropriate selection at 28°C and 200rpm. The o/n culture was harvested (4000 rcf, 15min, 4°C) and the pellet was re-dissolved in 15mL of infiltration buffer (10 mM MgCl₂, 10 mM MES-KOH, 150 µM Acetosyringone). 4-6week old *N. benthamiana* plants were obtained from the in-house gardeners. A syringe (without the cannula) was filled with the *agrobacteria* suspension and squeezed against the underside of the leaf until dark green discs

were observed. Tobacco plants were cultivated for 2d in the phyto-chamber at long day conditions.

6.1.11 Cultivation of *Arabidopsis* PSB-D cells

Arabidopsis landsberg erecta PSB-D suspension cell culture (*Arabidopsis* Biological Resource Centre) was grown in MSMO medium (0.443 % (w/v) Murashige and Skoog Salt mixture (US Biological), 3 % (w/v) sucrose, 0.5 mg/L NAA dissolved in 100 mM NaOH, 100 mg/L myo-inositol, 0.05 mg/L kinetin dissolved in DMSO, 0.4 mg/L thiamine, adjusted to pH 5.7 with 1 M KOH). Cells agitated at 130 rpm and 23 °C in the dark and were diluted weekly by transferring 7 mL culture into 43 mL fresh MSMO medium (compare Van Leene et al., 2011).

6.1.12 Transformation of *Arabidopsis* PSB-D cells

A. tumefaciens was transformed with the desired plant expression vector. 20 mL LB with appropriate antibiotics were inoculated with a pre-culture of a selected *A. tumefaciens* colony and incubated o/n at 28 °C at 200 rpm. *Agrobacteria* were pelleted by centrifugation for 15 min at 3000 rcf and washed in 40 mL sterile MSMO. Cells were vortexed, and the washing was repeated. OD600 was adjusted to 1.0 with MSMO.

For the actual transformation 3 mL of 3-day old *Arabidopsis* suspension cells (OD600: 1.2 - 1.3), 200 µl of the *Agrobacteria* solution (OD600 = 1.0) and 6 µL 100 mM Acetosyringone (dissolved in ethanol) were transferred into one well of a 6-well plate. The plate was closed with Micropore surgical tape and PSB-D cells and *Agrobacteria* were co-cultivated for 3 days at 130 rpm and 23 °C. To kill *Agrobacteria* and select for transformed cells the suspension was transferred into a 25 mL Erlenmeyer flask containing 8 mL MSMO supplemented with 500 µg/mL vancomycin and 500 µg/mL carbenicillin, 50 µg/mL kanamycin or 20 µg/mL Hygromycin B. PSB-D cells were incubated for 8 days and 10 mL of transformed cells were transferred into a 100 mL Erlenmeyer flask containing 25 mL MSMO supplemented with kanamycin/hygromycin, vancomycin and carbenicillin. After 7 days of incubation, as much sedimented cells as possible were transferred into a 100 mL Erlenmeyer flask containing 35 mL MSMO supplemented with plant selection only (kanamycin/Hygromycin B). Transformed cell culture was diluted weekly (see Section 6.1.11) maintaining plant selection markers.

6.1.13 Upscaling of *Arabidopsis* PSB-D cells

To obtain sufficient material for further analysis PSB-D cells were upscaled weekly in MSMO with appropriate selection. A typical set-up would increase the volume in the following steps:

50 mL 1-week old cell culture in 180 mL fresh MSMO medium; 180 mL cells into 5x 180 mL medium, 180 mL into 800 mL medium. 3 days after the final dilution, PSB-D cells were filtered through a double layer of Miracloth. 15 g portions were frozen in liquid nitrogen and stored at -80 °C.

6.2 Nucleic Acid based methods

6.2.1 Isolation of genomic DNA from *Arabidopsis* leaves

For extraction of genomic DNA from *A. thaliana* (Edwards et al., 1991) one leaf was harvested and frozen in liquid nitrogen in an 1.5 mL micro tube together with 2 glass beads. The leaf was ground with a frequency 30 Hz for 60s in a Qiagen TissueLyser II homogeniser. 400 µL Edward buffer (200 mM Tris pH 7.5, 250 mM NaCl, 25 mM EDTA and 0.5% (w/v) SDS) was added, the solution was vortexed and centrifuged at full speed for 5 min. 300 µL of the supernatant was transferred into a new tube and mixed with 300 µL of 100% isopropanol. After 2 min at room temperature the DNA was spun down for 5 min at full speed. The pellet was washed with 70% EtOH, the supernatant was removed, the pellets were left to dry and finally resuspended in 50 µL H₂O. All centrifugation steps were performed at RT.

6.2.2 Isolation of RNA from *Arabidopsis* seeds

Total RNA was isolated from seeds according to a previously described method (Vicent and Delsen, 1998). Here ~20 mg of seeds were used as starting material and harvested in 2 mL tubes containing one metal bead and frozen in liquid nitrogen. Seeds were ground with a frequency 30 Hz for a total of 60s in a Qiagen TissueLyser II homogeniser, refrozen every 20s. The extracted RNA was air dried and dissolved in 30 µL of H₂O. RNA concentration was measured on a NanoDrop ND1000 spectrophotometer (Peqlab) and the integrity of 18S and 28S rRNA was confirmed by agarose gel electrophoresis.

6.2.3 cDNA Synthesis

1.5 µg of extracted RNA was incubated with DNaseI (NEB) for 100 minutes at 37 °C. 1 µg of DNaseI digested RNA was used for cDNA synthesis with RevertAid Reverse Transcriptase and random hexamer primers. All steps were performed according to the manufacturer's description (Thermo Fisher Scientific).

6.2.4 Polymerase Chain Reaction (PCR)

6.2.4.1 PCR with *Diamond Taq* DNA polymerase

PCR with *Diamond Taq* (Eurogentec) was used for standard PCR-based validations. Polymerase Chain Reaction was performed in a 25 μ L reaction mixture, containing a final concentration of 1x reaction buffer, 0.02 mM dNTPs, 0.5 μ M forward and reverse primers and 0.04 units/ μ L *Diamond Taq*-DNA-polymerase. As DNA template e.g. 5 μ L of plant genomic DNA was used (Section 6.2.1). The PCR reaction was performed using a Tgradient or a T3000 PCR thermocycler (Biometra). Depending on the fragment size amplified PCR products were analysed on a 1-2% agarose gel.

Table 16 PCR Settings for *Diamond Taq*

PCR-Step	Temperature [°C]	Time [s]	Number of Cycles
Initial Denaturation	95	180	1
Denaturation	94	30	34
Annealing	Primer T _M - 2°C	30	
Elongation	72	60/1kb +15	
Final Elongation	72	420	1
Storage	10	∞	

6.2.4.2 PCR with *Herculase II* Polymerase

The proofreading *Herculase II* Fusion DNA Polymerase (Agilent) was used for cloning. Polymerase Chain Reaction was performed in a 50 μ L reaction mixture which contained 1x *Herculase II* reaction buffer, 250 μ M dNTPs, 0.25 μ M forward and reverse primer and 1 μ L of *Herculase II* DNA-polymerase. Typically, 20 ng of vector DNA or 100 ng of genomic DNA were used as DNA template. Amplified PCR products were analysed on a 1-2% agarose gel.

Table 17 PCR setting for *Herculase II* Polymerase

PCR-Step	Temperature [°C]	Time [s]	Number of Cycles
Initial Denaturation	95	120	1
Denaturation	95	20	34
Annealing	Primer T _M - 5°C	20	
Elongation	72	30/1kb +15	
Final Elongation	72	180	1
Storage	10	∞	

6.2.4.3 Overlap extension PCR

To introduce point mutations overlap extension PCR (Ho et al., 1989) was performed. Two PCR products were generated by *Herculase II* Polymerase. PCR product 1 was designed with the mutation in the reverse primer and PCR product 2 with the according mutation in the

forward primer. The two primers containing the desired mutation shared an overlapping region of about 18-25 nucleotides. The PCR fragments were validated on an agarose gel and used as templates for a third PCR containing the forward primer of PCR product 1 and the reverse primer of PCR product 2, giving rise to a DNA fragment with the desired mutation.

6.2.4.4 Real time quantitative PCR (qRT-PCR)

Disclaimer: Parts of this chapter was published in Journal of Plant Physiology (Michl-Holzinger et al., 2019)

For qRT-PCR analyses random hexamer-primed complementary DNA (Section 6.2.3) was prepared from total seed RNA (Section 6.2.2) and used with KAPA SYBR FAST Universal reagents (PEQLAB) in a Mastercycler ep realplex2 (Eppendorf). Targets were quantified with gene-specific primer pairs (Table 11), which were designed using the tool QuantPrime (Arvidsson et al., 2008). The normalised relative quantities (NRQ) were calculated according to (Hellemans et al., 2007) using the two reference genes AT4G12590 and AT4G02080 (Dekkers et al., 2012).

Table 18 PCR setting for qRT-PCR

PCR-Step	Temperature [°C]	Time [s]	Number of Cycles
Initial Denaturation	98	180	1
Denaturation	95	5	40
Annealing	60	15	
Elongation	72	8	
Melting curve	60-95	20 [min]	1

6.2.5 Agarose Gel Electrophoresis

Preparative as well as analytical agarose gels were made by adding 1-2% (w/v) agarose to 1x TAE buffer (40 mM Tris-Base pH 8.0, 1 mM Na₂EDTA). The mixture was boiled in a microwave until the agarose was dissolved. 0.005% (v/v) ethidium bromide was added to the slightly cooled solution and poured into a gel cassette with comb formers and left to solidify. Gels were put into gel chambers filled with 1x TAE buffer. DNA samples mixed with 6 x DNA loading dye (250 mM Tris pH 7.5, 10% (w/v) SDS, 30% (v/v) glycerol, 0.5 M DTT, 0.1% (w/v) bromophenol blue), as well as GeneRuler 1 kb DNA Ladder (Thermo Scientific) were loaded into the gel pockets. DNA fragments were separated at 130-150V. DNA and RNA fragments were visualized with a BioDoc Analyzer (Biometra) or a ChemiDoc MP (Bio-Rad).

6.2.6 Annealing of Oligonucleotides

For annealed oligo-cloning, top and bottom oligo were designed to complement the overhangs generated when digesting the vector backbone with the restriction-enzymes of choice. For details see: <https://www.addgene.org/protocols/annealed-oligo-cloning/>

Ordered oligonucleotides were resuspended in annealing buffer (10 mM Tris, pH 8.0, 50mM NaCl, 1mM EDTA). 2 µg of each oligo were mixed in a total volume of 50 µL and heated for 5 min at 95°C. The hot block was removed from the heating source and moved to RT, allowing for slow cooling from 95°C to RT (~1 h).

6.2.7 Restriction-ligation cloning

Restriction-Ligation based cloning was performed according to (Sambrook et al., 1989). Whenever necessary reactions were cleaned by the NucleoSpin Gel and PCR Clean-up kit (Macherey Nagel). PCR-fragments and plasmids were digested with commercial restriction enzymes (NEB, Thermo Fisher Scientific). Digested vector backbones were dephosphorylated with Antarctic Phosphatase (NEB). Ligations (NEB or Thermo Fisher Scientific) were carried out in an insert to vector ratio of 4:1. Typically 100 ng of vector were used. All buffers as well as reaction conditions were picked according to the manufacturer's description.

6.2.8 Gateway cloning

The respective sequence was transferred from gateway entry to destination vector according to the manufacturer's manual (Thermo Fisher Scientific).

6.2.9 Sequencing

Sequencing of PCR products or generated plasmids which included PCR amplification steps were sequenced with primers covering the amplified region. Sequencing was performed by the company MWG-Biotech (Germany).

6.3 Cell based methods

6.3.1 Preparation of chemically competent yeast cells

Yeast AH109 cells from a glycerol stock were used to inoculate 3mL YPAD (2% (w/v) tryptone, 1% (w/v) yeast extract, 2% (w/v) glucose and 0.004% (w/v) adenine-hemi-sulfate) starter culture (200 rpm, 30°C). The next day 50 mL YPAD medium was inoculated with the starter culture to an OD600 of 0.1 and was grown to an OD600 of 1.0. Yeast cell were pelleted by centrifugation (5 min, RT, 500 rcf) and subsequently washed with 25 mL sterile H₂O, 5 mL

sterile filtered SORB (100 mM LiOAc, 10 mM Tris, 1 mM EDTA, 1 M sorbitol; adjust to pH 8.0 with acetic acid) and 0.5 mL SORB. In the meantime, salmon sperm DNA (10 mg/mL) was heated at 90 °C for 5 min and immediately cooled on ice, to obtain single stranded DNA. The washed yeast pellet was re-suspended in 360 µL SORB buffer and mixed with 40 µL denatured salmon sperm DNA. Aliquots of 50 µL were stored at -80 °C.

6.3.2 Co-transformation of yeast cells by heat shock

Chemical competent yeast cells were thawed on ice. In the meantime, sterile PEG solution (40% (w/v) PEG 3350, 10 mM Tris-HCl pH 7.5, 1 mM EDTA, 100 mM LiAc) was prepared from autoclaved stock-solutions (50% (w/v) PEG 3350, 10x TE, 1 M LiAc). Thawed competent yeast cells were mixed with 500 ng of pGBKT7 and pGADT7 plasmid DNA. 300 µL PEG solution was added, mixed and incubated for 30 min at RT. After addition of 40 µL sterile DMSO and a heat shock for 15 min at 42°C, cells were pelleted (2 min at RT and 500g), resuspended in 100 µL sterile H₂O and plated on double dropout (DDO) plates (2% (w/v) glucose, 0.67% (w/v) yeast nitrogen base w/o amino acids, 2.2% (w/v) micro agar, 0.064% (w/v) -Leu/-Trp DO supplement, adjusted to pH 5.8 with 1 M KOH and autoclaved for 15min). DDO plates were incubated for 3-4 days at 30 °C.

6.3.3 Yeast-2-Hybrid (Y2H) Assay

Positive-selected yeast colonies were picked from DDO plates and resuspended in 200 µL sterile H₂O. Part of the yeast suspension was used to determine OD₆₀₀. The other part was used to adjust OD₆₀₀ to 1.0. A 1:10 dilution series of the yeast solution was prepared as following: 10⁰, 10⁻¹, 10⁻²). With a frogger the dilution series were plotted on DDO, triple dropout and quadruple dropout plates (TDO and QDO, see DDO except with -His/-Leu/-Trp DO or -Ade/-His/-Leu/-Trp DO supplement). The plates were incubated for 3-4 days at 30 °C.

6.3.4 Preparation of Rubidium Chloride competent cells

10 mL of LB with appropriate antibiotics were inoculated from a glycerol stock of the desired *E. coli* or *A. tumefaciens* strain and incubated o/n agitating at 37 °C or 28 °C. 100 mL LB media with selection were inoculated to an OD₆₀₀ of 0.1 with the o/n culture and grown until an OD₆₀₀ of ~ 0.75. Cell were harvested by centrifugation (2500 rcf, 10 min, 4 °C) and resuspended in 30 mL cold, sterile filtered TBF1 buffer (100 mM RbCl, 10 mM CaCl₂, 50mM MnCl₂, 30mM NaOAc; adjusted to pH 5.8 with acetic acid). Cells were incubated on ice for 90 min, harvested (2500 rcf, 10 min, 4 °C) and resuspended gently in 4 mL cold, sterile filtered TBF2 buffer (10 mM MOPS, 10 mM RbCl, 75 mM CaCl₂ and 15% (v/v) glycerol). 100 µL

aliquots of the Rubidium Chloride competent cells were frozen at -80 °C in pre-chilled (-80 °C) 1.5 mL micro tubes.

6.3.5 Transformation of *E. coli* and *A. tumefaciens* by heat shock

An aliquot of chemical competent *E. coli* or *A. tumefaciens* was thawed on ice and mixed gently with either half of the ligation reaction (section 6.2.7) or 100 ng of plasmid. For transformation of *E. coli* after 20 min on ice, a heat-shock was applied at 42 °C for 2 min. After 2 min on ice, 1 ml of LB medium was added to the reaction, incubated for 1 h at 37 °C and plated on solid LB with selection. For transformation of *A. tumefaciens*, after 5 min on ice the aliquot was frozen for 5 min in liquid N₂, a heat shock was performed for 5 min at 37°C and after another 5 min on ice 1 mL of LB medium was added and incubated for 2-4 h at 28°C. The transformed cells were plated on solid LB with selection.

6.3.6 Plasmid Miniprep

Single *E. coli* colonies were picked from a selective LB-plate and grown o/n in 4 mL LB-medium with appropriate selection at 37 °C and 200 rpm. The next day 2 mL of culture was harvested in a 2 mL micro tube (3 min, 5000 rcf, 4 °C) and resuspended in 200 µL P1 buffer (50 mM Tris-HCl pH 8.0, 10 mM EDTA, 100 µg/mL RNase A). For cell lysis 300 µL P2 buffer (200 mM NaOH, 1% SDS (w/v)) was added. After incubation for 5 min at room temperature the lysis was neutralized by adding 300 µL P3 buffer (3M KAc, pH 4.8 adjusted with glacial acetic acid). After 10 min incubation on ice, the cell debris were spun down (10 min, 12000 rcf, RT). 750 µL of the supernatant were transferred into a fresh 1.5 mL micro tube. By adding an equal amount of isopropanol the plasmid DNA was precipitated. After centrifugation (10 min, 12000 rcf, RT) the pellet was washed with 70 % (v/v) EtOH, dried and taken up in 50 µL H₂O. Obtained plasmid DNA was analysed by restriction enzyme digest.

6.3.7 Plasmid Midiprep

For large scale purification of pure plasmid DNA the remaining culture of the corresponding Mini Prep was used to inoculate 100 mL of selective LB medium. Plasmids were purified by the NucleoBond Xtra Midi kit (Macherey-Nagel) according to the manufacturer's instructions. After precipitation the pellet was resuspended in 100 µL H₂O. The plasmid DNA concentration was measured by a NanoDrop Spectrophotometer ND-100.

6.3.8 Protein expression in *E. coli*

A suitable expression strain of *E. coli* was transformed with the desired vector and plated on LB plates with selection. To test if cell express protein after IPTG induction, single colonies were picked and grown o/n at 37°C in 5 mL selective LB medium. The next day 5 mL of LB media with selection were inoculated with the starter culture to an OD₆₀₀ of 0.1. When an OD₆₀₀ of 0.7-0.8 was reached, a 100 µL aliquot of un-induced culture was taken and expression of recombinant proteins was induced by adding IPTG to a final concentration of 1 mM. Cells were grown for 2h at 37°C and another 100 µL aliquot was taken and OD₆₀₀ was measured. Aliquots were spun down (4°C, 4000 rcf, 1 min) and pellets were boiled in 1x SDS buffer with the volume adjusted to the density of growth obtained by the biophotometer. Protein expression after IPTG induction was observed by SDS-PAGE.

Large scale protein inoculation was performed either from a preculture (M15 expression strain) or directly from plate (B121 expression strains) in a volume of 4L. After 4h of IPTG induction at 37°C and 200 rpm the cells were harvested by centrifugation (4000 rcf, 15min and 4 °C), frozen in liquid N₂ and stored until further processing at -80°C.

6.4 Protein based methods

6.4.1 SDS-PAGE

Depending on the size of the analysed proteins, a resolving gel solution with either 9% (w/v), 12% (w/v) or 18% (w/v) acrylamide: bisacrylamide (30 : 0.15); 0.75 M Tris pH 8.8, 0.2 % (w/v) SDS, 0.1 % (w/v) APS and 0.02 % TEMED was poured into a Biorad Mini-Protean 3 Multi casting chamber. The setup was left to polymerize after the solution was covered with isopropanol. After polymerisation the isopropanol was removed and the stacking gel solution (5% (v/v) acrylamide mix Gel 30 (5 : 1), 140 mM Tris pH 6.8, 0.23 % (w/v) SDS, 0.11 % (w/v) APS and 0.06 % (v/v) TEMED) was poured on the separation gel. Comb formers were squeezed in and the setup was left to polymerize. Protein samples were mixed with a corresponding amount of 6 x SDS loading buffer (50 mM Tris pH 6.8, 0.002 % (w/v) bromophenol blue, 2.5 % (w/v) glycerol, 1 % (w/v) SDS and 143 mM β-mercaptoethanol) and boiled for 5 min at 95°C. The denatured samples were separated in SDS-PAGE gel chambers filled with 1x Laemmli running buffer (0.1 % (w/v) SDS, 3.03 g/L Tris, and 14.41 g/L glycine) at 200 V. Gels were stained with Coomassie Brilliant Blue solution or were used directly for Western blotting. Whenever indicated, 0.5% (v/v) TCE were added to resolving gels.

6.4.2 Native PAGE

10 mL gels were cast by mixing 7% native polyacrylamide gel solution (1x TBE-buffer (0,9 M Tris-Base, 0,9 M boric acid, 20 mM EDTA), 6% (v/v) acrylamide mix Gel 30, 0.6% (w/v) APS, 0.06% (w/v) TEMED) pouring into gel casting glass plates. A comb former was added and left to solidify. Samples were mixed with 10x DNA loading dye and loaded onto the native polyacrylamide gels. DNA-Protein samples were separated in 1x TBE buffer at 100V. The gel was incubated in an ethidium bromide bath (1x TBE, 0.01% (v/v) ethidium bromide) for 10 min at RT and washed twice with H₂O. For visualization the Biometra BioDoc Analyzer was used.

6.4.3 Acid Urea (AU) PAGE

AU PAGE was performed like described before (Shechter et al., 2007). 10 mL gels were cast by mixing AU polyacrylamide gel solution (15% acrylamide, 0.1 % bisacrylamide, 6M Urea, 5% (v/v) acetic acid, 0.6% (w/v) APS, 0.06% (w/v) TEMED) pouring into gel casting glass plates. A comb former was added and left to solidify. Samples were mixed with 2x loading dye (7.2% (w/v) Urea, 10% (v/v) acetic acid). Protein samples were separated in 5% acetic acid with the poles inverted at 200 V for 30-90 minutes. Gels were stained with CBB.

6.4.4 Coomassie Brilliant Blue staining (CBB)

Protein staining was performed by submerging the SDS- or AU-PAGE gel in Coomassie Brilliant Blue (CBB) solution (0.2 % (w/v) CBB G-250, 30 % (v/v) EtOH and 10 % (v/v) acetic acid), heating in the microwave and consecutive shaking for 15-20 min. Following, the gel was placed in destain solution (7.5 % (v/v) ethanol and 5 % (v/v) acetic acid) and destained o/n.

6.4.5 Protein Quantification

Protein concentrations of complex samples were determined by Bradford assay. 200 µL protein sample was mixed with 1 mL of Bradford-reagent (0.01 % Coomassie Blue G-250, 5 % (v/v) EtOH, 10 % (v/v) phosphoric acid) in a disposable spectrophotometer cuvette. After 10 min of incubation the absorbance at 595 nm was measured in a BioPhotometer (Eppendorf). Protein concentrations were obtained by comparing the measured absorbance with previously measured extinctions of a BSA calibration curve.

Protein concentrations of purified samples were estimated by NanoDrop Protein Quantification according to the manufacturer's protocol. Extinction coefficients were calculated with ProtParam (ExPASy).

6.4.5 Protein/Affinity Purification

6.4.5.1 6xHis-tagged proteins

His-tagged proteins were expressed as described in section 6.3.8 and purified under native conditions. Pellets were resuspended in freshly prepared Lysis buffer (500 mM NaCl, 50 mM NaH₂PO₄, 10 mM 2-Mercaptoethanol, 10 mM Imidazol, 10% Glycerol, 0.5% Triton-X-100, 0.5 mM PMSF, pH 8 adjusted with NaOH) in a volume of 10 mL/L culture. After sonification (5x, 30%, 30s with 40s breaks, UW2070 MS73 Sonicator) cell debris were removed by centrifugation at 10000 rcf for 20 min at 4°C (Sorvall LYNX 4000 equipped SS34 rotor). In the meanwhile, 0.4 mL/L culture Ni-NTA coated agarose beads (Qiagen) were washed 3 times with lysis buffer. The supernatant was transferred into a Falcon tube and the equilibrated beads were added. The suspension was incubated for 1h at 4°C, shaking on a Falcon-tube rotator. Subsequently, the beads were collected on an empty PD10 desalting column in the cold-room, washed 4x with washing buffer (500 mM NaCl, 50 mM NaH₂PO₄, 10 mM 2-Mercaptoethanol, 20 mM Imidazol, 10% Glycerol, 0.5% Triton-X-100, 0.5 mM PMSF, pH8 adjusted with NaOH). Collected beads were eluted 3x with 5 mL elution buffer (500 mM NaCl, 50 mM NaH₂PO₄, 10 mM 2-Mercaptoethanol, 250 mM Imidazol, 10% Glycerol, 0.5% Triton-X-100, 0.5 mM PMSF, pH8 adjusted with NaOH) for 15 min, shaking at RT. All steps, if not indicated otherwise, were performed at 4 °C or on ice, with pre-cooled buffers.

6.4.5.2 Hydrophobic Interaction Chromatography (HIC)

Truncated HMGbox proteins which were purified by 6xHis-tag affinity purification were further purified by hydrophobic interaction chromatography. The respective column of the FPLC System (Gradient Programmer GP250 (Pharmacia Biotech)) was washed with buffer B (10 mM Na₂HPO₄, 1 mM DTT, 1 mM EDTA, 0.5 mM PMSF, adjust to pH 7) and equilibrated by increasing ammonium sulphate salt concentration up to 1.8 M buffer A (10 mM Na₂HPO₄, 1 mM DTT, 1 mM EDTA, 0.5 mM PMSF, 1.8 M (NH₄)₂SO₄, adjusted to pH 7). The column with bound proteins was washed twice with buffer A and the flowthrough was collected for further analysis. Proteins were eluted by applying a linear gradient from 1.8 M to 0 M (NH₄)₂SO₄ and collected in 1 mL fractions at a flow rate of 2 mL/min by the Fraction Collector FRAC-100 (Amersham Biosciences). The elution profile was monitored spectrometrically at 280 nm. Selected fractions with high absorbance were tested by SDS-PAGE and stained with CBB. Fractions containing the desired pure protein in high amounts were desalted.

6.4.5.3 GST-tagged proteins

GST-tagged proteins were expressed (Section 6.3.8) in the BL21-CodonPlus(DE3)-RIL *E. coli* strain. The pellet of 2 L IPTG-induced culture was resuspended in 35 mL Lysis buffer (50 mM Tris-HCl pH 7.5, 500 mM NaCl, 0.05 % IGEPAL CA-630, 10 % glycerol, 2 mM DTT, 2 mM EDTA, 2 mM EGTA, 0.5 mM PMSF). After sonification (6x 30%, 15s with 60s breaks, UW2070 MS73 Sonicator) cell debris were removed by centrifugation at 40000 rcf for 60 min at 4°C (Sorvall LYNX 4000, equipped SS34 rotor). In the meantime, 1.8 mL Glutathione sepharose beads (Thermo Fisher Scientific) were equilibrated with lysis buffer and spun down for 2 min at 800 rcf at 4 °C. The supernatant was transferred into a falcon tube and the beads were added. The suspension was incubated for 80 min at 4°C rotating on a Falcon-tube rotator. Subsequently, the beads on an empty PD10 desalting column in the cold-room, washed 5x with lysis buffer. Collected beads were eluted 2x with 5 mL elution buffer (50 mM Tris-HCl pH 8.0, 20 mM reduced glutathione, 1 mM DTT) for 15 min whilst shaking at RT. All steps, if not indicated otherwise, were performed at 4 °C or on ice, with pre-cooled buffers. Protein fractions were validated by SDS-PAGE. Elution fractions containing the target protein were re-buffered and concentrated in buffer B using appropriate Amicon Ultra-15 Centrifugal filter devices.

6.4.5.4 GS-tagged proteins

A detailed protocol concerning GS affinity purifications coupled to Mass-spectrometry was published together with colleagues (Pfab et al., 2017). Minor modifications were used, e.g. the use of benzonase to reduce unspecific binding mediated by nucleic acids. Details on handling and materials remain valid. For all steps in the volumes from 0.5 – 2 mL protein low bind tubes were used (Eppendorf LoBind). IgG coupled beads were pelleted by a magnetic rack.

15 g of frozen cell suspension culture was transferred into in liquid nitrogen prechilled adapters and homogenized via the Tissue Lyser II (Qiagene) with a frequency 30 Hz for 1 min. Ground tissue was thawed on ice in 20 mL cold Extraction Buffer 1 (100 mM NaCl, 25 mM HEPES pH 7.4, 10 mM PMSF, 5 mM EGTA, 2 mM MgCl₂, 10% Glycerol, 0.05 % NP-40, protease inhibitor cocktail tablets (cOmplete, EDTA-Free, Roche)). The slurry was sonicated (5x, 30 sec at 30% intensity with 1 min breaks with a UW2070/MS73 Sonicator) and MgCl₂ (to a final concentration of 5 mM) and 50 U/mL Benzonase as added. After 30 min incubation at 4°C on a rotating wheel, cell debris were removed by centrifugation at 40000 rcf for 60 min at 4°C (Sorvall LYNX 4000, equipped SS34 rotor). Subsequently the supernatants were further cleared by PVDF syringe filters of 0.45 µm. Protein concentrations of the raw extract were measured by Bradford assay and adjusted within a set of samples by diluting them with extraction buffer.

100 μ L of magnetic IgG beads – prior washed 3x with extraction buffer – were added to the solution and left spinning for 1h at 4°C. The beads were centrifuged for 10 minutes at 2000 rcf and 4°C. The supernatant was discarded and the bead pellet was washed three times with 1 mL of cooled extraction buffer. Proteins were eluted by adding 300 μ L elution buffer (0.1 M glycine-HCl, adjusted to pH 2.7) and shaking for 5 min at RT at 700 rpm. After removal of the beads 1.2 mL of ice cold acetone was added. The protein precipitate was incubated at -20°C o/n. The proteins were pelleted by centrifugation (15 min, 12000 rcf, 4°C), washed 3x with ice cold acetone and taken up in 1 x PBS for in gel digestion and western blotting.

6.4.6 Desalting and Protein Concentration

For desalting and protein concentration Amicon Ultra-15 filter devices were used. Depending on the protein size an appropriate size cut-off was chosen. All steps were performed according to the manufacturer's description. Proteins were standardly rebuffed in buffer B (10 mM Na₂HPO₄, 1 mM DTT, 1 mM EDTA, 0.5 mM PMSF, adjust to pH 7). The concentrated, desalted proteins were aliquoted, frozen in liquid nitrogen and stored at -80 °C.

6.4.7 Electrophoretic mobility shift assay (EMSA)

100 ng of DNA and different concentrations of protein were incubated in 1x EMSA buffer (10 mM Tris-HCl pH 7.5, 50 mM NaCl, 5 mM MgCl₂, 1 mM EDTA, 1 mM DTT, 5% (v/v) Glycerol, 0.01 mg/mL BSA) for 10 min at RT in a total volume of 20 μ L. After the incubation DNA loading buffer was added and the samples were analysed with native PAGE (6% gel, Section 6.4.2)

6.4.8 Circular dichroism (CD)

With the help of Klaus Jürgen Tiefenbach the secondary structure of proteins was investigated by CD spectroscopy. BID-HMGboxes were diluted to 10 μ M in 50 mM KH₂PO₄ and analysed in a Jasco J-815 Circular Dichroism (CD) Spectropolarimeter using a 0.02 cm cell. The blank signal of the buffer was subtracted and the measured ellipticity was converted into mean residue ellipticity as described before (Myers et al., 1997).

6.4.9 GST-pulldowns

In a total reaction volume of 200 μ L, 0.5 μ M of target protein were mixed in equimolar ratios with either AtH2A-H2B or with bovine cytochrome C (Sigma Aldrich) and 1x GST buffer (0.2-0.35 M NaCl, 25 mM HEPES pH 7.5, 0.05 % (v/v) NP40, 5 mM DTT, 10 % (v/v) Glycerol, 2 mM MgCl₂). The mixture was incubated for 30 minutes at 30 °C. In the meantime, 20 μ L

glutathione sepharose beads were washed 3x with 500 μ L 1x GST buffer. After each washing step the beads were spun down at 800 rcf for 1 min. The equilibrated beads were added to the reaction mixture and the samples were incubated for 3 hours on a rotating wheel at 4 °C. The beads were pelleted, the supernatant was removed and the beads were washed three times with 500 μ L 1x GST buffer. For elution 40 μ L 1xSDS loading dye was added and the beads were boiled for 20 minutes at 95 °C. The supernatant was transferred into a new tube and analysed by SDS-PAGE.

6.4.10 “hot” CK2 *in vitro* phosphorylation assay

Radioactive *in vitro* Kinase assays were performed with [γ -³²P]ATP as previously described (Stemmer et al., 2002): A total volume of 20 μ L was incubated for 1 h at 37°C with 40 ng of purified recombinant maize CK2 α and 100 nCi of [γ -³²P]ATP in 1x CK2 buffer (25mM Tris/HCL pH 8.5, 10 mM MgCl₂, 1 mM DTT). Substrates contained up to 100 ng of protein. For the positive control 100 ng of HMGB2 was used which has been shown to be phosphorylated by CK2 (Stemmer et al., 2002). The phosphorylations were monitored by SDS-PAGE separation in 12% polyacrylamide gels and subsequent drying of the gels for 1h on a gel dryer. The dried polyacrylamide gel was facing a phosphor storage screen and stored in a light excluding cassette for ~45 minutes and scanned with a Cyclone Storage phosphorimager (Canberra Packard).

6.4.11 “cold” CK2 *in vitro* phosphorylation assay

Preparative phosphorylation was performed as previously described (Stemmer et al., 2002). In a total volume of 50 μ L, 20 μ g of SPT16-AID was incubated with 400 ng of purified recombinant maize CK2 α and 300 μ M ATP in 1x CK2 buffer (25mM Tris/HCL pH 8.5, 10 mM MgCl₂, 1 mM DTT) for 1h at 37°C. The assay was validated by AU-PAGE and by mass spectrometry.

6.4.12 ChIP-Seq

A detailed protocol concerning ChIP was published together with colleagues (Pfab et al., 2017). Minor modifications were used here, details on handling and materials remain valid. For all steps in the volumes from 0.5 – 2 mL protein low bind tubes were used (Eppendorf LoBind). Dynabeads and AMPure beads were pelleted by a magnetic rack.

6.4.12.1 Crosslinking

Plants were grown on ½ MS square plates for 14 days (Section 6.1.2) and 3 g of plant material was harvested into a 50 mL tube filled with 37 mL of cold fixation buffer (1% (v/v) formaldehyde 0.4 M sucrose, 10 mM HEPES-NaOH pH 8, 5 mM β-mercaptoethanol, 1x cOmplete EDTA free proteinase inhibitor tablets (Sigma-Aldrich)) and vacuum infiltrated for 10 min. The reaction was quenched by the addition of 2.5 mL 2.5M Glycine solution and subsequent vacuum infiltration for 5 min. The crosslinked seedlings were rinsed three times with H₂O. Excess water was removed by a paper towel. Plant material was frozen in liquid nitrogen and stored until chromatin isolation at -80°C.

6.4.12.2 Chromatin Preparation

The crosslinked, frozen plant material was transferred into in liquid nitrogen prechilled adapters and homogenized via the Tissue Lyser II (Qiagene) with a frequency 30 Hz for 1 min. Ground tissue was added to 30 mL cold Extraction Buffer 1 (0.4 M sucrose, 10 mM HEPES-NaOH pH 8, 5 mM β-mercaptoethanol, 1x cOmplete proteinase inhibitor tablets, 1x PhosSTOP phosphatase inhibitors (Sigma-Aldrich)) in a 50 mL Falcon tube and incubated on a rotating wheel at 4 °C for 20 min. The suspension was filtered through a double layer of Miracloth into a new 50 mL Falcon tube and centrifuged at 3000 rcf at 4 °C for 20 min. The pellet was resuspended in cold 1 mL Extraction Buffer 2 (0.25 M sucrose, 10 mM HEPES-NaOH pH 8, 10 mM MgCl₂, 1% (v/v) Triton X-100, 5 mM β-mercaptoethanol, 1x cOmplete proteinase inhibitor tablets, 1x PhosSTOP phosphatase inhibitors) and transferred into a new 1.5 mL tube and centrifuged at 12000 rcf at 4 °C for 10 min. Washing was repeated three times. 300 μL Extraction Buffer 3 (1.7 M sucrose, 10 mM HEPES-NaOH pH 8, 2 mM MgCl₂, 0.15% (v/v) Triton X-100, 5 mM β-mercaptoethanol, 1x cOmplete, 1x PhosSTOP) were added to a new 1.5 mL tube. The pellet was resuspended in 300 μL Extraction Buffer 3 and used to carefully overlay the 300 μL Extraction Buffer 3. The sucrose gradient was centrifuged at 16000 rcf at 4°C for 1h. After removal of the supernatant, the nuclei were frozen in liquid N₂ and stored at -80°C. The next day the pellet was resuspended in 600 μL Nuclei Lysis Buffer (50 mM HEPES-NaOH pH 8, 10 mM EDTA, 0.1% SDS, 1x cOmplete, 1x PhosSTOP) and incubated on ice for 30 min. The sample was split into two 300 μL parts and sonicated with 10 cycles (30 sec on/30 sec off) using Bioruptor Pico (Diagenode). The sample was re-merged and the chromatin solution was centrifuged at 20800 rcf and 4 °C for 10 min. The supernatant was transferred into a new tube and centrifugation was repeated. The supernatant was transferred into a new 1.5 mL tube containing Dynabeads (40μL/sample), which were washed 3x in 500μL ChIP dilution

buffer (1.1% Triton X-100, 1.2 mM EDTA, 16.7 mM HEPES-NaOH pH 8, 167 mM NaCl) for equilibration. The mixture was incubated at 4 °C with agitation for 2 hours to reduce the background signal.

6.4.12.3 Immunoprecipitation

The supernatant was split into 3 tubes a 200 µL and the Dynabeads were discarded. Supernatants were diluted with 800 µL of ChIP adjustment buffer (1.25% Triton X-100, 12.5 mM HEPES-NaOH pH 8, 188 mM NaCl, 1x cOmplete, 1x PhosSTOP). 3µL of the desired antibody (H3 (ab1791, Abcam) or S2P (ab5095, Abcam)) were added to each sample, except for one tube which served as the negative control. Samples were left rotating overnight at 4 °C.

6.4.12.4 Washing and Elution

Dynabeads (30µL/sample) were washed 3x with ChIP Dilution Buffer for equilibration. The pelleted beads were added to the chromatin solution containing the respective antibody. Samples were left rotating at 4 °C for 3 h. The beads were pelleted, 100 µL input sample were taken and the rest of the supernatant was discarded. Beads were washed 1 time with 0.5 mL of each wash buffer (LowSalt (150 mM NaCl, 0.1% SDS, 1% Triton X-100, 2 mM EDTA, 20 mM HEPES-NaOH pH 8), HighSalt (500 mM NaCl, 0.1% SDS, 1% Triton X-100, 2 mM EDTA, 20 mM HEPES-NaOH pH 8), LiCl-Wash (50 mM HEPES-NaOH pH 8, 0.25 M LiCl, 1% NP-40, 1% sodium deoxycholate (weigh in fresh), 1 mM EDTA), TE (10 mM TRIS-HCl pH 8, 1 mM EDTA), except twice with TE. After each washing step the samples rotated at 4 °C for 10 min. After the last washing step, the beads were pelleted, the supernatant was removed and DNA was eluted by adding 50 µL freshly made Elution Buffer (1 % SDS, 0.1 M NaHCO₃) and subsequent incubation at 65 °C for 15 min with gentle rotation. The supernatant was transferred into a new 0.5 mL tube, the elution was repeated, and the eluates were merged.

6.4.12.5 DNA extraction and Signal Quantification

The crosslinking was reversed by adding 4 µL of 5 M NaCl to 100 µL of the eluates and input controls followed by o/n incubation at 65°C with gentle rotation. Afterwards, 2 µL of 0.5 M EDTA and 1.5 µL 3 M TRIS-HCl pH 6.8 and 1 µL proteinase K (Thermo Fisher Scientific, 20 mg/mL) were added and incubated at 45°C for 3h in a thermocycler. DNA was purified with the NucleoSpin Gel and PCR Clean-up kit (Macherey Nagel) according to the manufacturer's manual for DNA clean-up of samples containing SDS. DNA was eluted 3x times with 17 µL buffer NE. 2 µL were used and dilute with 8 µL of H₂O for quantification with the Qubit Fluorometer. 1 µL was used for PCR reactions with actin primers.

6.4.12.6 Library preparation

Libraries were prepared using the NEBNext Ultra™ II DNA Library Prep Kit for Illumina with index primers NEBNext Multiplex Oligos for Illumina (Set 1-4) according to the manufacturer's protocol, using 20 ng starting material for H3 ChIP libraries and <5 ng starting material for S2P ChIP libraries. The following steps were included "Size Selection of Adaptor-ligated DNA" and "Cleanup of PCR Reaction" with AMPure beads and PCR target enrichment with 10 or 12 cycles respectively.

6.4.12.7 Quality control/ Sequencing of Libraries / Bioinformatic analysis

Quality controls and deep sequencing of the ready to sequence libraries were performed at the The Kompetenzzentrum Fluoreszente Bioanalytik (KFB). The read length was 75bp and the reading depth per biological replicate was 15 – 20 Million reads. Bioinformatic analysis of obtained datasets was performed by Simon Obermeyer with support of Uwe Schwartz (CCU Biology).

6.4.13 Western Blotting

Western blotting was performed either with nuclear protein extracts or proteins derived from GS-tag affinity purification (6.4.5.4). Nuclear protein extracts were prepared from 1 g plant material. Nuclei were extracted as described in section 6.4.12. However, nuclei were resuspended in 100 µL 1x Laemmli Buffer, SDS-loading buffer was added and samples were boiled for 10 min at 95°C. Sample was spun down at 16 000 rcf for 5 min and the supernatant was transferred into a new 1.5 ml micro centrifuge tube.

Proteins were separated by SDS-PAGE. Optionally proteins were stained with TCE after separation. Proteins were transferred onto Amersham Hybond LFP 0.2 PVDF membrane using a Mini-PROTEAN Tetra electrophoresis system containing the Mini Trans-Blot (Bio-Rad). Therefore, the membrane was activated beforehand for 30s in MeOH. The membrane, the 6 Whatman papers and the gel were equilibrated in blotting buffer (20% (v/v) methanol, 200 mM glycine, 20 mM Tris-Base and 0.01% (w/v) SDS) for 10 min. The blotting sandwich was set up avoiding any air bubbles: Three pieces of Whatman paper, the PVDF membrane, SDS-gel, three pieces of Whatman paper. Proteins were blotted to the membrane by applying 350 mA for 1h. After blotting the transfer was monitored by TCE staining (optionally). The membrane was incubated in blocking buffer (5% (w/v) skimmed milk powder, 20 mM Tris-HCl pH 7.5, 150 mM NaCl and 0.05% Tween 20 (v/v)) at 4°C on a Falcon tube rotator for 1h. The primary antibody (1:2000) was added and left rotating o/n. The following primary antibodies were used:

a-H3 (cat. no. ab1791, Abcam); a-H2B (cat. no. ab1790, Abcam); and a-SSRP1 and a-SPT16 (Duroux et al., 2004). The next day the membrane was washed 3x for 10 min at 4°C with washing buffer (20 mM Tris-HCl pH 7.5, 150 mM NaCl, 0.05% (v/v) Tween 20 and 1% (v/v) Triton X100). The blocking buffer, containing the secondary antibody in 1:5000 dilution, was added and left rotating for 2h at 4°C. The membrane was washed for 3 times in washing buffer. The blotting as well as antibody incubation and washing steps were performed at 4 °C. For chemiluminescent detection SuperSignal R West Pico Chemiluminescent substrate was used according to manufacturer's manual (Thermo Scientific). Chemiluminescence was detected using Multiimage FlurChem FC2 imager (Alpha Innotech) or ChemiDoc MP (Bio-Rad).

6.4.14 Mass-Spectrometry

6.4.14.1 MALDI-TOF

For quality control, mall purified proteins (<20 kDa) were analysed by MALDI-TOF in a 4800 instrument from Applied Biosystems like described before (Hamperl et al., 2013).

6.4.14.2 In-gel digestion of proteins

Samples analysed by shotgun proteomics were loaded on 4–15% precast polyacrylamide gels. Single bands were cut into one defined slice, whole lanes (IgG affinity purifications) were cut with a scalpel into 8-12 slices covering the whole molecular weight range. Each slice was cut further into small cuboids (~2x2mm). Cuboids were transferred into a 2 mL Eppendorf Safe-Lock Tubes and washed 3 times with different washing buffers for 30 min at RT whilst shaking (Washing Buffer 1: 50 mM NH₄HCO₃; 2: 37.5 mM NH₄HCO₃, 25% (v/v) acetonitrile; 3: 25 mM NH₄HCO₃; 50% (v/v) acetonitrile). After a final 10 min washing step with acetonitrile the gel pieces were lyophilized for 1h. Gel pieces were soaked in 20 µL of Trypsin solution (35 mM NH₄HCO₃, 0.04 µg/µL Trypsin). After 10 min, gel pieces were covered with 50 mM of NH₄HCO₃. The digest was performed o/n at 37 °C. The supernatant was transferred into a 0.5 mL collection tube (Eppendorf) and peptides were eluted at 37°C from the gel pieces in two 1h extractions steps (50 mM NH₄HCO₃). After a final extraction step for 30 min at RT (25 mM NH₄HCO₃, 50% (v/v) acetonitrile), all eluates were pooled, frozen in liquid N₂ and lyophilized.

6.5.14.3 LC-MS/MS

Peptides obtained from in-gel digestion were analysed like described in (Antosz et al., 2017). Depending on the assay additionally S/T phosphorylations were included as fixed modifications.

6.5 Confocal laser scanning microscope (CLSM)

CLSM was performed using a Leica SP8 equipped with a 10X NA 0.3, a 40X Oil NA 1.3 or a 63X Glycerol NA 1.3 objective. eGFP was excited with an Argon laser at 488 nm, mCherry was excited using an DPSS laser at 561 nm. The emission of eGFP or mCherry/TagRFP was detected at 500 - 550 nm or 570-620 nm. Roots, leaves or PSB-D suspension culture cells were mounted in H₂O on glass slides with coverslips.

6.5.1 Fluorescence recovery after photobleaching (FRAP)

The FRAP experiments were performed using a Leica SP8 confocal laser scanning microscope equipped with a 63X Glycerol NA 1.3 objective. Imaging was performed with the following settings: 256 x 256 pixel, 1800 Hz, bi-directional scanning mode. The best parameters for ROI size, time of bleaching and bleaching intensity were optimized around previous determined conditions (Pfab, 2017): ROI size 9 μm, bleaching pulse of six iterations (6 x 79 ms) at 100 % laser power (561 nm), 50 pre-bleach and 90 post-bleach images were acquired with 2% laser power. Although every parameter was altered, and leaves, roots and PSB-D cell suspension culture was tested, no satisfactory result was obtained. Obtained data was evaluated with the web-tool easyFRAP (Koulouras et al., 2018).

6.5.2 Förster resonance energy transfer (FRET)

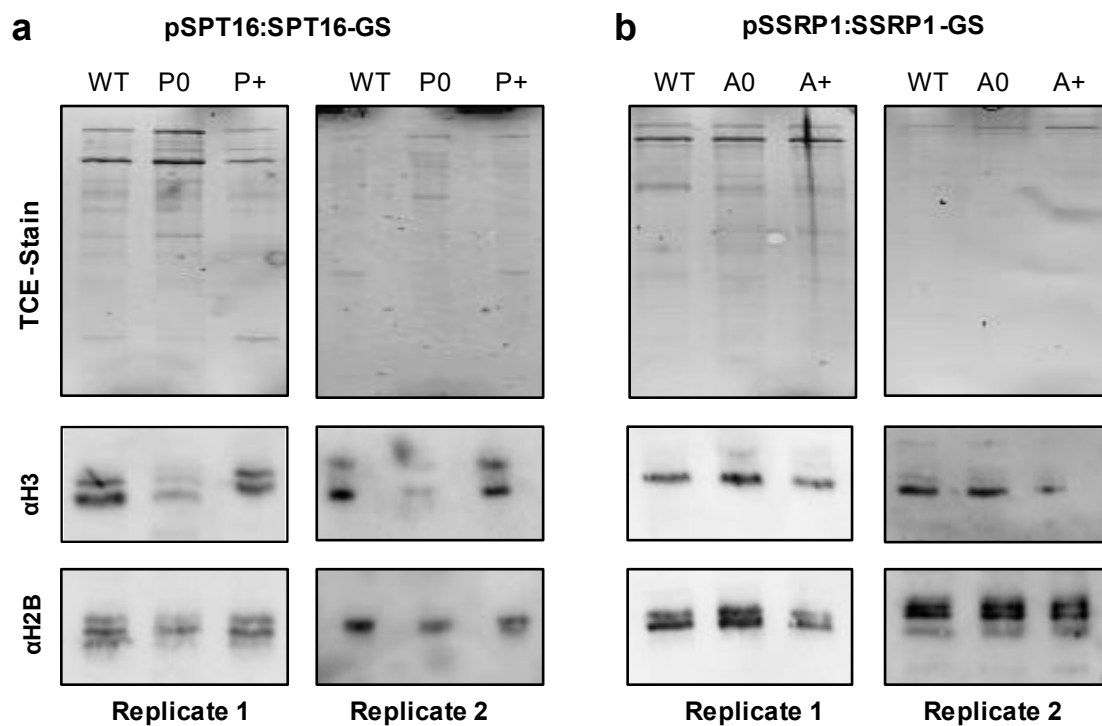
Förster resonance energy transfer - acceptor photobleaching (FRET-APB) and calculation of the FRET efficiencies were performed as described in (Weidtkamp-Peters and Stahl, 2017). *A. tumefaciens* was used to infiltrate a *Nicotiana benthamiana* leaf (Section 6.1.10). An infiltrated leaf piece (~ 0.5 x 0.5 cm) was mounted on a glass slide with the abaxial side facing up (Section 6.5). Moderate pressure was applied on the coverslip with tweezers to flatten the leaf. FRET was performed using a Leica SP8 confocal laser scanning microscope equipped with a 63X Glycerol NA 1.3 objective. eGFP was excited with an Argon laser at 488 nm and mCherry was excited/bleached with an DPSS laser at 561 nm. For acceptor bleaching, a circular area of 9 μm was bleached at 100% laser power (561 nm), for 60 iterations. Images were taken with the following settings: 256 x 256 pixel, 1400 Hz, no line averaging, sequential scan mode, pinhole 3, PMT detector gain of 800 V. If the fluorescent intensity dropped significantly in pre-bleached images, the measurement was discarded. FRET efficiency was calculated as follows:

$$Efficiency = \frac{(Intensity (Postbleach) - Intensity (Prebleach))}{Intensity (Prebleach)}$$

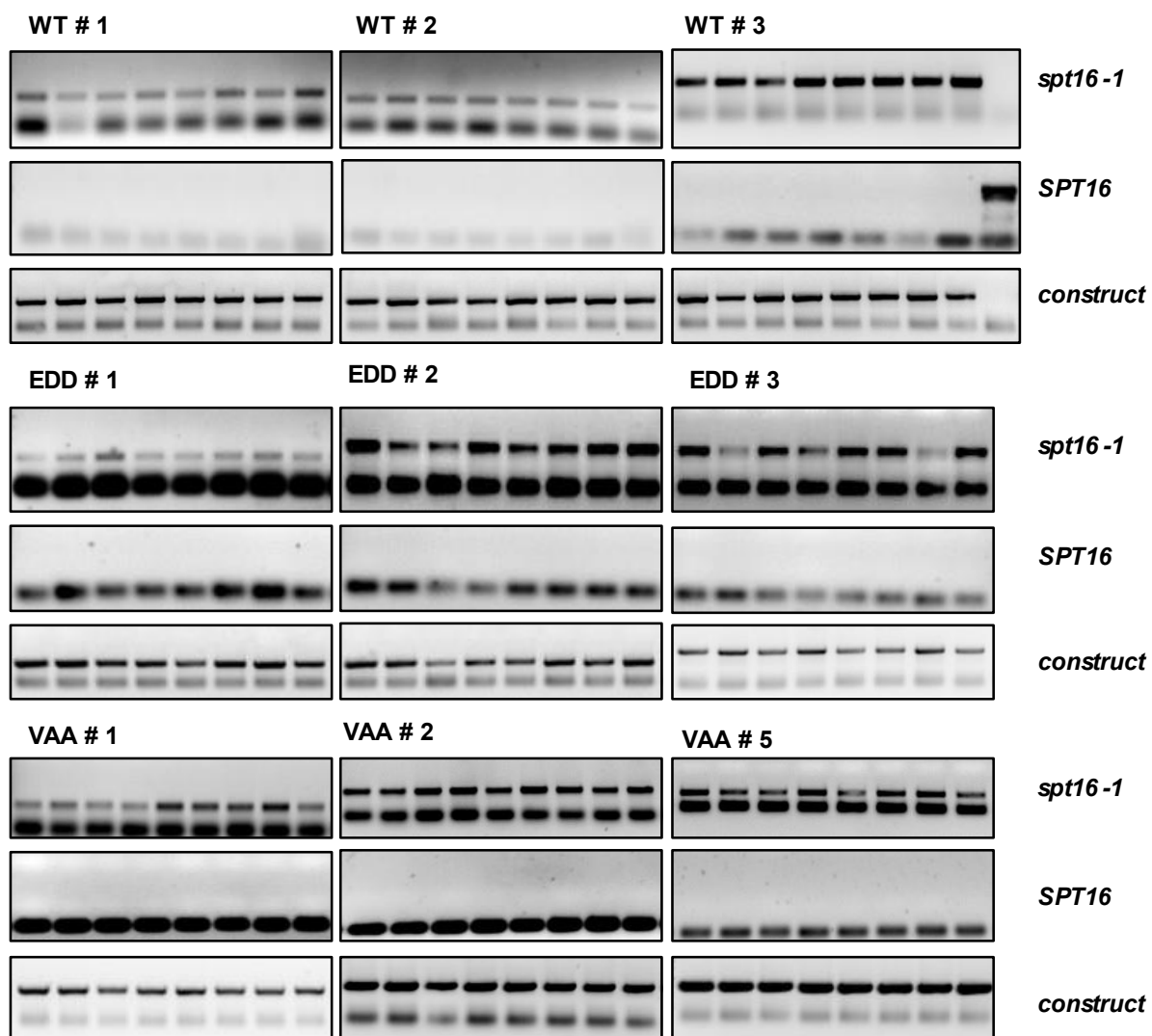
7 Supplementary

Supplementary Table 1 Subunits of CK2 co-purifying with SPT16-GS PTM

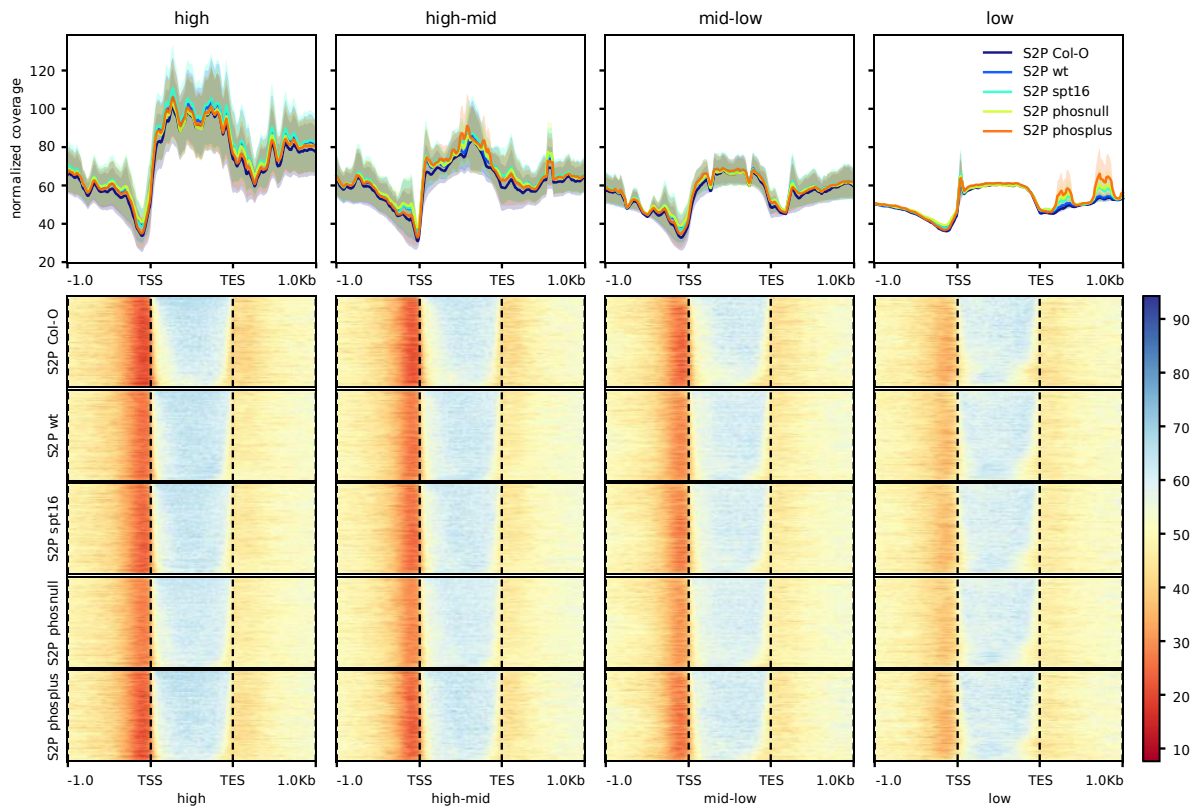
	SPT16-GS	Interactor	AGI	Complex
Rank	Score/#IPs			
38	810/2	CKA1	AT5G67380	CK2
33	1012/3	CKA2	AT3G50000	CK2
70	345/2	CKA3	AT2G23080	CK2
7	2096/3	CKA4	AT2G23070	CK2
22	1418/3	CKB1	AT5G47080	CK2
26	1132/3	CKB2	AT4G17640	CK2
35	962/3	CKB3	AT3G60250	CK2
34	1002/3	CKB4	AT2G44680	CK2



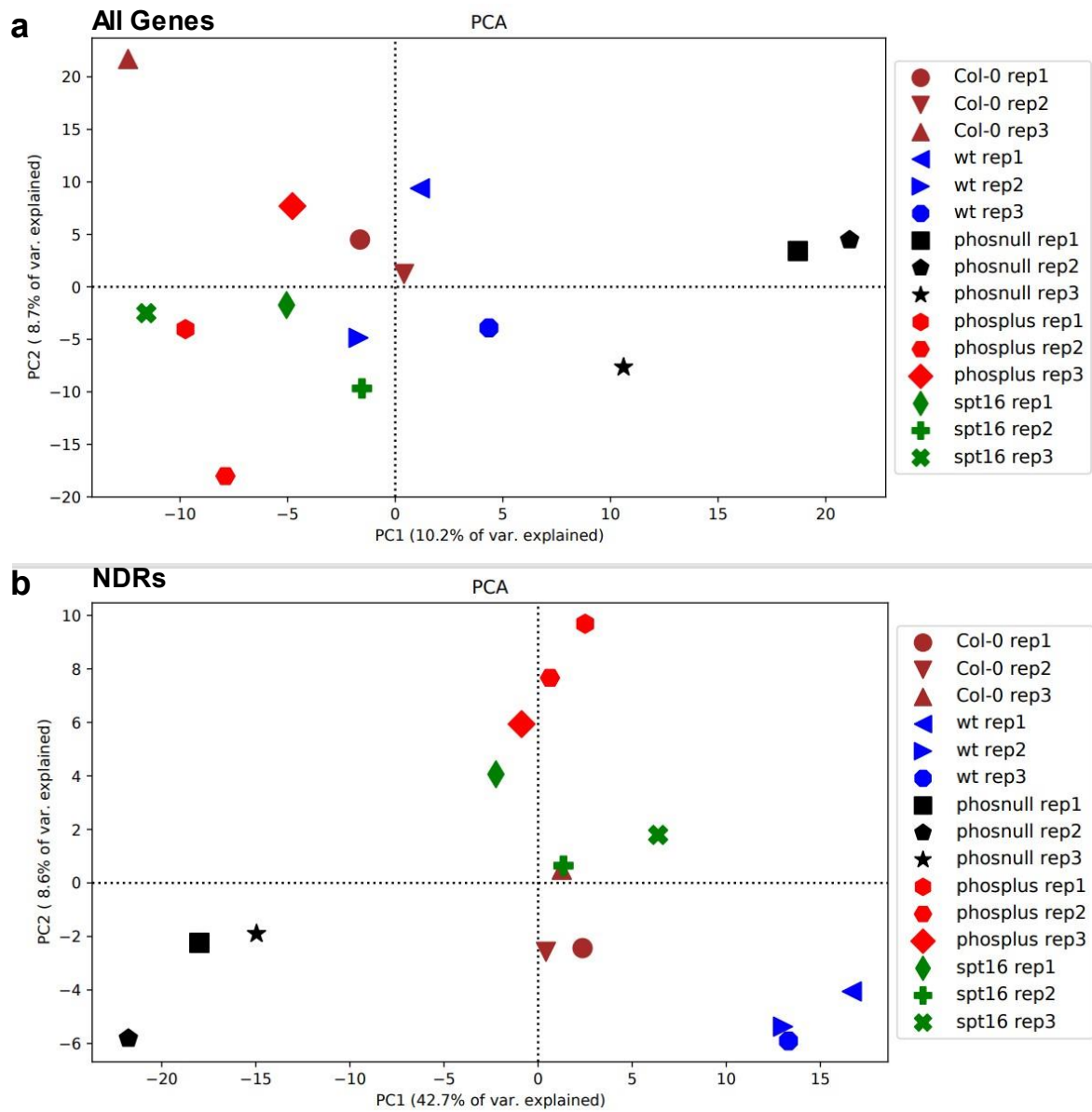
Supplementary Figure 1 H2B and H3 Immunoblot analysis of (a) Affinity Purification of SPT16 phospho-variants (b) Affinity Purification of SSRP1acetyl-variants



Supplementary Figure 2 Segregation analysis by genotyping PCR of double homozygous lines for *spt16-1* and the respective transgene. For Primers and details please refer to **Figure 21**



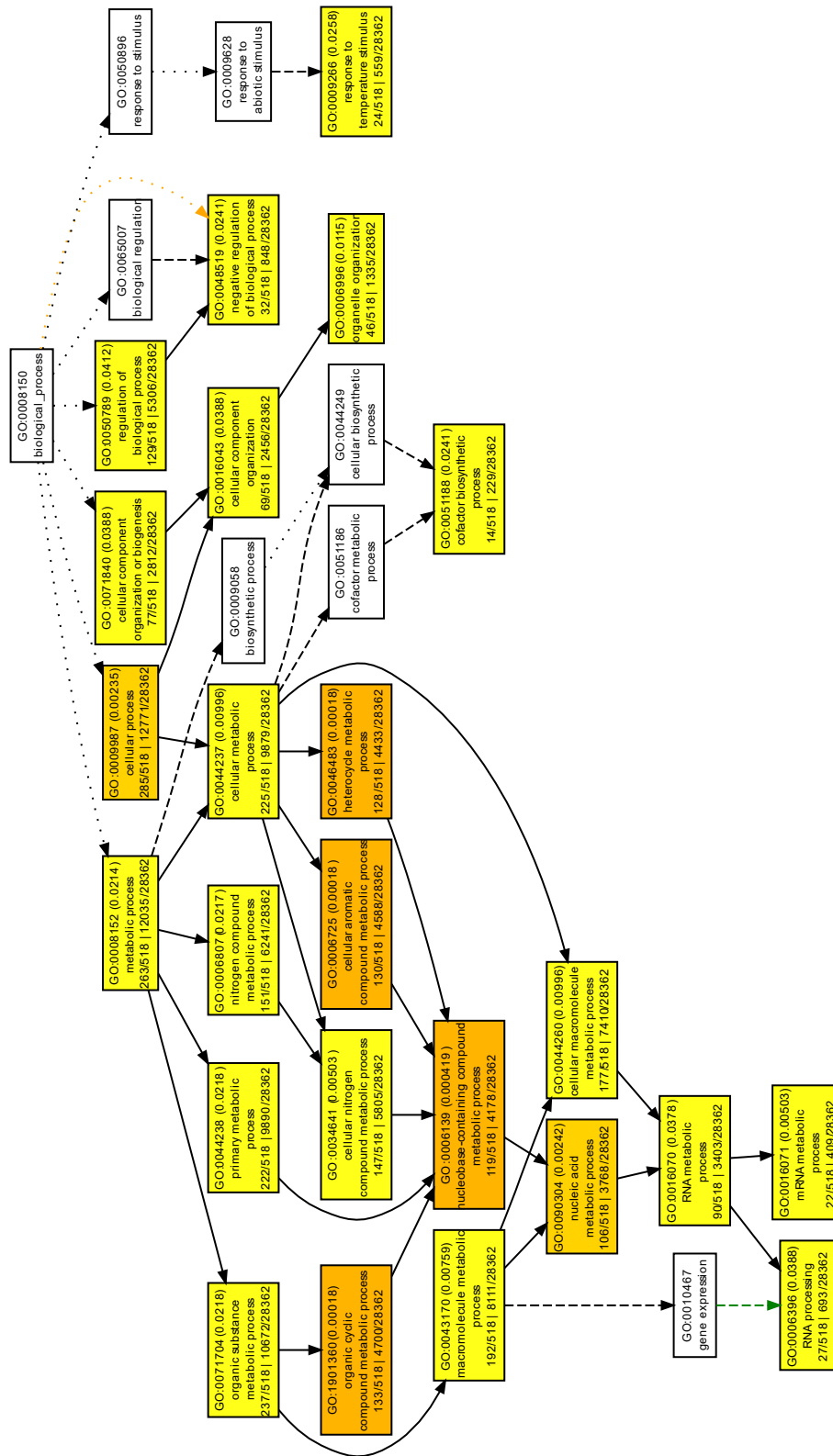
Supplementary Figure 3 Average S2P distribution over differentially expressed gens. Gene distribution over quartiles of high, mid-high, mid-low and low expressed genes determined by RNA-seq of 6 day old seedlings (Obermeyer unpublished). TSS = Transcription start site; TES = Transcription end site



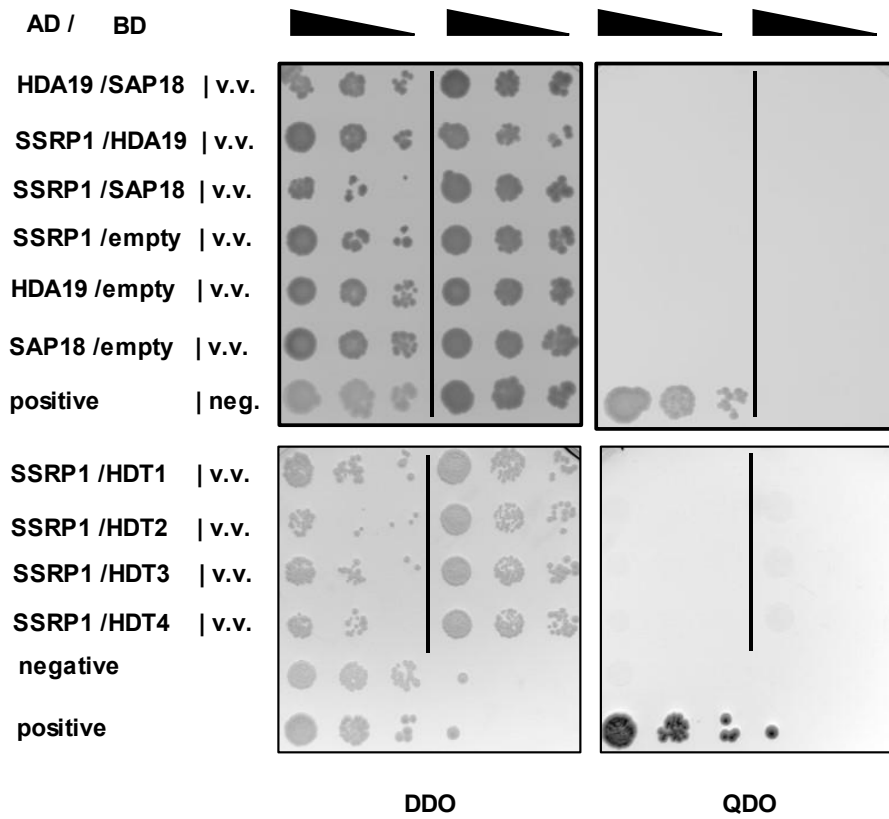
Supplementary Figure 4 PCA of α -H3 ChIP-seq analysis of Col-0, *spt16-1* and *spt16-1* phospho-variants.
(a) Over all genes **(b)** Over NDRs (-300bp to 0 bp upstream of TSS)

Rank	Motif	P-value	log P-value	% of Targets	% of Background	STD(Eg STD)	Best Match Details
1		1e-65	-1.515e+02	36.01%	1.19%	69.6bp (105.9bp)	PCF/Arabidopsis-Promoters/Homer(0.941) More Information Similar Motifs Found
2		1e-34	-7.981e+01	40.91%	8.90%	91.0bp (119.0bp)	Unknown4/Arabidopsis-Promoters/Homer(0.936) More Information Similar Motifs Found
3		1e-32	-7.495e+01	23.08%	1.80%	68.8bp (119.9bp)	VRN1(ABI3VP1)/col-VRN1-DAP-Seq(GSE100000) More Information Similar Motifs Found
4		1e-29	-6.862e+01	20.63%	1.43%	71.3bp (61.2bp)	E-box/Arabidopsis-Promoters/Homer(0.998) More Information Similar Motifs Found
5		1e-28	-6.512e+01	37.06%	8.89%	84.8bp (99.9bp)	RAMOSA1(MA1416.1)/Jaspar(0.936) More Information Similar Motifs Found
6		1e-27	-6.356e+01	52.45%	19.27%	80.7bp (115.3bp)	HuR(7)/HEK293-HuR-CLIP-Seq(GSE8788) More Information Similar Motifs Found
7		1e-26	-6.117e+01	48.95%	17.24%	74.7bp (107.3bp)	Hnmp1(RRM)/Xenopus_tropicalis-RNCMP1 More Information Similar Motifs Found
8		1e-24	-5.573e+01	11.19%	0.06%	68.9bp (38.6bp)	Unknown2/Arabidopsis-Promoters/Homer(0.936) More Information Similar Motifs Found
9		1e-19	-4.559e+01	25.52%	5.69%	79.2bp (97.6bp)	IRF3(IRF)/BMDM-Irf3-ChIP-Seq(GSE6733) More Information Similar Motifs Found
10		1e-16	-3.726e+01	15.38%	2.16%	64.4bp (56.4bp)	OP11(MacIsaac)/Yeast(0.827) More Information Similar Motifs Found
11		1e-15	-3.656e+01	22.38%	5.43%	73.2bp (111.6bp)	TFCP2(MA0145.3)/Jaspar(0.864) More Information Similar Motifs Found
12		1e-14	-3.271e+01	7.69%	0.19%	94.6bp (49.9bp)	MYB3R1(MYB)/col-MYB3R1-DAP-Seq(GSE100000) More Information Similar Motifs Found
13		1e-12	-2.980e+01	15.38%	2.99%	94.1bp (67.8bp)	SRSF10(RRM)/Homo_sapiens-RNCMP10 More Information Similar Motifs Found
14		1e-12	-2.971e+01	10.14%	1.01%	90.9bp (77.4bp)	PABPC5(RRM)/Homo_sapiens-RNCMP10 More Information Similar Motifs Found
15		1e-12	-2.803e+01	32.52%	13.75%	96.5bp (122.8bp)	SFL1(MacIsaac)/Yeast(0.891) More Information Similar Motifs Found

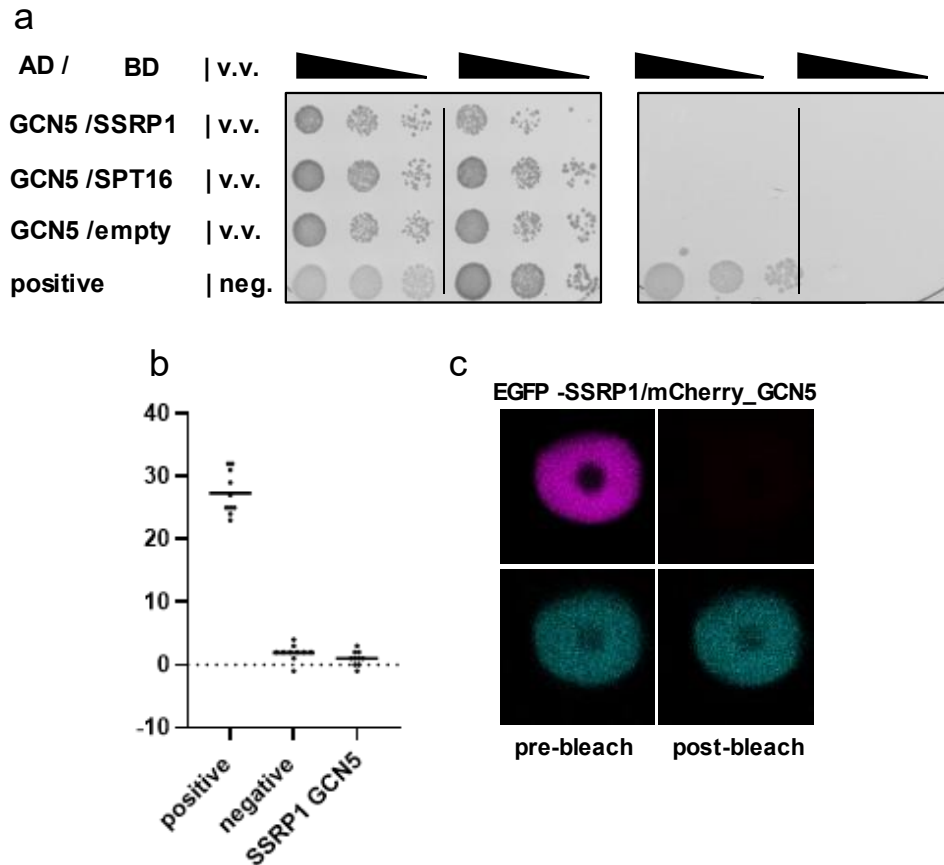
Supplementary Figure 5 *de novo* motif enrichment with HOMER (Heinz et al. 2010).



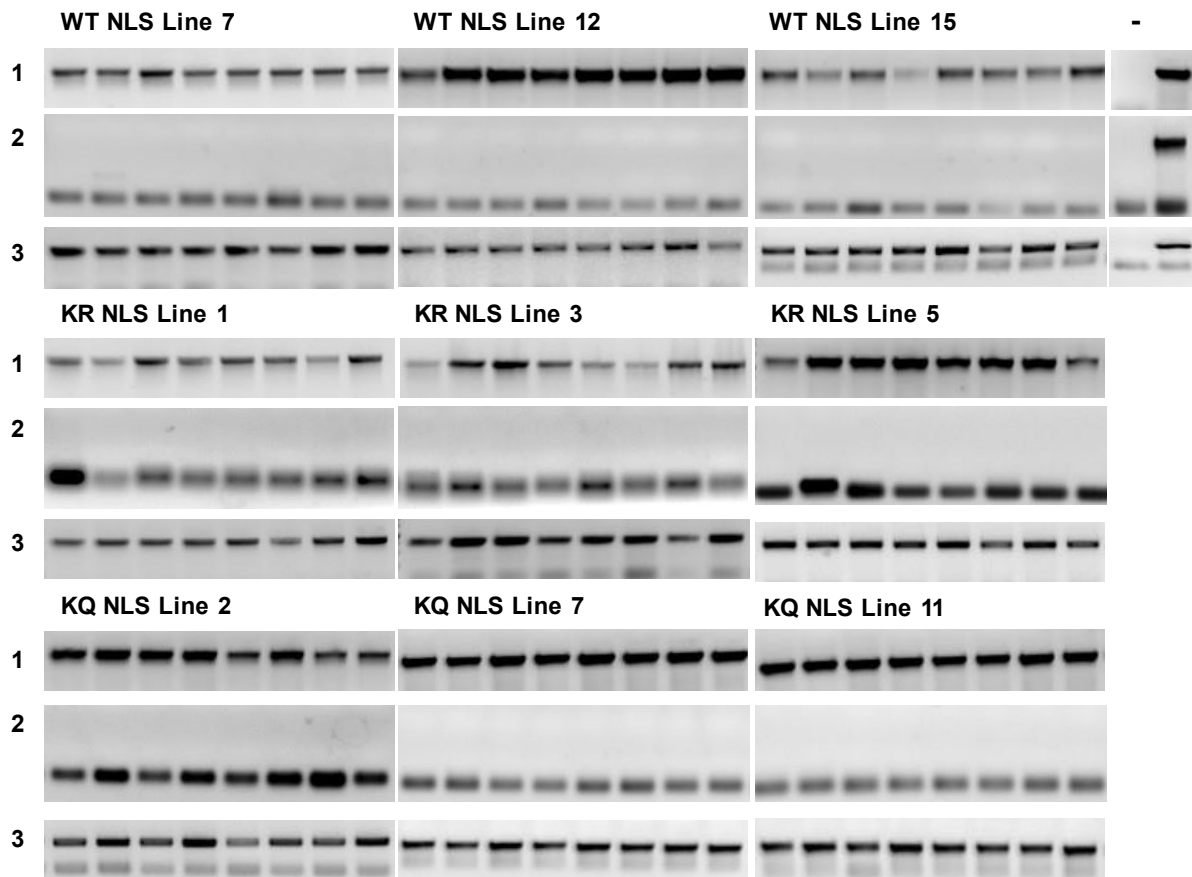
Supplementary Figure 6 Gene Ontology (GO) analysis was performed using the single enrichment analysis (SEA) of AgriGO (Tian et al. 2017). GO-analysis was performed with 648 genes which were significantly ($p < 0.05$) upregulated ($\geq 50\%$) in their H3 abundance in the NDR (-300 to 0 bp of TSS) of *Phos 0* compared to *WT*



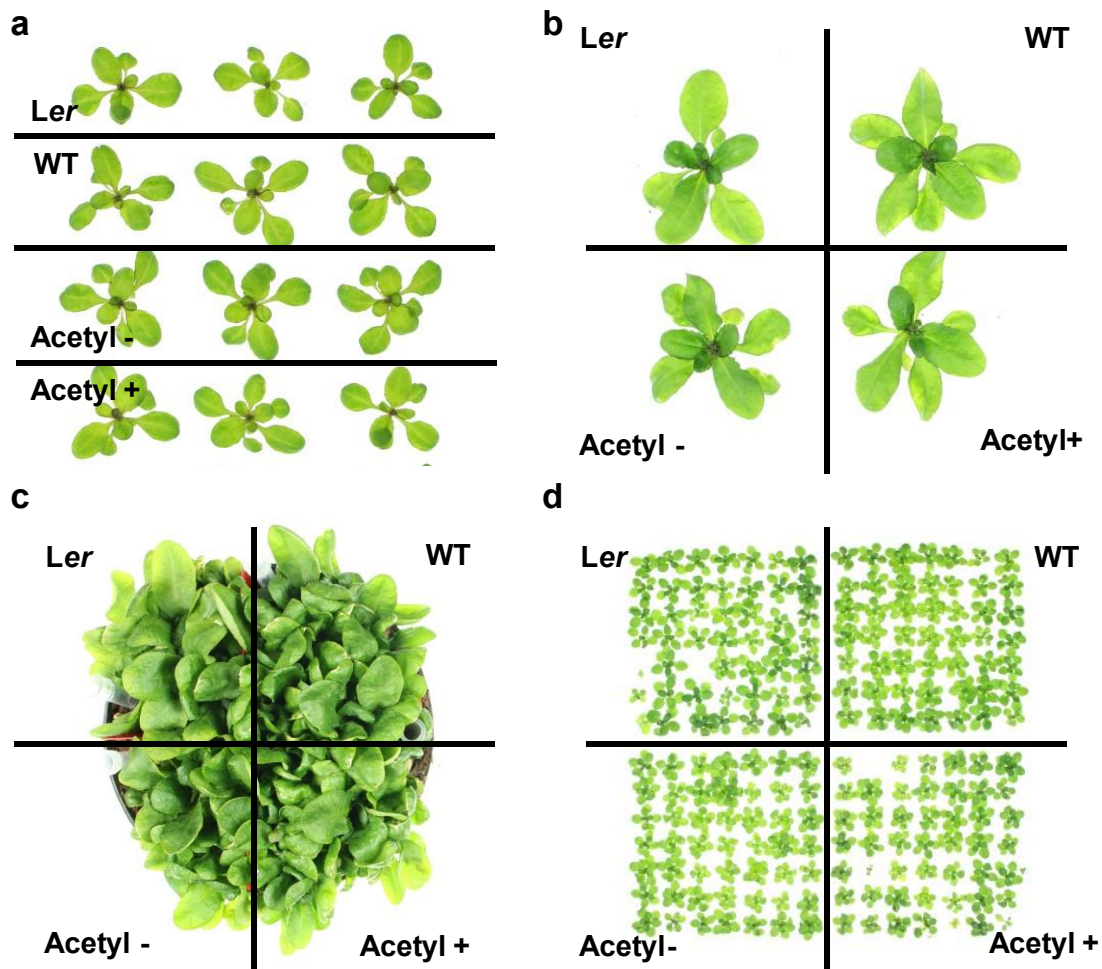
Supplementary Figure 7 Y2H displays no direct interaction between FACT and HDACs. Different combinations of bait- (DNA-binding domain = BD) and prey- (activation domain = AD) fusion proteins were spotted on dropout plates (DO) of yeast AH109 serial dilutions (100, 10⁻¹, 10⁻²). DDO (SD/ -LEU -TRP), and QDO (SD/ -LEU -TRP -HIS -ADE).. v.v. = vice versa



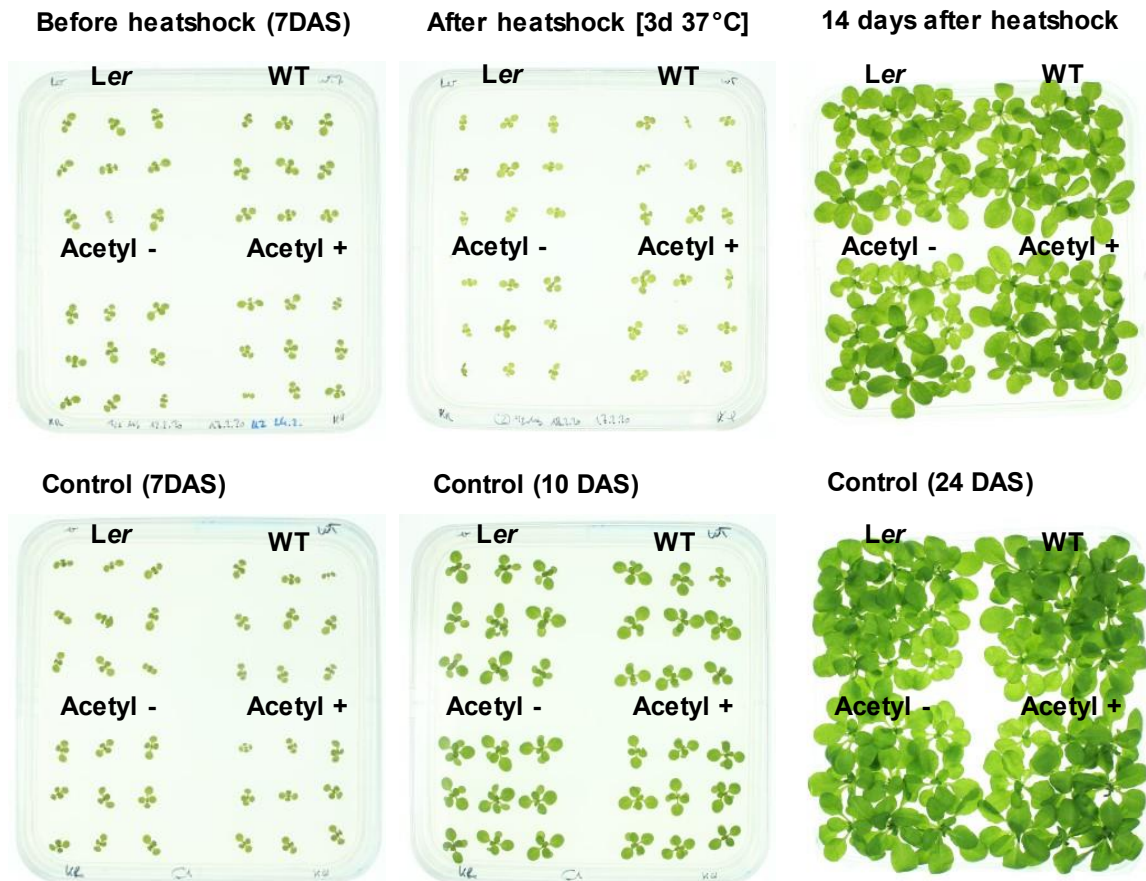
Supplementary Figure 8 Y2H and FRET assays display no direct interaction between FACT subunits and GCN5 (a) Different combinations of SSRP1, SPT16 or GCN5 AD or BD fusion proteins were spotted on synthetic dropout plates (b) FRET efficiencies [%] of 10 nuclei of the positive control (eGFP-NLS-mCherry fusion), negative control (eGFP-SSRP1 and mCherry-NLS) or the SSRP1/GCN5 interaction (eGFP-SSRP1, mCherry-GCN5). (c) Representative examples of donor and acceptor pre and post bleach. mCherry signals are displayed in magenta, eGFP signal in cyan. DDO (SD/ -LEU -TRP) and QDO (SD/ -LEU -TRP -HIS -ADE). Spotted were serial dilutions (10^0 , 10^{-1} , 10^{-2}) of yeast strain AH109.



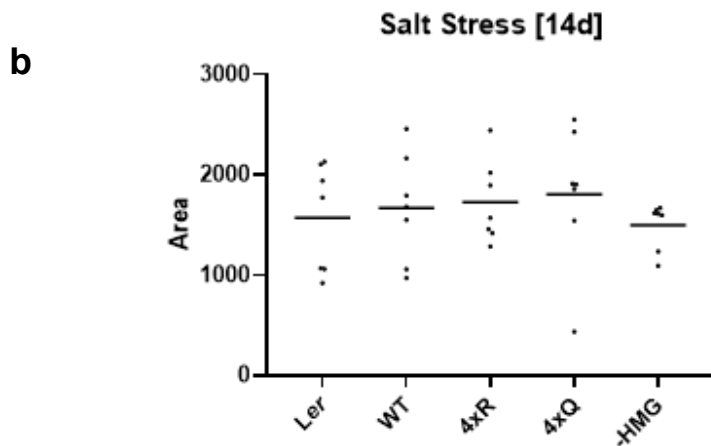
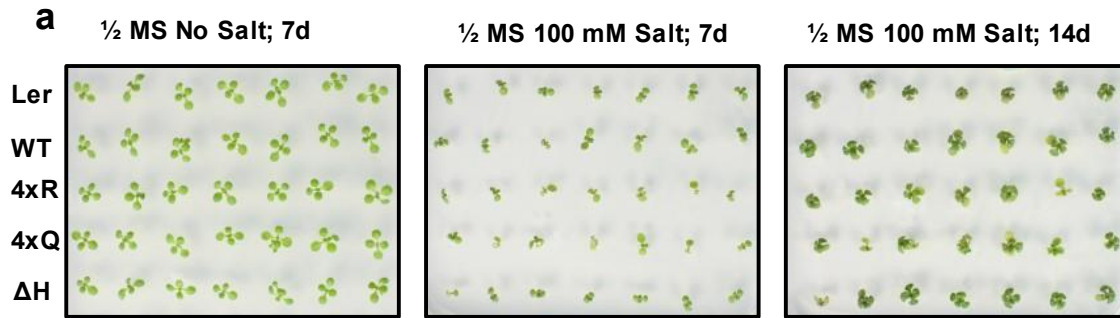
Supplementary Figure 9 Segregation analysis by genotyping PCR of double homozygous lines for *ssrp1-1* and the respective transgene. For Primers and details please refer to Figure 41



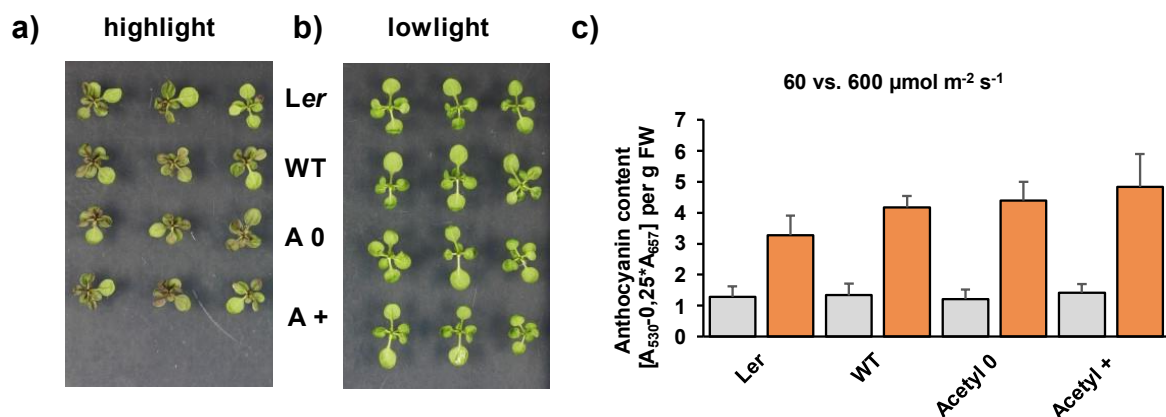
Supplementary Figure 10 *ssrp1-1* plants rescued with *pSSRP1:SSRP1* acetyl-variants show no defect when subjected cold stress (a) 20 Days cold treatment; (b, c, d) 40 days cold treatment; a,b,c were grown on soil, d on ½ MS plates, 16h light 8 h dark cycle at 4°C (Dong et al., 2006)



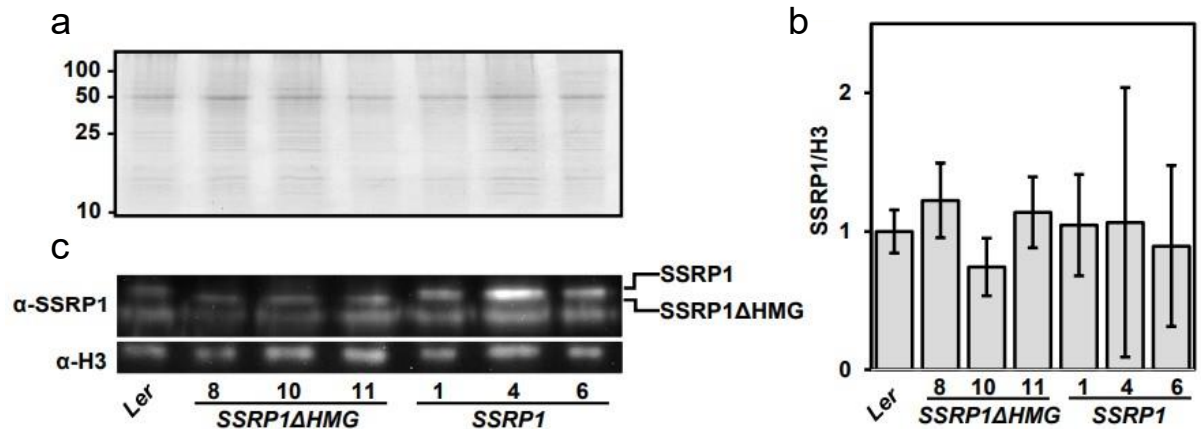
Supplementary Figure 11 *ssrp1-1* plants rescued with *pSSRP1:SSRP1* acetyl-variants show no defect when subjected to heat stress. Upper row: 7-day-old plantlets (left column) were heat treated for 3 days at 37°C (middle column) and recorded 14 days after heat treatment (Wu et al., 2010). Lower row: Same as upper row, but no heat treatment. 3 biological replicates were performed, one representative is shown here



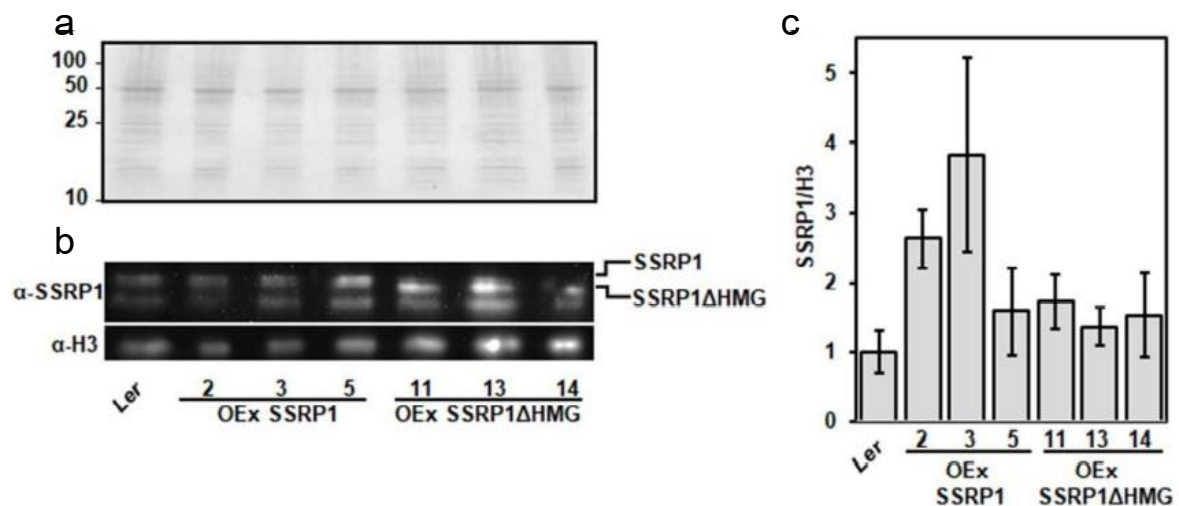
Supplementary Figure 12 *ssrp1-1* plants rescued with *pSSRP1:SSRP1* acetyl-variants show no defect when subjected to salt treatment (a) Plants were grown on $\frac{1}{2}$ MS plates for 3 days. Germinating Seedlings were transferred to $\frac{1}{2}$ MS plates containing 100 mM Salt, 16h light 8h dark cycle at 21°C (b) Quantification of leaf area, of 2 biological replicates with ImageJ. No significant difference was measured by one-way ANOVA and subsequent Tukey's pairwise analysis



Supplementary Figure 13 *ssrp1-1* plants rescued with *pSSRP1:SSRP1* acetyl-variants show no defect when subjected to highlight treatment 14-day-old plantlets were grown on plates containing 2% sucrose at lowlight (60 $\mu\text{mol m}^{-2} \text{s}^{-1}$) and (a) switched to highlight for 7 days (600 $\mu\text{mol m}^{-2} \text{s}^{-1}$) (b) continued growing at lowlight (c) Quantification of anthocyanin content. All plantlets of each replicate (n=9) were merged, and anthocyanin was extracted. 3 biological replicates were merged. No significant difference was measured by one-way ANOVA and subsequent Tukey's pairwise analysis

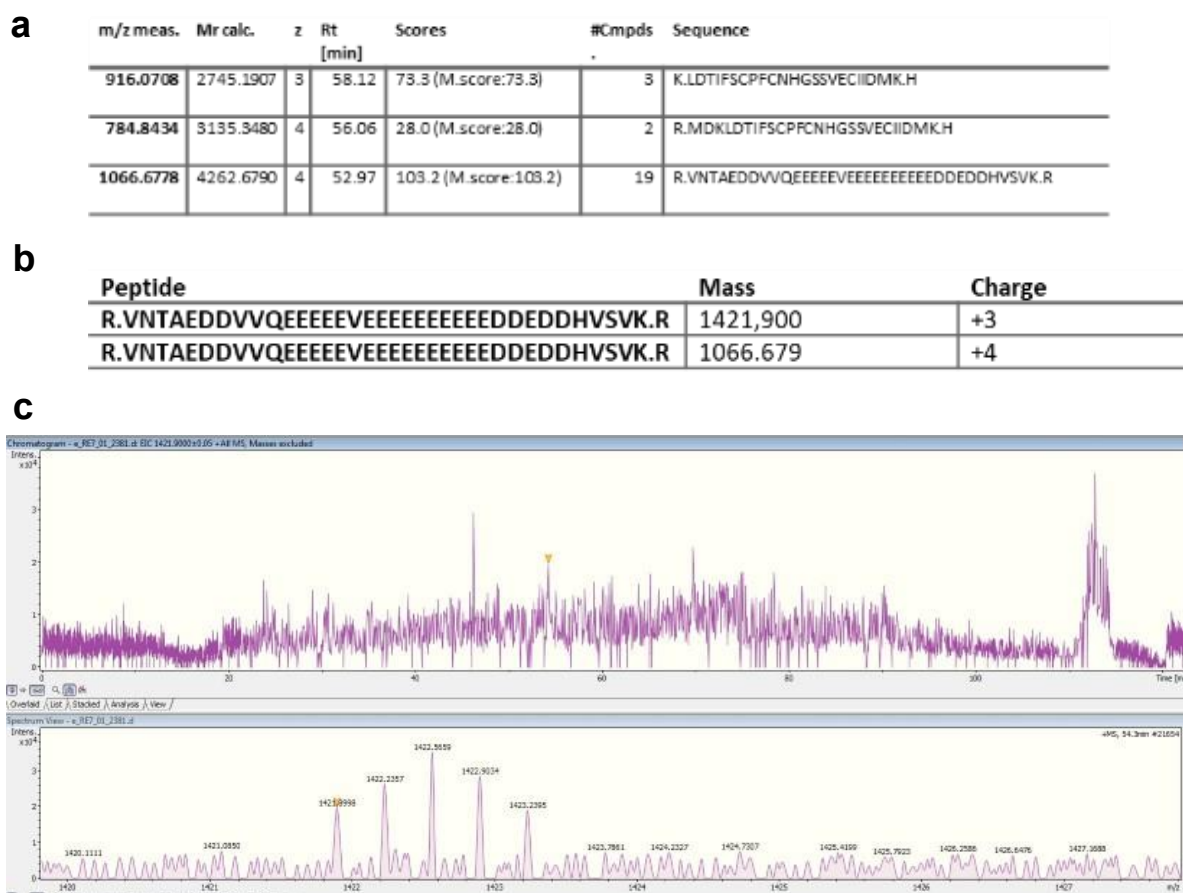


Supplementary Figure 14 Immunoblot analysis of the SSRP1 and SSRP1ΔHMG complementation plants. Nuclear protein extracts of *ssrp1-1* plants harbouring the expression constructs Ler plants were stained using Coomassie blue (a) and analysed by immunoblotting using α -SSRP1 antibodies and for comparison α -H3 antibodies (b). After transferring the protein onto the membrane, the membrane was cut horizontally and the upper part was incubated with the α -SSRP1 antibody while the lower part was incubated with the α -H3 antibody. α -SSRP1 in addition to SSRP1 detects a degradation product migrating below. Antibody binding was detected using a HRP-coupled secondary antibody and chemiluminescence detection. The slightly different migration positions of SSRP1 and SSRP1ΔHMG are indicated at the immunoblot. (c) Quantification of the relative amounts of SSRP1 and SSRP1ΔHMG. The band intensities of SSRP1/SSRP1ΔHMG relative to H3 were quantified using Image J. The histogram represents mean values \pm SD of three immunoblots.



Supplementary Figure 15 Protein levels of SSRP1 or SSRP1ΔHMG overexpression constructs. Immunoblot analysis of the SSRP1 and SSRP1ΔHMG overexpression plants. Nuclear protein extracts of *ssrp1-1* plants harbouring overexpression constructs and of Ler plants were stained using Coomassie blue (a) and were analysed by immunoblotting using α -SSRP1 antibodies and for comparison α -H3 antibodies (b). After transferring the protein onto the membrane, the membrane was cut horizontally, and the upper part was incubated with the α -SSRP1 antibody while the lower part was incubated with the α -H3 antibody. α -SSRP1 in addition to SSRP1 detects

a degradation product migrating below. Antibody binding was detected using a HRP-coupled secondary antibody and chemiluminescence detection. The slightly different migration positions of SSRP1 and SSRP1 Δ HMG are indicated at the immunoblot. (c) Quantification of the relative amounts of SSRP1 and SSRP1 Δ HMG. The band intensities of SSRP1/SSRP1 Δ HMG relative to H3 were quantified using Image J. The histogram represents mean values \pm SD of three immunoblots



Supplementary Figure 16 ELF1 is elusive in other AP-MS datasets. Manual screening reveals one single spectra in 3 Replicates of NRPB1-GS and SPT16-GS potentially correlating to ELF1 (a) Most likely spectra observed in the ELF1-GS AP-MS dataset (b) Overview of charge states of the highest abundant peptide (c) Exemplary peptide found in NRPB1-GS at the right retention time (upper panel), displaying appropriate Mass (lower panel)

References

- Aguilar-Gurrieri, C., Larabi, A., Vinayachandran, V., Patel, N.A., Yen, K., Reja, R., Ebong, I.-O., Schoehn, G., Robinson, C. V, Pugh, B.F., et al. (2016). Structural evidence for Nap1-dependent H2A–H2B deposition and nucleosome assembly. *EMBO J.* *35*, 1465–1482.
- Alonso-Blanco, C., Bentsink, L., Hanhart, C.J., Blankestijn-de Vries, H., and Koornneef, M. (2003). Analysis of natural allelic variation at seed dormancy loci of *Arabidopsis thaliana*. *Genetics* *164*, 711–729.
- Andrés-Barrao, C., Lafi, F.F., Alam, I., de Zélicourt, A., Eida, A.A., Bokhari, A., Alzubaidy, H., Bajic, V.B., Hirt, H., and Saad, M.M. (2017). Complete Genome Sequence Analysis of *Enterobacter* sp. SA187, a Plant Multi-Stress Tolerance Promoting Endophytic Bacterium. *Front. Microbiol.* *8*.
- Antosz, W. (2019). The role of *Arabidopsis* TFIIS in regulating transcript elongation : molecular and functional characterisation Wojciech Antosz.
- Antosz, W., Pfab, A., Ehrnsberger, H.F., Holzinger, P., Köllen, K., Mortensen, S.A., Bruckmann, A., Schubert, T., Längst, G., Griesenbeck, J., et al. (2017). The Composition of the *Arabidopsis* RNA Polymerase II Transcript Elongation Complex Reveals the Interplay between Elongation and mRNA Processing Factors. *Plant Cell* *29*, 854–870.
- Antosz, W., Deforges, J., Begcy, K., Bruckmann, A., Poirier, Y., Dresselhaus, T., and Grasser, K.D. (2020). Critical role of transcript cleavage in *Arabidopsis* RNA polymerase II transcriptional elongation. *Plant Cell* *32*, 1449–1463.
- Aoki, D., Awazu, A., Fujii, M., Uewaki, J., Hashimoto, M., Tochio, N., Umehara, T., and Tate, S. (2020). Ultrasensitive Change in Nucleosome Binding by Multiple Phosphorylations to the Intrinsically Disordered Region of the Histone Chaperone FACT. *J. Mol. Biol.* 106408.
- Arvidsson, S., Kwasniewski, M., Riaño-Pachón, D.M., and Mueller-Roeber, B. (2008). QuantPrime - A flexible tool for reliable high-throughput primer design for quantitative PCR. *BMC Bioinformatics* *9*, 1–15.
- Assenberg, R., Webb, M., Connolly, E., Stott, K., Watson, M., Hobbs, J., and Thomas, J.O. (2008). A critical role in structure-specific DNA binding for the acetyltable lysine residues in HMGB1. *Biochem. J.* *411*, 553–561.
- Badjatia, N., Rossi, M.J., Bataille, A.R., Mittal, C., Lai, W.K.M., and Pugh, B.F. (2021). Acute stress drives global repression through two independent RNA polymerase II stalling events in *Saccharomyces*. *Cell Rep.* *34*, 108640.
- Basnet, H., Su, X.B., Tan, Y., Meisenhelder, J., Merkurjev, D., Ohgi, K.A., Hunter, T., Pillus, L., and Rosenfeld, M.G. (2014). Tyrosine phosphorylation of histone H2A by CK2 regulates transcriptional elongation. *Nature* *516*, 267–271.
- Bedard, L.G., Dronamraju, R., Kerschner, J.L., Hunter, G.O., Axley, E.D., Boyd, A.K., Strahl, B.D., and Mosley, A.L. (2016). Quantitative analysis of dynamic protein interactions during transcription reveals a role for casein kinase II in PAF complex phosphorylation and regulation of H2B monoubiquitylation. *J. Biol. Chem.* *291*, jbc.M116.727735.
- Begum, N.A., Stanlie, A., Nakata, M., Akiyama, H., and Honjo, T. (2012). The histone chaperone Spt6 is required for activation-induced cytidine deaminase target determination through H3K4me3 regulation. *J. Biol. Chem.* *287*, 32415–32429.
- Bell, O., Tiwari, V.K., Thomä, N.H., and Schübeler, D. (2011). Determinants and dynamics of genome accessibility. *Nat. Rev. Genet.* *12*, 554–564.

- Bentsink, L., Jowett, J., Hanhart, C.J., and Koornneef, M. (2006). Cloning of DOG1, a quantitative trait locus controlling seed dormancy in *Arabidopsis*. *Proc. Natl. Acad. Sci. U. S. A.* *103*, 17042–17047.
- Bernecky, C., Herzog, F., Baumeister, W., Plitzko, J.M., and Cramer, P. (2016). Structure of transcribing mammalian RNA polymerase II. *Nature* *529*, 551–554.
- Bewley, J. (1997). Seed Germination and Dormancy. *Plant Cell* *9*, 1055–1066.
- Bigeard, J., Rayapuram, N., Bonhomme, L., Hirt, H., and Pflieger, D. (2014). Proteomic and phosphoproteomic analyses of chromatin-associated proteins from *Arabidopsis thaliana*. *Proteomics* *14*, 2141–2155.
- Bonaldi, T., Talamo, F., Scaffidi, P., Ferrera, D., Porto, A., Bachi, A., Rubartelli, A., Agresti, A., and Bianchi, M.E. (2003). Monocytic cells hyperacetylate chromatin protein HMGB1 to redirect it towards secretion. *EMBO J.* *22*, 5551–5560.
- Boulikas, T. (1994). Putative nuclear localization signals (NLS) in protein transcription factors. *J. Cell. Biochem.* *55*, 32–58.
- Boyes, D.C., Zayed, A.M., Ascenzi, R., McCaskill, A.J., Hoffman, N.E., Davis, K.R., and Görlach, J. (2001). Growth stage-based phenotypic analysis of *Arabidopsis*: a model for high throughput functional genomics in plants. *Plant Cell* *13*, 1499–1510.
- Brand, L., Hörler, M., Nüesch, E., Vassalli, S., Barrell, P., Yang, W., Jefferson, R. a, Grossniklaus, U., and Curtis, M.D. (2006). A versatile and reliable two-component system for tissue-specific gene induction in *Arabidopsis*. *Plant Physiol.* *141*, 1194–1204.
- Brázda, P., Krej, M., Kasiliauskaite, A., Klumpler, T., Vácha, R., Kubí, K., and Richard, Š. (2020). Yeast Spt6 Reads Multiple Phosphorylation Patterns of RNA Polymerase II C-Terminal Domain In Vitro. 4092–4107.
- Brewster, N.K., Johnston, G.C., and Singer, R.A. (2001). A bipartite yeast SSRP1 analog comprised of Pob3 and Nhp6 proteins modulates transcription. *Mol. Cell. Biol.* *21*, 3491–3502.
- Brower-Toland, B., Wacker, D.A., Fulbright, R.M., Lis, J.T., Kraus, W.L., and Wang, M.D. (2005). Specific contributions of histone tails and their acetylation to the mechanical stability of nucleosomes. *J. Mol. Biol.* *346*, 135–146.
- Bruhn, S.L., Pil, P.M., Essigmann, J.M., Housman, D.E., and Lippard, S.J. (1992). Isolation and characterization of human cDNA clones encoding a high mobility group box protein that recognizes structural distortions to DNA caused by binding of the anticancer agent cisplatin. *Proc. Natl. Acad. Sci. U. S. A.* *89*, 2307–2311.
- Cabrejos, M.E., Allende, C.C., and Maldonado, E. (2004). Effects of phosphorylation by protein kinase CK2 on the human basal components of the RNA polymerase II transcription machinery. *J. Cell. Biochem.* *93*, 2–10.
- Cairns, B.R. (2009). The logic of chromatin architecture and remodelling at promoters. *Nature* *461*, 193–198.
- Carrillo-Barral, N., Del Carmen Rodríguez-Gacio, M., and Matilla, A.J. (2020). Delay of germination-1 (DOG1): A key to understanding seed dormancy. *Plants* *9*.
- Chen, T., and Dent, S.Y.R. (2014). Chromatin modifiers and remodellers: regulators of cellular differentiation. *Nat. Rev. Genet.* *15*, 93–106.
- Chen, C., Shu, J., Li, C., Thapa, R.K., Nguyen, V., Yu, K., Yuan, Z., Kohalmi, S.E., Liu, J., Huang, S., et al. (2019a). RNA polymerase II-independent recruitment of SPT6L at transcription start sites in *Arabidopsis*. *47*, 6714–6725.
- Chen, F.X., Xie, P., Collings, C.K., Cao, K., Aoi, Y., Marshall, S.A., Rendleman, E.J.,

- Ugarenko, M., Ozark, P.A., Zhang, A., et al. (2017). PAF1 regulation of promoter-proximal pause release via enhancer activation. *Science* (80-.). 357, 1294–1298.
- Chen, P., Dong, L., Hu, M., Wang, Y.Z., Xiao, X., Zhao, Z., Yan, J., Wang, P.Y., Reinberg, D., Li, M., et al. (2018). Functions of FACT in Breaking the Nucleosome and Maintaining Its Integrity at the Single-Nucleosome Level. *Mol. Cell* 71, 284-293.e4.
- Chen, W.Q., Drapek, C., Li, D.X., Xu, Z.H., Benfey, P.N., and Bai, S.N. (2019b). Histone deacetylase *hda19* affects root cortical cell fate by interacting with scarecrow. *Plant Physiol.* 180, 276–288.
- Cheng, Y., and Patel, D.J. (2004). An efficient system for small protein expression and refolding. *Biochem. Biophys. Res. Commun.* 317, 401–405.
- Citterio, E., Van Den Boom, V., Schnitzler, G., Kanaar, R., Bonte, E., Kingston, R.E., Hoeijmakers, J.H.J., and Vermeulen, W. (2000). ATP-Dependent Chromatin Remodeling by the Cockayne Syndrome B DNA Repair-Transcription-Coupling Factor. *Mol. Cell. Biol.* 20, 7643–7653.
- Clough, S.J., and Bent, A.F. (1998). Floral dip: a simplified method for *Agrobacterium*-mediated transformation of *Arabidopsis thaliana*. *Plant J.* 16, 735–743.
- Costa, P.J., and Arndt, K.M. (2000). Synthetic lethal interactions suggest a role for the *Saccharomyces cerevisiae* Rtf1 protein in transcription elongation. *Genetics* 156, 535–547.
- CRICK, F. (1970). Central Dogma of Molecular Biology. *Nature* 227, 561–563.
- Dechassa, M.L., Sabri, A., Pondugula, S., Kassabov, S.R., Chatterjee, N., Kladdé, M.P., and Bartholomew, B. (2010). SWI/SNF Has Intrinsic Nucleosome Disassembly Activity that Is Dependent on Adjacent Nucleosomes. *Mol. Cell* 38, 590–602.
- Dekkers, B.J.W., Willems, L., Bassel, G.W., Van Bolderen-Veldkamp, R.P.M., Ligterink, W., Hilhorst, H.W.M., and Bentsink, L. (2012). Identification of reference genes for RT-qPCR expression analysis in *Arabidopsis* and tomato seeds. *Plant Cell Physiol.* 53, 28–37.
- Dissmeyer, N., and Schnittger, A. (2011). Use of Phospho-Site Substitutions to Analyze the Biological Relevance of Phosphorylation Events in Regulatory Networks. N. Dissmeyer, and A. Schnittger, eds. (Totowa, NJ: Humana Press), pp. 93–138.
- Dong, C.-H., Hu, X., Tang, W., Zheng, X., Kim, Y.S., Lee, B. -h., and Zhu, J.-K. (2006). A Putative *Arabidopsis* Nucleoporin, AtNUP160, Is Critical for RNA Export and Required for Plant Tolerance to Cold Stress. *Mol. Cell. Biol.* 26, 9533–9543.
- Duina, A. a (2011). Histone Chaperones Spt6 and FACT: Similarities and Differences in Modes of Action at Transcribed Genes. *Genet. Res. Int.* 2011, 625210.
- Duroux, M., Houben, A., Růžička, K., Friml, J., and Grasser, K.D. (2004). The chromatin remodelling complex FACT associates with actively transcribed regions of the *Arabidopsis* genome. *Plant J.* 40, 660–671.
- Dürr, J. (2013). The role of the transcription elongation factor SPT4-SPT5 in plant growth and development.
- Edwards, K., Johnstone, C., and Thompson, C. (1991). A simple and rapid method for the preparation of plant genomic DNA for PCR analysis. *Nucleic Acids Res.* 19, 1349.
- Ehara, H., Yokoyama, T., Shigematsu, H., Yokoyama, S., Shirouzu, M., and Sekine, S. (2017). Structure of the complete elongation complex of RNA polymerase II with basal factors. *Science* (80-.). 8552, 1–8.
- Ehara, H., Kujirai, T., Fujino, Y., Shirouzu, M., Kurumizaka, H., and Sekine, S. (2019). Structural insight into nucleosome transcription by RNA polymerase II with elongation factors.

747, 744–747.

Falbo, L., Raspelli, E., Romeo, F., Fiorani, S., Pezzimenti, F., Casagrande, F., Costa, I., Parazzoli, D., and Costanzo, V. (2020). SSRP1-mediated histone H1 eviction promotes replication origin assembly and accelerated development. *Nat. Commun.* *11*.

Farnung, L., Vos, S.M., and Cramer, P. (2018). Structure of transcribing RNA polymerase II-nucleosome complex. *Nat. Commun.* *9*, 5432.

Farnung, L., Ochmann, M., Engholm, M., and Cramer, P. (2021). Structural basis of nucleosome transcription mediated by Chd1 and FACT. *Nat. Struct. Mol. Biol.* *28*.

Finkelstein, R., Reeves, W., Ariizumi, T., and Steber, C. (2008). Molecular aspects of seed dormancy. *Annu. Rev. Plant Biol.* *59*, 387–415.

Formosa, T. (2012). The role of FACT in making and breaking nucleosomes. *Biochim. Biophys. Acta* *1819*, 247–255.

Formosa, T., and Winston, F. (2020). The role of FACT in managing chromatin: disruption, assembly, or repair? *Nucleic Acids Res.* *48*, 11929–11941.

Formosa, T., Eriksson, P., Wittmeyer, J., Ginn, J., Yu, Y., and Stillman, D.J. (2001). Spt16-Pob3 and the HMG protein Nhp6 combine to form the nucleosome-binding factor SPN. *EMBO J.* *20*, 3506–3517.

Frost, J.M., Kim, M.Y., Park, G.T., Hsieh, P.-H., Nakamura, M., Lin, S.J.H., Yoo, H., Choi, J., Ikeda, Y., Kinoshita, T., et al. (2018). FACT complex is required for DNA demethylation at heterochromatin during reproduction in Arabidopsis. *Proc. Natl. Acad. Sci.* *115*, E4720–E4729.

Goto, C., Hashizume, S., Fukao, Y., Hara-Nishimura, I., and Tamura, K. (2019). Comprehensive nuclear proteome of Arabidopsis obtained by sequential extraction. *Nucleus* *10*, 81–92.

Gouot, E., Bhat, W., Rufiange, A., Fournier, E., Paquet, E., and Nourani, A. (2018). Casein kinase 2 mediated phosphorylation of Spt6 modulates histone dynamics and regulates spurious transcription. 1–19.

Grasser, M., Kane, C.M., Merkle, T., Melzer, M., Emmersen, J., and Grasser, K.D. (2009). Transcript Elongation Factor TFIIS Is Involved in Arabidopsis Seed Dormancy. *J. Mol. Biol.* *386*, 598–611.

Gu, X.-L.L., Wang, H., Huang, H., and Cui, X.-F.F. (2012). SPT6L encoding a putative WG/GW-repeat protein regulates apical-basal polarity of embryo in Arabidopsis. *Mol. Plant* *5*, 249–259.

Gurova, K., Chang, H.W., Valieva, M.E., Sandlesh, P., and Studitsky, V.M. (2018). Structure and function of the histone chaperone FACT – Resolving FACTual issues. *Biochim. Biophys. Acta - Gene Regul. Mech.* *1861*, 892–904.

Hammond, C.M., Strømme, C.B., Huang, H., Patel, D.J., and Groth, A. (2017). Histone chaperone networks shaping chromatin function. *Nat. Rev. Mol. Cell Biol.* *18*, 141–158.

Hamperl, S., Brown, C.R., Garea, A.V., Perez-Fernandez, J., Bruckmann, A., Huber, K., Wittner, M., Babl, V., Stoeckl, U., Deutzmann, R., et al. (2013). Compositional and structural analysis of selected chromosomal domains from *Saccharomyces cerevisiae*. *Nucleic Acids Res.* *42*, 1–20.

Hartlepp, K.F., Fernández-Tornero, C., Eberharter, A., Grüne, T., Müller, C.W., and Becker, P.B. (2005). The Histone Fold Subunits of Drosophila CHRAC Facilitate Nucleosome Sliding through Dynamic DNA Interactions. *Mol. Cell. Biol.* *25*, 9886–9896.

He, M., Zhang, L., Wang, X., Huo, L., Sun, L., Feng, C., Jing, X., Du, D., Liang, H., Liu, M.,

- et al. (2013). Systematic Analysis of the Functions of Lysine Acetylation in the Regulation of Tat Activity. *PLoS One* 8.
- Heazlewood, J.I., Durek, P., Hummel, J., Selbig, J., Weckwerth, W., Walther, D., and Schulze, W.X. (2008). PhosPhAt: A database of phosphorylation sites in *Arabidopsis thaliana* and a plant-specific phosphorylation site predictor. *Nucleic Acids Res.* 36, 1015–1021.
- Heinz, S., Benner, C., Spann, N., Bertolino, E., Lin, Y.C., Laslo, P., Cheng, J.X., Murre, C., Singh, H., and Glass, C.K. (2010). Simple Combinations of Lineage-Determining Transcription Factors Prime cis-Regulatory Elements Required for Macrophage and B Cell Identities. *Mol. Cell* 38, 576–589.
- Hellemans, J., Mortier, G., De Paepe, A., Speleman, F., and Vandesompele, J. (2007). qBase relative quantification framework and software for management and automated analysis of real-time quantitative PCR data. *Genome Biol.* 8, R19.
- Heo, K., Kim, H., Choi, S.H., Choi, J., Kim, K., Gu, J., Lieber, M.R., Yang, A.S., and An, W. (2008). FACT-mediated exchange of histone variant H2AX regulated by phosphorylation of H2AX and ADP-ribosylation of Spt16. *Mol. Cell* 30, 86–97.
- Herzinger, S. (2018). Analysis of Transcript elongation Factors.
- Hetzl, J., Duttke, S.H., Benner, C., and Chory, J. (2016). Nascent RNA sequencing reveals distinct features in plant transcription. *Proc. Natl. Acad. Sci. U. S. A.* 113, 12316–12321.
- Ho, S.N., Hunt, H.D., Horton, R.M., Pullen, J.K., and Pease, L.R. (1989). Site-directed mutagenesis by overlap extension using the polymerase chain reaction. *Gene* 77, 51–59.
- Hollender, C., and Liu, Z. (2008). Histone deacetylase genes in *Arabidopsis* development. *J. Integr. Plant Biol.* 50, 875–885.
- Holzinger, P. (2015). Molecular Characterization of the Histone Chaperone FACT.
- Jeronimo, C., Poitras, C., and Robert, F. (2019). Histone Recycling by FACT and Spt6 during Transcription Prevents the Scrambling of Histone Modifications. *Cell Rep.* 28, 1206-1218.e8.
- Johnson, J.M., French, S.L., Osheim, Y.N., Li, M., Hall, L., Beyer, A.L., and Smith, J.S. (2013). Rpd3- and Spt16-Mediated Nucleosome Assembly and Transcriptional Regulation on Yeast Ribosomal DNA Genes. *Mol. Cell. Biol.* 33, 2748–2759.
- Jones, D.T., and Cozzetto, D. (2015). DISOPRED3: Precise disordered region predictions with annotated protein-binding activity. *Bioinformatics* 31, 857–863.
- Joo, Y.J., Ficarro, S.B., Chun, Y., Marto, J.A., and Buratowski, S. (2019). In vitro analysis of RNA polymerase II elongation complex dynamics. *Genes Dev.* 1–12.
- Kalashnikova, A.A., Winkler, D.D., McBryant, S.J., Henderson, R.K., Herman, J.A., DeLuca, J.G., Luger, K., Prenti, J.E., and Hansen, J.C. (2013). Linker histone H1.0 interacts with an extensive network of proteins found in the nucleolus. *Nucleic Acids Res.* 41, 4026–4035.
- Kaljanac, M. (2014). Transcript elongation factors FACT and TFIIS in *A. thaliana*.
- Kato, H., Okazaki, K., and Urano, T. (2013). Spt6: Two fundamentally distinct functions in the regulation of histone modification. *Epigenetics* 8, 1249–1253.
- Keller, D.M., and Lu, H. (2002). p53 serine 392 phosphorylation increases after UV through induction of the assembly of the CK2.hSPT16.SSRP1 complex. *J. Biol. Chem.* 277, 50206–50213.
- Kiefhaber, C. (2016). Chromatin remodeling histone chaperones in *Arabidopsis thaliana*.
- Kim, S., Piquerez, S.J.M., Ramirez-Prado, J.S., Mastorakis, E., Veluchamy, A., Latrasse, D., Manza-Mianza, D., Brik-Chaouche, R., Huang, Y., Rodriguez-Granados, N.Y., et al. (2020).

- GCN5 modulates salicylic acid homeostasis by regulating H3K14ac levels at the 5' and 3' ends of its target genes. *Nucleic Acids Res.* *48*, 5953–5966.
- Koenig, T., Menze, B.H., Kirchner, M., Monigatti, F., Parker, K.C., Patterson, T., Steen, J.J., Hamprecht, F.A., and Steen, H. (2008). Robust prediction of the MASCOT score for an improved quality assessment in mass spectrometric proteomics. *J. Proteome Res.* *7*, 3708–3717.
- Koulouras, G., Panagopoulos, A., Rapsomaniki, M.A., Giakoumakis, N.N., Taraviras, S., and Lygerou, Z. (2018). EasyFRAP-web: A web-based tool for the analysis of fluorescence recovery after photobleaching data. *Nucleic Acids Res.* *46*, W467–W472.
- Krogan, N.J., Kim, M., Ahn, S.H., Zhong, G., Kobor, M.S., Cagney, G., Emili, A., Shilatifard, A., Buratowski, S., and Greenblatt, J.F. (2002). RNA Polymerase II Elongation Factors of *Saccharomyces cerevisiae*: a Targeted Proteomics Approach. *Society* *22*, 6979–6992.
- Krohn, N.M., Stemmer, C., Fojan, P., Grimm, R., and Grasser, K.D. (2003). Protein kinase CK2 phosphorylates the high mobility group domain protein SSRP1, inducing the recognition of UV-damaged DNA. *J. Biol. Chem.* *278*, 12710–12715.
- Kubinski, K., Zielinski, R., Hellman, U., Mazur, E., and Szyszka, R. (2006). Yeast elf1 factor is phosphorylated and interacts with protein kinase CK2. *J Biochem Mol Biol* *39*, 311–318.
- Kujirai, T., and Kurumizaka, H. (2020). Transcription through the nucleosome. *Curr. Opin. Struct. Biol.* *61*, 42–49.
- Kujirai, T., Ehara, H., Fujino, Y., Shirouzu, M., Sekine, S., and Kurumizaka, H. (2018). Structural basis of the nucleosome transition during RNA polymerase II passage. *598*, 595–598.
- Kumar, A., and Vasudevan, D. (2020). Structure-function relationship of H2A-H2B specific plant histone chaperones. *Cell Stress Chaperones* *25*, 1–17.
- Van Leene, J., Witters, E., Inzé, D., and De Jaeger, G. (2008). Boosting tandem affinity purification of plant protein complexes. *Trends Plant Sci.* *13*, 517–520.
- Van Leene, J., Eeckhout, D., Persiau, G., Van De Slijke, E., Geerinck, J., Van Isterdael, G., Witters, E., and De Jaeger, G. (2011). Isolation of Transcription Factor Complexes from Arabidopsis Cell Suspension Cultures by Tandem Affinity Purification. In *Plant & Cell Physiology*, pp. 195–218.
- Van Leene, J., Eeckhout, D., Cannoot, B., De Winne, N., Persiau, G., Van De Slijke, E., Vercruyse, L., Dedecker, M., Verkest, A., Vandepoele, K., et al. (2015). An improved toolbox to unravel the plant cellular machinery by tandem affinity purification of Arabidopsis protein complexes. *Nat Protoc* *10*, 169–187.
- Lei, B., and Berger, F. (2020). H2A Variants in Arabidopsis: Versatile Regulators of Genome Activity. *Plant Commun.* *1*, 100015.
- Leng, X., Thomas, Q., Rasmussen, S.H., and Marquardt, S. (2020). A G(enomic)P(ositioning)S(ystem) for Plant RNAPII Transcription. *Trends Plant Sci.* *25*, 744–764.
- Li, H., Torres-Garcia, J., Latrasse, D., Benhamed, M., Schilderink, S., Zhou, W., Kulikova, O., Hirt, H., and Bisseling, T. (2017). Plant-Specific Histone Deacetylases HDT1/2 Regulate GIBBERELLIN 2-OXIDASE2 Expression to Control Arabidopsis Root Meristem Cell Number. *Plant Cell* *29*, 2183–2196.
- Van Lijsebettens, M., and Grasser, K.D. (2014). Transcript elongation factors: shaping transcriptomes after transcript initiation. *Trends Plant Sci.* *1*, 1–10.
- Lilley, D.M.J., and Clegg, R.M. (1993). The Structure of the Four-Way Junction in DNA. *Annu.*

Rev. Biophys. Biomol. Struct. 22, 299–328.

Liu, H., Ding, Y., Zhou, Y., Jin, W., Xie, K., and Chen, L.L. (2017). CRISPR-P 2.0: An Improved CRISPR-Cas9 Tool for Genome Editing in Plants. *Mol. Plant* 10, 530–532.

Liu, M.J., Seddon, A.E., Tsai, Z.T.Y., Major, I.T., Floer, M., Howe, G.A., and Shiu, S.H. (2015). Determinants of nucleosome positioning and their influence on plant gene expression. *Genome Res.* 25, 1182–1195.

Liu, Y., Koornneef, M., and Soppe, W.J.J. (2007). The absence of histone H2B monoubiquitination in the *Arabidopsis* hub1 (rdo4) mutant reveals a role for chromatin remodeling in seed dormancy. *Plant Cell* 19, 433–444.

Liu, Y., Geyer, R., van Zanten, M., Carles, A., Li, Y., Hörold, A., van Nocker, S., and Soppe, W.J.J. (2011). Identification of the *Arabidopsis* reduced dormancy 2 gene uncovers a role for the polymerase associated factor 1 complex in seed dormancy. *PLoS One* 6, 1–8.

Liu, Y., Zhou, K., Zhang, N., Wei, H., Tan, Y.Z., Zhang, Z., Carragher, B., Potter, C.S., D'Arcy, S., and Luger, K. (2020). FACT caught in the act of manipulating the nucleosome. *Nature* 577, 426–431.

Lolas, I.B. (2008). Characterization of *Arabidopsis* plants harboring mutations in the genes encoding the chromatin associated FACT complex.

Lolas, I.B., Himanen, K., Grønlund, J.T., Lynggaard, C., Houben, A., Melzer, M., Van Lijsebettens, M., and Grasser, K.D. (2010). The transcript elongation factor FACT affects *Arabidopsis* vegetative and reproductive development and genetically interacts with HUB1/2. *Plant J.* 61, 686–697.

Luger, K., Mäder, A.W., Richmond, R.K., Sargent, D.F., and Richmond, T.J. (1997). Crystal structure of the nucleosome core particle at 2.8 Å resolution. *Nature* 389, 251–260.

Luger, K., Dechassa, M.L., and Tremethick, D.J. (2012). New insights into nucleosome and chromatin structure: an ordered state or a disordered affair? *Nat. Rev. Mol. Cell Biol.* 13, 436–447.

Malarkey, C.S., and Churchill, M.E.A. (2012). The high mobility group box : the ultimate utility player of a cell. *Trends Biochem. Sci.* 37, 553–562.

Markusch, H. (2018). Characterisation of *Arabidopsis* Transcript Elongation Factors.

Markusch, H. (2020). *Arabidopsis* Transcription elongation factor 1 has histone chaperone like qualities.

Martin, B.J.E., Chruscicki, A.T., and Howe, L.J. (2018). Transcription promotes the interaction of the facilitates chromatin transactions (FACT) complex with nucleosomes in *saccharomyces cerevisiae*. *Genetics* 210, 869–881.

Matsuzaki, H., Daitoku, H., Hatta, M., Aoyama, H., Yoshimochi, K., and Fukamizu, A. (2005). Acetylation of Foxo1 alters its DNA-binding ability and sensitivity to phosphorylation. *Proc. Natl. Acad. Sci. U. S. A.* 102, 11278–11283.

Mayanagi, K., Saikusa, K., Miyazaki, N., Akashi, S., Iwasaki, K., Nishimura, Y., Morikawa, K., and Tsunaka, Y. (2019). Structural visualization of key steps in nucleosome reorganization by human FACT. *Sci. Rep.* 9, 1–14.

Mayer, A., Lidschreiber, M., Siebert, M., Leike, K., Söding, J., and Cramer, P. (2010). Uniform transitions of the general RNA polymerase II transcription complex. *Nat. Struct. Mol. Biol.* 17, 1272–1278.

McCullough, L., Connell, Z., Petersen, C., and Formosa, T. (2015). The Abundant Histone Chaperones Spt6 and FACT Collaborate to Assemble, Inspect, and Maintain Chromatin

Structure in *Saccharomyces cerevisiae*. *Genetics* 201, 1031–1045.

McCullough, L.L., Connell, Z., Xin, H., Studitsky, V.M., Feofanov, A. V., Valieva, M.E., and Formosa, T. (2018). Functional roles of the DNA-binding HMGB domain in the histone chaperone FACT in nucleosome reorganization. *J. Biol. Chem.* 293, 6121–6133.

McDonald, S.M., Close, D., Xin, H., Formosa, T., and Hill, C.P. (2010). Structure and Biological Importance of the Spn1-Spt6 Interaction, and Its Regulatory Role in Nucleosome Binding. *Mol. Cell* 40, 725–735.

Meggio, F., and Pinna, L.A. (2003). One-thousand-and-one substrates of protein kinase CK2? *FASEB J.* 17, 349–368.

Mehrtens, F., Kranz, H., Bednarek, P., and Weisshaar, B. (2005). The Arabidopsis transcription factor MYB12 is a flavonol-specific regulator of phenylpropanoid biosynthesis. *Plant Physiol.* 138, 1083–1096.

Michl-Holzinger, P., Mortensen, S.A., and Grasser, K.D. (2019). The SSRP1 subunit of the histone chaperone FACT is required for seed dormancy in Arabidopsis. *J. Plant Physiol.* 236, 105–108.

Miyagi, A., Tsunaka, Y., Uchihashi, T., Mayanagi, K., Hirose, S., Morikawa, K., and Ando, T. (2008). Visualization of Intrinsically Disordered Regions of Proteins by High-Speed Atomic Force Microscopy. *ChemPhysChem* 9, 1859–1866.

Molitor, A.M., Bu, Z., Yu, Y., and Shen, W.H. (2014). Arabidopsis AL PHD-PRC1 Complexes Promote Seed Germination through H3K4me3-to-H3K27me3 Chromatin State Switch in Repression of Seed Developmental Genes. *PLoS Genet.* 10.

Montacié, C., Durut, N., Opsomer, A., Palm, D., Comella, P., Picart, C., Carpentier, M.-C., Pontvianne, F., Carapito, C., Schleiff, E., et al. (2017). Nucleolar Proteome Analysis and Proteasomal Activity Assays Reveal a Link between Nucleolus and 26S Proteasome in *A. thaliana*. *Front. Plant Sci.* 8, 1–13.

Mortensen, S.A. (2012). Molecular analysis of the transcript elongation factor TFIIS and the histone chaperone FACT in *Arabidopsis thaliana*.

Mortensen, S. a., and Grasser, K.D. (2014). The seed dormancy defect of Arabidopsis mutants lacking the transcript elongation factor TFIIS is caused by reduced expression of the DOG1 gene. *FEBS Lett.* 588, 47–51.

Mortensen, S. a., Sønderkær, M., Lynggaard, C., Grasser, M., Nielsen, K.L., and Grasser, K.D. (2011). Reduced expression of the DOG1 gene in Arabidopsis mutant seeds lacking the transcript elongation factor TFIIS. *FEBS Lett.* 585, 1929–1933.

Myers, J.K., Pace, C.N., and Scholtz, J.M. (1997). Helix propensities are identical in proteins and peptides. *Biochemistry* 36, 10923–10929.

Mylonas, C., and Tessarz, P. (2019). NET-prism enables RNA polymerase-dedicated transcriptional interrogation at nucleotide resolution. *RNA Biol.* 16, 1156–1165.

Naito, Y., Yamada, T., Matsumiya, T., Ui-Tei, K., Saigo, K., and Morishita, S. (2005). dsCheck: highly sensitive off-target search software for double-stranded RNA-mediated RNA interference. *Nucleic Acids Res.* 33, W589-91.

Nishino, Y., Eltsov, M., Joti, Y., Ito, K., Takata, H., Takahashi, Y., Hihara, S., Frangakis, A.S., Imamoto, N., and Ishikawa, T. (2012). Human mitotic chromosomes consist predominantly of irregularly folded nucleosome fibres without a 30-nm chromatin structure. *EMBO J.* 31, 1644–1653.

Noe Gonzalez, M., Blears, D., and Svejstrup, J.Q. (2020). Causes and consequences of RNA

polymerase II stalling during transcript elongation. *Nat. Rev. Mol. Cell Biol.*

Nonogaki, H. (2014). Seed dormancy and germination-emerging mechanisms and new hypotheses. *Front. Plant Sci.* 5, 233.

Orphanides, G., LeRoy, G., Chang, C.-H.H., Luse, D.S., and Reinberg, D. (1998). FACT, a Factor that Facilitates Transcript Elongation through Nucleosomes. *Cell* 92, 105–116.

Orphanides, G., Wu, W.H., Lane, W.S., Hampsey, M., and Reinberg, D. (1999). The chromatin-specific transcription elongation factor FACT comprises human SPT16 and SSRP1 proteins. *Nature* 400, 284–288.

Osakabe, A., Lorković, Z.J., Kobayashi, W., Tachiwana, H., Yelagandula, R., Kurumizaka, H., and Berger, F. (2018). Histone H2A variants confer specific properties to nucleosomes and impact on chromatin accessibility. *Nucleic Acids Res.* 46, 7675–7685.

Osman, A. (2004). Yeast Two-Hybrid Assay for Studying Protein–Protein Interactions. *Methods Mol Biol.* 270.

Osman, S., and Cramer, P. (2020). Structural Biology of RNA Polymerase II Transcription: 20 Years On. *Annu. Rev. Cell Dev. Biol.* 36, 1–34.

Pandey, R., Müller, A., Napoli, C.A., Selinger, D.A., Pikaard, C.S., Richards, E.J., Bender, J., Mount, D.W., and Jorgensen, R.A. (2002). Analysis of histone acetyltransferase and histone deacetylase families of *Arabidopsis thaliana* suggests functional diversification of chromatin modification among multicellular eukaryotes. *Nucleic Acids Res.* 30, 5036–5055.

Pass, D.A., Sornay, E., Marchbank, A., Crawford, M.R., Paszkiewicz, K., Kent, N.A., and Murray, J.A.H. (2017). Genome-wide chromatin mapping with size resolution reveals a dynamic sub-nucleosomal landscape in *Arabidopsis*. *PLoS Genet.* 13, 1–18.

Pathak, R., Singh, P., Ananthakrishnan, S., Adamczyk, S., Schimmel, O., and Govind, C.K. (2018). Acetylation-Dependent Recruitment of the FACT Complex and Its Role in Regulating Pol II Occupancy Genome-Wide in *Saccharomyces cerevisiae*. *Genetics* 209, genetics.300943.2018.

Pendle, A.F., Clark, G.P., Boon, R., Lewandowska, D., Lam, Y.W., Andersen, J., Mann, M., Lamond, A.I., Brown, J.W.S., and Shaw, P.J. (2005). Proteomic analysis of the *Arabidopsis* nucleolus suggests novel nucleolar functions. *Mol. Biol. Cell.*

Petes, S.J., and Lis, J.T. (2012). Overcoming the nucleosome barrier during transcript elongation. *Trends Genet.* 28, 285–294.

Pfab, A. (2017). Molecular and functional studies on the transcript elongation factor FACT and the SAGA-DUBm subunit ENY2 in *Arabidopsis thaliana*.

Pfab, A., Antosz, W., Holzinger, P., Bruckmann, A., Griesenbeck, J., and Grasser, K.D. (2017). Analysis of In Vivo Chromatin and Protein Interactions of *Arabidopsis* Transcript Elongation Factors. (Humana Press, New York, NY), pp. 105–122.

Pfab, A., Breindl, M., and Grasser, K.D. (2018a). The *Arabidopsis* histone chaperone FACT is required for stress-induced expression of anthocyanin biosynthetic genes. *Plant Mol. Biol.* 96, 367–374.

Pfab, A., Grønlund, J.T., Holzinger, P., Längst, G., and Grasser, K.D. (2018b). The *Arabidopsis* Histone Chaperone FACT: Role of the HMG-Box Domain of SSRP1. *J. Mol. Biol.* 430, 2747–2759.

Philpott, a, Krude, T., and Laskey, R. a (2000). Nuclear chaperones. *Semin. Cell Dev. Biol.* 11, 7–14.

Prather, D., Krogan, N.J., Emili, A., Jack, F., Winston, F., and Greenblatt, J.F. (2005).

Identification and Characterization of Elf1 , a Conserved Transcription Elongation Factor in *Saccharomyces cerevisiae* Identification and Characterization of Elf1 , a Conserved Transcription Elongation Factor in *Saccharomyces cerevisiae*. *25*, 10122–10135.

Ramachandran, S., Ahmad, K., and Henikoff, S. (2017). Transcription and Remodeling Produce Asymmetrically Unwrapped Nucleosomal Intermediates. *Mol. Cell* *68*, 1038-1053.e4.

Reynolds, C.R., Islam, S.A., and Sternberg, M.J.E. (2018). EzMol: A Web Server Wizard for the Rapid Visualization and Image Production of Protein and Nucleic Acid Structures. *J. Mol. Biol.* *430*, 2244–2248.

Ricci, M.A., Manzo, C., Lakadamyali, M., and Cosma, M.P. (2015). Chromatin Fibers Are Formed by Heterogeneous Groups of Nucleosomes In Vivo Article Chromatin Fibers Are Formed by Heterogeneous Groups of Nucleosomes In Vivo. 1145–1158.

Roeder, A.H.K., and Yanofsky, M.F. (2006). Fruit Development in Arabidopsis.

Romeis, T., Ludwig, A.A., Martin, R., and Jones, J.D. (2001). Calcium-dependent protein kinases play an essential role in a plant defence response. *EMBO J.* *20*, 5556–5567.

Röttgers, K., Krohn, N.M., Lichota, J., Stemmer, C., Merkle, T., and Grasser, K.D. (2000). DNA-interactions and nuclear localisation of the chromosomal HMG domain protein SSRP1 from maize. *Plant J.* *23*, 395–405.

Roudier, F., Ahmed, I., Bérard, C., Sarazin, A., Mary-Huard, T., Cortijo, S., Bouyer, D., Caillieux, E., Duvernois-Berthet, E., Al-Shikhley, L., et al. (2011). Integrative epigenomic mapping defines four main chromatin states in Arabidopsis. *EMBO J.* *30*, 1928–1938.

Roy, A., Kucukural, A., and Zhang, Y. (2010). I-TASSER: a unified platform for automated protein structure and function prediction. *Nat. Protoc.* *5*, 725–738.

Rutowicz, K., Lirski, M., Mermaz, B., Teano, G., Schubert, J., Mestiri, I., Kroteń, M.A., Fabrice, T.N., Fritz, S., Grob, S., et al. (2019). Linker histones are fine-scale chromatin architects modulating developmental decisions in Arabidopsis. *Genome Biol.* *20*, 1–22.

Safina, A., Cheney, P., Pal, M., Brodsky, L., Ivanov, A., Kirsanov, K., Lesovaya, E., Naberezhnov, D., Neshet, E., Koman, I., et al. (2017). FACT is a sensor of DNA torsional stress in eukaryotic cells. *Nucleic Acids Res.* *45*, 1925–1945.

Sambrook, J., Fritsch, E.F., and Maniatis, T. (1989). *Molecular Cloning: A Laboratory Manual*, Second Edition.

Sansó, M., Vargas-Pérez, I., Quintales, L., Antequera, F., Ayté, J., and Hidalgo, E. (2011). Gcn5 facilitates Pol II progression, rather than recruitment to nucleosome-depleted stress promoters, in *Schizosaccharomyces pombe*. *Nucleic Acids Res.* *39*, 6369–6379.

Saunders, A., Werner, J., Andrulis, E.D., Nakayama, T., Hirose, S., Reinberg, D., and Lis, J.T. (2003). Tracking FACT and the RNA Polymerase II Elongation Complex Through Chromatin in Vivo. *301*, 1094–1097.

Schier, A.C., and Taatjes, D.J. (2020). Structure and mechanism of the RNA polymerase II transcription machinery. *Genes Dev.* *34*, 465–488.

Schmid, M., Davison, T.S., Henz, S.R., Pape, U.J., Demar, M., Vingron, M., Schölkopf, B., Weigel, D., and Lohmann, J.U. (2005). A gene expression map of Arabidopsis thaliana development. *Nat. Genet.* *37*, 501–506.

Sekar, R.B., and Periasamy, A. (2003). Fluorescence resonance energy transfer (FRET) microscopy imaging of live cell protein localizations. *J. Cell Biol.* *160*, 629–633.

Sequeira-Mendes, J., Araguez, I., Peiro, R., Mendez-Giraldez, R., Zhang, X., Jacobsen, S.E., Bastolla, U., and Gutierrez, C. (2014). The Functional Topography of the Arabidopsis Genome

- Is Organized in a Reduced Number of Linear Motifs of Chromatin States. *Plant Cell* 26, 2351–2366.
- Shandilya, J., and Roberts, S.G.E. (2012). *Biochimica et Biophysica Acta* The transcription cycle in eukaryotes : From productive initiation to RNA polymerase II recycling. *BBA - Gene Regul. Mech.* 1819, 391–400.
- Shechter, D., Dormann, H.L., Allis, C.D., and Hake, S.B. (2007). Extraction, purification and analysis of histones. *Nat Protoc* 2, 1445–1457.
- Sievers, F., Wilm, A., Dineen, D., Gibson, T.J., Karplus, K., Li, W., Lopez, R., McWilliam, H., Remmert, M., Söding, J., et al. (2011). Fast, scalable generation of high-quality protein multiple sequence alignments using Clustal Omega. *Mol. Syst. Biol.* 7.
- Song, F., Chen, P., Sun, D., Wang, M., Dong, L., Liang, D., Xu, R., and Zhu, P. (2014). Cryo-EM Study of the Chromatin Fiber Tetranucleosomal Units. 376–381.
- St-Denis, N., Gabriel, M., Turowec, J.P., Gloor, G.B., Li, S.S.C., Gingras, A.C., and Litchfield, D.W. (2015). Systematic investigation of hierarchical phosphorylation by protein kinase CK2. *J. Proteomics* 118, 49–62.
- Stemmer, C., Schwander, A., Bauw, G., Fojan, P., and Grasser, K.D. (2002). Protein kinase CK2 differentially phosphorylates maize chromosomal high mobility group B (HMGB) proteins modulating their stability and DNA interactions. *J. Biol. Chem.* 277, 1092–1098.
- Stillman, D.J. (2010). Nhp6: A small but powerful effector of chromatin structure in *Saccharomyces cerevisiae*. *Biochim. Biophys. Acta - Gene Regul. Mech.* 1799, 175–180.
- Stros, M., Launholt, D., Grasser, K.D., Štros, M., Launholt, D., and Grasser, K.D. (2007). The HMG-box: a versatile protein domain occurring in a wide variety of DNA-binding proteins. *Cell. Mol. Life Sci.* 64, 2590–2606.
- Stuwe, T., Hothorn, M., Lejeune, E., Rybin, V., Bortfeld, M., Scheffzek, K., and Ladurner, A.G. (2008). The FACT Spt16 “peptidase” domain is a histone H3-H4 binding module. *Proc. Natl. Acad. Sci. U. S. A.* 105, 8884–8889.
- Takahata, S., Yu, Y., and Stillman, D.J. (2009). The E2F functional analogue SBF recruits the Rpd3(L) HDAC, via Whi5 and Stb1, and the FACT chromatin reorganizer, to yeast G1 cyclin promoters. *EMBO J.* 28, 3378–3389.
- Thorbecke, C. (2019). Functional characterisation of the putative *Arabidopsis thaliana* transcription elongation factor ELF1.
- Tian, T., Liu, Y., Yan, H., You, Q., Yi, X., Du, Z., Xu, W., and Su, Z. (2017). AgriGO v2.0: A GO analysis toolkit for the agricultural community, 2017 update. *Nucleic Acids Res.* 45, W122–W129.
- Tiwari, P., Kaila, P., and Guptasarma, P. (2019). Understanding anomalous mobility of proteins on SDS-PAGE with special reference to the highly acidic extracellular domains of human E- and N-cadherins. *Electrophoresis* 40, 1273–1281.
- Tomson, B.N., and Arndt, K.M. (2013). The many roles of the conserved eukaryotic Paf1 complex in regulating transcription, histone modifications, and disease states. *Biochim. Biophys. Acta - Gene Regul. Mech.* 1829, 116–126.
- Tripodi, F., Nicastro, R., Busnelli, S., Cirulli, C., Maffioli, E., Tedeschi, G., Alberghina, L., and Coccetti, P. (2013). Protein kinase CK2 holoenzyme promotes start-specific transcription in *saccharomyces cerevisiae*. *Eukaryot. Cell* 12, 1271–1280.
- True, J.D., Muldoon, J.J., Carver, M.N., Poorey, K., Shetty, S.J., Bekiranov, S., and Auble, D.T. (2016). The Mot1 ATPase and Spt16 Histone Chaperone Co-Regulate Transcription through

Preinitiation Complex Assembly and Nucleosome Organization. *J. Biol. Chem.* 291, jbc.M116.735134.

Tsien, R.Y., Bacsikai, B.J., and Adams, S.R. (1993). FRET for studying intracellular signalling. *Trends Cell Biol.* 3, 242–245.

Tsunaka, Y., Toga, J., Yamaguchi, H., Tate, S.I., Hirose, S., and Morikawa, K. (2009). Phosphorylated intrinsically disordered region of FACT masks its nucleosomal DNA binding elements. *J. Biol. Chem.* 284, 24610–24621.

Tsunaka, Y., Fujiwara, Y., Oyama, T., Hirose, S., and Morikawa, K. (2016). Integrated molecular mechanism directing nucleosome reorganization by human FACT. *Genes Dev.* 30, 673–686.

Tsunaka, Y., Ohtomo, H., Morikawa, K., and Nishimura, Y. (2020). Partial Replacement of Nucleosomal DNA with Human FACT Induces Dynamic Exposure and Acetylation of Histone H3 N-Terminal Tails. *IScience* 23.

Ülker, B., Peiter, E., Dixon, D.P., Moffat, C., Capper, R., Bouché, N., Edwards, R., Sanders, D., Knight, H., and Knight, M.R. (2008). Getting the most out of publicly available T-DNA insertion lines. *Plant J.* 56, 665–677.

Venkatesh, S., and Workman, J.L. (2015). Histone exchange, chromatin structure and the regulation of transcription. *Nat. Rev. Mol. Cell Biol.* 16, 178–189.

Vicient, C.M., and Delsen, M. (1998). Isolation of Total RNA from Arabidopsis. 412–413.

Vinayachandran, V., Reja, R., Rossi, M.J., Park, B., Rieber, L., Mittal, C., Mahony, S., and Pugh, B.F. (2018). Widespread and precise reprogramming of yeast protein-genome interactions in response to heat shock. *Genome Res.* 28, 1–10.

Vos, S.M., Farnung, L., Boehning, M., Wigge, C., Linden, A., Urlaub, H., Cramer, P., Dsif, I.I., and Spt, P.A.F. (2018). Structure of activated transcription complex Pol II–DSIF–PAF–SPT6. *Nature* 560, 607–612.

Vos, S.M., Farnung, L., Linden, A., Urlaub, H., and Cramer, P. (2020). Structure of complete Pol II–DSIF–PAF–SPT6 transcription complex reveals RTF1 allosteric activation. *Nat. Struct. Mol. Biol.* 27, 668–677.

Waese, J., Fan, J., Pasha, A., Yu, H., Fucile, G., Shi, R., Cumming, M., Kelley, L., Sternberg, M., Krishnakumar, V., et al. (2017). ePlant: Visualizing and Exploring Multiple Levels of Data for Hypothesis Generation in Plant Biology. *Plant Cell* 29, tpc.00073.2017.

Wagner, F.R., Dienemann, C., Wang, H., Stützer, A., Tegunov, D., Urlaub, H., and Cramer, P. (2020). Structure of SWI/SNF chromatin remodeller RSC bound to a nucleosome. *Nature* 579, 448–451.

Wang, L., Du, Y., Lu, M., and Li, T. (2012). ASEB: A web server for KAT-specific acetylation site prediction. *Nucleic Acids Res.* 40, 376–379.

Wang, T., Liu, Y., Edwards, G., Krzizike, D., Scherman, H., and Luger, K. (2018). The histone chaperone FACT modulates nucleosome structure by tethering its components. *Life Sci. Alliance* 1, e201800107.

Wang, Y., Wang, L., and Gong, Z. (2019). Regulation of Acetylation in High Mobility Group Protein B1 Cytosol Translocation. *DNA Cell Biol.* 38, 491–499.

Wang, Z., Xing, H., Dong, L., Zhang, H., Han, C., Wang, X., and Chen, Q. (2015). Egg cell-specific promoter-controlled CRISPR / Cas9 efficiently generates homozygous mutants for multiple target genes in Arabidopsis in a single generation. *Genome Biol.* 1–12.

Warren, C., and Shechter, D. (2017). Fly Fishing for Histones: Catch and Release by Histone

- Chaperone Intrinsically Disordered Regions and Acidic Stretches. *J. Mol. Biol.* *429*, 2401–2426.
- Weber, C.M., Ramachandran, S., and Henikoff, S. (2014). Nucleosomes are context-specific, H2A.Z-Modulated barriers to RNA polymerase. *Mol. Cell* *53*, 819–830.
- Wei, Y., Thyparambil, A.A., and Latour, R.A. (2014). Protein helical structure determination using CD spectroscopy for solutions with strong background absorbance from 190 to 230 nm. *Biochim. Biophys. Acta - Proteins Proteomics* *1844*, 2331–2337.
- Weidtkamp-Peters, S., and Stahl, Y. (2017). The Use of FRET/FLIM to Study Proteins Interacting with Plant Receptor Kinases. pp. 163–175.
- Wilkins, M.R., Gasteiger, E., Bairoch, A., Sanchez, J.-C., Williams, K.L., Appel, R.D., and Hochstrasser, D.F. (1999). Protein Identification and Analysis Tools in the ExPASy Server. In *2-D Proteome Analysis Protocols*, (New Jersey: Humana Press), pp. 531–552.
- Winkler, D.D., and Luger, K. (2011). The histone chaperone FACT: structural insights and mechanisms for nucleosome reorganization. *J. Biol. Chem.* *286*, 18369–18374.
- Winkler, D.D., Muthurajan, U.M., Hieb, A.R., and Luger, K. (2011). Histone chaperone FACT coordinates nucleosome interaction through multiple synergistic binding events. *J. Biol. Chem.* *286*, 41883–41892.
- Winston, F., Chaleff, D.T., Valent, B., and Fink, G.R. (1984). Mutations affecting Ty-mediated expression of the HIS4 gene of *Saccharomyces cerevisiae*. *Genetics* *107*, 179–197.
- Wu, S., Wang, L., Yeh, C., Lu, C., and Wu, S. (2010). Isolation and characterization of the *Arabidopsis* heat-intolerant 2 (hit2) mutant reveal the essential role of the nuclear export receptor EXPORTIN1A (XPO1A) in plant heat tolerance. *Plant Cell* *22*, 833–842.
- Xing, H., Dong, L., Wang, Z., Zhang, H., Han, C., Liu, B., Wang, X., and Chen, Q. (2014). A CRISPR/Cas9 toolkit for multiplex genome editing in plants. *Plant Cell* *26*, 1–12.
- Yang, J., Zhang, X., Feng, J., Leng, H., Li, S., Xiao, J., Liu, S., Xu, Z., Xu, J., Li, D., et al. (2016). The Histone Chaperone FACT Contributes to DNA Replication-Coupled Nucleosome Assembly. *Cell Rep.* *14*, 1128–1141.
- Yelagandula, R., Stroud, H., Holec, S., Zhou, K., Feng, S., Zhong, X., Muthurajan, U.M., Nie, X., Kawashima, T., Groth, M., et al. (2014). The Histone Variant H2A.W Defines Heterochromatin and Promotes Chromatin Condensation in *Arabidopsis*. *Cell* *158*, 98–109.
- Yin, R., Messner, B., Faus-Kessler, T., Hoffmann, T., Schwab, W., Hajirezaei, M.R., Von Saint Paul, V., Heller, W., and Schäffner, A.R. (2012). Feedback inhibition of the general phenylpropanoid and flavonol biosynthetic pathways upon a compromised flavonol-3-O-glycosylation. *J. Exp. Bot.* *63*, 2465–2478.
- Van Zanten, M., Koini, M.A., Geyer, R., Liu, Y., Brambilla, V., Bartels, D., Koornneef, M., Fransz, P., and Soppe, W.J.J. (2011). Seed maturation in *Arabidopsis thaliana* is characterized by nuclear size reduction and increased chromatin condensation. *Proc. Natl. Acad. Sci. U. S. A.* *108*, 20219–20224.
- Zhang, T., Zhang, W., and Jiang, J. (2015). Genome-wide nucleosome occupancy and positioning and their impact on gene expression and evolution in plants. *Plant Physiol.* *168*, 1406–1416.
- Zhang, Y., Fonslow, B.R., Shan, B., Baek, M.-C., and Yates, J.R. (2013). Protein Analysis by Shotgun/Bottom-up Proteomics. *Chem. Rev.* *113*, 2343–2394.
- Zheng, J., Chen, F., Wang, Z., Cao, H., Li, X., Deng, X., Soppe, W.J.J., Li, Y., and Liu, Y. (2012). A novel role for histone methyltransferase KYP/SUVH4 in the control of *Arabidopsis*

primary seed dormancy. *New Phytol.* *193*, 605–616.

Zhou, C., Labbe, H., Sridha, S., Wang, L., Tian, L., Latoszek-Green, M., Yang, Z., Brown, D., Miki, B., and Wu, K. (2004). Expression and function of HD2-type histone deacetylases in Arabidopsis development. *Plant J.* *38*, 715–724.

Zhou, J., Applegate, C., Alonso, A.D., Reynolds, D., Orford, S., Mackiewicz, M., Griffiths, S., Penfield, S., and Pullen, N. (2017). Leaf-GP: An open and automated software application for measuring growth phenotypes for arabidopsis and wheat. *Plant Methods* *13*, 1–17.

Zhou, K., Gaullier, G., and Luger, K. (2019). Nucleosome structure and dynamics are coming of age. *Nat. Struct. Mol. Biol.* *26*, 3–13.

Zhou, K., Liu, Y., and Luger, K. (2020). Histone chaperone FACT FACilitates Chromatin Transcription: mechanistic and structural insights. *Curr. Opin. Struct. Biol.* *65*, 26–32.

Zimmermann, L., Stephens, A., Nam, S.Z., Rau, D., Kübler, J., Lozajic, M., Gabler, F., Söding, J., Lupas, A.N., and Alva, V. (2018). A Completely Reimplemented MPI Bioinformatics Toolkit with a New HHpred Server at its Core. *J. Mol. Biol.* *430*, 2237–2243.